STUDY OF GENERATION AND TRANSPORT OF RUNAWAY ELECTRONS IN ADITYA AND ADITYA-U TOKAMAK

By
HARSHITA RAJ
PHYS06201304012

Institute for Plasma Research, Gandhinagar

A thesis submitted to the

Board of Studies in Physical Sciences

In partial fulfillment of requirements

for the Degree of

DOCTOR OF PHILOSOPHY

of

HOMI BHABHA NATIONAL INSTITUTE

July, 2019

Homi Bhabha National Institute[1]

Recommendations of the Viva Voce Committee

As members of the Viva Voce Committee, we certify that we have read the dissertation prepared by Ms. Harshita Raj entitled "STUDY OF GENERATION AND TRANSPORT OF RUNAWAY ELECTRONS IN ADITYA AND ADITYA-U TOKAMAK" and recommend that it may be accepted as fulfilling the thesis requirement for the award of Degree of Doctor of Philosophy.

Chairman - Prof. P.K. Chattopadhyay		Date: 22/01/20
Guide / Convener - Dr. Joydeep Ghosh	Ghosh	Date: 22.01.20
Examiner - Prof. Ashish Ganguli		Date: 28/01/20
Member 1- Dr. Raju Daniel		Date: 22/01/20
Member 2- Dr. R. Srinivasan		Date: 22.01.20
Technology Adviser - Prof. Y.C Saxena		Date: 22/01/20

Final approval and acceptance of this thesis is contingent upon the candidate's submission of the final copies of the thesis to HBNI.

I hereby certify that I have read this thesis prepared under my direction and recommend that it may be accepted as fulfilling the thesis requirement.

Date: 22.01.20

Place: IPR, Gandhinagar

Ghosh

Signature

Guide: Dr. Joydeep Ghosh

[1] This page is to be included only for final submission after successful completion of viva voce.

STATEMENT BY AUTHOR

This dissertation has been submitted in partial fulfillment of requirements for an advanced degree at Homi Bhabha National Institute (HBNI) and is deposited in the Library to be made available to borrowers under rules of the HBNI.

Brief quotations from this dissertation are allowable without special permission, provided that accurate acknowledgement of source is made. Requests for permission for extended quotation from or reproduction of this manuscript in whole or in part may be granted by the Competent Authority of HBNI when in his or her judgment the proposed use of the material is in the interests of scholarship. In all other instances, however, permission must be obtained from the author.

Harshita Raj

Harshita Raj

DECLARATION

I, hereby declare that the investigation presented in the thesis has been carried out by me. The work is original and has not been submitted earlier as a whole or in part for a degree / diploma at this or any other Institution / University.

Harshita Raj

Harshita Raj

List of Publications arising from the thesis

1. "Effect of periodic gas-puffs on drift-tearing modes in ADITYA/ADITYA-U tokamak discharges" by *Harshita Raj,* T. Macwan, et al. *Nucl. Fusion **60**, 036012 (2020).*

2. "Generation and Transport of Runaway Electrons during Sawteeth Crash in the ADITYA Tokamak" by *Harshita Raj,* J. Ghosh, R. L. Tanna, et al., *Nucl. Fusion* ***58***, *076004 (2018).*

3. "Overview of Recent Experimental Results from ADITYA Tokamak" by R. Tanna, J. Ghosh, P. Chattopadhyay, *Harshita Raj* et al., *Nucl. Fusion* ***57,*** *102008 (2017).*

4. "Overview of Operation and Experiments in the ADITYA-U Tokamak" by R. Tanna, *Harshita Raj* et al., *Nucl. Fusion* ***59***, *112006 (2019).*

5. "Origin of Harmonics of Drift Tearing Modes in ADITYA tokamak" by *Harshita Raj*, J. Ghosh, A. Sen et al., Submitted Manuscript - *Nucl. Fusion (NF-102943).*

6. "Experimental observation of edge fluctuation induced Runaway electron loss in ADITYA-U tokamak" by *Harshita Raj, J. Ghosh, R. L. Tanna, et* al. (To be submitted).

7. "Runaway electron induced neutral emission source in ADITYA and ADITYA-U tokamak" *Harshita Raj, J. Ghosh, R. L. Tanna, et* al. (To be submitted).

8. "Plasma Production and Preliminary Results from the ADITYA Upgrade Tokamak" by R. Tanna, J. Ghosh, P. Chattopadhyay, *Harshita Raj* et al., *Plasma Sci. Technol.* ***20***, *074002 (2018).*

9. "Automation of ADITYA tokamak plasma position control DC power supply" by B. Arambhadiya, *Harshita Raj* et al., *Fusion Engineering and Design* ***112***, *714 (2016).*

10. "Dynamics of Neon Ions after Neon Gas Seeding into Tokamak Plasma" by N. Bisai, M. B. Chowdhuri, S. Banerjee, *Harshita Raj* et al., *Nucl. Fusion* ***59***, *126013 (2019).*

11. "Novel Approach of Pulsed-Glow Discharge Wall Conditioning in ADITYA Upgrade Tokamak" by K. A. Jadeja**,** J. Ghosh**,** Kiran Patel**,** K. M. Patel**,** B. G. Arambhadiya**,** R. L. Tanna**,** K. S. Acharya**,** S.B. Bhatt**,** M. B. Chowdhuri**,** R. Manchanda**,** Minsha Shah**,** S. Ghosh**,** Vara Prasad Kella**,** T. Macwan**,** *Harshita Raj*, et al., *Nucl. Fusion* ***59***, *086005 (2019).*

Manchanda, Minsha Shah, S. Ghosh, Vara Prasad Kella, T. Macwan, *Harshita Raj*, et.al, *Nucl. Fusion 59 086005 (2019)*

12."Observation of Poloidal asymmetry in measured neutral temperatures in ADITYA-U tokamak plasma", Nandini Yadava, J. Ghosh, M.B. Chowdhuri, R. Manchanda, Sripathi Punchithaya, R. Dey, *Harshita Raj* et.al, *Nucl. Fusion 59 106003 (2019)*

13."Observations of Toroidal Plasma Rotation in Aditya-U Tokamak" by G. Shukla , K. Shah , M. B. Chowdhuri , *Harshita Raj,* et. al *Nucl. Fusion 59 (2019), 106049.*

14."Runaway electron mitigation with supersonic molecular beam injection (SMBI) in ADITYA-U tokamak", S. Banerjee, *Harshita Raj* et.al, Submitted Manuscript - *Nucl. Fusion (NF-103388)*

15."Studies of edge plasma parameters along with the neutrals of ADITYA-U tokamak using combined UEDGE-DEGAS2 code" by Ritu Dey , *Harshita Raj* et. al. Submitted Manuscript - *Nucl. Fusion -102929*

Date: 31 July 2019

Harshita Raj.

Harshita Raj

Publications in International Conference:

1. "Control of Magnetohydodynamic modes by periodic gas-puffing in ADITYA and ADITYA-Upgrade Tokamak" by *Harshita Raj*, et.al at 2nd Asia-Pacific Conference on Plasma Physics (AAPPS-DPP 2018), Kanazawa, Japan- Invited Talk

2. "Origin of Harmonics of Drift Tearing Mode in ADITYA tokamak", by *Harshita Raj*, et.al at *27th IAEA Fusion Energy Conference (FEC-2018), Gandhinagar India* -Invited Talk

3. "Generation and Transport of Runaway electrons in ADITYA tokamak" by *Harshita Raj* et.al at *13th Carolus Magnus Summer School on Plasma and Fusion Energy Physics*, from 3-14 September (CMSS-2018) in Netherlands.

4. "Observations of MHD modes prior to Disruption in ADITYA-Upgrade Tokamak", by *Harshita Raj et.al.*, *9th ITER International School (IIS-2017)*, 20th – 24th March, 2017, Aix en Provence, France

5. "A Study of Anomalous transportation of Sawtooth generated Runaway electrons observed in ADITYA tokamak", *Harshita Raj*, Joydeep Ghosh, R. L. Tanna, et.al at *10th APFA-2015 Conference*, Gandhinagar, India. (*Best Paper Award*)

As Co-Author

6. "Overview of Operation and Experiments in the ADITYA-U Tokamak", by R.L.Tanna, *Harshita Raj*, et.al at *27th IAEA Fusion Energy Conference (FEC-2018), Gandhinagar India*

7. "Runaway Electron Mitigation Using Supersonic Molecular Beam Injection in the Aditya-U Tokamak" by S.Banerjee, *Harshita Raj*, et.al, *at 27th IAEA Fusion Energy Conference (FEC-2018), Gandhinagar India*

8. "Studies of the gas puff effect on edge plasma of Aditya tokamak using coupled DEGAS2-UEDGE code" by R. Dey, *Harshita Raj*, et.al, at *27th IAEA Fusion Energy Conference (FEC-2018), Gandhinagar India*

Publications in National Conference:

1. "Dynamics of Runaway electrons in presence of MHD modes in ADITYA-U tokamak", by *Harshita Raj, et.al* at *33rd National Symposium on Plasma Science & Technology (PSSI-2018)*, Ahmedabad, Gujarat, India. (Oral presentation) (Awarded with *Best Oral Award*)

2. "Analysis of multiple Magnetohydodynamic modes in ADITYA-Upgrade Tokamak", Harshita Raj, *et.al* at *32nd National Symposium on Plasma Science & Technology (PSSI-2017)*, Ahmedabad, Gujarat, India. (Oral presentation)

3. "Experimental observations and LUKE code simulations of Runaway electrons in ADITYA tokamak" Harshita Raj, et.al at *31th National Symposium on Plasma Science & Technology (PSSI-2016)*, Coimbatore ,Tamil Nadu, India.

4. "Effect of multiple Gas-puffs on Plasma density and temperature in ADITYA tokamak", Harshita Raj, et.al at *30th National Symposium on Plasma Science and Technology (PSSI-2015)*, SINP, Kolkata, India (*Z.H. Sholapurwala Award for Fusion Science*)

5. "Generation and Transport of Saw-Teeth Induced Runaway Electrons in ADITYA Tokamak, Harshita Raj, Joydeep Ghosh, R. L. Tannaet.al at *29th National Symposium on Plasma Science & Technology (PSSI-2014)*, Kottayam (Kerala).

6. "ADITYA Tokomak high current, long pulse and high temperature current discharges", Harshita Raj et.al at *Plasma Scholars' Colloquium (PSC-2015)* , Jadavpur University, Kolkata

Dedicated to

My Parents Rajesh and Subhadra

ACKNOWLEDGEMENTS

First and foremost, I express my sincere gratitude for my thesis supervisor Dr. Joydeep Ghosh for nurturing and supporting me, pushing me beyond my limits and showing immense faith in me throughout my Ph.D. tenure. I have thoroughly enjoyed our long discussions in the corridors and cafeteria of IPR which ranged beyond the Runaway electron, MHD and Tokamak physics. Our discussions truly enabled me find the joy of doing Physics, and solving problems. I am also thankful to him for motivating me to explore all aspects of Tokamak physics and giving me the liberty to do experiments and operation. I will forever be grateful for his wisdom, guidance, criticism, support, and patience. Dr. Ghosh has shaped me to be the scientist that I am today.

I am immensely grateful to Mr. Rakesh Tanna, for mentoring me, sharing his 20 years' experience of tokamak operation and also for sharing the operation desk with me for the past 5 years. It was his dedication towards the ADITYA operation that motivated me to learn and enjoy the tokamak Operation. His friendly, fun-loving and humorous nature made the control room a space full of life and happiness for me. I must thank him for the constant support as well as criticism throughout my research work which helped me to maintain my focus.

I was lucky to have a great and energetic lot of sincere and hardworking lab mates Tanmay, Sharvil Kaushalendar, Suman, Rohit, Kaushal Bhai and Kumar Bhai. I am thankful to them for their constant support in my research. Due to their company I have thoroughly enjoyed my time in the ADITYA-U which full of discussions, jokes, laughter and celebration. My sincere thanks also goes to the support group Madan ji, Varia ji Sandrakiya ji for always being helpful and sharing their knowledge and experience.

I convey my thanks to Doctoral Committee members Prof.Y.C. Saxena, Prof. P. K. Chattopadhyay, Dr. D. Raju and Dr. R. Srinivasan for their valuable suggestions and guidance throughout my PhD tenure. I am also forever grateful to Prof. A.Sen for being an excellent teacher, strong supporter, and research collaborator. His positivity and strong belief in me helped me immensely in a multifaceted way.

The generous help of Mrs. Ranjana, Mr. Jayesh, Mr. Umesh, Dr. Atrey from diagnostic group, Mr. Bharat and Mrs. Pramila from electronics group was instrumental for carrying out various experiments and studies for my thesis work on ADITYA-and ADITYA-U tokamak. I must thank them for their kind support.

I would like to thank Prof. S. Sengupta, Prof. R. Ganesh, Prof. S. Mukerjee, Dr. M. Kundu, Dr. D. Sharma, Prof. P. K. Chattopadhyay, Dr.Joydeep Ghosh, Dr. Shantanu Karkari, and Dr. A. Chattopadhyay for teaching various important courses which helped me to build a strong foundation of basic plasma physics. I am indebted to all the teachers, who have taught me till post-graduation.

I thank my seniors Manjeet di, Sayaka da, Soumen da, Arghya da, Surabhi, Vidhi di, and my batch mates Sagar, Atul, Meenakshi, Pallavi, Prabhakar, Sandeep, Chetan, Alam, Deepak, and all other seniors and juniors at IPR hostel who made my hostel life a delightful memory. I will always fondly remember our shared laughter, silly fights, *late-night walks, encouragement, coffee, conversations, tea-breaks, and festivals at the IPR hostel. I was also fortunate enough to enjoy joyous playtime with the lovely little kids Myra, Pari, Somu, Sampriya and others at the IPR crèche who filled my days with happiness and positivity with their unconditional love and innocence.*

I genuinely thank Harsh Raj, Ashwin Kumar and Binu Kumari for the numerous adventurous road-trips, great weekends, for taking care of me, and providing me an escape from Tokamak research in Ahmedabad. I also thank my sisters Shrishti, Amrita and brothers Sushant, Utsav and Utkarsh for constantly motivating and supporting in spite of being far away from me.

Lastly, I want to express my deep gratitude for the most important people in my life. I thank my mother Subhadra Kumari, for being my constant source of energy and inspiration to be fearless. I thank my father Kumar Rajesh, the guiding force in my life, the man who always makes me understand my duties and motivates me to achieve my potential. I also am thankful to my late grandfather Shri Sant Prasad for instilling a deep sense of respect for academia in me at a very young age.

CONTENTS

ACKNOWLEDGEMENTS 11

CONTENTS 13

ABSTRACT 25

Chapter 1 Introduction 41

1.1 Need for a better energy source 41

1.2 Nuclear Fusion: The Cosmic Power Source 42

1.3 Fusion on Earth 44

1.4 Runaway Electrons 48

1.4.1 Dreicer Generation 48

1.4.2 Secondary/ Avalanche Generation 51

1.4.3 RE Radiation Losses 52

1.4.3.1 Synchrotron radiation 53

1.4.3.2 Bremsstrahlung 54

1.4.3.3 Cherenkov Radiation 54

1.4.3.4 Collisional damping 55

1.5 RE Loss and Confinement 55

1.5.1 Radial drift of RE orbit 56

1.5.2 RE diffusion due to magnetic fluctuations 57

1.6 RE Mitigation Techniques 60

1.7 Motivation 62

1.8 Outline of the Thesis 63

Chapter 2 The ADITYA and ADITYA-Upgrade Tokamak 65

2.1 Tokamak 65

2.1.1 Lawson / Ignition Criterion 65

2.1.2 Magnetic confinement in Tokamak 66

2.1.3 Tokamak Equilibrium 70

2.1.4 Heating in Tokamak 71

2.1.5 Particle transport in Tokamak 72

2.2 Magnetohydrodynamic Instabilities 73
2.2.1 Ideal MHD Modes 74
2.2.2 Resistive MHD Modes 76
2.2.3 Neutral Dynamics 78
2.2.4 Electrostatic fluctuation 79
2.3 ADITYA tokamak (1989-2015) 80
2.3.1 Vacuum vessel and vacuum system 80
2.3.2 Gas fuelling System 81
2.3.3 Magnetic Coils 81
2.4 ADITYA-Upgrade (2016 – present) 84
2.4.1 New Vacuum Vessel of ADITYA-U 85
2.4.2 Error field measurement experiments in ADITYA-U 88
2.4.3 ADITYA Pulsed Power System (APPS) 89
2.5 Diagnostics 90
2.5.1 Magnetic measurements 90
2.5.2 Microwave Interferometry 91
2.5.3 Soft X-Ray 92
2.5.4 Hard X-ray measurements 93
2.5.5 Spectroscopy 94
2.5.6 Mirnov Coils 95
2.6 Diagnostics in ADITYA-U 96
2.6.1 Mirnov Coils in ADITYA-U 96
2.6.2 Langmuir Probes 97
2.6.2.1 Density measurement: 100
2.6.2.2 Floating Potential measurement: 102
2.6.2.3 Temperature measurement: 102
2.7 Basic Studies in ADITYA and ADITYA-U tokamak 105
2.7.1 Confinement time studies in ADITYA tokamak 105
2.7.2 Operation at Parameter Space of ADITYA 109
2.7.3 Observation of Anomalous Inward Pinch Velocity in ADITYA 110

2.8 ADITYA-U Operation 113
2.8.1 Basic studies in ADITYA-U 113
2.8.2 Phase II Operation of ADITYA-U 115
2.9 Analysis of Mirnov data 116
2.9.1 Mode Rotation frequency 117
2.9.2 Island structure: 119
2.9.3 SVD Technique 121
2.10 Summary 122
Chapter 3 Sawtooth Instability Generated Runaway Electrons and their Transport **123**
3.1 Sawteeth Generated Runaway electrons in ADITYA 124
3.1.1 Sawteeth Instability 124
3.2 Experimental Observations of correlated SXR and HXR bursts in ADITYA/ADITYA-U 127
3.3 Sawtooth generated Runaway electrons in ADITYA/ADITYA-U 132
3.3.1 Sawteeth Induced Electric Field 136
3.3.2 Generation of REs by Sawteeth Induced Electric Field 137
3.4 Radial Transport of Sawteeth generated REs 139
3.4.1 Fast Radial transport of REs 139
3.4.2 Magnetic Island Characterization and Evolution 140
3.5 Conclusion 143
Chapter 4 Drift tearing modes and its interplay with Runaway electrons in ADITYA and ADITYA-U tokamak **147**
4.1 Relation between REs and 2/1 Drift Tearing Modes and its Harmonics in ADITYA and ADITYA-U tokamak 149
4.1.1 Drift Tearing mode and its Harmonics in ADITYA and ADITYA-U tokamak 149
4.1.2 Threshold conditions for the observation of harmonics of 2/1 mode 157
4.1.3 Correlation of Presence and absence of Harmonics of 2/1 mode with Hard X-Ray 160
4.2 Modulation of drift-tearing mode using short periodic gas-puff pulses and their effect on RE dynamics 165

4.2.1 Impact of multiple periodic gas-puffs on MHD modes 170
4.2.2 Influence of MHD modulation using short gas-puff pulses on RE dynamics 181
4.3 Discussion and Conclusion 183
Chapter 5 Influence of Turbulent Fluctuations in Edge Density and Floating Potential on RE loss in ADITYA-U 187
5.1 Introduction 187
5.2 Experimental Observation 188
5.2.1 Variation in HXR emission intensity with short gas-puff pulses 188
5.3 Turbulent Electrostatic Edge Fluctuation 193
5.3.1 Edge Fluctuation in ADITYA-U Tokamak 194
5.3.2 Effect of Turbulent edge fluctuations on REs Loss 198
5.3.3 Effect of edge/SOL turbulence on Sawteeth generated REs 202
5.4 Discussion and conclusion 205
Chapter 6 Summary and Conclusion 209
Future Scope 215
References 217

ABSTRACT

Chapter 1: Introduction

The development of the human race, in its never-ending struggle to improve its standard of living, is invariably bound to a persistently rising energy demand. Nuclear Fusion, two lighter atomic nuclei fusing to form a heavier nucleus, releasing energy, is envisaged to play a significant role in providing a sustainable, secure and safe solution to tackle the global energy demands. After decades of collective international efforts, energy generation through controlled nuclear fusion reactions is on the horizon and the tokamak is the leading candidate for a fusion reactor. The tokamak is a toroidal device in which plasma is confined by magnetic fields and heated to high temperatures in order to fuse the fuel nuclei to obtain fusion energy [1]. The plasma parameters required for net energy gain (efficiency Q > 1) through fusion reactions are quantified by the Lawson criterion [2] , which necessitates the triple product of plasma density (n_e), temperature (T) and confinement time (τ_e), $n_e \, T\tau_e > 3 \times 10^{21} m^{-3} keVs$, for efficient production of fusion energy with Deuterium-Tritium (D-T). A steady progress has been made towards achieving this 'magic' number in tokamaks worldwide and with a commitment to demonstrate steady-state fusion, the largest tokamak International Thermonuclear Experimental Reactor (ITER) is being constructed in France by putting together a unique international collaboration [3]. Although numerous insurmountable challenges have been overcome to demonstrate controlled thermonuclear fusion in tokamak [4,5,6], few challenges are still left to be adequately addressed for realising a commercial fusion reactor. These challenges include avoidance and/or mitigation of runaway electrons (REs) [7], magnetohydrodynamic (MHD) instabilities leading to plasma disruptions [8], edge localized modes (ELMs) [9] etc., which are, catastrophic for the safety and integrity of a tokamak. In this thesis, a detailed experimental study of REs has been carried out to understand the physics mechanisms of their generation as well as their losses from the plasma along with basic studies of Magnetohydrodynamic (MHD) instabilities, electrostatic instabilities, plasma confinement etc. in ADITYA/ADITYA-U tokamak.

Runaway electrons are the electrons that are collisionally decoupled from the bulk plasma and accelerate freely to very high energies (~ several tens of MeVs). They pose a severe threat to the peripheral plasma facing components as well as to the vacuum vessel of a tokamak machine. Scaling of the energy of the RE beam produced during plasma disruption in tokamaks like Tore-Supra, JET [10,11], etc portrays a very alarming projection for ITER [8]. It is predicted that in ITER disruptions, a large amount of highly energetic REs (>100 MJ) is likely to be produced through the hot-tail generation and avalanche mechanism [12]. If not mitigated at an early stage, kinetic energy carried by the high energy RE beam can severely damage plasma facing components as a result of a highly localised RE deposition [8]. Therefore, a comprehensive understanding of REs generation and its loss is of utmost priority in order to develop reliable REs mitigation and control methods to ensure the success of ITER.

The RE generation mechanisms have been extensively studied both theoretically and experimentally and understood up to a fair extent. However, the loss or mitigation mechanisms of the REs are rather ambiguous till date and demand much more experimental as well as theoretical investigation. There are several known mechanisms for the generation as well as the loss of REs from the plasma and the RE content in a tokamak is determined by the combined effect of both processes. Drecier's (primary) generation mechanism [13,14] and avalanche (secondary) [15] are the two established REs generation mechanism. In a Maxwellian distribution every electron experiences a friction force, due to its collision with other electrons, this friction force is also called collisional drag force. Dreicer theory explains that in presence of a strong parallel electric field, energetic electrons in a Maxwellian distribution can overcome the collisional drag force, acting on them and start accelerating, ultimately they ‘runaway' from the Maxwellian distribution [13,14] and become so-called Runaway electrons. Several sources of the parallel electric field exist in conventional/superconducting tokamaks, such as the applied ohmic electric field, electric field generated during plasma disruption [12], electric field generated by MHD instabilities [] (e.g.: Sawteeth instability), etc. In secondary/avalanche generation, the existing REs with sufficiently high energy ‘knock-out’ the thermal electrons to runaway regime through large angle electron-electron scattering, while itself remaining in runaway regime, leading to an avalanche effect in the REs population growth [15]. These RE generation theories provide a basic understanding of REs in tokamak but do not explain the experimental observations completely. Most of the present-day tokamaks exhibit the presence of critical field required for RE generation which exceeds the theoretically predicted critical electric field (Connor- Hastie) by a factor of 2-10 [14]. The discrepancy has been often attributed to the presence of several RE loss processes in tokamak and limitations of available RE diagnostics [15,16]. The RE loss processes like collisional loss and drift orbit loss along with RE energy loss due to synchrotron radiations are taken into consideration while modeling the total RE population [17]. Apart from these loss processes, magnetic and electrostatic fluctuations, present in the tokamak plasmas, are also known to facilitate the RE loss at a rate faster than the above-mentioned processes [18]. Enhanced RE loss due to stochastic magnetic fluctuation inherent to plasma or due to externally applied Resonant Magnetic Perturbations (RMP) which causes the ergodization of the magnetic surface at the edge has been investigated both theoretically [19,20] and in experiments [20, 21,22]. Contrary to this, in several tokamaks like COMPASS [23] and TEXTOR [24], the presence of magnetic islands has caused suppression of REs loss during the current flat-top. RE transport across the magnetic field and eventual loss to the limiter/diverter and plasma peripheral material surfaces, play a major role in determining overall dynamics of REs in a tokamak and also holds the key to the development of a reliable RE mitigation system for ITER. A comprehensive understanding of REs cross-field transport in the dynamic magnetic topology of a tokamak remains a challenge and indispensable to develop a reliable RE mitigation technique for ITER.

This thesis is focused on REs generation and transport due to the intrinsic and externally controlled magnetic and edge instabilities in ADITYA and ADITYA-U tokamak. Being medium-size tokamak with moderate plasma currents $(80 - 150\ kA)$ and plasma duration $(100 - 300\ ms)$, REs do not attain catastrophic energy levels and hence they can be studied in a controlled manner in ADITYA/ADITYA-U tokamak. The studies presented in this thesis aim to provide a wider and more inclusive perspective on the complex inter-dynamics of REs, Magnetohydrodynamic (MHD) instabilities/modes and the edge fluctuations. RE generation and loss mechanisms influenced by intrinsic MHD fluctuations, such as the Sawteeth and tearing instabilities, are studied by analyzing a large number of discharges over a wide range of macroscopic operation and plasma parameters. To obtain more insight into the interaction of MHD with the REs, the amplitude and rotation frequency of the low-m MHD modes have been altered during a course of a single discharge by injection of periodic gas puffs. These periodic gas puffs also lead to the modification of edge fluctuations. These alterations in amplitude and rotation frequency of MHD modes as well as in amplitude of edge turbulent fluctuations have been observed to influence significantly the RE dynamics in ADITYA/ADITYA-U. The results have been consolidated to provide a broader perspective of RE generation and loss in various dynamic tokamak plasma scenario during the current flat-top. The thesis is arranged as follows: The experimental set-up, diagnostics, and discharge characterisation in terms of confinement times along with the experimental results of inward transport of fuel gas during gas puffs in ADITYA/ADITYA-U tokamak are described in Chapter 2. Chapter 3 presents the sawtooth instability (m/n=1/1) generated RE and their transport in ADITYA/ADITYA-U. Experimental results of the effect of MHD instabilities and their variations with periodic gas-puffs on RE loss in ADITYA/ADITYA-U tokamak are presented in Chapter 4. The experimental observations of RE loss due to edge fluctuations are described in Chapter 5. The results are discussed and summarized in Chapter 6 along with the future scope.

Chapter 2: Experimental set-up, Diagnostics, and Discharge characteristics

ADITYA tokamak [22, 23] was a medium-sized ohmically heated tokamak with a circular poloidal limiter having a major radius of $R = 75\ cm$ and a minor (plasma) radius $a = 25\ cm$ with 20 toroidal magnetic field coils. The plasma boundary in ADITYA was defined by a poloidal ring limiter with graphite tiles located at one toroidal location inside the vacuum vessel having a rectangular cross-section. Base pressure of $\sim 5 \times 10^{-8}$ Torr was maintained inside the vessel and the hydrogen gas was injected inside the vessel at filling pressure of $\sim 8 - 10 \times 10^{-5}$Torr for plasma discharges. The results presented in this thesis are from plasma discharges with axisymmetric toroidal magnetic field, $B_{\phi} \sim 0.75 - 1.25\ T$; peak loop voltage, $V_L \sim 18 - 20\ V$ ($E \sim 4 - 5\ V/m$); plasma current, $I_p \sim 80 - 160\ kA$ and plasma duration of $\sim 80 - 250\, ms$. The central chord-average density, $n_e \sim 1 - 5 \times 10^{19} m^{-3}$ and central chord-average electron temperature, $T_e \sim 300 - 700\, eV$.

During the course of this thesis, the ADITYA tokamak [24] has been upgraded to ADITYA-U [26] tokamak with the aim of conducting experiments in shaped plasma configurations. All the major magnetic coils, such as the ohmic transformer coils, toroidal magnetic field coils and vertical magnetic field coils of ADITYA have been reused in ADITYA-U. The major radius ($R = 75\, cm$) and minor radius of circular cross-section plasma ($a = 25\, cm$) are also kept the same in ADITYA-U. The new inclusions in ADITYA-U are: a new vacuum vessel of circular cross-section, two new sets of diverter (shaping) coils, a continuous toroidal graphite belt limiter on high magnetic field (inboard) side, as well as two poloidal limiters located on low magnetic field (outboard) side at two toroidal locations 180^0 apart ($\varphi = 90° \, and \, 270°$). ADITYA-U has been operated in limiter (toroidal belt limiter) configuration, with operation parameters similar to ADITYA and discharges with circular cross-section have been obtained, so far. The plasma parameters of ADITYA-U discharges are: plasma current $I_p \sim 80 - 170\, kA$, plasma duration (t) ~ $80 - 330\, ms$, the chord-averaged central electron density $n_e \sim 1 - 6 \times 10^{19} m^{-3}$, chord averaged central electron temperature $(T_e) \sim 300 - 500\, eV$, and toroidal magnetic field $(B_\phi) \sim 0.8 - 1.3\, T$. The RE experiments carried out in ADITYA have been repeated in ADITYA-U. Results from both the machines with discharges having similar plasma parameters but different limiter configurations have been analysed and presented in this thesis.

The standard tokamak diagnostics have been used for the present study which includes: external magnetic sensors for measurements of plasma current (I_p), loop voltage (V_L), plasma column position, etc. Seven-channel microwave interferometer is used for line averaged electron density measurements. The electron temperature has been measured using a two-filter soft X-ray spectrometer. Standard spectroscopic diagnostics for the temporal evolution of hydrogen neutral (H_α) and impurity (oxygen and carbon) spectral emissions and bolometers for the total radiation power (P_{RAD}) have been used. In ADITYA-U (ADITYA), the poloidal magnetic fluctuations ($\widetilde{\dot{B_\theta}}$) have been detected by two sets (one set) of 16 Mirnov coils distributed at equal angle separation in the poloidal periphery, inside the vessel at two diametrically opposite toroidal locations. The Hard X-rays (HXR) induced due to RE's interaction with limiter are detected by a 3-inch diameter NaI (Tl) scintillator detector. This lead-shielded detector is collimated to view the limiter and located at the equatorial plane of the machine. As a part of developmental work of this thesis, a matrix of 15 Langmuir probes arranged in different radial, poloidal, as well as toroidal locations have been designed, developed and installed to investigate the SOL and edge plasmas of ADITYA-U.

At the end of this chapter, typical discharges from ADITYA [25] and ADITYA-U [26] are presented. In these discharges, the density at the current flat-top has been maintained using periodic gas puffs. The estimation of global energy confinement time (τ_E) for ADITYA discharges and its scaling with density has been carried out and compared with neo-ALCATOR scaling law for [25] ohmically heated plasma discharges. In several discharges with improved ohmic confinement anomalous inward pinch velocities have been observed [25]. The pinch velocities have been estimated by measuring the time delay between the peaks in the temporal evolution of H_α emission and of Soft X-ray (SXR) emission and chord averaged electron density, during a gas puff pulse.

Chapter 3: Sawtooth Instability (m/n=1/1) Generated Runaway Electrons and their Transport in ADITYA

The sawtooth instability is an ideal MHD instability, during which the core temperature and density rise slowly and quickly crash down, periodically. This effect is most evident in line integrated Soft X-Ray (SXR) measurements of the plasma core, since SXR intensity, is strongly dependent on plasma density and temperature, hence used as a preferred tool to investigate the sawtooth instability [27,28]. The sawtooth instability is believed to be a manifestation of m/n= 1/1 internal kink mode (where m is poloidal mode number and n is toroidal mode number) during which plasma core is radially displaced, leading to reconnection at the q=1 flux surface, followed by its return to the center. It is commonly observed in most tokamaks when $q\ (0)\ < 1$, including ADITYA and ADITYA-U. In typical discharges of ADITYA, bursts of hard X-ray (HXR) due to the interaction of runaway electrons (RE) with limiter, during sawteeth activity were regularly observed. These HXR bursts were highly correlated in time with each sawtooth-crash, which suggested that each sawtooth-crash event generated/accelerated these runaway electrons, which then yielded the HXR bursts after their interaction with the limiter. Detailed investigations revealed that the electric field induced in the toroidal direction due to change in poloidal magnetic field during the sawtooth crash [28] is several times higher than the critical electric field required for runaway generation. The induced toroidal electric field during each sawtooth crash generates the REs, which then travel to the limiter to give a HXR burst. Furthermore, it was observed that in the later period of the plasma current flat-top of the discharge, no HXR bursts were accompanied by the sawtooth crash, although the sawteeth activity prevailed. This observation indicated a difference in radial transport of runaway electrons in the initial and later parts of plasma current flat-top in same discharge. During the initial phase of plasma current flat-top, the appearance of the HXR bursts were found to be due to enhanced loss of sawtooth-crash generated REs, facilitated by the overlapping of inflated magnetic islands (m/n = 2/1 and 3/1) present in the intermediate plasma region between core and the limiter. In the later phase, where magnetic islands did not overlap and good magnetic surfaces prevailed between the islands, the radial transport of REs was constrained, leading to the absence of correlated HXR bursts with the sawtooth crash. From the observations and analysis, it has been concluded that ergodization due to island overlapping in intermediate region facilitates the rapid loss of REs generated due to sawtooth crash, leading to HXR bursts. And well-formed islands separated by good magnetic surfaces between them substantially reduce the transport of the REs [29].

Chapter 4: Effect of Resistive Magnetohydrodynamic (MHD) Instabilities on Runaway Electrons in ADITYA and ADITYA-U tokamak

In this chapter, the effect of resistive MHD instabilities on runaway electron dynamics in ADITYA and ADITYA-U tokamak is presented. At the outset, a large number of discharges (>3000) with different resistive MHD (low m, n) modes with different amplitudes and frequencies have been analysed and studied in correlation with the HXR data to obtain a heuristic picture of the dependence of RE dynamics on MHD mode amplitudes and frequencies. Later in the chapter, the effect of varying the amplitude and frequencies of MHD modes in a controlled manner using periodic gas puffs on RE dynamics during a course of a single discharge is presented.

i) Resistive tearing modes & their influence on Runaway Electrons in ADITYA and ADITYA-U

A class of instabilities that is able to change the topology of the equilibrium magnetic field via the process of magnetic reconnection is known to be driven by the free energy associated with the nature of the current density profile sustaining the equilibrium field. Resistive tearing instabilities belong to this class of instability [30]. In a magnetically confined tokamak plasma, these instabilities lead to the formation of magnetic islands which can cause significant degradation of plasma confinement [8]. In high-frequency regimes, these modes often get coupled with drift wave, hence called drift tearing (DT) modes, and the magnetic islands associated with these DT modes rotate poloidally in electron diamagnetic drift direction with frequencies close to diamagnetic drift frequencies i.e $\omega^* = \frac{k_y\, T_e}{eB\, L_n}$, where k_y = wavenumber and L_n = density scale length [30]. As commonly measured in other tokamak, these rotating islands are observed as perturbed poloidal magnetic fluctuations, acquired by Mirnov coils (magnetic pick-up loops) placed around the poloidal periphery of the plasma [313].The frequency spectra of the poloidal magnetic field fluctuation exhibit coherent peaks corresponding to different modes present in the plasma. In the purely ohmic discharges of ADITYA as well as of ADITYA Upgrade MHD modes rotating with a frequency close to the electron diamagnetic frequency have been observed and identified as DT modes. Large number of discharges (>5000 discharges) have been studied using various numerical routines like Fast Fourier Transform (FFT), Singular value decomposition (SVD) technique and contour plots to obtain the DT mode rotation frequencies and island structures. It has been found that m/n = 2/1 mode and its harmonics are predominantly present in the majority of discharges with varying amplitudes and mode rotation frequencies. In ADITYA-U, the emergence of harmonics of m/n = 2/1 mode strongly depends on the amplitude and rotation frequency of m/n = 2/1 DT mode and it is found that the harmonics cease to exist when m/n = 2/1 rotation frequency exceeds 14 kHz. Furthermore, the dynamics of REs is found to be strongly correlated with the presence and absence of these harmonics in both ADITYA and ADITYA-U. Significantly higher HXR emission has been observed in discharges with a single small m/n = 2/1 DT mode exists with no harmonics, whereas reduced HXR emissions are observed in discharges having m/n = 2/1 DT mode with large amplitude ($\widetilde{B_\theta} > 50\ Gauss$) predominates along with its harmonics (up to 7). The appearance and disappearance of harmonics are also correlated with lower and higher intensities of HXR emission respectively have also been observed during the course of discharge in several discharges. These observations indicate reduced RE loss in presence of large well-formed (m/n = 2/1) islands compared to that in discharges with small or no islands. These results are in line with the theory predicting trapping of REs in MHD islands having width larger than a threshold width [19]. A sudden increase in the island widths and appearance of harmonics of m/n = 2/1 mode coinciding with strong reduction in HXR emission during the course of a single discharge also suggest that the trapping of REs in the island may be increasing the saturated island width as predicted theoretically, leading to higher amplitudes of these DT modes and subsequent harmonics generation.

ii) Modulation of amplitude and rotation frequency of MHD by periodic gas puffs and their influence on RE dynamics in ADITYA and ADITYA-U

In order to substantiate the results described in the previous section, the mode rotation frequency and amplitude of the m/n= 2/1 mode were modulated by periodic gas puff pulses in ADITYA and ADITYA-U. Periodic gas-puffing has been extensively used in most discharges of ADITYA and ADITYA-U, primarily to maintain the plasma density. The gas puff pulse width has been varied from ~1 – 5 ms, and the time gap between two pulses has been varied from ~ 4 – 8 ms. Each of these gas puff injects $\sim 10^{16} - 10^{18}$ hydrogen neutrals in the vessel depending upon the gas-puff pulse width. In presence of periodic gas puffs at the plasma current flat-top, the mode rotation frequency and the amplitude of m/n = 2/1 mode have been observed to vary in tandem with the gas puffs. This has been observed in more than 7000 discharges from ADITYA and ADITYA-U. The existing mode rotation frequency decreases by $\sim 20 - 50$ % within 1-2 ms after the injection of a gas puff. The DT mode regains its original frequency within 2 - 4 ms and the cycle is repeated after each gas-puff pulse. The observed decrease in mode rotation frequency of m/n = 2/1 mode is found to be proportional to the amount of gas puffed. The decrease in temperature and increase in the density scale length at the edge due to injected gas leads most possibly lead to a reduction in drift frequency (ω^*), which ultimately leads to a decrease in DT island rotation frequency. Further, it has been observed that the amplitude of the mode is also reduced immediately after each gas-puff. However, in subsequent 1 – 3 ms, the amplitude grows again to its value, which it had prior to the gas puff until the next gas-puff again reduces it. Similar signatures of significant decrease and increase have been observed in HXR emission intensity with the application of each gas-puff. This periodic amplitude modulation of HXR emission intensity with gas-puff shows a weak time-correlation with MHD modulation, indicative of a relation between of MHD modes and RE loss. However, detailed investigation of events during a single gas puff revealed that the onset time of MHD mode suppression lags or leads the HXR emission reduction. Often, the HXR emission intensity remains suppressed even well after the MHD amplitudes retain their original (high) values after going through suppression due to gas puff and the overall duration of suppression of MHD mode amplitude also does not match with that of the HXR emission. Further, the fall-time of HXR emission after each gas-puff always remains much faster than the time required for the REs to reach to the limiter from the m=2 surface even with Rochester-Rosenbluth diffusivities calculated from the observed amplitudes of MHD mode [18]. Furthermore, in a large number of discharges with very low MHD amplitudes and no detectable islands, the MHD amplitude remains indifferent to the periodic gas-puffs, i.e., devoid of any periodic activity. Interestingly, the periodic variations in HXR emissions are still observed in such discharges. These observations strongly indicate the presence of another factor controlling the RE dynamics in ADITYA/ADITYA-U, which is strongly affected by the gas-puffs as well. Extensive investigations reveal that another factor influencing the RE dynamics is the edge turbulent fluctuations in density and floating potential, which is described in the next chapter.

Chapter 5: Influence of Turbulent Fluctuations in Edge Density and Floating Potential on RE loss in ADITYA-U

In this chapter, experimental evidence substantiating the role of turbulent fluctuations in density and floating potential at the plasma edge and SOL regions of ADITYA/ADITYA-U in RE loss is presented and discussed. Turbulent fluctuations in density and temperature of the edge region are commonly observed in almost all tokamaks and their basic characteristics are fairly universal. Edge turbulence dominantly consists of broadband plasma density and potential fluctuations. It has been recognized for many years that the cross-field plasma transport through the edge is dominated by these turbulent fluctuations leading to loss of thermal particles from the plasma. By carrying out controlled experiments in which the edge turbulence is periodically suppressed using periodic gas puffs, it has been shown that the turbulent fluctuations present in the edge region of ADITYA/ADITYA-U not only facilitate the loss of thermal particles but also strongly influence the RE loss rate. As mentioned in the preceding chapter, when multiple gas-puff pulses are applied during the plasma current flat-top, the temporal evolution of HXR intensity also modulates in amplitude exhibiting prominent peaks with a full width at half maxima (FWHM) ~ 2 ms, following each gas puff in ADITYA and ADITYA-U. These variations in HXR amplitude remain absent in discharges without the gas puffs. Previous experiments in ADITYA have demonstrated that injection of short pulses of gas leads to a concomitant suppression of edge fluctuations. Detailed analysis of edge density and potential fluctuations and their suppression in presence of gas puffs, studied using a set of Langmuir probes in the edge and SOL region, revealed that that periodic suppression of turbulent density and potential fluctuations coincide with the reduction in the HXR intensity. It has been observed that the HXR amplitude is reduced by $\sim 60 - 80$ % of its value prior to the suppression when the edge/SOL turbulence is suppressed by gas puffs during a discharge. The frequency spectra of time series of HXR intensity show similar characteristics as that of the frequency spectra of density and potential indicating that the REs present in the edge region are significantly influenced by the prevailing turbulent fluctuations in density and potential. A heuristic model of RE loss in the presence of MHD oscillations associated with m/n=2/1 DT modes and edge turbulent fluctuations in density and potential based on several discharges has been developed and presented. These observations provide a basis to explore the possibility of a new RE mitigation scheme based on enhancing seed RE loss with the assistance of external turbulent perturbations of density and potential in the edge/SOL region of a tokamak.

Chapter 6: Discussion, Summary and Future Scope

This chapter presents a discussion and summary of the results presented in this thesis along with future works. The dedicated experiments on REs dynamics in ADITYA and ADITYA-U have demonstrated significant dependence of RE dynamics on MHD instabilities and edge turbulent fluctuations. These instabilities substantially enhance the loss of REs and hence should be duly included in estimations of RE growth rates in a tokamak. It has been shown that the Sawteeth instability (m/n=1/1) crash generate

REEs and presence of stochastic magnetic fields due to the overlapping of m/n=2/1 and m/n=3/1 islands enhance the radial transport of these REs. Analysing a large number of discharges, it has been established that there exists a strong correlation between the RE population in a discharge and the MHD amplitude and frequency. MHD (m/n=2/1) modes with high amplitude ($\frac{\widetilde{B_\theta}}{B_\theta} > 5 \times 10^{-4}$) and low rotation frequency ($\omega^* < 14\,kHz$) exhibit harmonics and such discharges are charachterised by low HXR emission. Whereas, discharges with lower amplitude ($\frac{\widetilde{B_\theta}}{B_\theta} < 5 \times 10^{-4}$) m/n = 2/1 mode and higher rotation frequency ($\omega^* > 14\,kHz$) mostly lead to the observation of high HXR emission in ADITYA and ADITYA-U tokamak. These results indicate a reduction in RE loss in presence of large well-formed islands most possibly due to trapping of REs in the islands. Multiple periodic gas puffs have been injected to modulate the MHD mode characteristics and edge turbulent fluctuations during the current flat-top of discharges, in a controlled manner, to study their impact on the RE dynamics. These periodic gas puffs lead to a periodic modulation of the rotation frequency, as well as of the amplitude of m/n=2/1 mode. The neutrals injected by gas puff decrease the edge temperature and increase the density scale length, thereby decreasing the diamagnetic drift frequency which leads to the decrease in rotation frequency of the observed drift tearing modes. Although, gas-puff induced frequency and amplitude modulation of MHD modes does seem to have some influence on the RE loss, the fast variations in HXR emission amplitude during and after each gas puff can not be explained by the RE diffusion estimates using the Rochester and Rosenbluth model. It has also been shown that in the discharges where the MHD amplitude remains very low, the gas puffs lead to negligible variation in MHD amplitude and frequency. However, even in absence of periodic MHD modulation, strong periodic modulations in HXR intensities still prevail in such discharges. Further investigations revealed that in these discharges suppression of RE loss coincides perfectly in time with the edge density and potential fluctuation suppression after each gas puff and RE loss increases simultaneously with the edge fluctuation. The edge fluctuations suppression by the gas injection has been quite well established in ADITYA. Obseravtion of reduction in HXR emission at the same time instant indicate suppression of RE loss during that time. Periodic HXR peaks (due to periodic RE loss) are also found to coincide with distinct peaks in time profile of H_α line emission intensity, indicative of the increase in neutrals after REs loss to the limiters. These observations provide evidence of neutral recycling by REs in ADITYA/ADITYA-U tokamak. These results provide a significant insight of a RE loss mechanism through edge/SOL turbulent fluctuations in density and potential and may bridge the gap between the experimental observations and theoretical estimations of critical electric field requirements for RE generation in tokamaks. Furthermore, based on these observations, a mitigation technique for REs using broadband electrostatic fluctuations will also be thought through. In addition to the RE studies, the effect of periodic gas puffs on plasma confinement has also been studied and results on observations of anomalous inward pinch during the gas puffs are also reported in this thesis. Enhancing RE loss by externally inducing broadband electrostatic fluctuations through some means, such as biasing an electrode with time-varying (fluctuating) voltages placed inside the plasma remains one of the important future work of this thesis. Further, studies of controlling the MHD island rotations with DC biased electrode induced $E \times B$ plasma rotations and their effect in RE dynamics will also be carried out in future.

Chapter 6
Summary and Conclusion

In this chapter, the thesis is concluded and the results obtained are summarized. Along with the conclusion and summary, the future scope of this thesis work is also presented. This thesis is mainly focused on REs generation and transport due to the intrinsic and externally controlled magnetic and electrostatic edge/SOL turbulence in ADITYA and ADITYA-U tokamaks. Being medium-size tokamak with moderate plasma currents ($80 - 150\ kA$) and plasma duration ($100 - 300\ ms$), REs do not attain catastrophic energy levels and hence they can be studied in a controlled manner in ADITYA/ADITYA-U tokamak. The studies presented in this thesis aim to provide a wider and more inclusive perspective on the complex inter-dynamics of REs, Magnetohydrodynamic (MHD) instabilities/modes and the edge fluctuations in relation with each other.

One of the important results presented in this thesis is the direct experimental evidence of RE dynamics being influenced by the edge/SOL electrostatic turbulence. It has been observed that the electrostatic fluctuations present in edge/SOL region of ADITYA/ADITYA-U tokamak facilitate the RE diffusion with a diffusion coefficient $\sim 1.2\ m^2/sec$, which is comparable to that being obtained in presence of magnetic fluctuations in several tokamaks. Several thoughtful experiments are conceived and carried out in ADITYA/ADITYA-U tokamak in order to understand the RE generation and loss mechanisms influenced by intrinsic MHD fluctuations, such as the Sawteeth and tearing instabilities, by analyzing a large number of discharges over a wide range of macroscopic operation and plasma parameters. It has also been observed that the sawtooth crash induced toroidal electric field is capable of generating/accelerating REs. Overlapping of MHD islands creating a schotastic layer increases the RE loss from the bulk plasma, whereas a single large well-formed island seems to confine the REs. To obtain more insight into the interaction of MHD with the REs, the amplitude and rotation frequency of the low-m MHD modes have been altered during a course of a single discharge by injection of periodic gas puffs. These periodic gas puffs also lead to the modification of edge electrostatic turbulence. These alterations in the amplitude of edge/SOL electrostatic turbulence fluctuations have been observed to influence significantly the RE dynamics in ADITYA/ADITYA-U. The results have been consolidated to provide a broader perspective of RE generation and loss in various dynamic tokamak plasma scenario during the current flat-top.

In typical discharges of ADITYA as well as in ADITYA-U, bursts of hard Xray (HXR) during sawteeth activity, highly correlated in time with each sawtooth crash were regularly observed. The discharges in ADITYA show that sawtooth-crash event leads to generation/acceleration of runaway electrons, which then yield the HXR bursts after their interaction with the limiter. Detailed investigations revealed that the electric field induced in the toroidal direction due to change in the poloidal magnetic field during the sawtooth crash is several times higher than the critical electric field required for runaway generation. The induced toroidal electric field during each sawtooth crash generates the REs, which then travel to the limiter to give HXR bursts. Furthermore, it has been observed that in the later period of the plasma current flattop of the discharge, no HXR bursts were accompanied by the sawtooth crash, although the sawteeth activity prevailed. This observation indicated a difference in radial transport of runaway electrons in the initial and later parts of plasma current flattop in the same discharge. During the initial phase of plasma current flat-top, the appearance of the HXR bursts were found to be due to enhanced loss of sawtoothcrash generated REs, facilitated by the overlapping of inflated magnetic islands (m/n = 2/1 and 3/1) present in the intermediate plasma region between the core and the limiter. In the later phase, where magnetic islands did not overlap and good magnetic surfaces prevailed between the islands, the radial transport of REs was constrained, leading to the absence of correlated HXR bursts with the sawtooth crash. From the observations and analysis, it has been concluded that ergodization due to island overlapping in the intermediate region facilitates the rapid loss of REs generated due to sawtooth crash, leading to HXR bursts. And well-formed islands separated by good magnetic surfaces between them substantially reduce the transport of the REs. Similar observations of sawtooth-crash induced HXR bursts are observed in ADITYA-U discharges where the magnetic fluctuations are inherently low. These HXR bursts are influenced by controlling the edge/SOL electrostatic turbulence using short gas-puff injection.

After demonstrating the deterministic effect of the topology of two magnetic islands on RE loss in ADITYA tokamak, the effect of the single island on RE dynamics has been investigated in ADITYA/ADITYA-U tokamak. A large number of discharges (>3000) with different resistive MHD (low m, n) modes with different amplitudes and frequencies have been analyzed to segregate discharges with single magnetic island, which is majorly found to be m/n= 2/1 drift tearing modes. the dynamics of REs is found to be strongly correlated with the presence and absence of these harmonics in both ADITYA and ADITYA-U. Significantly higher HXR emission has been observed in discharges with a single small m/n = 2/1 DT mode exists with no harmonics, whereas reduced HXR emissions are observed in discharges having m/n = 2/1 DT mode with large amplitude ($\widetilde{B_\theta} > 50\ Gauss$) predominates along with its harmonics (up to 7). The appearance and disappearance of harmonics are also correlated with lower and higher intensities of HXR emission respectively have also been observed during the course of discharge in several discharges. These observations indicate reduced RE loss in presence of large well-formed (m/n = 2/1) islands compared to that in discharges with small or no islands. These results are in line with the available theories on the subject, predicting trapping of REs in MHD islands having a width larger than a threshold width. A sudden increase in the island widths and appearance of harmonics of m/n = 2/1 mode coinciding with strong reduction in HXR emission during the course of a single discharge also suggest that the trapping of REs in the island may be increasing the saturated island width as predicted theoretically, leading to higher amplitudes of these DT modes and subsequent harmonics generation.

In order to understand the dependence of island width and rotation frequency on RE loss, the mode rotation frequency and amplitude of the m/n= 2/1 mode were modulated by periodic gas puff pulses in ADITYA and ADITYA-U. In presence of periodic gas puffs at the plasma current flat-top, the mode rotation frequency and the amplitude of m/n = 2/1 mode have been observed to vary in tandem with the gas puffs. This has been observed in more than 7000 discharges from ADITYA and ADITYA-U. The existing mode rotation frequency, as well as amplitude, decreases by $\sim 20 - 50\ \%$ within $1 -$

$2\ ms$ after the injection of a gas puff. The observed decrease in mode rotation frequency of m/n = 2/1 mode is found to be proportional to the amount of gas puffed. The decrease in temperature and increase in the density scale length at the edge due to injected gas leads most possibly lead to a reduction in drift frequency (ω^*), which ultimately leads to a decrease in DT island rotation frequency. A strong signature of this modulation has been observed in the RE dynamics in the form of periodic peaks in HXR signal intensity following each gas puff. This periodic amplitude modulation of HXR emission intensity exhibited very strong correlation with the gas-puff , but a weak time-correlation with MHD modulation. Detailed investigation of events during a single gas puff revealed that the onset time of MHD mode suppression lags or leads the HXR emission reduction. Furthermore, in a large number of discharges with very low MHD amplitudes and no detectable islands, the MHD amplitude remains indifferent to the periodic gas-puffs, i.e., devoid of any periodic activity. Interestingly, the periodic variations in HXR emissions are still observed in such discharges. These observations strongly indicate the presence of another factor controlling the RE dynamics in ADITYA/ADITYA-U, which is strongly affected by the gas-puffs as well. Extensive investigations of a large number of discharge parameters reveals that the factor influencing the RE dynamics is the edge turbulent fluctuations in density and floating potential.

To establish the role of turbulent fluctuations in density and floating potential, at the plasma edge and SOL regions of ADITYA-U, in RE loss has been persued. By carrying out controlled experiments in which the edge turbulence is periodically suppressed using periodic gas puffs, it has been shown that the turbulent fluctuations present in the edge region of ADITYA/ADITYA-U not only facilitate the loss of thermal particles but also strongly influence the RE loss rate. As mentioned in the preceding chapter, when multiple gas-puff pulses are applied during the plasma current flat-top, the temporal evolution of HXR intensity also modulates in amplitude exhibiting prominent peaks with a full width at half maxima (FWHM) ~ 2 ms, following each gas puff in ADITYA and ADITYA-U. These variations in HXR amplitude remain absent in discharges without the gas puffs. Detailed analysis of edge density and potential fluctuations and their suppression in presence of gas puffs, studied using a set of Langmuir probes in the edge and SOL region, revealed a strong correlation between the periodic suppression of edge/SOL electrostatic turbulence and the periodic reduction in the HXR intensity. It has been observed that the HXR amplitude is reduced by $\sim 60 - 80\ \%$ of its value prior to the suppression when the edge/SOL turbulence is suppressed by gas puffs during a discharge. The frequency spectra of time series of HXR intensity show similar characteristics as that of the frequency spectra of density and potential indicating that the REs present in the edge region are significantly influenced by the prevailing turbulent fluctuations in density and potential. These observations provide a basis to explore the possibility of a new RE mitigation scheme based on enhancing seed RE loss with the assistance of external turbulent perturbations of density and potential in the edge/SOL region of a tokamak.

Based on the above experimental observations, an interpretation is presented that is consistent with the statement that the RE dynamics in ADITYA and AIDTYA-U tokamak is generally influenced by a combination of magnetic and electrostatic (edge/SOL) turbulence. There are discharges in which one weigh more than the other. In the following a heuristic model of RE loss in the presence of magnetic fluctuations and electrostatic turbulence based in several discharges has been proposed:

The REs are believed to be dominantly generated around plasma core by the primary mechanism in presence of the toroidal electric field, these REs gain energy and their orbits shift as their energy increases with time, ultimately they are lost to the limiter emitting HXR emission. Other RE loss mechanisms like synchrotron loss and collisional loss also contribute to the RE loss but due to short discharge time duration, smaller limiter radius and relatively lower RE energy ($\sim 1 - 3\ MeV$), they do not significantly control RE loss or overall RE dynamics in ADITYA or ADITYA-U. In addition to the drift-orbit loss having relatively slower time-scales, the RE diffusion in ADITYA and ADITYA-U are found to be mainly dependent on the amplitude of magnetic fluctuations associated with different MHD modes and that of electrostatic turbulence in edge/SOL. A RE generated in the center of the plasma needs to travel radially outward through the entire plasma region, whose characteristics continuously varies throughout its radial extent, in order to get lost to the limiter. While approaching the limiter through the plasma region, if a RE encounters a magnetic fluctuation due to the presence of a large saturated magnetic island it may get confined in the island if the island size is larger than the critical island width for runaway trapping. Whereas if it finds a stochastic magnetic fluctuation region due to island overlapping of any other reason, it rapidly crosses this region with Rechester–Rosenbluth diffusion coefficient. Here it has been assumed that the MHD island is not so big that it touches the limiter, because in that case, the RE can directly be thrown to the limiter with trespassing the significant plasma region. After crossing the stochastic region, it continues to move radially outward due to orbit drift. Finally, once the RE reaches the edge region of the plasma, where the electrostatic turbulence prevails, it diffuses quickly towards the limiter under the influence of the turbulence. Hence, contributions of electrostatic turbulence need to be included in the estimations of the overall RE diffusion coefficient. The signature of the above-mentioned proposition of RE transport is observed in several ADITYA-ADITYA-U discharges. A time-slice from the plasma current flat-top in a representative discharge showing the MHD mode amplitude and HXR emission intensity in the presence of gas-puff pulse injections (vertical arrows) is shown in figure 6.1. It can be clearly seen from the figure that as soon as the MHD mode amplitude increases sharply at $\sim 62\ ms$, the HXR intensity also increases significantly, however after that when a gas –puff pulse is applied at $\sim 66\ ms$, the HXR intensity decreases, where the edge turbulence decreases, although the MHD mode amplitude remain almost constant. The mean of the HXR intensity has been observed to be decreasing even though the MHD mode amplitude remains constant in the period $\sim 63\ to\ 75\ ms$. Trapping of REs in the island may be a possibility during this time. This trend in HXR intensity is repeated in the period $\sim 115\ to\ 130\ ms$.

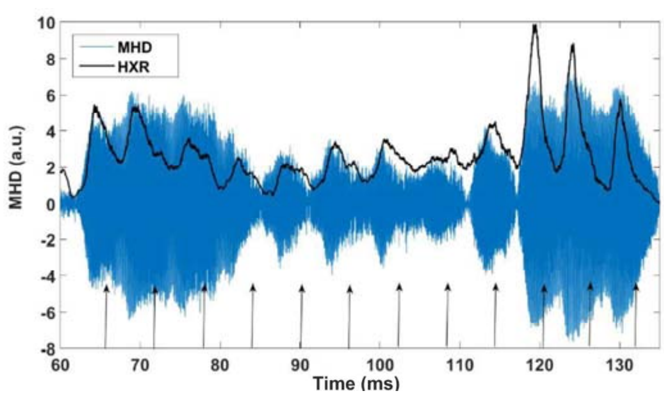

Figure 6.1: Plot showing the time evolution of MHD activity, HXR intensity and gas puff from shot #31375

Apart from the above, several basic experiments and analysis have been carried out in this thesis work to understand the basic operation of ADITYA tokamak, such as confinement time analysis and comparison with the scaling laws, fueling of the tokamak plasma, etc. A set of Langmuir probes have been developed from scratch and installed in ADITYA-U tokamak along with the operation of several existing diagnostic has been accomplished in this thesis. Furthermore, during this thesis period, the ADITYA tokamak has been upgraded to ADITYA-U tokamak, which has provided a unique opportunity to observe and contribute to the process of building a complex machine like tokamak.

Future Scope

The results obtained during the course of this thesis provide significant insight into RE loss mechanism in different discharge scenarios. The experimental results on statistically significant number discharge with various MHD activity and island configurations may be utilised to model the MHD induced RE loss and compare with simulations. The RE dynamics with the inclusion of the effect of edge/SOL turbulent fluctuations may be explored through proper modelling and simulations. Modelling of RE dynamics including the loss induced by edge fluctuations may be a step ahead in bridging the gap between the experimental observations and theoretical estimations of critical electric field requirements for RE generation in tokamaks. Furthermore, based on these observations, a mitigation technique for REs using broadband electrostatic fluctuations also is thought through. Enhancing RE loss by externally inducing broadband electrostatic fluctuations through some means, such as biasing an electrode with time-varying (fluctuating) voltages placed inside the plasma remains one of the important future work of this thesis. In addition to the RE studies, the effect of periodic gas puffs on plasma confinement has also been studied and results on observations of anomalous inward pinch due to the pulsed periodic gas puffs opens a possibility to explore better fuelling schemes. Further, studies of controlling the MHD island rotations with DC biased electrode induced $E \times B$ plasma rotations and their effect in RE dynamics will also be carried out in the future. Significant results indicating non-linear coupling of 2/1 mode opens new venue to test and study various non-linear MHD models and their limitation which would contribute significantly to enhance our understanding of 2/1 MHD mode dynamics which is the prime culprit of triggering disruptions. The extensive study and understanding of external gas fueling on MHD mode rotation, can be instrumental in carrying out a wide number of experiments including MHD studies, transport , drift studies etc.

ABSTRACT

Chapter 1: Introduction

The development of the human race, in its never-ending struggle to improve its standard of living, is invariably bound to a persistently rising energy demand. Nuclear Fusion, two lighter atomic nuclei fusing to form a heavier nucleus, releasing energy, is envisaged to play a significant role in providing a sustainable, secure and safe solution to tackle the global energy demands. After decades of collective international efforts, energy generation through controlled nuclear fusion reactions is on the horizon and the tokamak is the leading candidate for a fusion reactor. The tokamak is a toroidal device in which plasma is confined by magnetic fields and heated to high temperatures in order to fuse the fuel nuclei to obtain fusion energy [1]. The plasma parameters required for net energy gain (efficiency Q > 1) through fusion reactions are quantified by the Lawson criterion [2] , which necessitates the triple product of plasma density (n_e), temperature (T) and confinement time (τ_e), $n_e T\tau_e > 3 \times 10^{21} m^{-3} keVs$, for efficient production of fusion energy with Deuterium-Tritium (D-T). A steady progress has been made towards achieving this 'magic' number in tokamaks worldwide and with a commitment to demonstrate steady-state fusion, the largest tokamak International Thermonuclear Experimental Reactor (ITER) is being constructed in France by putting together a unique international collaboration [3]. Although numerous insurmountable challenges have been overcome to demonstrate controlled thermonuclear fusion in tokamak [4,5,6], few challenges are still left to be adequately addressed for realising a commercial fusion reactor. These challenges include avoidance and/or mitigation of runaway electrons (REs) [7], magnetohydrodynamic (MHD) instabilities leading to plasma disruptions [8], edge localized modes (ELMs) [9] etc., which are, catastrophic for the safety and integrity of a tokamak. In this thesis, a detailed experimental study of REs has been carried out to understand the physics mechanisms of their generation as well as their losses from the plasma along with basic studies of Magnetohydrodynamic (MHD) instabilities, electrostatic instabilities, plasma confinement etc. in ADITYA/ADITYA-U tokamak.

Runaway electrons are the electrons that are collisionally decoupled from the bulk plasma and accelerate freely to very high energies (~ several tens of MeVs). They pose a severe threat to the peripheral plasma facing components as well as to the vacuum vessel of a tokamak machine. Scaling of the energy of the RE beam produced during plasma disruption in tokamaks like Tore-Supra, JET [10,11], etc portrays a very alarming projection for ITER [8]. It is predicted that in ITER disruptions, a large amount of highly energetic REs (>100 MJ) is likely to be produced through the hot-tail generation and avalanche mechanism [12]. If not mitigated at an early stage, kinetic energy carried by the high energy RE beam can severely damage plasma facing components as a result of a highly localised RE deposition [8]. Therefore, a comprehensive understanding of REs generation and its loss is of utmost priority in order to develop reliable REs mitigation and control methods to ensure the success of ITER.

The RE generation mechanisms have been extensively studied both theoretically and experimentally and understood up to a fair extent. However, the loss or mitigation mechanisms of the REs are rather ambiguous till date and demand much more experimental as well as theoretical investigation. There are several known mechanisms for the generation as well as the loss of REs from the plasma and the RE content in a tokamak is determined by the combined effect of both processes. Drecier's (primary) generation mechanism [13,14] and avalanche (secondary) [15] are the two established REs generation mechanism. In a Maxwellian distribution every electron experiences a friction force, due to its collision with other electrons, this friction force is also called collisional drag force. Dreicer theory explains that in presence of a strong parallel electric field, energetic electrons in a Maxwellian distribution can overcome the collisional drag force, acting on them and start accelerating, ultimately they 'runaway' from the Maxwellian distribution [13,14] and become so-called Runaway electrons. Several sources of the parallel electric field exist in conventional/superconducting tokamaks, such as the applied ohmic electric field, electric field generated during plasma disruption [12], electric field generated by MHD instabilities [] (e.g.: Sawteeth instability), etc. In secondary/avalanche generation, the existing REs with sufficiently high energy 'knock-out' the thermal electrons to runaway regime through large angle electron-electron scattering, while itself remaining in runaway regime, leading to an avalanche effect in the REs population growth [15]. These RE generation theories provide a basic understanding of REs in tokamak but do not explain the experimental observations completely. Most of the present-day tokamaks exhibit the presence of critical field required for RE generation which exceeds the theoretically predicted critical electric field (Connor- Hastie) by a factor of 2-10 [14]. The discrepancy has been often attributed to the presence of several RE loss processes in tokamak and limitations of available RE diagnostics [15,16]. The RE loss processes like collisional loss and drift orbit loss along with RE energy loss due to synchrotron radiations are taken into consideration while modeling the total RE population [17]. Apart from these loss processes, magnetic and electrostatic fluctuations, present in the tokamak plasmas, are also known to facilitate the RE loss at a rate faster than the above-mentioned processes [18]. Enhanced RE loss due to stochastic magnetic fluctuation inherent to plasma or due to externally applied Resonant Magnetic Perturbations (RMP) which causes the ergodization of the magnetic surface at the edge has been investigated both theoretically [19,20] and in experiments [20, 21,22]. Contrary to this, in several tokamaks like COMPASS [23] and TEXTOR [24], the presence of magnetic islands has caused suppression of REs loss during the current flat-top. RE transport across the magnetic field and eventual loss to the limiter/diverter and plasma peripheral material surfaces, play a major role in determining overall dynamics of REs in a tokamak and also holds the key to the development of a reliable RE mitigation system for ITER. A comprehensive understanding of REs cross-field transport in the dynamic magnetic topology of a tokamak remains a challenge and indispensable to develop a reliable RE mitigation technique for ITER.

This thesis is focused on REs generation and transport due to the intrinsic and externally controlled magnetic and edge instabilities in ADITYA and ADITYA-U tokamak. Being medium-size tokamak with moderate plasma currents $(80 - 150\ kA)$ and plasma duration $(100 - 300\ ms)$, REs do not attain catastrophic energy levels and hence they can be studied in a controlled manner in ADITYA/ADITYA-U tokamak. The studies presented in this thesis aim to provide a wider and more inclusive perspective on the complex inter-dynamics of REs, Magnetohydrodynamic (MHD) instabilities/modes and the edge fluctuations. RE generation and loss mechanisms influenced by intrinsic MHD fluctuations, such as the Sawteeth and tearing instabilities, are studied by analyzing a large number of discharges over a wide range of macroscopic operation and plasma parameters. To obtain more insight into the interaction of MHD with the REs, the amplitude and rotation frequency of the low-m MHD modes have been altered during a course of a single discharge by injection of periodic gas puffs. These periodic gas puffs also lead to the modification of edge fluctuations. These alterations in amplitude and rotation frequency of MHD modes as well as in amplitude of edge turbulent fluctuations have been observed to influence significantly the RE dynamics in ADITYA/ADITYA-U. The results have been consolidated to provide a broader perspective of RE generation and loss in various dynamic tokamak plasma scenario during the current flat-top. The thesis is arranged as follows: The experimental set-up, diagnostics, and discharge characterisation in terms of confinement times along with the experimental results of inward transport of fuel gas during gas puffs in ADITYA/ADITYA-U tokamak are described in Chapter 2. Chapter 3 presents the sawtooth instability (m/n=1/1) generated RE and their transport in ADITYA/ADITYA-U. Experimental results of the effect of MHD instabilities and their variations with periodic gas-puffs on RE loss in ADITYA/ADITYA-U tokamak are presented in Chapter 4. The experimental observations of RE loss due to edge fluctuations are described in Chapter 5. The results are discussed and summarized in Chapter 6 along with the future scope.

Chapter 2: Experimental set-up, Diagnostics, and Discharge characteristics

ADITYA tokamak [22, 23] was a medium-sized ohmically heated tokamak with a circular poloidal limiter having a major radius of $R = 75\ cm$ and a minor (plasma) radius $a = 25\ cm$ with 20 toroidal magnetic field coils. The plasma boundary in ADITYA was defined by a poloidal ring limiter with graphite tiles located at one toroidal location inside the vacuum vessel having a rectangular cross-section. Base pressure of $\sim 5 \times 10^{-8}$ Torr was maintained inside the vessel and the hydrogen gas was injected inside the vessel at filling pressure of $\sim 8 - 10 \times 10^{-5}$Torr for plasma discharges. The results presented in this thesis are from plasma discharges with axisymmetric toroidal magnetic field, $B_\phi \sim 0.75 - 1.25\ T$; peak loop voltage, $V_L \sim 18 - 20\ V$ ($E \sim 4 - 5\ V/m$); plasma current, $I_p \sim 80 - 160\ kA$ and plasma duration of $\sim 80 - 250\, ms$. The central chord-average density, $n_e \sim 1 - 5 \times 10^{19} m^{-3}$ and central chord-average electron temperature, $T_e \sim 300 - 700\, eV$.

During the course of this thesis, the ADITYA tokamak [24] has been upgraded to ADITYA-U [26] tokamak with the aim of conducting experiments in shaped plasma configurations. All the major magnetic coils, such as the ohmic transformer coils, toroidal magnetic field coils and vertical magnetic field coils of ADITYA have been reused in ADITYA-U. The major radius ($R = 75\, cm$) and minor radius of circular cross-section plasma ($a = 25\, cm$) are also kept the same in ADITYA-U. The new inclusions in ADITYA-U are: a new vacuum vessel of circular cross-section, two new sets of diverter (shaping) coils, a continuous toroidal graphite belt limiter on high magnetic field (inboard) side, as well as two poloidal limiters located on low magnetic field (outboard) side at two toroidal locations 180^0 apart ($\varphi = 90° \; and \; 270°$). ADITYA-U has been operated in limiter (toroidal belt limiter) configuration, with operation parameters similar to ADITYA and discharges with circular cross-section have been obtained, so far. The plasma parameters of ADITYA-U discharges are: plasma current $I_p \sim 80 - 170\, kA$, plasma duration (t) ~ $80 - 330\, ms$, the chord-averaged central electron density $n_e \sim 1 - 6 \times 10^{19} m^{-3}$, chord averaged central electron temperature $(T_e) \sim 300 - 500\, eV$, and toroidal magnetic field $(B_\phi) \sim 0.8 - 1.3\, T$. The RE experiments carried out in ADITYA have been repeated in ADITYA-U. Results from both the machines with discharges having similar plasma parameters but different limiter configurations have been analysed and presented in this thesis.

The standard tokamak diagnostics have been used for the present study which includes: external magnetic sensors for measurements of plasma current (I_p), loop voltage (V_L), plasma column position, etc. Seven-channel microwave interferometer is used for line averaged electron density measurements. The electron temperature has been measured using a two-filter soft X-ray spectrometer. Standard spectroscopic diagnostics for the temporal evolution of hydrogen neutral (H_α) and impurity (oxygen and carbon) spectral emissions and bolometers for the total radiation power (P_{RAD}) have been used. In ADITYA-U (ADITYA), the poloidal magnetic fluctuations ($\widetilde{\dot{B}_\theta}$) have been detected by two sets (one set) of 16 Mirnov coils distributed at equal angle separation in the poloidal periphery, inside the vessel at two diametrically opposite toroidal locations. The Hard X-rays (HXR) induced due to RE's interaction with limiter are detected by a 3-inch diameter NaI (Tl) scintillator detector. This lead-shielded detector is collimated to view the limiter and located at the equatorial plane of the machine. As a part of developmental work of this thesis, a matrix of 15 Langmuir probes arranged in different radial, poloidal, as well as toroidal locations have been designed, developed and installed to investigate the SOL and edge plasmas of ADITYA-U.

At the end of this chapter, typical discharges from ADITYA [25] and ADITYA-U [26] are presented. In these discharges, the density at the current flat-top has been maintained using periodic gas puffs. The estimation of global energy confinement time (τ_E) for ADITYA discharges and its scaling with density has been carried out and compared with neo-ALCATOR scaling law for [25] ohmically heated plasma discharges. In several discharges with improved ohmic confinement anomalous inward pinch velocities have been observed [25]. The pinch velocities have been estimated by measuring the time delay between the peaks in the temporal evolution of H_α emission and of Soft X-ray (SXR) emission and chord averaged electron density, during a gas puff pulse.

Chapter 3: Sawtooth Instability (m/n=1/1) Generated Runaway Electrons and their Transport in ADITYA

The sawtooth instability is an ideal MHD instability, during which the core temperature and density rise slowly and quickly crash down, periodically. This effect is most evident in line integrated Soft X-Ray (SXR) measurements of the plasma core, since SXR intensity, is strongly dependent on plasma density and temperature, hence used as a preferred tool to investigate the sawtooth instability [27,28]. The sawtooth instability is believed to be a manifestation of m/n= 1/1 internal kink mode (where m is poloidal mode number and n is toroidal mode number) during which plasma core is radially displaced, leading to reconnection at the q=1 flux surface, followed by its return to the center. It is commonly observed in most tokamaks when $q\ (0)\ < 1$, including ADITYA and ADITYA-U. In typical discharges of ADITYA, bursts of hard X-ray (HXR) due to the interaction of runaway electrons (RE) with limiter, during sawteeth activity were regularly observed. These HXR bursts were highly correlated in time with each sawtooth-crash, which suggested that each sawtooth-crash event generated/accelerated these runaway electrons, which then yielded the HXR bursts after their interaction with the limiter. Detailed investigations revealed that the electric field induced in the toroidal direction due to change in poloidal magnetic field during the sawtooth crash [28] is several times higher than the critical electric field required for runaway generation. The induced toroidal electric field during each sawtooth crash generates the REs, which then travel to the limiter to give a HXR burst. Furthermore, it was observed that in the later period of the plasma current flat-top of the discharge, no HXR bursts were accompanied by the sawtooth crash, although the sawteeth activity prevailed. This observation indicated a difference in radial transport of runaway electrons in the initial and later parts of plasma current flat-top in same discharge. During the initial phase of plasma current flat-top, the appearance of the HXR bursts were found to be due to enhanced loss of sawtooth-crash generated REs, facilitated by the overlapping of inflated magnetic islands (m/n = 2/1 and 3/1) present in the intermediate plasma region between core and the limiter. In the later phase, where magnetic islands did not overlap and good magnetic surfaces prevailed between the islands, the radial transport of REs was constrained, leading to the absence of correlated HXR bursts with the sawtooth crash. From the observations and analysis, it has been concluded that ergodization due to island overlapping in intermediate region facilitates the rapid loss of REs generated due to sawtooth crash, leading to HXR bursts. And well-formed islands separated by good magnetic surfaces between them substantially reduce the transport of the REs [29].

Chapter 4: Effect of Resistive Magnetohydrodynamic (MHD) Instabilities on Runaway Electrons in ADITYA and ADITYA-U tokamak

In this chapter, the effect of resistive MHD instabilities on runaway electron dynamics in ADITYA and ADITYA-U tokamak is presented. At the outset, a large number of discharges (>3000) with different resistive MHD (low m, n) modes with different amplitudes and frequencies have been analysed and studied in correlation with the HXR data to obtain a heuristic picture of the dependence of RE dynamics on MHD mode amplitudes and frequencies. Later in the chapter, the effect of varying the amplitude and frequencies of MHD modes in a controlled manner using periodic gas puffs on RE dynamics during a course of a single discharge is presented.

i) Resistive tearing modes & their influence on Runaway Electrons in ADITYA and ADITYA-U

A class of instabilities that is able to change the topology of the equilibrium magnetic field via the process of magnetic reconnection is known to be driven by the free energy associated with the nature of the current density profile sustaining the equilibrium field. Resistive tearing instabilities belong to this class of instability [30]. In a magnetically confined tokamak plasma, these instabilities lead to the formation of magnetic islands which can cause significant degradation of plasma confinement [8]. In high-frequency regimes, these modes often get coupled with drift wave, hence called drift tearing (DT) modes, and the magnetic islands associated with these DT modes rotate poloidally in electron diamagnetic drift direction with frequencies close to diamagnetic drift frequencies i.e $\omega^* = \frac{k_y T_e}{eB L_n}$, where k_y = wavenumber and L_n = density scale length [30]. As commonly measured in other tokamak, these rotating islands are observed as perturbed poloidal magnetic fluctuations, acquired by Mirnov coils (magnetic pick-up loops) placed around the poloidal periphery of the plasma [313].The frequency spectra of the poloidal magnetic field fluctuation exhibit coherent peaks corresponding to different modes present in the plasma. In the purely ohmic discharges of ADITYA as well as of ADITYA Upgrade MHD modes rotating with a frequency close to the electron diamagnetic frequency have been observed and identified as DT modes. Large number of discharges (>5000 discharges) have been studied using various numerical routines like Fast Fourier Transform (FFT), Singular value decomposition (SVD) technique and contour plots to obtain the DT mode rotation frequencies and island structures. It has been found that m/n = 2/1 mode and its harmonics are predominantly present in the majority of discharges with varying amplitudes and mode rotation frequencies. In ADITYA-U, the emergence of harmonics of m/n = 2/1 mode strongly depends on the amplitude and rotation frequency of m/n = 2/1 DT mode and it is found that the harmonics cease to exist when m/n = 2/1 rotation frequency exceeds 14 kHz. Furthermore, the dynamics of REs is found to be strongly correlated with the presence and absence of these harmonics in both ADITYA and ADITYA-U. Significantly higher HXR emission has been observed in discharges with a single small m/n = 2/1 DT mode exists with no harmonics, whereas reduced HXR emissions are observed in discharges having m/n = 2/1 DT mode with large amplitude ($\widetilde{B_\theta} > 50\ Gauss$) predominates along with its harmonics (up to 7). The appearance and disappearance of harmonics are also correlated with lower and higher intensities of HXR emission respectively have also been observed during the course of discharge in several discharges. These observations indicate reduced RE loss in presence of large well-formed (m/n = 2/1) islands compared to that in discharges with small or no islands. These results are in line with the theory predicting trapping of REs in MHD islands having width larger than a threshold width [19]. A sudden increase in the island widths and appearance of harmonics of m/n = 2/1 mode coinciding with strong reduction in HXR emission during the course of a single discharge also suggest that the trapping of REs in the island may be increasing the saturated island width as predicted theoretically, leading to higher amplitudes of these DT modes and subsequent harmonics generation.

ii) Modulation of amplitude and rotation frequency of MHD by periodic gas puffs and their influence on RE dynamics in ADITYA and ADITYA-U

In order to substantiate the results described in the previous section, the mode rotation frequency and amplitude of the m/n= 2/1 mode were modulated by periodic gas puff pulses in ADITYA and ADITYA-U. Periodic gas-puffing has been extensively used in most discharges of ADITYA and ADITYA-U, primarily to maintain the plasma density. The gas puff pulse width has been varied from ~1 – 5 ms, and the time gap between two pulses has been varied from ~ 4 – 8 ms. Each of these gas puff injects $\sim 10^{16} - 10^{18}$ hydrogen neutrals in the vessel depending upon the gas-puff pulse width. In presence of periodic gas puffs at the plasma current flat-top, the mode rotation frequency and the amplitude of m/n = 2/1 mode have been observed to vary in tandem with the gas puffs. This has been observed in more than 7000 discharges from ADITYA and ADITYA-U. The existing mode rotation frequency decreases by $\sim 20 - 50$ % within 1-2 ms after the injection of a gas puff. The DT mode regains its original frequency within 2 - 4 ms and the cycle is repeated after each gas-puff pulse. The observed decrease in mode rotation frequency of m/n = 2/1 mode is found to be proportional to the amount of gas puffed. The decrease in temperature and increase in the density scale length at the edge due to injected gas leads most possibly lead to a reduction in drift frequency (ω*), which ultimately leads to a decrease in DT island rotation frequency. Further, it has been observed that the amplitude of the mode is also reduced immediately after each gas-puff. However, in subsequent 1 – 3 ms, the amplitude grows again to its value, which it had prior to the gas puff until the next gas-puff again reduces it. Similar signatures of significant decrease and increase have been observed in HXR emission intensity with the application of each gas-puff. This periodic amplitude modulation of HXR emission intensity with gas-puff shows a weak time-correlation with MHD modulation, indicative of a relation between of MHD modes and RE loss. However, detailed investigation of events during a single gas puff revealed that the onset time of MHD mode suppression lags or leads the HXR emission reduction. Often, the HXR emission intensity remains suppressed even well after the MHD amplitudes retain their original (high) values after going through suppression due to gas puff and the overall duration of suppression of MHD mode amplitude also does not match with that of the HXR emission. Further, the fall-time of HXR emission after each gas-puff always remains much faster than the time required for the REs to reach to the limiter from the m=2 surface even with Rochester-Rosenbluth diffusivities calculated from the observed amplitudes of MHD mode [18]. Furthermore, in a large number of discharges with very low MHD amplitudes and no detectable islands, the MHD amplitude remains indifferent to the periodic gas-puffs, i.e., devoid of any periodic activity. Interestingly, the periodic variations in HXR emissions are still observed in such discharges. These observations strongly indicate the presence of another factor controlling the RE dynamics in ADITYA/ADITYA-U, which is strongly affected by the gas-puffs as well. Extensive investigations reveal that another factor influencing the RE dynamics is the edge turbulent fluctuations in density and floating potential, which is described in the next chapter.

Chapter 5: Influence of Turbulent Fluctuations in Edge Density and Floating Potential on RE loss in ADITYA-U

In this chapter, experimental evidence substantiating the role of turbulent fluctuations in density and floating potential at the plasma edge and SOL regions of ADITYA/ADITYA-U in RE loss is presented and discussed. Turbulent fluctuations in density and temperature of the edge region are commonly observed in almost all tokamaks and their basic characteristics are fairly universal. Edge turbulence dominantly consists of broadband plasma density and potential fluctuations. It has been recognized for many years that the cross-field plasma transport through the edge is dominated by these turbulent fluctuations leading to loss of thermal particles from the plasma. By carrying out controlled experiments in which the edge turbulence is periodically suppressed using periodic gas puffs, it has been shown that the turbulent fluctuations present in the edge region of ADITYA/ADITYA-U not only facilitate the loss of thermal particles but also strongly influence the RE loss rate. As mentioned in the preceding chapter, when multiple gas-puff pulses are applied during the plasma current flat-top, the temporal evolution of HXR intensity also modulates in amplitude exhibiting prominent peaks with a full width at half maxima (FWHM) ~ 2 ms, following each gas puff in ADITYA and ADITYA-U. These variations in HXR amplitude remain absent in discharges without the gas puffs. Previous experiments in ADITYA have demonstrated that injection of short pulses of gas leads to a concomitant suppression of edge fluctuations. Detailed analysis of edge density and potential fluctuations and their suppression in presence of gas puffs, studied using a set of Langmuir probes in the edge and SOL region, revealed that that periodic suppression of turbulent density and potential fluctuations coincide with the reduction in the HXR intensity. It has been observed that the HXR amplitude is reduced by $\sim 60 - 80\ \%$ of its value prior to the suppression when the edge/SOL turbulence is suppressed by gas puffs during a discharge. The frequency spectra of time series of HXR intensity show similar characteristics as that of the frequency spectra of density and potential indicating that the REs present in the edge region are significantly influenced by the prevailing turbulent fluctuations in density and potential. A heuristic model of RE loss in the presence of MHD oscillations associated with m/n=2/1 DT modes and edge turbulent fluctuations in density and potential based on several discharges has been developed and presented. These observations provide a basis to explore the possibility of a new RE mitigation scheme based on enhancing seed RE loss with the assistance of external turbulent perturbations of density and potential in the edge/SOL region of a tokamak.

Chapter 6: Discussion, Summary and Future Scope

This chapter presents a discussion and summary of the results presented in this thesis along with future works. The dedicated experiments on REs dynamics in ADITYA and ADITYA-U have demonstrated significant dependence of RE dynamics on MHD instabilities and edge turbulent fluctuations. These instabilities substantially enhance the loss of REs and hence should be duly included in estimations of RE growth rates in a tokamak. It has been shown that the Sawteeth instability (m/n=1/1) crash generate

REs and presence of stochastic magnetic fields due to the overlapping of m/n=2/1 and m/n=3/1 islands enhance the radial transport of these REs. Analysing a large number of discharges, it has been established that there exists a strong correlation between the RE population in a discharge and the MHD amplitude and frequency. MHD (m/n=2/1) modes with high amplitude ($\frac{\widetilde{B_\theta}}{B_\theta} > 5 \times 10^{-4}$) and low rotation frequency ($\omega^* < 14\ kHz$) exhibit harmonics and such discharges are charachterised by low HXR emission. Whereas, discharges with lower amplitude ($\frac{\widetilde{B_\theta}}{B_\theta} < 5 \times 10^{-4}$) m/n = 2/1 mode and higher rotation frequency ($\omega^* > 14\ kHz$) mostly lead to the observation of high HXR emission in ADITYA and ADITYA-U tokamak. These results indicate a reduction in RE loss in presence of large well-formed islands most possibly due to trapping of REs in the islands. Multiple periodic gas puffs have been injected to modulate the MHD mode characteristics and edge turbulent fluctuations during the current flat-top of discharges, in a controlled manner, to study their impact on the RE dynamics. These periodic gas puffs lead to a periodic modulation of the rotation frequency, as well as of the amplitude of m/n=2/1 mode. The neutrals injected by gas puff decrease the edge temperature and increase the density scale length, thereby decreasing the diamagnetic drift frequency which leads to the decrease in rotation frequency of the observed drift tearing modes. Although, gas-puff induced frequency and amplitude modulation of MHD modes does seem to have some influence on the RE loss, the fast variations in HXR emission amplitude during and after each gas puff can not be explained by the RE diffusion estimates using the Rochester and Rosenbluth model. It has also been shown that in the discharges where the MHD amplitude remains very low, the gas puffs lead to negligible variation in MHD amplitude and frequency. However, even in absence of periodic MHD modulation, strong periodic modulations in HXR intensities still prevail in such discharges. Further investigations revealed that in these discharges suppression of RE loss coincides perfectly in time with the edge density and potential fluctuation suppression after each gas puff and RE loss increases simultaneously with the edge fluctuation. The edge fluctuations suppression by the gas injection has been quite well established in ADITYA. Obseravtion of reduction in HXR emission at the same time instant indicate suppression of RE loss during that time. Periodic HXR peaks (due to periodic RE loss) are also found to coincide with distinct peaks in time profile of H_α line emission intensity, indicative of the increase in neutrals after REs loss to the limiters. These observations provide evidence of neutral recycling by REs in ADITYA/ADITYA-U tokamak. These results provide a significant insight of a RE loss mechanism through edge/SOL turbulent fluctuations in density and potential and may bridge the gap between the experimental observations and theoretical estimations of critical electric field requirements for RE generation in tokamaks. Furthermore, based on these observations, a mitigation technique for REs using broadband electrostatic fluctuations will also be thought through. In addition to the RE studies, the effect of periodic gas puffs on plasma confinement has also been studied and results on observations of anomalous inward pinch during the gas puffs are also reported in this thesis. Enhancing RE loss by externally inducing broadband electrostatic fluctuations through some means, such as biasing an electrode with time-varying (fluctuating) voltages placed inside the plasma remains one of the important future work of this thesis. Further, studies of controlling the MHD island rotations with DC biased electrode induced $E \times B$ plasma rotations and their effect in RE dynamics will also be carried out in future.

Chapter 1
Introduction

"Nothing in life is to be feared, it is only to be understood. Now is the time to understand more, so that we may fear less." —Marie Curie

1.1 Need for a better energy source

The commercialization of coal and other natural resources gave rise to the first industrial revolution in the 18th century. Since then, humans have mostly relied on natural resources for their energy needs. Even today, energy derived from natural resources contributes up to $70 - 80\ \%$ of total energy consumption in most countries. The current situation gives rise to two major problems: i) The shrinking reserves of the natural resources, and ii) Global warming due to increased greenhouse gases in the atmosphere. The natural resources such as oil, coal, and gas are foreseen to be extinct by the end of this century [1]. One of the main drawbacks for using natural resources is the amount of hydrocarbons that are emitted during the various stages of energy production. This has led to an increase in the greenhouse gases in the atmosphere, which consists mainly of CO_2 and the hydrocarbons (e.g. methane). The greenhouse cover, although necessary for trapping the earth's heat, is proving to be detrimental as the concentration of greenhouse gases is increasing day by day, owing to the incessant pollution caused by the human race. This has led to a steady increase in the average global temperature of the earth, commonly known as "Global Warming". In a landmark report by the UN Intergovernmental Panel on Climate Change (IPCC), climate scientists have warned that there are only a dozen years to mitigate the effects of global warming beyond which even half a degree rise in the global temperature will significantly worsen the risks of drought, floods and, extreme heat which will likely affect hundreds of millions of people [1,2]. In addition, humans will also be confronted by a critical energy crisis as soon as 2050, due to an expected rise of 4 billion in global population and constant need for better living standards which could lead to a two to threefold increase in energy consumption, which cannot be met because of the shrinking reserves of fossil fuels. Renewable energy such as wind and solar, which make up about 20 percent of the electricity mix today, would have to increase to as much as 67 percent [2,3]. Due to the intermittent nature, dependence on daily weather as well as the technical challenge of energy storage scalability, solar power, and wind power are not dependable alternatives as an energy source. The recent failure of Germany's renewables energy transition, the Energiewende, was a reality check for unrealistic goals of replacing fossil fuels [4–6]. Nuclear fission is a technologically feasible option, however, radiation damages and devastating accidents in the past have instilled a fear against its utilization as a mainstream energy source [7,8]. A new energy source compatible with environmental needs, economically viable and independent of weather and climate changes is the only way to sail the human race through this double crisis. There is no superior new energy source on the horizon other than the controlled thermonuclear fusion which offers the following :

- A secure, long-term and massive source of energy supply
- Negligible and short-lived radioactive waste
- Inherent safety features
- Abundant fuel supplies
- Clean energy source, free of greenhouse gas emission.

On current estimates, the cost of fusion-generated electricity is predicted to be broadly comparable to that obtained from fission, renewables and fossil fuels. Fusion, therefore, could have a key role to play in the energy market of the future, with the potential to produce at least 20% of the world's electricity by 2100 [3].

1.2 Nuclear Fusion: The Cosmic Power Source

Fusion is the cosmic energy source of the Sun and stars. In the tremendous heat and gravity at the core of these stellar bodies, hydrogen nuclei collide, fuse into heavier helium nuclei and release a tremendous amount of energy in the process [9]. At such high temperatures found in the stars, electrons separate from their atomic nuclei due to high-energy collisions, and the resulting mixture of free electrons and ionized nuclei is called plasma: the fourth and most common state of visible matter in the universe. Plasma physics is the study of how this amalgam of electrical charges behaves differently from a neutral gas [10]. For fusion to occur, the repulsive Coulomb forces between the positively charged nuclei must be overcome, which can be achieved by increasing their temperature. Hence the process is termed as thermonuclear fusion. The difference in the sum of the masses of the two light nuclei and the mass of the fusion products is converted into energy, according to Einstein's well-known equation, $E = mc$^2. Achieving the controlled thermonuclear fusion is equivalent to creating our very own sun on earth, an exemplar of collective endeavors of the human race. Fusion science has identified the deuterium (D) and tritium (T) fusion reaction as the most efficient fusion reaction which produces the highest energy gain at the "lowest" temperatures[11]. In this reaction two hydrogen isotopes, deuterium and tritium, fuse resulting in a helium nucleus and a neutron:

$$D + T \rightarrow He(3.5\, MeV) + n(14.1\, MeV) \qquad \ldots 1.1$$

where D denotes the hydrogen isotope deuterium (^2_1H), T is tritium (^3_1H), He is helium (^4_2He), and n is neutron (^1_0n). The produced energy is shared by the fusion products: most of the energy in the D-T fusion is produced in the form of a 14.1 MeV neutron while the helium nuclei, also called α-particle, receives 3.5 MeV of energy. In practical units, $1\ kg$ of a D-T mixture produces as much energy as the energy produced by $10000\ \mathrm{m}^3$ of crude oil [12]. Once the fuel supply is shut off, the reactions in a Fusion reactor will stop, hence there will be no off-site radiation-related calamities, even from a severe accident. When the neutron penetrates the reactor walls, it induces radioactivity in the reactor which has a shorter half-life time (of the order of $15 - 25$ years), as compared with the radioactive waste of fission reactors, and research is in progress to develop even lower activity materials. In a fission reactor fuel is stored for a long time which can cause the unfortunate accidents under adverse conditions, while in a fusion device fuel is continuously supplied, which makes it more resilient to a melt-down; instead, a technical failure tends to result in a direct termination of the burn.

1.3 Fusion on Earth

There are two different approaches to achieve controlled fusion: inertial and magnetic confinement. The former Inertial Confinement Fusion (ICF) involves small solid fuel pellets of D-T mixture that are irradiated with extremely powerful lasers, causing them to implode and rise in temperature [13]. The extremely high density, together with the high temperature fuses deuterium and tritium. However, there are enormous difficulties in focussing the laser beams equally around the fuel pellet, or in controlling the Rayleigh-Taylor instability which needs to be addressed yet [14]. Apart from the ICF exhibit low fusion triple product due to very low confinement time ($< 10^{-9}s$) in spite of very high fuel densities ($\sim 10^{25} cm^{-3}$).

The other approach, known as magnetic confinement is the most successful principle of fusion energy generation on earth at the moment. It uses strong magnetic fields around which the ions and electrons of plasma tend to gyrate, thereby remain confined in the direction perpendicular to the field [15]. The energetic neutrons which will be generated by the fusion reactions will not interact with the field and leave the plasma leading to a large flux on the material walls, which will be absorbed by blanket module and ultimately utilized to generate electricity. The charged alpha particles which will be generated by the fusion reactions with energy much larger than plasma temperature will remain confined in the magnetic trap and will re-heat the plasma. When this heating caused by the fusion products is sufficient to sustain the fusion reactions that stage is called an ignited reactor [16–18]. In a controlled nuclear fusion power plant, three following conditions must be satisfied:

- High temperature (T_e): (~10 keV) More than 10 times hotter than at the center of the Sun >100,000,000°C, required to incite highly energetic collisions at extreme speed.
- High plasma density (n): ($\sim 5 \times 10^{20}$ m^{-3}) To increase the probability of collisions.
- High confinement time (τ_E): ($\sim$ few seconds) To hold the plasma and allow continuous fusion reactions to take place.

The triple product $n\tau_E\, T_e$ is a figure-of-merit for a fusion reactor. For the deuterium-tritium (D-T) reaction the triple product is:

$$n\tau_E\, T_e > 5 \cdot 10^{21} keV.s.m^{-3} \qquad \dots (1.2)$$

The above criterion is the so-called Lawson criterion [19]. In order to have a reasonable cross-section for the deuterium-tritium reaction, a temperature of 1 to 10 keV is needed [16].

In 1955 Homi J. Bhabha who chaired the First International Conference on Peaceful Uses of Atomic Energy dared to predict in its opening ceremony that "a method of controlled release of the energy of nuclear fusion would be discovered in the next 20 years"[20].

Inspired by the idea of Oleg Lavrentiev [20] and developed in the 1950s by Soviet physicists Igor Tamm and Andrei Sakharov, tokamak is basically a toroidal "magnetic cage" (shaped like a doughnut) designed to confine and heat the plasma and has achieved the highest value of fusion triple product so far [21]. It has a strong toroidal magnetic field provided by external coils and a poloidal magnetic field induced by the plasma current which adds a helical twist to the resultant magnetic field lines. Each field line creates a toroidal surface of constant pressure, called flux surface, to which plasma is bound. The magnetic cage, therefore, can be viewed as a series of nested flux surfaces. To generate the plasma, a suitable amount of fuel (Hydrogen or Deuterium) is prefilled in the vessel. The plasma current is then induced via transformer action, where a changing current is driven through a conducting loop called ohmic coil placed in the centre of the tokamak vessel, inducing a voltage (loop voltage) which breaks down the neutral gas to a plasma state and drives the plasma current to heat the plasma thus formed. Additional non-inductive currents and plasma heating are obtained through the injection of high energy neutral particles and electromagnetic waves [22,23]. There are also external coils generating additional fields for plasma shaping and position control. The electrons/ions gain energies from the loop voltage and lose energy in collisions with other ions and electrons, which are usually balanced hence the electrons are settled in the thermal/ Maxwellian distribution and are usually referred to the background plasma [24]. These electrons should ideally be infinitely confined in the magnetic cage of tokamaks by gyrating the helical field lines and escaping in the perpendicular/radial direction by much slower diffusion processes [25,26]. However in reality due to the presence of finite resistivity and magnetohydrodynamic (MHD) instabilities, the magnetic cages are torn at some weak points leading to leakage of the electrons and ions, causing faster radial loss of plasma [27,28]. Further, the density and temperature gradients inside the tokamak plasma lead to electrostatic and magnetic fluctuations in plasma density, floating potential and plasma temperature. These fluctuating quantities lead to enhanced particle and energy transport across the magnetic field lines, thus degrading the confinement [29,30]. The tokamak plasma is a complex non-linear system with numerous variable dependent on each other. Numerous insurmountable challenges have been overcome to demonstrate controlled thermonuclear fusion in tokamak [JET] with a peak D-T fusion power of 16.1 MW in 1997, which made tokamak the toughest contender for a fusion reactor design [31]. Motivated by the results of JET and other machines and propelled by the urgency to build a new age energy source, the International Thermonuclear Experimental Reactor (ITER), the largest tokamak was envisioned and designed [10]. The International Thermonuclear Experimental Reactor (ITER) is a global project which aims to demonstrate controlled ignition and extended burn of deuterium-tritium plasmas in a tokamak. The ultimate goal is to achieve a steady-state operation and a power output larger than the power input. The giant reactor is currently under construction in Cadarache, France and is an epitome of human perseverance which holds promises for a better and cleaner future. The success of ITER can demonstrate the scientific and technological feasibility of fusion energy for peaceful purposes and open the avenue for a clean and abundant energy source. After more than 5 decades of global research on the colossal scientific and technical problem of controlled nuclear fusion, it will soon be a reality with the tokamak as the most promising design candidate for a fusion reactor. DIII-D and Alcator C-Mod tokamaks have recently achieved the highest peak fusion gain, $Q_{DT,,equiv} \sim 0.5$, achieved on a medium scale ($R < 2\,m$) tokamak in a newly discovered state of tokamak plasma that could sharply boost the performance of future fusion reactors, Super H mode regime. Super H-Mode access is predicted to allow ITER to achieve its goals (Q = 10) at $I_p < 15\,MA$, based on both theoretical prediction and observed normalized performance [32].

However, there remain certain challenges such as avoidance and/or mitigation of runaway electrons, (RE) [33], magnetohydrodynamic (MHD) instabilities leading to plasma disruptions [34], edge localized modes (ELMs) [35], etc., which are catastrophic for the safety and integrity of a tokamak. This thesis is dedicated to studying the runaway electrons which have been theoretically predicted to form intense collimated beams with alarming energies in larger tokamaks, which have the potential to destroy the plasma-facing components. Abrupt loss of plasma current, so-called disruptions often occurs in tokamaks [36], which induces a large electric field leading to high RE generation which grows exponentially to create relativistic RE beams under adverse conditions. The presence of the RE population is known from the very beginning of the tokamak research and their threats have also been identified in the fusion community since early days as they presented serious threat to the early small/medium tokamaks (e.g. TEXTOR, TFTR, ORMAK) even with relatively low RE beam currents [37,38]. After witnessing their damages to plasma-facing components in tokamaks like JET and Tora-Supra [39][40], it has been demonstrated that the generation rate of runaway electrons increases with the machine size [17, 18]. Theoretical models predict that up to 70% of the pre-disruptive plasma current could be carried by the REs which would have several tens of MeV energy in large and reactor-like tokamaks (ITER), the research on runaway electrons has been accelerated. The kinetic energy carried by this RE beam can severely damage plasma-facing components (PFC) and blanket modules because of a highly localized RE deposition. Besides the high cost of the plasma-facing components and blanket modules, the time to fabricate and replace those parts may delay or halt the ITER project for a considerable period of time. Moreover, the worst-case scenario (with very low possibility) of the RE damage to ITER predicts leakage of cooling liquids into the vacuum chamber that can put a halt to the entire ITER project [41]. The very design of ITER with plasma current ~ 5 - 20 MA, which makes it suitable to demonstrate controlled fusion, also make it prone to the generation of disastrous RE beams which may end up carrying currents of over 60% of the plasma current but in a much smaller and intensive beam [42]. The problem of runaway electron mitigation is considered critical as it threatens the safety of the tokamak, thus threatens the whole project of ITER and future tokamaks.

1.4 Runaway Electrons

The existence of runaway electrons is not unique to tokamaks, in principle, REs can appear in any form of plasma. The first detailed study of these REs, also called 'energetic electrons' has probably been carried out to explain the phenomena of thunderbolts [43]. REs are common in many astrophysical and atmospheric plasma like the solar flares [44], solar wind [45], mesosphere [46], etc. When a subtle balance between the electric field force, F_E , accelerating the electrons and collisional drag/friction force, F_{coll}, decelerating the electrons is maintained, the distribution of plasma electrons broadly remain the Maxwellian. The friction force on an electron in a Maxwellian distribution is a non-monotonic function of its velocity, v, which is maximum at its thermal velocity, $v = v_{th}$. For electrons with $v > v_{th}$, the collisional friction force (F_{coll}) decreases quadratically as given by the following relation [47],

$$\nu_{coll} = \frac{ne^4 \ln \Lambda}{4\pi\varepsilon_0{}^2 m_e{}^2 v_e{}^3} \propto v_e{}^{-3} \quad \ldots 1.3$$

$$F_{coll} = m_e v_e \nu_{coll} \quad \ldots 1.4$$

where, ν_{coll} is the collision frequency, n is plasma density, $\ln \Lambda$ is coulomb logarithm, m_e is electron mass and v_e is electron velocity. When this friction force becomes smaller than the parallel electric field force acting on the electrons $F_{coll} < eE$, those electrons 'runaway' from the thermal electron population in velocity space [48]. Due to the toroidal geometry, the magnetic field acts as an "infinite racetrack" for the runaway electrons, which keep gaining energy by accelerating and millions of toroidal revolutions of the tokamak each second. The two main RE generation mechanisms are (a) Dreicer/Primary and (b) Avalanche/Secondary.

1.4.1 Dreicer Generation

H. Dreicer accomplished the first detailed theoretical model of REs in 1960s [47,49] assuming an infinite, homogeneous, cylindrical, non-relativistic, fully ionised, quasi-steady-state plasma in an electric field, with an electron distribution function close to a Maxwellian, which is based on calculating a quasi-steady state electron distribution affected by the electric field and the collisions, and studying the electron flow in the momentum space. The critical electric E_c is the minimum Electric field required for RE generation in plasma at which the electrons with light-like velocity runaway. The Dreicer electric field is the electric field above which all electron population will runaway. They are given by the following equations and represented graphically in figure 1.1.

$$E_c = \frac{n_e e^3 ln\Lambda}{4\pi\varepsilon_o mc^2} \qquad \ldots 1.5$$

$$E_D = \frac{n_e e^3 ln\Lambda}{4\pi\varepsilon_o T_e} \qquad \ldots 1.6$$

where n_e~ plasma density and $ln\Lambda$~ coulomb logarithm.

$$ln\Lambda \ = \ 23 - log(\sqrt{n_e(cm^{-3})}.T_e^{-3/2}(eV)) \qquad T_e < 10\ eV$$

$$= \ 24 - log(\sqrt{n_e(cm^{-3})}.T_e^{-1}(eV)) \qquad T_e > 10\ eV \qquad \ldots 1.7$$

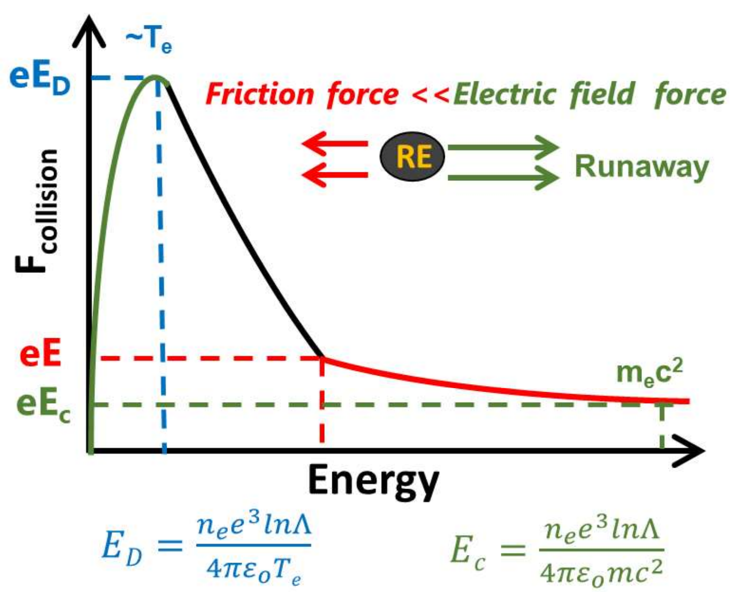

Figure 1.1: Plot showing Energy versus collisional friction force on electrons in a Maxwellian distribution along with energy required for runaway.

The process of runaway leaves a void in the tail of the thermal population which is replenished by collisions, thus making primary RE generation a continuous process, with a growth rate dependent on background plasma parameters. The primary generation rate has been studied and refined over decades [50–52]. The latest growth rate including the non-relativistic effects given by Connor and Hastie [53]:

$$\lambda_{RE} = kvn_e\, \mathcal{E}_D^{\ -3(1+Z_{eff})/16}\, exp\left[-\frac{\mathcal{E}_D}{4} - \sqrt{\mathcal{E}_D(1+Z_{eff})}\right] \quad \ldots 1.8$$

where $\mathcal{E}_D = E/E_D$, and Z_{eff} is the effective charge state of the plasma and is a factor in order of unity. In the limit $\mathcal{E}_D \gg T_e/m_e c^2$ the relativistic effects significantly change the RE birth rate which becomes:

$$\lambda_{RE}^{rel} = \lambda_{RE}\ exp\left(-\frac{T_e}{m_e c^2}\left[\frac{\mathcal{E}_D^2}{8} + 2\sqrt{\frac{1+Z_{eff}}{3}}\,\mathcal{E}_D^{2/3}\right]\right) \quad \ldots 1.9$$

The RE generation rate essentially depends on n_e, T_e, E and Z_{eff} in both cases. Lower n_e, and high T_e, E and Z_{eff} favor higher RE generation. During the start-up of a tokamak discharge, plasma is formed by the ionization of a gas which requires a strong electric field and n_e is relatively lower as compared to current flat-top. However, their formation is usually avoided by maintaining a higher gas/plasma density or lowering breakdown loop voltage. During the current flat-top, the E is much lower and the n_e is higher which leads to lower RE growth rates [20]. However, magneto-hydrodynamic (MHD) events are known to induce strong longitudinal electric field which may drive a significant population of REs [54] during the current flat-top. Generation of supra-thermal electrons has been observed during sawteeth crashes several tokamaks like T-10 [55] DIII-D [56]TCV [57] and ADITYA [58] is attributed to the high parallel electric field induced during the sawteeth crash. The induced electric field has been modeled and estimated in works by Wesson [54] and Kadomstev [59]. Although the generation of new REs has been debated in some experimental studies [60], the possibility of RE acceleration to high energies remains a possibility to explain the appearance of non-thermal electrons during sawteeth bursts.

Another RE generation mechanism during the thermal quench (TQ) i.e. the first phase of disruptions in large fusion devices called 'hot-tail' mechanism was theoretically predicted by Fleischmann and Zweben [61]. During the current quench, the sudden cooling of plasma which is too fast for the energetic tail electrons with very low collisionality to get thermalized, enabling/inducing them to become REs. This hot-tail mechanism is later used to explain RE generation during the pellet injection in DIII-D by Harvey et al. [62]. The Decrier and hot tail generation mechanism drive the thermal electrons to runaway regime depending on the prevailing background plasma characteristics and therefore are called primary mechanisms.

1.4.2 Secondary/ Avalanche Generation

The REs are also known to be generated by the collision of existing REs with sufficiently high energy with the thermal electrons. In this generation mechanism called avalanche mechanism or secondary mechanism, the colliding RE 'knock-out' the thermal electron to runaway regime while itself remaining in runaway regime. The knocked-out REs with sufficient energy further knocks-out more thermal electrons to RE regime, thereby causing an avalanche of REs production. After being theoretically predicted by Sokolov in 1979[63], the secondary generation has been observed experimentally in the TEXTOR tokamak [37] for the first time. The growth rate of RE density, γ_A , produced through secondary generation avalanche is given as

$$\gamma_A = \frac{n_r \nu_{ee}(\mathcal{E}_D - 1)}{c_z ln\lambda}\left(1 - \mathcal{E}_D^{-1} + \frac{4\left(Z_{eff}+1\right)^2}{c_z^2\left(\mathcal{E}_D^2+3\right)}\right) \qquad \ldots\ 1.10$$

where $c_z = \sqrt{3(Z_{eff}+5)/\pi}$, $\mathcal{E}_D = E/E_D$, ν_{ee} is electron-electron collision frequency and Z_{eff} is the effective charge state of the plasma.

In simpler terms under approximations, the time scale of secondary generation is given as $\tau_{sec} = \frac{2me\ c\ ln\Lambda\ aZ_{eff}}{e\ E}$. The secondary generation mechanism is the dominant mechanism of RE generation during disruption and is responsible for post disruption RE beam generation. The problem of REs is identified as a more critical threat to large tokamaks, after the disruption generated RE beams displayed their destructive potential in several large tokamaks, including TFTR [65], Tore Supra [39] JT-60U [66] and JET [42,67]. In 1997 Rosenbluth et. al estimated that few tens of MeV of post-disruption RE beams carrying the majority of pre-disruptive current may be generated in ITER, based on avalanche generation mechanism which drew wide attention in the fusion community on the grave issue of REs [68]. A detailed study and kinetic modeling of RE generation during avalanche mechanism due to 'knock-on' collisions using numerical tools have been carried out by E. Nilsson in her Ph.D. thesis. It explores the effect of toroidicity [69] and trapped electron effect on RE generation by both primary and secondary mechanisms[70].

Although the RE generation mechanisms have been investigated in-depth, the experimental evidence exhibit discrepancy in comparison with existing generation models. Through an extensive joint ITPA experiment, which investigated data from DIII-D, C-Mod, FTU, KSTAR, and TEXTOR tokamaks during the quiescent current flattop, Granetz et al [71] have reported that for a significant RE production, a critical electric field 3-10 times higher than that predicted by Connor and Hastie is required for significant RE production. The study strongly indicated the presence of other dominant RE loss mechanisms in addition to collisional damping, which determines the RE population. The RE experiments have played a catalytic role in motivating dedicated theoretical and modeling efforts to understand the additional RE loss mechanisms in quiescent and dynamic tokamak discharge scenario. Lack of unambiguous data of REs with low energy and low population, due to the finite lower threshold of sensitivity of detectors is also considered to be a factor responsible for the discrepancy between theory and experimental results [72,73]. The total population of REs and their energy distribution in plasma is strongly determined by their loss mechanism prevailing in the plasma. The major RE loss mechanisms are discussed in the following section.

1.4.3 RE Radiation Losses

The power gained by an RE in the presence of a toroidal field in the absence of any loss is given as: [48]

$$P_E = ecE_{tor} = ecV_{loop}/2\pi R \qquad \ldots 1.11$$

An electron with relativistic energies ($>$ 10s MeV) is subjected to various radiation losses. These losses contribute to the slowing down of the REs in addition to the collisional friction force. Synchrotron radiation and bremsstrahlung (free-free collisions or braking radiation) and Cherenkov radiation are some of the radiation losses influencing the maximum attainable energies of the REs. These radiations are also utilized as an important diagnostic tool to study the RE and to measure their properties.

1.4.3.1 Synchrotron radiation

Synchrotron radiation is the radiation emitted by highly energetic charged particles undergoing acceleration perpendicular to the direction of their motion [72]. Due to the presence of a strong magnetic field REs in tokamak follow a circular motion around the field lines and the synchrotron emission radiated by them is [72]

$$P_{syn} = \frac{e^4}{6\pi\varepsilon_0 m_e^2 c} B^2 p_\perp^2 \qquad \dots 1.12$$

where B is the toroidal field, and

$$p_\perp^2 \sim \gamma^2 (v_\perp/c)^2 = \gamma^2 \sin^2\theta\,(v/c)^2 \sim \gamma^2\theta^2 \qquad \dots 1.13$$

where $\theta = v_\perp/v_\parallel$ is the pitch angle of the RE, $v_\perp$ is the perpendicular velocity of RE, v is the total velocity of RE and γ is the Lorentz factor. This radiation loss increases with energy and pitch angle hence limiting the maximum energy attained by an RE. It effectively introduces a decelerating force on RE given by [72]

$$F_s = \frac{2}{3}\frac{e^2}{4\pi\varepsilon_0}\left(\frac{v}{c}\right)^3 \gamma^4 \langle\frac{1}{R^2}\rangle \qquad \dots 1.14$$

where $\langle\frac{1}{R^2}\rangle$ is the field line curvature averaged over gyromotion. Stahl et.al showed that synchrotron radiation losses may partially explain the higher threshold of the critical electric field for RE generation, which has been observed in the ITPA joint experiment by Granetz et al [74]. In a Ph.D. thesis by A.Stahl [75], it has also been argued that the assumption of the presence of electrons with light like speed, which was inherent to the estimation for the critical electric field for RE [75], is an overestimation. A finite Maxwellian plasma has a distribution width determined by its thermal temperature. Simulations carried out incorporating these details resulted in significant reduction in the growth rate of RE at a given electric field [76]. For tokamaks with high RE energies, the synchrotron radiation acts as an important source of information of RE and its dynamics. The interpretation of the synchrotron radiation is not straight forward due to its dependence on pitch angle as well as energy [77,78].

1.4.3.2 Bremsstrahlung

Bremsstrahlung radiation is emitted when an energetic electron slows down after Coulomb interaction with other charged particles. Bremsstrahlung is also one of the energy loss channels for the REs [79,80]. The broadband spectrum of bremsstrahlung radiation from an electron scattered by an ion is dependent on electron velocity v, an atomic number of the scattering ion Z and collisional parameter, b. [81]

$$P(\lambda) = \frac{4\pi^3}{3}\frac{Z^2 e^6}{m_e^2 c^3 b^2 v^2} exp(-\frac{4\pi cb}{\lambda v}) \qquad \ldots 1.15$$

The decelerating force on an RE due to bremsstrahlung is given as [81]

$$F_B = \frac{4}{137} n_e\left(Z_{eff} + 1\right) m_e c^2 \gamma r_e^2 \left(ln\, 2\gamma - \frac{1}{3}\right) \qquad \ldots 1.16$$

where r_e is classical electron radius.

The bremsstrahlung radiation from REs interacting with the limiter in ADITYA and ADITYA-U, i.e Hard X-Rays (HXR) are the source of information of RE and their dynamics in ADITYA/ADITYA-U tokamak, which will be discussed in next chapter.

1.4.3.3 Cherenkov Radiation

A charged particle passing with a velocity faster than its phase velocity in a dielectric medium cause excitation of electromagnetic waves and emit Cherenkov radiation. Due to the wide range of wave phase velocity in the plasma, the resonance condition for Cherenkov radiation, $\omega = k.v$ can be easily satisfied. Detectors based on this radiation are also being developed and used to study the RE dynamics in several tokamaks like COMPASS [82], and FTU [83]. The effect has recently been investigated in detail in a thesis by Liu Chang [84] as an attempt to understand the experimentally observed large critical field and improve the theoretical RE model. The drag force associated with the Cherenkov radiation can be as large as $\sim 20\%$ of the collisional drag force in typical runaway electron experiments. Combined with the synchrotron radiation reaction force, the correction is still not enough to explain the observed critical electric field. The Cherenkov radiation is significant for relativistic runaway electrons. The radiation electromagnetic fields can also cause pitch angle scattering of REs in momentum-space through wave-particle interaction and enhance their diffusion. The effect has been used to explain the abrupt growth of electron cyclotron emission (ECE) signals in a runaway electron experiment that was recently conducted on the DIII-D tokamak [85].

1.4.3.4 Collisional damping

Collisional damping is another factor that can increase the effective friction compared to the classical estimate is partially ionized atoms. The effect is especially dominant for heavy ions such as argon or tungsten, which are often present during or after disruptions and may cause a significant slowing-down of REs. The massive gas injection (MGI) technique which was primary RE mitigation scheme for ITER relied on this mechanism [86]. However, it has been estimated that an injection of $\sim 10^{26}$ heavy impurity particles in $\sim 20 - 30\ ms$ would be required to achieve effective mitigation of RE beams in ITER. The task is a technological challenge and it can have serious implications on the cryopumps and tritium breeding plants in ITER. Moreover, some experiments in DIII-D [62] and JET [40,87] show that the injection of pure Argon or Neon can often cause the generation of a large population of REs instead of mitigating them.

1.5 RE Loss and Confinement

Apart from the above mentioned RE generation and energy loss mechanism the spatial dynamics of REs in a tokamak also determines the ultimate RE population present in a tokamak plasma. The ITPA joint experiments and several other observations in several tokamaks like the limitations of MGI scheme and RMP scheme of RE mitigation in the past few years have compelled the RE physics community to explore and improve the understanding of RE dynamics. Although a strong effort is being dedicated to the RE dynamics and loss in tokamaks a reliable model for RE dynamics in a tokamak is far from complete. The current understanding is limited to that described by single-particle dynamics in a quiescent plasma in toroidal geometry. In the simplest model, the RE electrons are continuously accelerated in tokamak in the presence of the electric field and are strongly confined by the toroidal field. The radial loss of REs is determined by radial orbit drift, the stochastic magnetic field which may be driven externally or generated due to intrinsic MHD activity as well as electromagnetic and electrostatic fluctuations in the plasma edge [88].

1.5.1 Radial drift of RE orbit

Like thermal electrons REs also gyrate around the magnetic field lines and follow the magnetic flux surfaces. However, the REs are forced radially outward because of another fundamental effect called drift orbit effect. The acceleration of a runaway particle implies a change in its angular momentum with respect to the axis of the tokamak. Since the canonical angular momentum of the particle should be conserved, this change causes a shift of the runaway orbit away from the flux surface [89,90]. The effective safety factor is $q_P = \frac{\Delta\varphi}{2\pi}$, where $\Delta\varphi$the increment in toroidal angle per one poloidal turn is for an RE. For lower energy electrons with the relativistic factor $\gamma \geq 1$ and $v_{RE} \ll c$, the effective poloidal magnetic field and electron orbits coincide with magnetic field lines. With the increase in the RE energy, the effective safety factor and corresponding drift surfaces start shifting outwards with respect to the equilibrium flux surface. Figure 1.2 shows the radial shift of drifted RE orbits with different energies simulated for TEXTOR tokamak [33]. The orbit marked by REs with lowest energy $\sim 10\ keV$ and has negligible drift as compared to the equilibrium surface and therefore have $q_P \approx q_\psi$(equilibrium safety factor). The consecutive surfaces correspond to drifted orbit of REs with higher energies, $10\ MeV, 20\ MeV, 40 MeV, and\ 46\ MeV$. As apparent from the figure, the radial shift '$\boldsymbol{\delta}$' increases with the RE energy and the shape of RE orbit also elongates horizontally. This drift orbit also imposes a maximum limit to RE energy for a tokamak depending on its size and the loop voltage, beyond which the REs will hit the limiter and get lost.

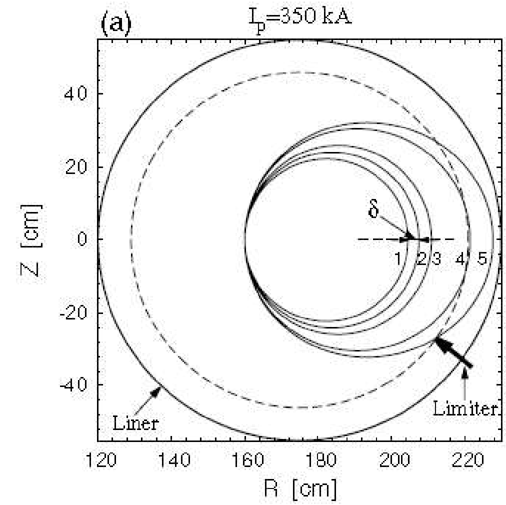

Figure 1.2: Guiding-center orbits of electrons corresponding to the different energies in the plasma with the plasma current I_P = 350 kA and the toroidal field B_T = 2.5 T: curves 1-5 correspond to energies E = 10 keV, 10 MeV, 20 MeV, 40MeV, and 46 MeV, respectively. (TEXTOR tokamak)

The radial shift of the outermost point R_o of the RE orbit from the magnetic surface is obtained as [91]

$$\delta \approx \frac{(R_o - R_i)E}{E_c R_o\, B_\theta} = \frac{2\tilde{q}E}{E_c B_T} \qquad \dots 1.18$$

where $\tilde{q} = \frac{rB_T}{R_o B_\theta}$ and $r = (R_o - R_i)/2$, and R_i is the innermost point of the RE orbit. Such drift of electron orbits can be quantified by the outward drift velocity v_{dr} , which can be approximated as [91]:

$$v_{dr} \approx \frac{R_o E_\phi}{R_o\, {B_\theta}^*}\left(1 - \frac{RT_{av}}{R_o T}\right) \qquad \dots 1.19$$

where ${B_\theta}^*$ are the effective poloidal B field for RE and average transition time

$T_{av} = \frac{2\pi q_p R_o}{v_\phi}$

1.5.2 RE diffusion due to magnetic fluctuations

Traditionally, the REs have been detected by monitoring the HXR emission intensity, generated by REs hitting mainly the limiter, due to radial RE transport. There has always been an inconsistency between the radial diffusion coefficient ($10^{-2} - 10^{-1}\ m^2/s$) from measured HXR emissions and the estimated collisional diffusion coefficient for REs ($10^{-4} m^2/s$) in tokamaks [33,92]. This mismatch has often been attributed to the non-axisymmetric magnetic perturbations, which can be sub-divided into small scale microturbulence [93,94] and large scale magnetic fluctuations due to MHD modes [95].

Single-particle RE dynamics including electric field acceleration, collisions with the plasma and deceleration due to radiation losses have been studied in detail [88,96]. Due to their very low coulomb collision frequency, the RE dynamics is also strongly sensitive to the magnitude and nature of the magnetic fluctuations, which has been studied in experiments and theoretically over the last two decades [92,97]. The magnetic stochasticity is mostly credited to enhance the RE loss. The effect of the fluctuations via an effective friction force characterized by a frequency of collisions with the fluctuations proportional to the fluctuation induced radial diffusion coefficient in a single test particle study by Solis et al [61]. Intensive fluctuations of electric and magnetic fields not only cause anomalous electron losses, depleting the runaway population but also alter and determine the spatial distribution of REs, limit their maximum attainable energy. The diffusion coefficient of RE is given as [88]

$$D_{RE} = K_{\tilde{B}} v_{||} + \frac{K_{\tilde{E}}}{v_{||}} + 2\sqrt{(K_{\tilde{B}} K_{\tilde{E}})} cos\alpha \qquad \dots 1.20$$

$$K_{\tilde{E}} = L_{||} v_{\tilde{E}}{}^2 \qquad \dots 1.21$$

$$K_{\tilde{B}} = L_{||} \tilde{b} \qquad \dots 1.22$$

where $K_{\tilde{B}} v_{||}$ and $\frac{K_{\tilde{E}}}{v_{||}}$ are the diffusion coefficients due to magnetic fluctuations and electrostatic fluctuations respectively. α is the phase difference between the magnetic and electrostatic fluctuations, connection length, $L_{||} = \pi q_0 R_0$, $\tilde{b} = \widetilde{B_r}/B_0$ where $\widetilde{B_r}$ is the radial component of MHD fluctuations.

In ADITYA tokamak a localized vertical magnetic perturbation applied at one toroidal location has been used to mitigate REs [98]. Suppression of REs by the external magnetic perturbations has been intensively discussed since the late 1990s [97,99–103]. The Resonant Magnetic Perturbations (RMPs) have been used as a means of RE mitigation in several tokamaks like TEXTOR[87,92], COMPASS-C [104], ASDEX [105], JET[106], J-TEXT[107], DIII-D[108] with limited success by altering the magnetic topology of the edge plasma. The RMPs can also suppress the secondary RE generation by enhancing seed RE diffusion[109]. The suppression of disruption generated REs by the RMPs in ITER tokamak has been explored in [102]. However, in some experiments in JET[110] and DIII-D [111], RMPs have not succeeded in RE suppression.

The experimental observation of 'runaway snakes' in TEXTOR tokamak[112] is an excellent example of the dominance of MHD modes on RE dynamics in tokamaks. The study shows that after pellet injection, MHD stochasticity is triggered and the REs that are confined in the central region, escape radially out through the stochastic channel. The remaining REs stay confined in a small region, most probably in the magnetic islands forming the so-called 'RE snakes'. RE confinement in localized regions in tokamak has also been observed in several other tokamaks like J-TEXT[113], DIII-D [114] etc. Experiments in HL-2A also showed diminished RE loss in the presence of a single magnetic island as compared to discharges with multiple islands[99]. A.H Boozer has analytically explored the possibility of RE confinement inside the core of a well-formed large magnetic island with a width greater than a critical island width given by [95]

$$\frac{\delta_i}{\psi_t} \approx \sqrt{\left(\frac{2\,\rho_e}{\Delta_\iota a}\right)} \qquad \dots 1.21$$

where δ_i is half-width of the island, $\psi_t$the enclosed toroidal flux, ι is the rotational transform, ρ_e is the parallel electron gyroradius, $\rho_e \equiv \gamma m_e v_\parallel / eB$ and $\Delta_\iota \equiv |\psi_t d\iota / d\psi_t|$. The author also attempts to estimate the accelerating electric field in an island and the change in the size of an island by the runaway electron current. However, the idea/notion of RE confinement in MHD islands is in the early stage of development and detailed theoretical and experimental investigations are required to establish this.

With $v_{||}$ in the denominator, the second term in the RE diffusion equation (Eq. 1.20) due to magnetic and electrostatic fluctuations given by Solis et al.,[88] implies that the contribution of electrostatic fluctuations in RE diffusion decreases as the velocity of the particle increases. Based on the above, it is quite a widely accepted fact that magnetic turbulence dominates runaway transport but electrostatic turbulence dominates thermal transport [88,90,115]. Therefore, the effect of magnetic fluctuations on REs has been studied for quite a long time both experimentally and theoretically. However, very few experimental studies are reported demonstrating the effect or non-effect of electrostatic fluctuations on REs [116]. As can be seen from figure 9 of reference [116] in ASDEX tokamak, the RE flux increases significantly when the discharge makes the transition to L-mode from the Ohmic mode. The RE flux again decreases significantly, well below of its value in the Ohmic mode, when the discharge makes a transition from L to H mode. As it is well known that the electrostatic fluctuations in the edge/SOL make similar transitions at Ohmic to L to H modes, an indirect correlation may be foreseen between the electrostatic fluctuations and the RE flux.

1.6 RE Mitigation Techniques

Several techniques have been proposed for runaway mitigation. Massive gas injection (MGI) is commonly used due to its straightforward implementation. Several experimental investigations on tokamak disruptions [14, 15, 16, 17, 18] have been conducted to investigate the effect of massive gas injection (MGI) on the runaway suppression in different machines. Enormous amounts of neutral gas ($> 10^{21}$ atoms) are injected into the vacuum vessel. The REs are collisionally suppressed by an increased density at the start of the current quench [19]. The main drawback of this technique is the slow impurity delivery and a poor mixing efficiency [16]. Moreover, the injection hardware and technologies available to date are not capable of complete runaway suppression during tokamak disruptions. Experiments showing enhanced RE generation after impurity pellet injection in some experiment also raises a concern [62,117] . An alternative concept for mitigation of REs is to deconfine the REs before they have time to gain high energies from the induced toroidal electric fields. Perturbation fields which cause an enhancement of the RE loss can be initiated, e.g. by externally applied non-axisymmetric magnetic fields. The perturbation fields that are resonant with the specific magnetic surface give rise to the ergodization. In the ergodic layer, the radial transport of the particles is enhanced [20, 21]. The position control of the runaway beam also is an attractive option in case the applied runaway mitigation methods fail and many high energy REs are generated. Control of the runaway beam position has been demonstrated in Tore-Supra [22], DIII-D [23], COMPASS[118] and TEXTOR [24]. The interaction between runaway beam and the wall can be minimized by keeping the beam within the "safe zone". This offers an opportunity to apply other mitigation methods such as massive gas injection and runaway current ramp-down to dissipate the runaway energy. [91]

Following previous experiments [2] and recent modeling efforts [3], it appears that improved understanding of the link between the complex dynamics of evolution of perturbed magnetic surfaces during the disruption and RE generation and losses represents a key contribution towards safe operation of ITER. However, this task is quite challenging, due to short timescales and significant radiation loads that can lead to saturation or degradation of many diagnostic signals. Disruptions are interesting but complex processes for studying the birth of runaway electrons since they include magnetohydrodynamic (MHD) instabilities, anomalous transport and complex evolution of the magnetic field topology [11]. Modeling the evolution of the temperature and electric field in disruptions would require a proper description of the thermal quench including radiative or convective loss mechanisms and MHD instabilities. The coupling of a kinetic code capable of handling 3D magnetic topologies and open field lines with a fluid code such as JOREK [14]. In this respect, it is essential to understand the response of REs to magnetic perturbations under controlled conditions, i.e. in the current flat-top phase of the discharge. Subsequently, the knowledge so acquired can be extended towards plasma disruption timescales with support of the relevant MHD codes [60]. It has also been suggested in the literature that by drastically increasing the plasma density, by injection of fast gas puffs [47], “killer” pellets [32, 48], or liquid jets [49], the critical runaway field would rise and thereby directly inhibit runaway acceleration. These schemes can also lead to ergodisation of the magnetic field which removes from the plasma fast electrons that would otherwise act as seed electrons for the avalanche. If successful, as indicated by the experimental results of gas puffing and pellet injection from the DIII-D tokamak [50], these schemes would reduce the runaway population to a manageable level. [119,120]

1.7 Motivation

Scaling the energy of the RE beam produced during plasma disruption in presently operating big machines like JET, portrays a very alarming projection for ITER with REs attaining energies $> 10\ MeV$. Hence, owing to the potential threat, posed by these high energy REs to the peripherals of a tokamak for the safe operation of the future nuclear fusion power plants based on the tokamak principle, REs are considered as the second-highest priority for the ITER [27,41]. Looking at a huge number of publications since the last few decades on REs, it is quite safe to state that complete understanding of all aspects of REs is far from complete. A serious global effort is underway to overcome the threats of REs through experiments as well as theory and simulations for ensuring the safety of large fusion reactors. The REs are known since the birth of tokamak and the generation mechanism of REs is understood to an extent, however, the loss or mitigation mechanisms of these REs are very poorly understood. There are several mechanisms for generation as well as for loss of REs from the plasma and the RE content in any plasma depends on the rates of generation and loss. In spite of small collisional interaction of REs with bulk plasma, there exists a hidden interplay between the runaways and the bulk plasma and the instabilities present therein, which are yet to be fully explored experimentally. The role of magnetic field topology or MHD activity in RE dynamics (including RE generation, confinement as well in their loss) is becoming progressively evident with experience gained through various RE experiments in several tokamaks. From an experimental viewpoint, deciding between the two potential candidate mechanisms influencing the RE transport, i.e., the magnetic turbulence and the electrostatic turbulence, still drives a strong motivation for RE studies in tokamaks. Further, deriving a comprehensive RE mitigation technique from these studies and understandings also motivate basic studies of REs in tokamaks. The main objective of this thesis work is to study the interaction between the bulk plasma instabilities, including magnetic and electrostatic turbulence, and RE dynamics leading to generation, confinement and loss of REs in ADITYA and ADITYA-U tokamaks through devising careful experiments and analysis. Due to the destructive nature of REs, with the damage being proportional to the RE energies, the RE experimentation remains limited in large/reactor-like tokamaks, such as JET etc., since the significant population of runaways, necessary for detailed studies of the RE, can severely damage in-vessel components. However, with relatively low plasma current in comparison to larger devices, ADITYA/ADITYA-U is a suitable machine for RE studies as the RE cannot achieve very high energies and cause severe damage to the vessel and the peripherals. In short, the major objectives of this thesis are:

- RE generation due to MHD instabilities, such as Sawteeth instabilities.
- RE transport losses in the presence of overlapping magnetic islands.
- RE confinement in the presence of single large m/n = 2/1 MHD island.
- Effect of periodic modulation of island width/MHD amplitude on RE dynamics
- Effective role of edge fluctuations on RE loss

1.8 Outline of the Thesis

This thesis presents the results of dedicated experiments exploring the dynamics of runaway electrons in ADITYA/ADITYA-U tokamak. The runaway electrons are highly energetic electrons which are collisionally decoupled from the rest of background thermal plasma, accelerate to high energies in presence of a parallel electric field and may form intense beams ($\sim 10 - 100\ MW$) which can destroy any material in its way. Chapter-1 has been written as a general introduction for non-expert readers to establish the concept of a tokamak, runaway electrons, and phenomena affecting the dynamics of runaways in a tokamak namely, magnetohydrodynamics and edge electrostatic fluctuations, which will lay the foundation for rest of the thesis. Chapter-1 also includes a brief review of prior research work on runaway electrons and motivation for the experiments described in this thesis. Chapter 2 describes the ADITYA tokamak, its transformation to the ADITYA-Upgrade tokamak, experimental methods and the various diagnostic techniques used for studying runaway electrons during the current flat top. This chapter includes the details of the Langmuir probes designed and developed to study the edge plasma dynamics in ADITYA-U.

The sawteeth (MHD) instability generated/accelerated REs and their radial transport in the presence of two magnetic islands as observed and studied in ADITYA/ADITYA-U is presented in Chapter 3. In Chapter 4 the Dynamics of 2/1 drift tearing (MHD) mode and its impact on RE dynamics in ADITYA and ADITYA-U tokamak is described. Chapter-3 also includes the results from experiments where the mode rotation frequency and amplitude of m/n = 2/1 mode have been varied in a controlled way during a plasma discharge to study its effect on REs dynamics. Chapter 5 discusses the novel experimental results and analysis suggesting a significant role of edge fluctuations on the RE dynamics. The effect of the REs on neutral hydrogen dynamics in ADITYA/ADITYA-U tokamak is also presented, which has been observed due to the modification of edge fluctuations during a discharge and its subsequent effect on the REs. Finally, the results of various RE experiments conducted in ADITYA/ADITYA-U tokamak are summarised in Chapter 6 along with the future scope of this thesis work.

Chapter 2
The ADITYA and ADITYA-Upgrade Tokamak

In this chapter, a basic concept of Tokamaks, and details about its sub-systems has been presented. This chapter also provides details of ADITYA tokamak, confinement time study of high parameter discharges from ADITYA as well as diagnostics used in studies presented in this thesis. During the course of this thesis work, the upgrade of ADITYA to ADITYA-U has been carried out and most of the studies presented in this thesis have been carried out in both ADITYA and ADITYA-U tokamaks. A brief section consolidating the upgrade process and ADITYA-Upgrade tokamak details have also been reported. Finally, the details of the design and installation of a set of Langmuir probes have been presented.

2.1 Tokamak

In a fusion reactor, the helical B fields required for plasma confinement can be generated entirely through external field coils (stellarator concept) or through a combination of external field coils and B fields generated by the plasma current (tokamak concept). The tokamak is the most promising [1], well-developed and studied magnetic confinement concept due to its relative simplicity and successes in achieving high fusion triple product, which is a necessary criterion to achieve economically viable fusion. A schematic of tokamak machine is presented in figure 2.1.

2.1.1 Lawson / Ignition Criterion

The criterion derived by Lawson [20,31,122], also known as the break-even condition, is the condition on plasma density, temperature and confinement time, for which the total fusion power generated by D-T reaction is equal to the external power that heats the plasma in a fusion reactor. The criterion is :

$$n\,T\tau_E > 5 \times 10^{21} s.keV.m^{-3} \qquad \text{...(2.1)}$$

where n is the ion density, T is the ion temperature and τ_E is the energy confinement time. When the total fusion power generated exceeds the heating power and heat loss in a fusion reactor, the ignition condition is achieved and $Q = \frac{P_{Fusion}}{P_{Heat}} > 1$. The optimal temperature for the plasma in a fusion reactor is around 15 keV. To maximize the density and confinement plasma is confined in magnetic traps of different configurations, amongst which the tokamaks are most advanced.

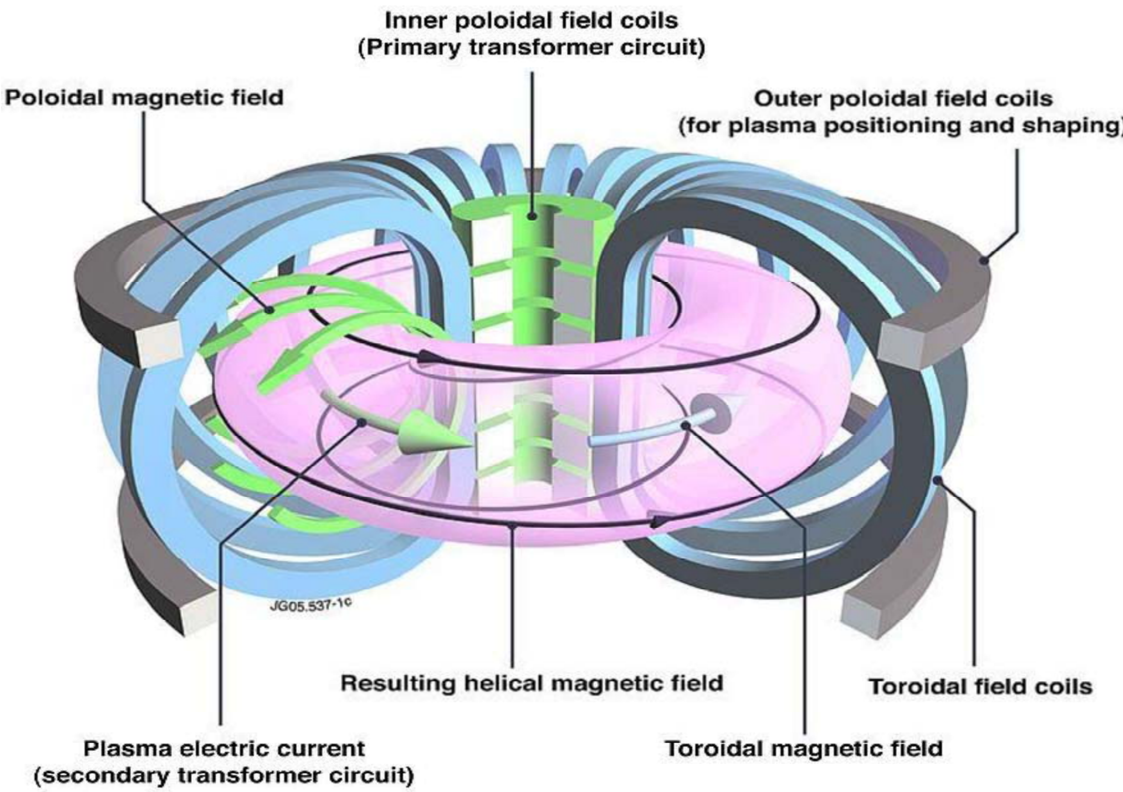

Figure 2.1: Schematic of a tokamak showing different coils, magnetic field and plasma current. P.C.: euro-fusion.org

2.1.2 Magnetic confinement in Tokamak

In tokamaks, magnetic fields are used to confine the plasma since the charged particles follow the field lines due to the Lorentz force ($F = q\vec{v} \times \vec{B}$). To get rid of the end losses the field lines are closed, which requires a toroidal geometry. The smaller poloidal cross-section is defined by minor radius (a) and the larger toroidal cross-section is defined by major radius (R) in a tokamak as marked in figure 2.2. The vacuum chamber is a torus, wrapped by poloidal (TF) coils generating magnetic field along the toroidal direction) as shown in figure 2.1. The axial toroidal magnetic field, $B_T \sim 1 - 8\,T$. Due to the toroidal geometry the B_T decreases with increasing major radius (R), $B_T \sim \frac{1}{R}$, hence the inboard poloidal cross-section at smaller R is called high field side and the outboard side is called low field side. Because of this gradient in the B field, the charge-dependent grad B drift ($\nabla B \times \vec{B}$) separates ions and electrons vertically and creates an electric field (E) perpendicular to B_T. The ∇B drift, along with the drift caused by centrifugal force acting on the charged particles due to curvature of the magnetic field, is given as

$$v_{R+\nabla B} = \frac{m}{q}\frac{\vec{B} \times \nabla B}{B^3}\left(\frac{1}{2}v_\perp^2 + v_\parallel^2\right) \qquad \ldots(2.2)$$

where $v_\perp$ is the perpendicular thermal velocity and $v_\parallel$ is the toroidal velocity. The vertical E field thus form exerts a charge independent $E \times B_T$ force on plasma can cause a collective radial motion of plasma towards the outer wall with a drift velocity given as [123]:

$$v_{E\times B} = \frac{\vec{E} \times \vec{B}}{B^2} \qquad \ldots(2.3)$$

These drifts in tokamak have been schematically represented in figure 2.2. The toroidal plasma current (I_p) resolves this issue by generating a poloidal magnetic field (B_θ), which adds a twist/ helicity to the toroidal magnetic field as shown in figure 2.1. The poloidal magnetic field counters the charge separation by short-circuiting it and inducing a poloidal current flow of charged particles. The plasma current is driven by the application of a toroidal E field generated by the ohmic coil which lies in the central bore of the tokamak as shown in figure 2.1.

The resultant magnetic field lines due to the TF coils and the plasma current have helical geometry, $= \sqrt{B_T^2 + B_\theta^2}$. Electrons and ions spiral along the helical magnetic field lines and experience a continuous change in the magnetic field, and consequently, the drifts caused by the separation of charges will only persist for a short time before being reversed, and in the time average they will cancel out. Figure 2.2 shows the orientation of the toroidal field, charge separation and different drifts in poloidal cross-section

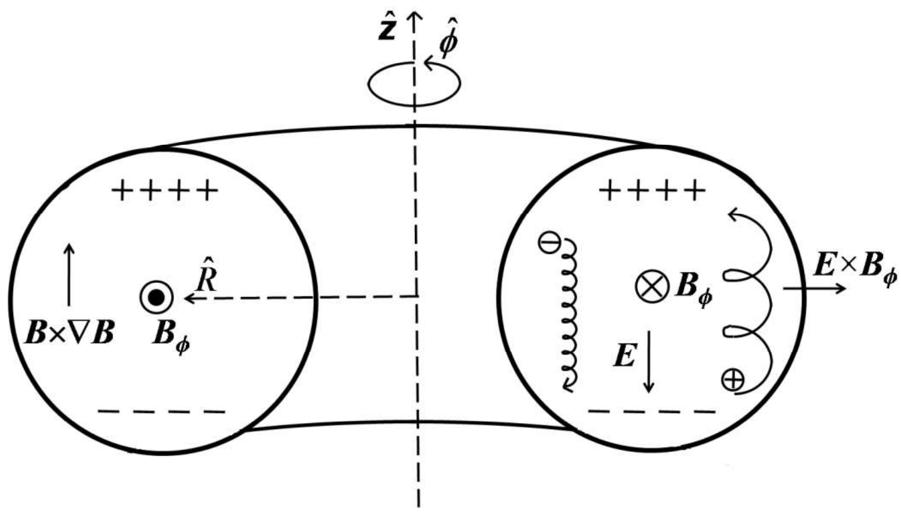

Figure 2.2: Tokamak schematic showing orientation of the toroidal field, charge separation and different drifts in poloidal cross-section

The helicity or the pitch of the field lines is the ratio of the number of toroidal turns (n) traversed by a field line to the number of poloidal turns (m), $\iota = n/m$. The the inverse of rotational transform $q = \frac{1}{\iota}$, is generally used to characterize the field lines and can be calculated as [124]

$$q = \frac{rB_T}{RB_\theta} \qquad ...(2.4)$$

where r is the radial location of the respective flux surface and R is tha major radius.A magnetic field line with rational q value closes on itself after a finite number of toroidal turns, such magnetic surface is called a rational flux surface as shown in figure 2.3. The field lines with irrational q values do not close on themselves, and thereby form magnetic surfaces with infinite turns. The electrons and ions gyrate about the field lines forming the flux surfaces, with a gyration radius

$$r_L = \frac{mv_\perp}{q_c B} \qquad ...(2.5)$$

where m and q_c are the mass and charge of the charge species respectively and $v_\perp$is their thermal velocity. The ion Larmour radius is quantized as the minimum separation distance between two adjacent magnetic flux surfaces. These nested toroidal flux surfaces together form a magnetic cage which confines the plasma in a tokamak and restrict the perpendicular/radial loss to the periphery.

The q value of any flux surface is of great importance as it determines its stability, and the q value of the last flux surface (q_{edge}) essentially determines the stability of the whole plasma column, hence also termed as a safety factor. Higher q_{edge}values offer better stability against MHD instabilities, although they come at the expense of a lower plasma current. Therefore, the tokamak operation is optimised attain maximum current while avoiding low n MHD disruptive kink instabilities, which are prone to be excited at ration q surfaces (explained in section 2.2). For standard aspect ratio tokamaks, this current limit is typically set by external kink mode and is usually violated when q_{edge} ≤ 2 [10,27].

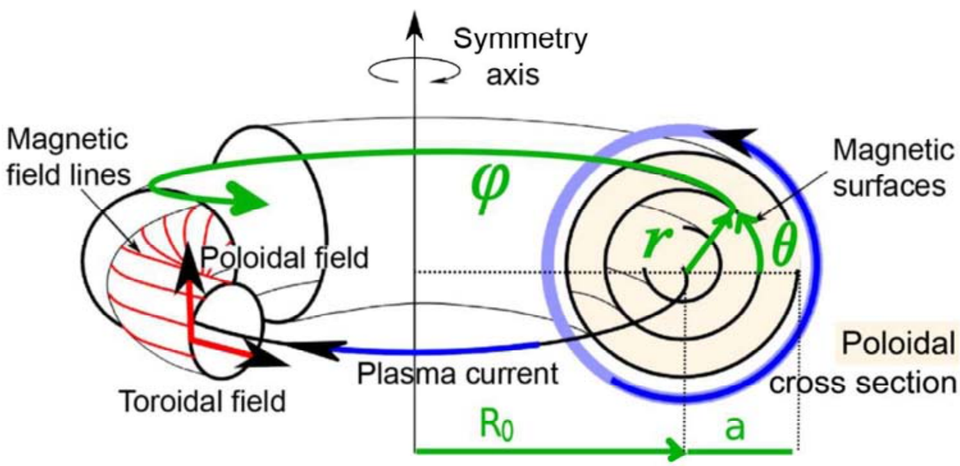

Figure 2.3: Plot showing flux surfaces, toroidal, poloidal and radial coordinates, major and minor radius in a tokamak

Due to the toroidal geometry of tokamak, the poloidal magnetic flux is concentrated more on the inner high field side, due to smaller surface area for each flux surface as compared to the outer low field side with a larger surface area. To even out this asymmetry the centroid of the flux surfaces are displaced outward by a distance (Δ_s) with respect to boundary flux, and is known as the 'Shafranov shift' [10,125]. This shift is controlled by imposing a vertical magnetic (B_V) field generated by external poloidal field coils (as shown in figure 2.1), to maintain the plasma equilibrium by providing the necessary force inward ($j \times B_V$) to counterbalance the horizontally expanding plasma column due to the plasma pressure and magnetic forces. Figure 2.4 shows nested flux surfaces with different helicity with their centroid displaced by Grad Shafranov shift.

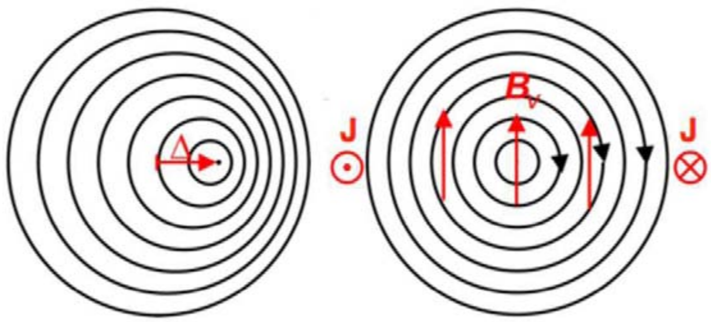

Figure 2.4: Poloidal schematic of (a) flux surfaces in a tokamak with shifted centroids (b) flux surfaces after application of vertical magnetic field B_V.

2.1.3 Tokamak Equilibrium

Plasma equilibrium and instabilities are generally described by the magnetohydrodynamics (MHD) theory, which is a valid approach for high-temperature plasmas, as the electrical conductivity increases with electron temperature T_e $\left(\sigma \sim T_e^{\frac{3}{2}}\right)$ and for timescales that are short with respect to a typical current-redistribution time. The MHD theory treats the plasma as an ideal fluid with infinite electrical conductivity. It includes the continuity equation, the momentum equation, the equation of state and Maxwell's equations along with Ampere's equation [28,34,126].

$$\frac{\partial \rho}{\partial t} + \nabla . \rho \mathrm{v} = 0$$ *Mass continuity:* ...(2.6)

$$\rho \frac{\partial \mathrm{v}}{\partial t} = j \times B - \nabla \mathrm{p}$$ *Momentum continuity:* ...(2.7)

$$\frac{d}{dt}\left(\frac{p}{\rho^{\Gamma}}\right) = 0$$ *Equation of state* ...(2.8)

$$E + \mathrm{v} \times B = \eta j = 0$$ *Generalized Ohms Law (Ideal MHD ,η = 0):* ...(2.9)

$$\nabla \times E = -\frac{\partial B}{\partial t} \qquad \textit{Faraday's Law:} \qquad ...(2.10)$$

$$\nabla \times B = \mu_o j \qquad \textit{Ampere's Law:} \qquad ...(2.11)$$

$$\nabla . B = 0 \qquad \textit{Gauss's Law:} \qquad ...(2.12)$$

where E is the electric field, B the magnetic field, j the current density, ρ the mass density, v the fluid velocity, p the pressure, $\Gamma = 5/3$ and $d/dt = \partial/\partial t + v \cdot \nabla$ is the convective derivative. These equations can well describe the magnetic equilibrium of plasma in the presence of an electric and magnetic field. For tokamak equilibrium (static), the velocity v and its derivative $\partial v/\partial t$ in equation 2.7 are assumed to be zero, thus giving the ideal MHD force balance equation [10,34,127]

$$j \times B = \nabla \mathrm{p} \qquad \textit{Force balance equation:} \qquad ...(2.13)$$

The equations show that the plasma pressure gradient force $\nabla \mathrm{p}$ is balanced by the magnetic force $j \times B$ in the equilibrium in static equilibrium. Also taking the dot product of equation 2.13 with B and p , we find that

$$B.[j \times B] = B.\nabla \mathrm{p} = 0 \qquad ...(2.14)$$

$$j.[j \times B] = j.\nabla \mathrm{p} = 0 \qquad ...(2.15)$$

It means that the magnetic flux surfaces are isobaric in nature (p= constant) and the current density is also constant at every flux surface. These ideal MHD equations describe the basic equilibrium as well as dynamics of tokamak quite well. Due to the toroidal geometry, and presence of strong gradients in current density, magnetic field and plasma density in the tokamak equilibrium is a naturally unstable system, which continually tries to expand radially out. Most of the tokamak research revolves around understanding and overcoming these instabilities by external means/technology.

2.1.4 Heating in Tokamak

The plasma current is an essential component of the tokamak equilibrium and is driven by transformer action through an ohmic coil situated at the central bore of the vacuum vessel. The plasma inside vacuum vessel acts as the secondary winding in which the ohmic E field is induced. The ohmic E field also serves additional purposes of initially ionizing the working gas and subsequently heating the plasma by ohmic heating power, $P_{OH} = R_p . {I_p}^2$ (where R_p is the electrical resistance of the plasma torus and I_p the plasma current). As required by Lawon criterion heating plasma to $\sim 10\ keV$ is essential to achieve fusion. However, ohmic heating alone cannot heat plasma enough to achieve fusion like condition due to MHD limitation on maximum plasma current. Secondly, the R_p and hence the ohmic-heating power decreases proportionally with ${T_e}^{3/2}$, where T_e is the plasma temperature [10]. Therefore, additional heating schemes like the injection of energetic neutral particles [128] and injection of electromagnetic power [22,129] to plasma are used to achieve and maintain a desirable temperature. Fast neutral particles cross the magnetic field unimpeded, gets ionized by collisions, and then transfers their energy to the plasma. Owing to the Lorentz force, injection of EM waves causes oscillations of the plasma particles, which is then transferred to background plasma via thermalization. This coherent oscillation energy transfer is maximized by tuning applied electromagnetic waves to specific frequencies of ion or electron cyclotron frequencies, which leads to resonance (strong wave energy absorption) and efficient plasma heating. These heating methods are collectively called auxiliary heating, $P_{tot} = P_{OH} + P_{aux}$. The total energy W of the plasma increases at a rate $\frac{dW}{dt} = P_{tot} - \frac{W}{\tau_E}$, where the last term accounts for losses (by convection, conduction, and radiation) characterized by τ_E, the so-called energy-confinement time. The energy loss rate in a tokamak is much greater than the classical diffusion.

2.1.5 Particle transport in Tokamak

As described in section 2.1.1, in a tokamak, plasma is confined in the nested magnetic surfaces. In the zeroth-order approximation, while moving along the nested surfaces, trajectories of particles on the inner surfaces do not mix up with those on the outer surfaces. In the central region, high-temperature plasma is confined and separated from the cold plasma at the edge. Plasma parameters (temperature and density) gradually decrease from center to the edge[10,12]. This inhomogeneity in the plasma significantly degrades the plasma confinement. Primarily, the plasma energy and density are lost due to a temperature gradient, density gradient, electric fields and gradients in a magnetic field. Particles travel across the B field to the walls along the gradients by diffusion. In straight cylindrical plasma diffusion understood in terms of Coulomb collisions and called as ‘classical transport’. In classical transport particles suffer collisions with a collision frequency ν and collision allows the particle to diffuse at step length equal to the Larmour radius, r_L . This gives a diffusion coefficient $D_{\perp} \sim \nu r_L^2$ and hence diffusion coefficient across the magnetic field scaled as $1/B^2$. A comprehensive theory based on inter-particle collisions of particle and energy transport for toroidal system with magnetic surfaces has been studied in detail by Hinton and Hazeltine [25]. In toroidal plasma, transport fluxes enhance above the straight cylinder geometry because of internal convective flows and loss of poloidal symmetry because the toroidal field is stronger on the inside than on the outside of the torus, and is described by ‘neoclassical transport’ which incorporates the toroidal effects [10,24,26]. In tokamaks, the measured values of transport across the magnetic field in tokamaks often exceed the losses predicted by the classical or the neo-classical theories and therefore called as anomalous transport, which is not completely understood. It is believed that these additional losses are probably due to the growth of one or more of the instabilities to which tokamak plasmas are theoretically prone. The tokamak equilibrium is indeed linearly stable against large variety of known modes. However, the nonlinear consequences of such instabilities numerically challenging to calculate, a difficulty exceeded by that of experimentally measuring fluctuating quantities and their correlation in tokamak plasma. The anomalous transport in plasma is believed to arise from turbulent diffusion caused by electrostatic or electromagnetic fluctuations caused by micro-instabilities. The presence of magnetic islands which short circuit two flux surfaces at different radial location also enhances the particle transport and decreases the achievable confinement time [27]. The origin of these islands will be described in the coming sections.

2.2 Magnetohydrodynamic Instabilities

In a state of equilibrium, the plasma pressure is well balanced by the magnetic forces. Any perturbations to this state which occur inevitably in real systems change the force balance. These perturbations are represented in the following form [10,34,126]:

$$\xi = \xi_0(r).\cos(m\theta + n\phi - \omega t), \qquad \text{...(2.16)}$$

where $\xi_0(r)$ is radial displacement component, m is the poloidal mode, n is the toroidal mode and ω is the mode rotation frequency of the magnetic perturbation. These perturbations occur under suitable conditions and may grow and lead to the growth of MHD instabilities at mode rational surfaces. If not controlled they often lead to sudden violent termination (quench) of the plasma current, the so-called disruption. These MHD instabilities strongly affect particle transport and plasma confinement. Several studies have indicated that the MHD activity has a strong effect on the RE dynamics [88,93–96]. Tokamak plasma is prone to a variety of macroscopic instabilities due to the presence of free energy sources due to (1) *current gradient* and (2) *pressure gradient* in combination with *adverse magnetic field curvature,* inherent to the tokamak scheme, which is converted into kinetic energy to drive MHD instabilities. These instabilities are divided into two categories: (i) *Ideal modes*- which grow in a perfectly conducting plasma, and (ii) *Resistive modes*- which survive due to the finite resistivity of the plasma.

The rational surfaces are prone to various Magnetohydrodynamic (MHD) instabilities, whereas the irrational surfaces are resilient to the MHD instabilities. Also, magnetic surfaces with higher safety factor have better stability and low q rational surfaces are desired to remain sufficiently far from the plasma edge. The MHD equilibrium of plasma is discussed in the next section 2.2.1.

2.2.1 Ideal MHD Modes

Ideal MHD instabilities are fast timescale disruptive instabilities which evolve at Alfven timescales (microseconds) at their mode rational surface (q=m/n). The Ideal MHD provides a necessary but not sufficient condition for the stability of the plasma and describes the stability limits, determined by magnetic energy, thermal pressure, and inertial forces in perfectly conducting plasma placed in a magnetic configuration. The ratio of kinetic pressure to magnetic pressure in a tokamak, called the plasma beta, is the factor determining the growth of ideal MHD modes in plasma. It is also a measure of the efficiency of plasma confinement by a magnetic field. [10,16,130]

$$\beta = \frac{p}{B^2/2\mu_o} \qquad \text{...(2.17)}$$

$$\beta_p = \frac{\langle p \rangle}{\langle B_p \rangle^2 / 2\mu_o} \quad ...(2.18)$$

$$\beta_t = \frac{\langle p \rangle}{\langle B_t \rangle^2 / 2\mu_o} \quad ...(2.19)$$

where, $\beta_p$is the poloidal beta, β_t is the toroidal beta. The fusion power density scales as β^2, which makes high beta operation highly desirable trait for an economically viable fusion device. However, the onset of instabilities places limits on the achievable plasma beta, described by Troyon limit. For circular plasma, it is given as $\beta_N \approx 2.5 - 3.5$, where [10,27,131]

$$\beta_N = \frac{\langle \beta_t \rangle}{I_p / a B_t} \quad ...(2.20)$$

The energy variation principle is widely used for the analysis of the ideal MHD stability of the plasma equilibria , which is based on the idea that any equilibrium is unstable if a perturbation lowers the potential energy of the system. Change in potential energy (δW) of plasma due to a magnetic perturbation ξ is written as: [10,34,126,132]

$$\delta W = -1/2 \int B.\frac{B}{8\pi} + \gamma p_0 (\nabla.\xi)^2 + (\xi.\nabla p_0)\nabla.\xi + \frac{B_1}{\mu_0} - j_0.(B_1 \times \xi) d\tau \quad ...(2.21)$$

where the indexes (0/1) describe the equilibrium and the perturbed quantities respectively.

$$\delta W(\xi^*, \xi) \geq 0 \quad ...(2.22)$$

is a necessary and sufficient condition for plasma equilibrium to be stable. The equation 2.21 indicates that the energy required to perturb the equilibrium magnetic field (either field line bending or compression) are positive and stabilizing. The third and fifth term proportional to the pressure gradient and current density respectively can be negative and may drive instabilities. The instabilities where ∇p_0 acts as a predominating destabilizing factor, lead to pressure-driven modes like interchange modes and ballooning modes [10,34,126]. Similarly, the plasma current gradient may generate current-driven modes, the modes with long parallel wavelengths ($k_{||}$) and macroscopic perpendicular wavelengths ($k_\perp$) ($k_{||}/k_\perp << 1,\ k_\perp a \sim 1$) are the most dangerous and are called kink modes. Depending on the perturbation of the plasma boundary, they can be divided into internal kink modes which are excited well inside the plasma boundary and external kink modes which are excited close to the plasma boundary which can disrupt the plasma. These modes can now be avoided by tailoring the plasma current and pressure gradients in tokamaks. An MHD instability is characterized by (i) poloidal (m) and the toroidal (n) mode numbers that determine its helicity, (ii) frequency of the mode (ω) represents the rotation frequency of the instability (iii) growth and decay of the instability are characterized by the growth rate parameter (γ) and the displacement eigenfunction (ξ) represents the shift of the magnetic field lines due to the MHD mode.

2.2.2 Resistive MHD Modes

Due to the presence of finite resistivity, resistive MHD instabilities (tearing modes) can grow in plasma, which shall otherwise be stable in an ideal scenario. These instabilities often lead to the formation of magnetic islands. For the island growth, field lines must 'reconnect', which requires a finite plasma resistivity in the region where reconnection takes place to change the topology of the flux surfaces [10,34,126,133,134]. The flux tube associated with the island winds around the torus-like the field line itself, kinking the magnetic surface it has manifested on as shown in figure 2.5. The resistive MHD model with finite η suggests that plasma resistivity makes little contribution to the stability of magnetic perturbations in tokamaks, but becomes crucial when ξ lies parallel to the background magnetic field. For a perturbation with wavenumber k this criterion is fulfilled when, $k \cdot B_0 = 0$ at the mode resonant surface with $q = m/n$, where m and n are toroidal and poloidal mode number of the perturbation. The localized resistivity near such rational surfaces determine the stability as well as the growth rate of a mode, which is generally determined by the parameter Δ' which was first defined by Furth et al, such that a positive Δ' means instability [10,34,126,135]. The Δ' is a measure of discontinuity in perturbation flux function ψ in the inner and outside of the resistive mode rational layer and is defined as: [34]

$$\Delta' = \frac{\psi'(r_s+\varepsilon) - \psi'(r_s-\varepsilon)}{\psi(r_s)} \qquad \varepsilon \longrightarrow 0, \qquad \ldots(2.23)$$

where r_s is the mode resonant surface. For $\Delta' > 0$, an instability occurs and generates an island. The discontinuity generally increases with island width and the growth rate of an island may be estimated using Rutherford's equation [136]

$$\frac{dW}{dt} = 1.22\frac{\eta}{\mu}\,\Delta'(W) \qquad \textit{...(2.24)}$$

where η is plasma resistivity and μ is plasma permeability.

Magnetic islands short-circuit flux surfaces and deteriorate the confinement by allowing heat and particles to flow rapidly across the plasma cross-section along the field lines in the island region, rather than by slow diffusion across flux surfaces [10,27]. These islands are known to rotate poloidally with a poloidal frequency of several kHz due to the combined effect of the electron diamagnetic drift and the $E_r \times B_\varphi$drift [137–139]These modes are usually studied with the help of magnetic coils called Mirnov coils. In extreme situations, these modes often stop to rotate and uncontrolled growth of a low mode number tearing mode can lead to disruption with a total loss of the plasma [140–142]. Disruptions can prove catastrophic for devices like ITER [24,106,143,144]and future reactor size tokamaks and hence need to be avoided or prevented in such tokamaks. This limits the operational space for tokamaks with tearing modes, particularly their high beta and low collisionality counterpart, the neoclassical tearing modes (NTMs), providing a limiting factor on the plasma beta [10,27,145] The growth rate, saturation, and stability of tearing modes have therefore received extensive attention both experimentally [146–148] and theoretically.

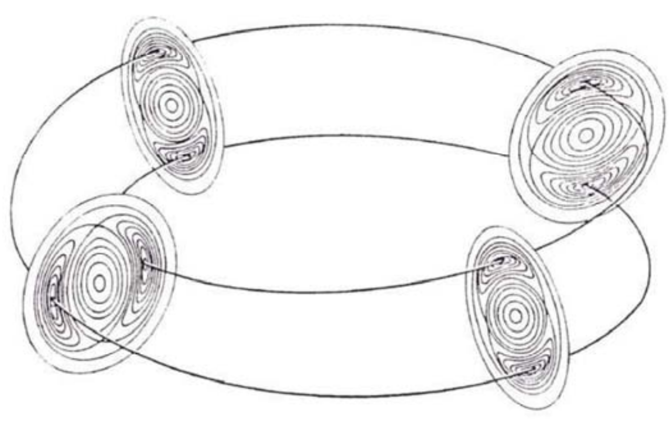

Figure 2.5: Example of a m/n=2/1 tearing mode spatial structure.

Several linear [135,138,139,149,150], as well as non-linear resistive MHD theories [32,33,43], have been put forward to understand the growth and saturation of these modes. These studies suggest that, in low beta tokamaks, the classical resistive tearing modes are driven by unfavorable plasma current density gradient and in high beta regimes the neoclassical tearing modes (NTM) driven by the bootstrap current [126,139,151]play pivotal roles. The classical resistive tearing instability, a purely growing mode, changes its character when electron pressure gradient effects are important [152–154]. In the regime where the electron diamagnetic frequency is larger than the tearing mode growth rate, the growth rate of the unstable mode is significantly reduced. In this so-called linear 'Drift-tearing' regime, the magnetic islands rotate in the electron diamagnetic drift direction with frequencies close to the diamagnetic drift frequency, ω^* [146]. In the non-linear phase, the pressure gradient around the magnetic islands is flattened and the diamagnetic drift frequency is modified. The amount of flattening depends on the perpendicular transport and the electron temperature. The island width is believed to be closely linked to the island rotation frequency [137,146,155]. Experimental evidence suggesting a significant role of the magnetic island/MHD modes on RE dynamics have also been observed in several tokamaks like TEXTOR [33,156]COMPASS [60]and ADITYA [58,157]. The RE loss seems to be closely related to the magnetic topology of the plasma. However, it is not clearly understood so far. Numerical Simulations integrating MHD and RE dynamics are extremely expensive therefore dedicated experiments exploring the dynamics of REs in presence of MHD modes are very important to understand the complete RE dynamics. This thesis explores various MHD modes observed in ADITYA and their effect on RE dynamics as well.

2.2.3 Neutral Dynamics

There exist different sources of neutral in a tokamak, passive source (particle recycling from the material surface) and active source (gas-puffs/SMBI/pellet injection). However, the amount of gas in the wall is large compared with that in the plasma, therefore the recycling is considered to be a significant fueling source in tokamaks. Wherever they come from, they enter in the plasma and interact with plasma particles and decide the global plasma parameter of a discharge. Also, understanding of neutral particle dynamic in a tokamak is very essential since it contributes to alter the edge parameter and then influence the plasma performance. Furthermore, it provides a deeper insight into the formation of edge transport barrier in H-mode plasma [158] Furthermore, it can be effective to achieve active density control via neutral particle recycling [159] The neutrals are known to affect the energy and particle fluxes to the vessel wall diverter plates and/or limiter tiles, which lead to wall erosion and production of impurities [160]. Experiments and simulations [161–166], to achieve a fair understanding of neutral particle transport is being pursued worldwide in many tokamaks such as JET, TFTR, DIII-D, TEXTOR, ADITYA, etc. As for example, Colchin R.J. et al [40] measured neutral hydrogen density near X point in the DIII-D tokamak. There are various simulation codes available to study the edge neutral particle dynamics. It is well known that the charged plasma species are typically treated via fluid models while the neutral species are typically treated via Monte Carlo techniques. So the neutral particle transport codes are coupled with the plasma fluid codes to describe the complete edge plasma behavior in different tokamaks. The widely used codes are B2-EIRENE [167], DEGAS2-UEDGE [168], SOLPS-ITER [169].

2.2.4 Electrostatic fluctuation

The edge of a tokamak plasma is turbulent in nature and believed to be mostly dominated by electrostatic turbulence. The particle diffusion in a tokamak should follow the neoclassical transport theory, in the absence of turbulence and there should have been no confinement degradation. Unfortunately, experiments have shown that the observed electron transport is about one order of magnitude larger than the neoclassical value, which is attributed to electrostatic micro-turbulence driven by temperature and pressure gradients. A number of experimental scenarios that lead to improved confinement such as L–H transition phenomenon triggered by a sufficient level of auxiliary heating of the plasma are linked to suppression of edge turbulence and creation of transport barrier (pedestal) due to the enhancement of $E \times B$ shear, near the plasma edge. The edge fluctuations are studied in this thesis with the help of Langmuir probes. Gas puff induced concomitant suppression of edge fluctuation has been observed and studied in detail in ADITYA tokamak [170] which lead to improving the particle confinement too. Although the edge dynamic is widely accepted to control the thermal particle transport, the role of these edge fluctuations on RE dynamics has not been explored much. The edge fluctuations suppression due to periodic gas puff has been studied extensively in ADITYA-U and its effect on RE loss has been presented in this thesis.

2.3 ADITYA tokamak (1989-2015)

ADITYA tokamak was a medium-size, ohmically heated, air-core tokamak with a poloidal graphite limiter as shown in figure 2.6 having a major radius, $R \sim 75\ cm$ and minor radius, $a \sim 25\ cm$ [171]. The machine consisted of a stainless-steel vacuum vessel with rectangular cross-section; vacuum pumps; gas fuelling system; pulsed power supply unit; electromagnetic coils for ohmic heating, toroidal magnetic field (B_T), and vertical field (B_v); diagnostics and data acquisition system. The following subsections describe all these sub-systems briefly.

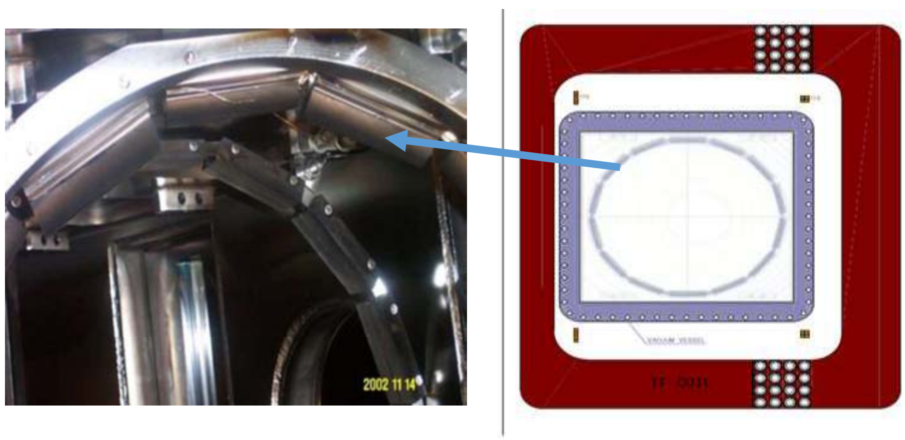

Figure 2.5: Graphite circular poloidal ring limiter of ADITYA tokamak

2.3.1 Vacuum vessel and vacuum system

The vacuum vessel of ADITYA had a rectangular cross-section and was made of 4 quadrants of SS-304L material with a square cross-section of side $60\ cm$. A base pressure of $\sim 10^{-7} - 10^{-8} Torr$ was maintained with four Ultra High Vacuum (UHV) pumping Lines including two Turbo Molecular Pumps (1900 $L/s\ N_2$) & two Cryogenic Pumps (9500 $L/s\ H_2O$) which were backed by rotary pumps with pumping speed of $60\ m^{-3}/hr$. In real conditions the finite amount of oxygen and carbon impurities are always present inside the vacuum vessel, often deposited on the vessel walls. The vessel wall also acts as a large reservoir of the fuel gas, i.e hydrogen (H_2) for ADITYA, which is desorbed during the discharge to provide an excess of fuel, through plasma-wall interaction. The deposited monolayers of impurities are also desorbed during the plasma discharge which can affect the plasma discharge adversely. High level of impurity in discharges also leads to higher runaway electron generation. Therefore, to control and remove impurities deposited on the vessel wall the vacuum vessel, glow discharge cleaning [172] pulse discharge cleaning as well as electron cyclotron resonance cleaning were regularly carried out

2.3.2 Gas fuelling System

The fuel H_2 gas was injected into the vessel from a constant pressure reservoir through fast response piezo-electric valve located at the bottom of the vacuum vessel at a single toroidal location. The vessel was pre-filled at a working pressure of $\sim 10^{-4} - 10^{-5} Torr$ before application of the loop voltage, depending upon the vacuum and impurity level. Thereafter series of short pulses of H_2 gas is injected to the vacuum vessel during the current flat-top. The gas puffing was carried out using a piezo-electric valve ($500\ SCCM\ at\ 100\ V$) located at 10 cm radially (on the bottom port). The voltage applies to the piezo-electric valve. The amount of injected gas is controlled in such a way that there is no significant change in the plasma current and its equilibrium.

2.3.3 Magnetic Coils

ADITYA tokamak contains three principal sets of magnetic field coils namely the TF coils, TR coils and BV coils. In addition, there are two pairs of Fast Feedback Coils (FFB) place symmetrically around the vacuum vessel and within TF coil frames.

2.3.3.1 Ohmic Transformer Unit

The ADITYA tokamak was powered by the central solenoid (TR1) placed at the center of the machine, which generated the toroidal electric field in the vacuum vessel by transformer action. Loop voltage (V_L) $\sim 15 - 25\ V$ was induced by the central solenoid for $2 - 4\ ms$ for a gas breakdown. It was gradually decreased over $30 - 40\ ms$ during the plasma current ramp-up and thereafter maintained at $1.5 - 2.5\ V$ during the current flat-top phase. The vertical (B_z) component of the magnetic field induced by TR1 passing through the plasma cross-section act as an error field. This error field was minimized with the help of compensation coils TR2, TR3, TR4 and TR5 coils which were placed in the toroidal plane, at a symmetrical distance from the mid-plane (Z=0) in the vertical direction. All the compensation coils were connected in series with central solenoid TR1 coil and powered by ohmic pulse power supply. A schematic of these coils is shown in figure 2.7.

2.3.3.2 Toroidal field coils

There were 20 TF coils, each weighing $\sim 500\ kg$in ADITYA tokamak. Each of the TF coils had a rectangular cross-section, with a bore of $0.78\,m \times 0.9\,m$ and outer dimension $of\ 1.03\,m \times 1.26\,m$, made up of two C sections (Fig. 2.5 (b)). The C-sections, consisting of 6 turns each, are consolidated (by vacuum pressure impregnation) and are bolted to each other with insulation to avoid turn-to turn contact. The TF coils were placed 18° apart toroidally. The turns of the TF coils were made from ETP copper and epoxy impregnated fiberglass was used for a turn to turn insulation. The TF coils were cooled by passing demineralized (D.M) chilled water through the cooling tubes embedded in and soldered to the inner surface of each turn. These toroidal magnetic field coils were designed to generate a maximum of $B_T \sim 1.5\ T$.

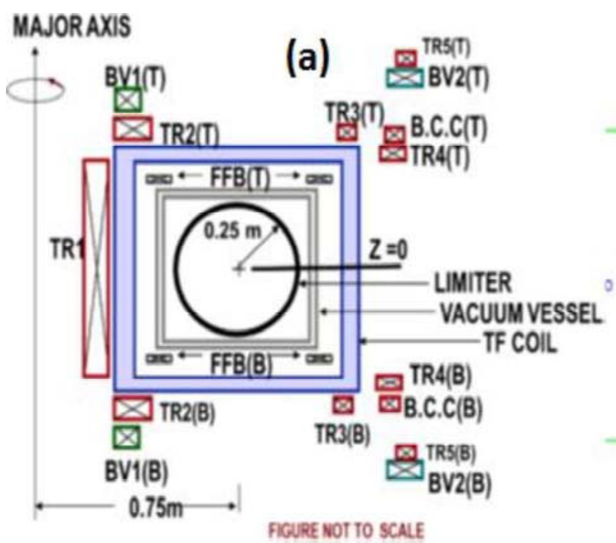

Figure 2.6: Schematic of (a) vacuum vessel and magnetic coils in ADITYA (b) TF coil with dimensions in mm.

2.3.3.3 Vertical Field Coils

The horizontal plasma column shift due to Shafranov shift and hoop forces are compensated by imposing a vertical magnetic field, which is generated by 2 sets of vertical field coils. The vertical magnetic field required for plasma position equilibrium can be approximated as:

$$B_v = -\frac{\mu_0 I_p}{4\,\pi R}\left(ln\frac{8R}{a} - \Lambda - 1/2\right) \qquad \ldots 2.25$$

where $\Lambda = \beta_p + \frac{l_i}{2} - 1$, and l_i is the internal inductance of plasma current. A vertical magnetic field of 4 G/kA was sufficient to maintain the position of plasma current in ADITYA tokamak. figure 2.7 shows the schematic of all magnetic coils as well as the vacuum vessel of ADITYA tokamak. The mechanical and electrical specifications of each coil of ohmic, TF and BV system are shown in Table 2.1.

Table 2.1: design and electrical specification of magnetic coils in ADITYA

PARAMETERS	TR1	TR2	TR3	TR4	TR5	BV1	BV2	TF
No. of coils	1	2	2	2	2	2	2	20
Turns/coil	174	56	3	4	1	60	22	6
Inner Radius (cm)	17.5	28.0	121	150	160	30	155	-
Outer radius (cm)	27.5	49.0	124	156	164	45.2	171.0	-
Vertical Width (cm)	100	15.0	3.6	6.04	2.5	11.2	3.6	-
Resistance/coil (mΩ)	9.4	5.3	0.9	1.5	2.6	11.0	17.6	0.27
Inductance/coil (mH)	5.6	2.2	0.1	0.25	1.2	4.0	4.4	0.05

2.4 ADITYA-Upgrade (2016 – present)

The main objectives of upgradation of ADITYA tokamak are to obtain shaped plasma operation in open divertor configuration. The major alterations in ADITYA-U are tabulated in Table 2.2.

Table 2.2: The major alteration in ADITYA-U from ADITYA tokamak

ADITYA	ADITYA-U
Poloidal Ring Limiter	Toroidal Belt Limiter
Circular Plasmas	Circular / Shaped Plasma
Pre-fixed controls	Real-time controls
$\frac{B_{err}}{B_T} \sim 1.5 \times 10^{-3}$	$\frac{B_{err}}{B_T} \sim 5 - 7 \times 10^{-4}$

As the toroidal field (TF) coils, Ohmic transformer (OT) coils and the main vertical field (BV) coils of ADITYA are reused in ADITYA-U, the machine dimensions remains the same, i.e., major radius R = 0.75 m, minor (plasma) radius, r = 0.25 m and maximum toroidal magnetic field = 1.5 T. Three sets of new divertor coils have been installed in ADITYA-U by replacing the existing rectangular cross-section vacuum vessel of ADITYA with a new circular-shaped vacuum vessel. It has been done to create additional space between the new vessel and TF coils to accommodate additional poloidal (divertor) coils. ADITYA has been dismantled to its base level. Other new components installed in ADITYA-U are: new buckling cylinder, main divertor coils (inner), auxiliary divertor coils, outer divertor coils, fast feedback coils, a toroidal belt of graphite limiters and quarter poloidal limiters at two toroidal locations. The ADITYA-U tokamak is designed to achieve following plasma parameters: circular plasma with a plasma current of $\sim 150 - 250\ kA$, plasma duration of $\sim 250 - 300\ ms$, chord averaged electron density in the range of $3 - 5 \times 10^{19}\ m^{-3}$, and electron temperature of $\sim 500 - 1000\ eV$. In addition, it is designed to achieve shaped plasmas with a plasma current of $\sim 100\text{–}150\ kA$, elongation (k) $\sim 1.1\text{–}1.2$, and triangularity ~ 0.45 [173]. The schematic of all magnetic coils including the new inclusions as well as the vacuum vessel of ADITYA tokamak is shown in figure 2.8.

2.4.1 New Vacuum Vessel of ADITYA-U

The new circular cross-section vacuum vessel of ADITYA-U made up of SS-304L with an inner diameter of 61 cm and a wall thickness of 1 cm [174]. It has a volume of $1.6\ m^{-3}$and a total surface area of $16\ m^{-2}$. The new toroidal vacuum vessel has been designed with two semi-tori having electrical isolation at two junctions [175]. The electrical isolation has been provided by using Viton O-rings at two junctions with inter-space pumping port. In order to accommodate as many numbers of conventional and advanced diagnostics, gas-feed valves, RF systems viz., the ADITYA-U vessel is designed to have 114 direct standard CF and customized ports openings (including 4 tangential ports) on vessel compared to 48 ports in the previous vessel. As per designed criterions, the ADITYA-U vessel has been designed in CATIA-V5 following all the ultra-high vacuum system protocols and the ASME standards. The vacuum vessel is bakable up to $\sim 150°\ C$ using current filaments wrapped around the vessel. Limiter tiles of ADITYA-U are made up of fusion grade high purity graphite IG-430. The toroidal belt limiter ($r \sim 25\ cm$) has been assembled at the high field side, as shown in figure 2.9 (b). At the low field side, one pair of poloidal limiters ($r \sim 25\ cm$) covering 1/4th of poloidal periphery and one poloidal rings of safety limiter ($r \sim 28\ cm$) are installed at different toroidal locations as shown in figure 2.9 (a).

Following the successful assembly, integrated power testing of magnet coils up to the design parameters has been carried out. Following the successful integrated power testing of magnet coils up to the design parameters, basic diagnostics along with data acquisition systems were installed for the plasma operation. After the installation of the plasma-facing component (PFC) in the new vacuum vessel of ADITYA-U, plasma operations have been resumed in the upgraded machine in a graphite toroidal belt limiter configuration with hydrogen plasma. The first discharge in ADITYA-U has been obtained on December 1, 2016. Before the starting of the operations the error field are measured thoroughly. During the intial phase of this thesis work, the author was actively involved in these measurements, hence it is being briefly discussed in the next section.

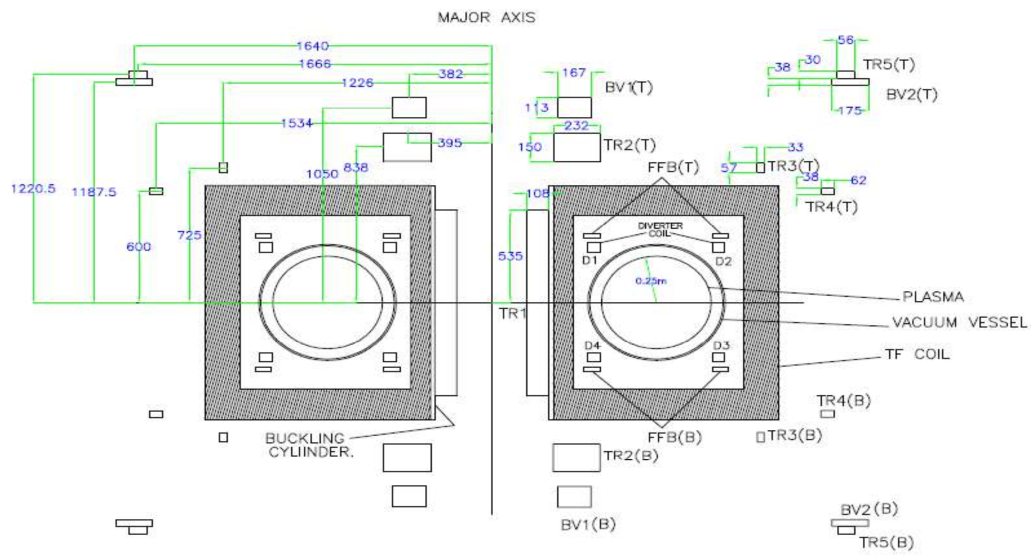

Figure 2.7: Schematic of ADITYA-U tokamak including all magnetic coils and vacuum vessel

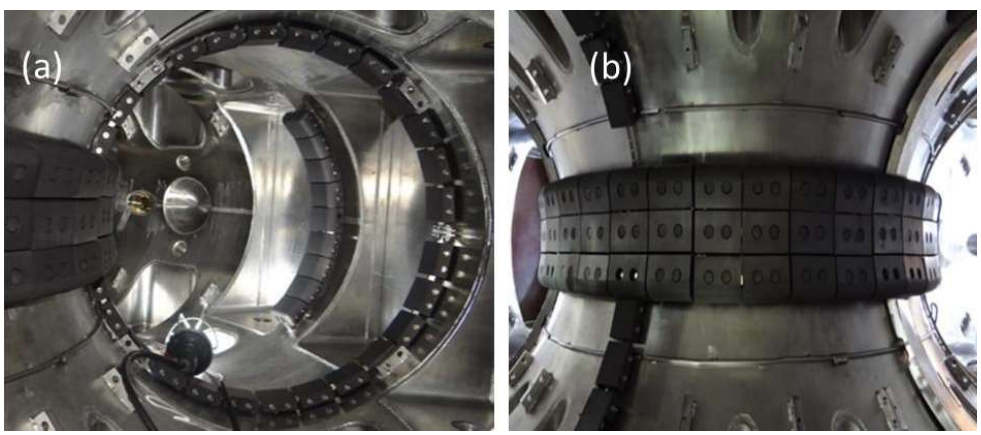

Figure 2.8: (a) Poloidal limiter, safety limiter and (b) toroidal limiter

Magnetic Coil	dR (mm)	dZ (mm)	R(mm)	Z (mm)	No. Of Turns	Max Current (kA)
TR-1	107.50	1040.00	226.25	0.00	174	20
TR-2 (T)	230.5	160.00	395.3	843.00	56	20
TR-2 (B)	230.5	157.00	395.3	-839.52	56	20
TR-3 (T)	34.83	60.00	1223.19	728.06	-3	20
TR-3 (B)	35.16	59.50	1226.00	-727.00	-3	20
TR-4 (T)	64.46	38.20	1534.00	602.09	4	20
TR-4 (B)	65.40	38.67	1530.07	-601.00	4	20
TR-5_1 (T)	34.00	15.50	1627.00	1148.00	-1	20
TR-5_1 (B)	35.00	16.00	1627.00	1147.50	-1	20
TR-5_2(T)_CTC	55.00	13.00	1642.5	1162.50	-1	20
TR-5_2(B)_CTC	55.00	13.00	1642.5	1162.50	-1	20
BV-1 (T)	164.05	120.03	379.81	1052.70	-60	12.5
BV-1 (B)	169.37	117.33	382.00	1051.00	-60	12.5
BV-2 (T)	181.55	38.63	1642.04	1188.50	-22	12.5
BV-2 (B)	179.50	38.00	1641.00	1189.00	-22	12.5
Main Divertor Inner (T)	55.00	65.00	462.5	297	6	25
Main Divertor Inner (B)	55.00	65.00	462	-297	6	25
Main Divertor Outer (T)	28.00	13.12	1062.88	337.5	1	25
Main Divertor Outer (B)	28.14	13.26	1062.88	-337.5	1	25
Aux. Divertor Inner (T)	55.00	21.66	470	430	2	25
Aux. Divertor Inner (B)	55.00	21.66	470.4	-430	2	25
Fast Feedback Inner (T)	29.43	15.20	475	392	1	2
Fast Feedback Inner (B)	29.23	14.96	470	-392	1	2
Fast Feedback Outer (T)	28.14	12.91	1087.5	377	-1	2
Fast Feedback Outer (B)	28.34	13.35	1087.5	-377	-1	2

Table 2.3: Position measurement of all magnetic coils after complete assembly. (T) denotes top coils and (B) denotes the bottom coils.

2.4.2 Error field measurement experiments in ADITYA-U

A dedicated effort has been made to reduce the error magnetic field in ADITYA-U by ensuring precise positioning of the magnetic coils. The losses of electrons due to the error magnetic field in the breakdown phase must be minimized to improve the operation window. The error field measurements are carried out with the help of a triple-axis Hall probe. The total error magnetic field, B_{error}, and its vertical component, B_z inside the vacuum vessel, due to Ohmic coil system, have been measured at two different toroidal locations as a function of radius (R) and height (Z) and estimated for designed value current 20 kA for Ohmic coil. The total error magnetic field B_{error} and its vertical components B_z at different radial location (R) shown figure 2.10 (a) and (b) respectively. The minimum B_z component of error field due to Ohmic coils in ADITYA-U is found to be ~ 0.5 G / 1 kA current in Ohmic coils, which is half in magnitude as compared to error field in ADITYA tokamak [176]. This decrease in the error field has significantly enhanced the operation window in terms of pre-fill gas pressure from $10^{-5}\ Torr$ (in ADI) to $10^{-4}\ Torr$ (in ADITYA-U).

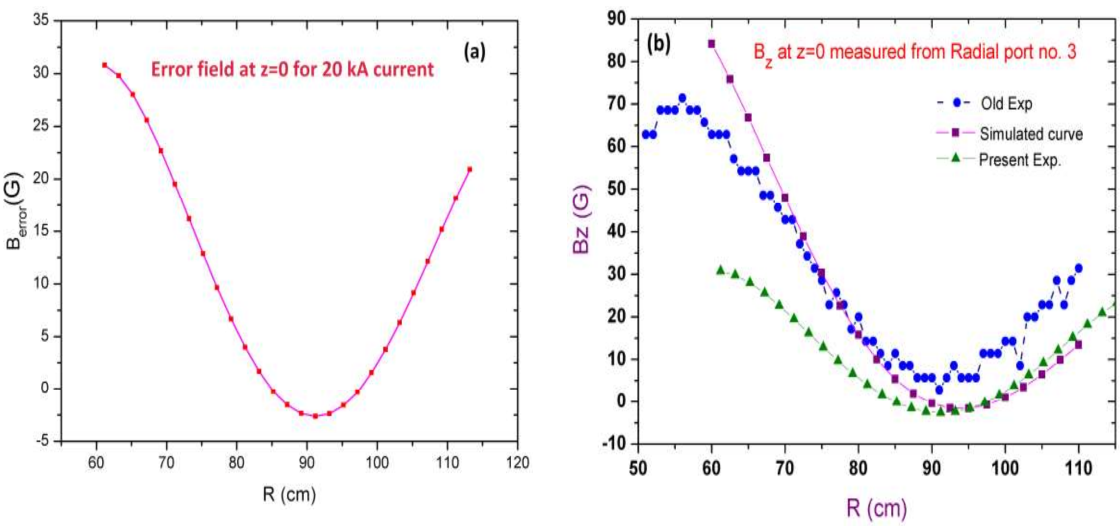

Figure 2.9: (a) Plot showing radial profile of error field at the z=0 plane of the ADITYA-U tokamak. (b) Comparison of error field (B_z) measurement carried out for ADITYA and ADITYA-U tokamak and simulated curve of error field.

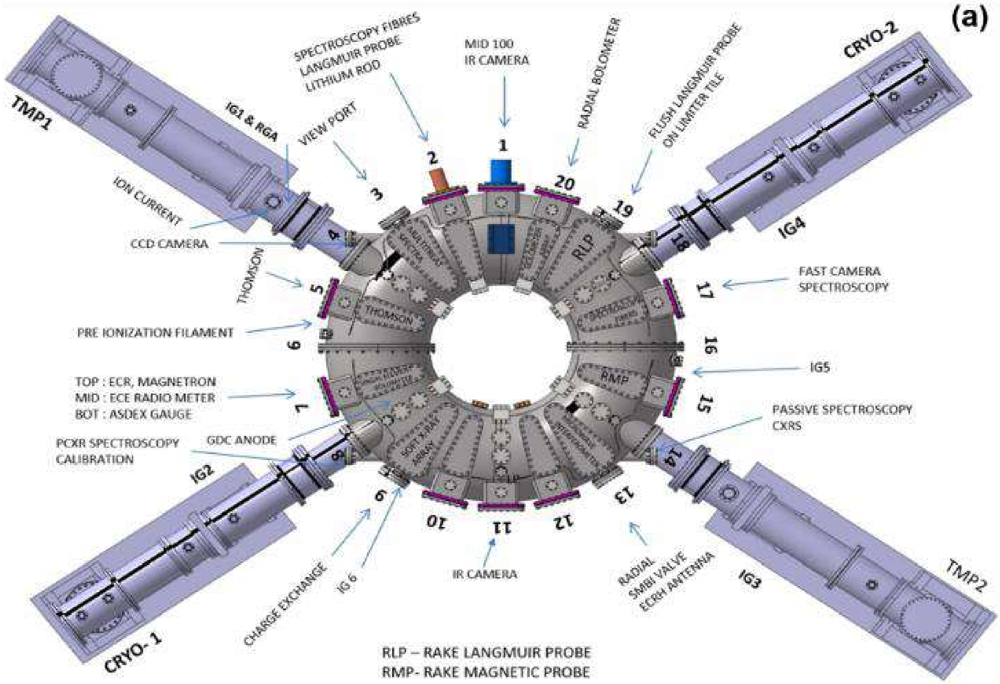

Figure 2.10: Schematic showing location of different diagnostics in ADITYA-U

2.4.3 ADITYA Pulsed Power System (APPS)

The Ohmic coils (TR1- TR5), TF magnet coils (TF1-TF20) and vertical field (B_V) coils of ADITYA and ADITYA-U are powered by a pulsed power system (APPS) which mainly consisted of three pulsed power supplies i.e Ohmic power supply ($\pm 20\ kA, 2\ kV$), TF power supply ($50\ kA, 380\ V$) and Vertical field power supply ($12.5\ kA, 2.2\ kV$). The power supply consists of a 132kV/ 11kV sub-station which includes the reactive power compensation system, pulse shaping units, and the control instrumentation. The waveform defining the magnitude, shape, and duration of current pulses to be applied to the ohmic, TF and BV coils were pre-programmed before each discharge according to the experimental requirements. Waveshaping unit consists of VCB (Vacuum Circuit Breaker), switches, capacitor ($1200\ \mu F, 22\ kV$) resistors ($1.8\ \Omega, 36\ MJ$) which provide 3 steps switching for regulating the loop voltage-time profile as indicated in figure 2.12(c). The mutual coupling between Ohmic coils (TR coils) and BV coils was nullified using an anti-transformer. The AC power is converted to DC by a thyristor-based, air-cooled 12-pulse line commutated converters. The converters led to a ripple noise in loop voltage of ~ 6% with a constant frequency of 600 Hz. Despite its low magnitude, the frequency of ~600 Hz is often observed in several diagnostics channels e.g. Mirnov Coils, Soft X-Ray, microwave interferometer signals, etc. Analog controllers, logic cards and interlocks were provided for operation through Computer/VME interfaces for generating desired current waveforms, as shown in figure 2.12 (c).

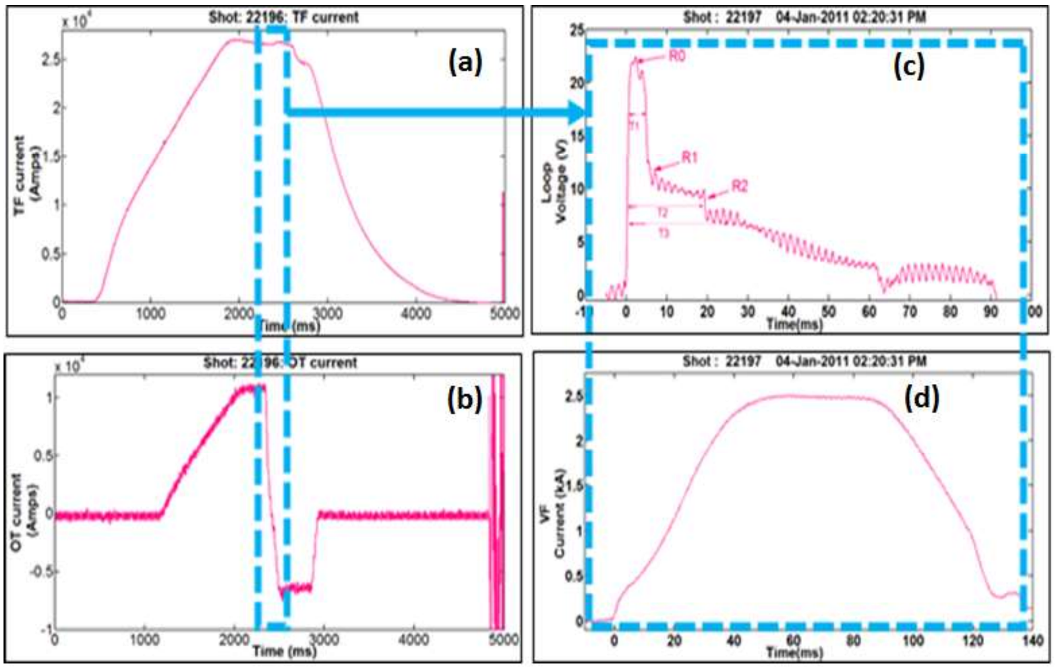

Figure 2.11: Waveform of current applied to (a) TF coil (b) Ohmic coil (c) Loop Voltage and (d) BV coils.

2.5 Diagnostics

The plasma thus generated, confined and heated in ADITYA tokamak are studied with the help of several diagnostics as shown in figure 2.11. The main diagnostics used for the studies presented in this thesis are discussed in this section.

2.5.1 Magnetic measurements

The plasma current was measured with a Rogowski coil wound around the poloidal periphery of the vacuum vessel. The loop voltage is measured with two single turns toroidal pickup coil located at the high field side and low field side of the tokamak. The diamagnetic flux i.e. the difference between the total toroidal flux with plasma and that in the absence of plasma, was used to measure the β_p. It was measured with a pickup loop called diamagnetic loop, poloidally enclosing the plasma and a compensating loop of six turns made of polyimide-insulated wire which shielded the electrostatic pick-up.

2.5.2 Microwave Interferometry

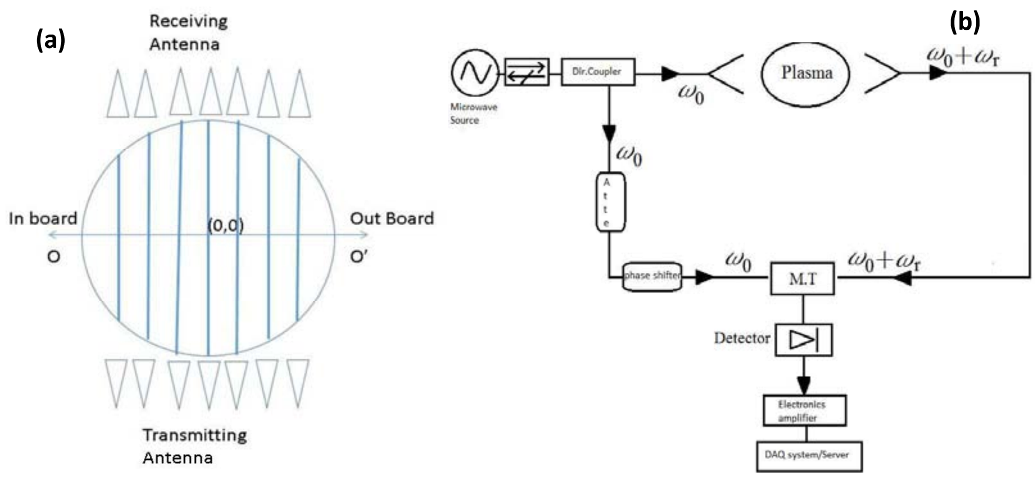

Figure 2.12: a) Schematic showing location of different interferometer chords in poloidal cross-section on ADITYA (b) Block diagram of homodyne interferometer system.

Microwave Interferometer is a powerful diagnostic for measurement of line averaged electron density. An electromagnetic wave experiences a phase difference (ϕ) while passing through the plasma with respect to the reference arm due to change in the refractive index of the medium which is dependent on the plasma density. This phase information gives a line average plasma density $\overline{n_e} = 2\varepsilon_0 m_e c\omega\phi/e^2L$ where ω is the frequency of microwave and L is the path length of the chord. There are two types of technique for phase measurement: (1) Homodyne (2) Heterodyne.

Schematic of a typical homodyne interferometer system is shown in figure 2.13 (a).The system consists of has seven channels viewing plasma at r=-21,-14,-7,0,+7,+14 and 21 cm as indicated in figure 2.13 (a).

A 140 GHz Heterodyne Interferometer system with real-time density signal for density feedback was installed at the top and bottom port of the ADITYA Tokamak. A 140 GHz microwave beam, transmitting from the top port with transmitting antenna, traverses through the plasma, and receiving at the bottom port with receiving antenna. The phase difference between reference and plasma path is measured in terms of phase shift and can measure the density from the phase shift with the help of the above equation.

It is a single channel system, which gives a real-time density signal that can be used for the density feedback of the Tokamak. Schematic block diagram of heterodyne interferometer system is shown in the figure 2.14.

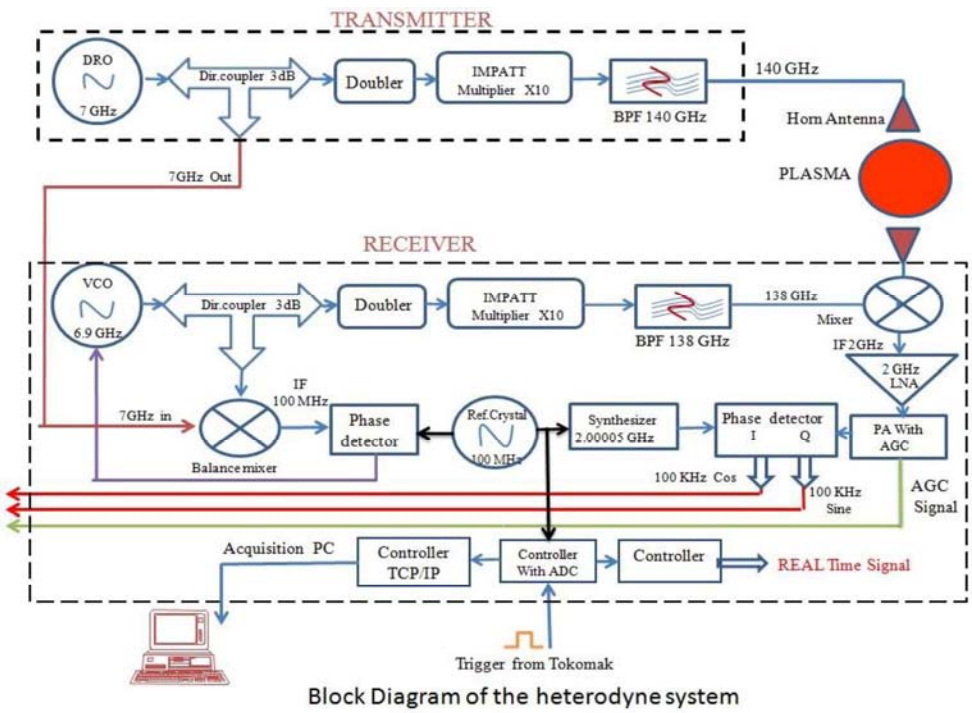

Figure 2.13: Block diagram of heterodyne density measurement system

2.5.3 Soft X-Ray

The Soft-X ray (radiation between 100eV and 10keV) emitted from plasma core is a measure of plasma density and temperature. SXR intensity measurements provide valuable insight/information about the plasma parameters [10,177]. The intensity of Soft-X ray(SXR) radiation is a measure of plasma density (n_e), electron temperature (T_e) and effective ion charge (Z_{eff}). The SXR power detected by the silicon surface barrier diode detectors depends on $exp\left(-\frac{E}{T_e}\right)$ where E is the cut-off energy of SXR for transmission through the metal (Be) foil which depends on the foil thickness [178]. F.C. Jahoda et. al. provided the technique to measure T_e with soft x-ray diagnostic in the year 1960. In this technique, two photodiode detectors with different foil thickness view same plasma volume in such a way that n_e, T_e and Z_{eff} are same in this volume, then ratio of the SXR intensity measured by these detectors provides T_e measurements, which is expressed as follow [178].

$$R = I1/I2 = \exp((E_1 - E_2)/T_e) \qquad \ldots 2.26$$

where R =ratio of SXR intensity

$I1, I2$ are SXR intensity measured by two photodiode detector

$E1, E2$ are cut off energy for metallic foils.

In ADITYA the line averaged electron temperature was measured using the transmission ratios of soft X-ray flux detected by identical detectors through two Beryllium foils of 25 μm and 70 μm thickness [178]

2.5.4 Hard X-ray measurements

In ADITYA the REs were studied by detecting HXRs using a 3 inch NaI(Tl) scintillator detector coupled with photo-multipliers [98]. The lead shielded detector was placed ~5 m away from the vessel at the equatorial plane of ADITYA and collimated to view the limiter cross-section as shown in figure 2.15(b). The detector was calibrated using the standard HXR sources Caesium-137 and Cobalt. The energetic REs emit HXRs with energy less than their kinetic energy via bremsstrahlung, when they interact with the limiter. Owing to the high density of the graphite limiter as compared to the plasma, the contribution of plasma volume generated HXR is negligible as compared to limiter generated HXR. Hence, it is safe to assume that the observed HXR intensity is proportional to the lost REs, which ultimately depends on the total RE population in plasma. Figure 2.15 (a) shows the location and viewing angle of the HXR detector which was same in ADITYA and ADITYA-U tokamak. Figure 2.15(b) presents a cartoon of REs (red line) interacting with the limiter inside the vessel, and emitting photons (black line) which is then detected by the HXR detector.

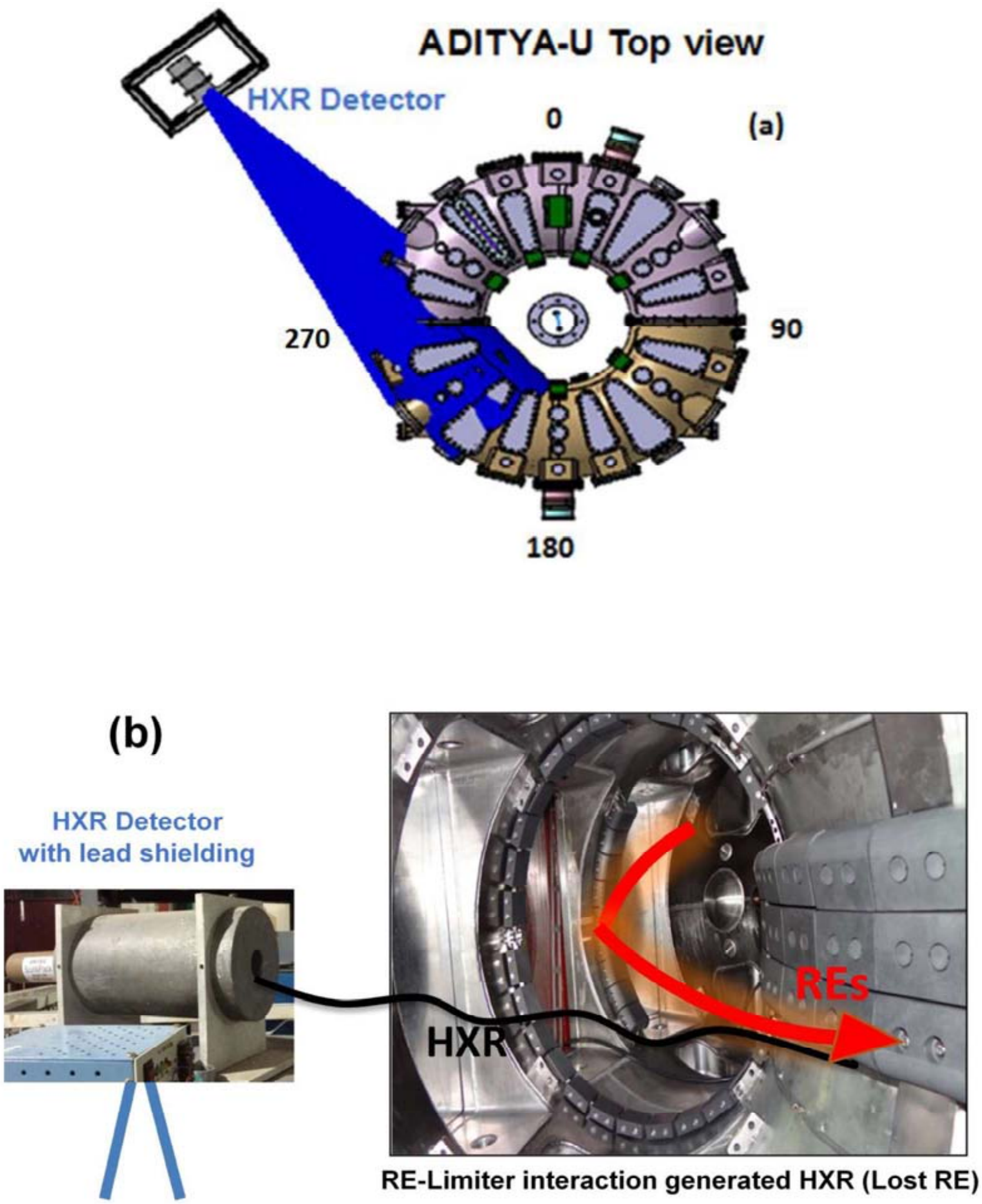

Figure 2.14: (a) Top view of HXR diagnostic viewing ADITYA-Tokamak (with toroidal co-ordinates) (b) Schematic of HXR diagnostic in ADITYA-U

2.5.5 Spectroscopy

The amount and profile of neutrals and impurity species strongly determine as well as get influenced by various phenomena like MHD, particle transport, edge turbulence, etc. Therefore, continuous monitoring of spectral line emission from neutral hydrogen, CIII, and OII ions during a plasma discharge is done to estimate the particle fluxes of these impurity species from various plasma-facing components. Filter based photomultiplier tube (PMT) detectors are used for this purpose. The PMT has multi-alkaline anode layer with peak sensitivity at 450 nm wavelength [179]. Spectral emission was detected by collecting emission from plasma using optical fiber and filtering light using interference filter and fed to PMT. The interference filter had a wavelength bandwidth of 0.5 nm. The applied bias is about 400-500 V and signal voltage gain is optimally kept at 10^6. The temporal evolution of these spectral lines provides information about the impurity contamination and influx in a plasma discharge.

2.5.6 Mirnov Coils

Mirnov coils (magnetic pickup coils) are widely used as diagnostic to study the MHD activity in tokamaks. They detect the voltage induced by magnetic fluctuations $\dot{B_\theta}$ and $\dot{B}_r$ associated with the MHD modes or magnetic islands present inside the plasma. The magnetic islands are known to rotate under a combined influence diamagnetic drift rotation and $E_r \times B_T$ rotation, with several kHz. The change in magnetic flux through the probes due to this poloidal rotation induces a voltage that is detected by the Mirnov coils. Magnetic perturbations strength falls with distance as $\sim r^{-(m+1)}$, where m is the poloidal mode number. By making measurements at different poloidal and toroidal locations the structure of magnetic islands (m, n), as well as their amplitudes and frequencies, can be determined. A poloidal array of 16 Mirnov coils distributed at equal poloidal separation at one toroidal location. These probe signals are acquired at a sampling frequency of $\sim 50\ kHz$. The MHD activities are complex non-linear dynamic processes that determine as well as depend on several other plasma parameters including the REs. Although being a celebrated topic it has been extensively studied theoretically and numerous approximation models are used to describe different MHD events, a complete and accurate picture of MHD instabilities still remains a future goal. Nevertheless the experiments have helped in uncovering many mysteries in tokamak like that of sawtooth oscillations, even in absence of theoretical background. The experiments provide a required set of approximations as well as direction for the theories to be developed. The magnetic islands, which are a manifestation of resistive tearing modes can be studied in great detail with the help of Mirnov coils.

2.6 Diagnostics in ADITYA-U

Most of the diagnostics used in ADITYA-U have the same specifications as in ADITYA e.g. SXR, HXR, bolometer, magnetic diagnostics, spectroscopy diagnostics. Several diagnostics are upgraded and some new diagnostics are installed in ADITYA-U. This includes new Mirnov coils and Langmuir probes. As the Langmuir probe development for ADITYA-U is a part of this thesis work, it has been described in detail.

2.6.1 Mirnov Coils in ADITYA-U

The new machine is equipped with two sets of Mirnov garlands, each of which contains sixteen individual probes that are distributed uniformly at an equal poloidal separation of 22.5^{o}. The probes are made of 176 turns of Kapton insulated copper wire ($d = 6\ mm$), with a rectangular cross-section ($35 \times 15\ mm^2$). The coil inductance (L) ~ $60\ \mu H$ and resistance (R) ~3Ω , and response time (L/R) ~ $20\ \mu s$. The coils are placed at toroidally opposite location inside vacuum vessel in a SS casing at $r\sim\ 28.5\ cm$. Each probe has been calibrated (in-situ) by passing current (10 kA-50 kA) through a toroidal conductor placed at different positions ($r = (0,2,4,8,10) cm$ & $z = (0,4,8) cm$) inside the vacuum chamber and measuring the voltage induced in each mirnov coil. A snapshot of the experimental setup is shown in figure 2.16 (b). Details of the calibration experiment can be found in reference [180]. Figure 2.16 shows the schematic of the Mirnov probes. The data is acquired at a sampling frequency of 100 kHz.

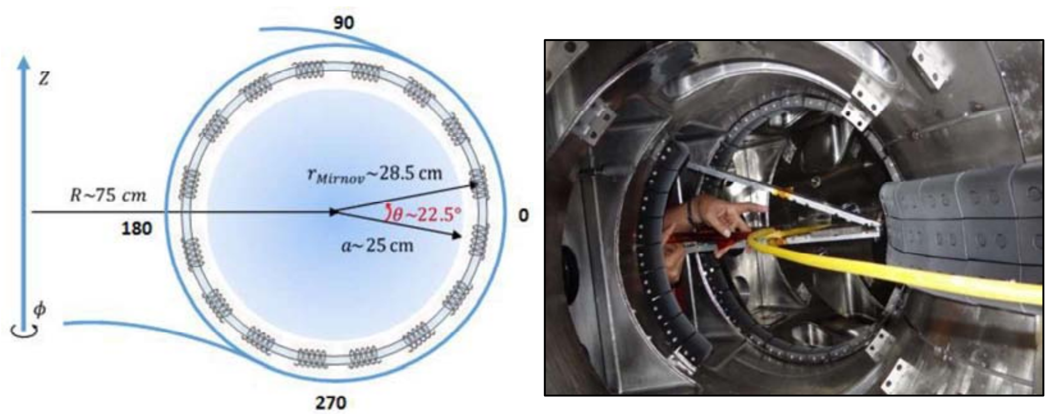

Figure 2.15: (a) Schematic of 1 set of Mirnov garland with 16 coils in poloidal cross section of ADITYA-U (with poloidal co-ordinates) (b) View inside vacuum vessel during Mirnov calibration experiment, showing toroidal conductor (yellow) and its support structure.

2.6.2 Langmuir Probes

Langmuir probe is the simplest, oldest and most widely used probe to study low density and temperature plasma such as the tokamak edge. It was invented by Irving Langmuir and has a history as old as 'plasma' itself. By measuring the voltage-current (I-V) characteristic of metallic tip or wire immersed into the plasma, one can find the density, temperature, and potential of the plasma. A matrix of 15 Langmuir probes arranged in different radial, poloidal, as well as toroidal locations has been designed, developed and installed to investigate the SOL and edge plasma of ADITYA-U. The Molybdenum probes have a mushroom-shaped tip with a diameter $\sim 4\ mm$ (figure 2.17 (d)). Probes are placed inside non-machinable alumina (Al_2O_3) ceramic bushes of different radial length as depicted in figure 2.17 (c).

The probes have been designed to withstand a maximum heat-load possible for edge plasma with $T_e = 50\ eV, n_e = 10^{19}\ \mathrm{m}^{-3}$ for a time duration of ~ 500 ms, which is much higher than the design parameters of ADITYA-U. The ceramic bush is bolted to a support structure consisting of two SS plate with a thickness of 3 mm, extending over one-quarter of the poloidal cross-section at $r \sim 28\ cm$ and bolted to the vessel. Figure 2.17 (a) drawing of one of the SS plates with holes to hold the bolts and Langmuir probe and (b) shows the plate curvature after bending it. The two plates have been designed such that they cover quarter poloidal cross-section inside the vessel at $\sim 28\ cm$ after assembling and bolting to vessel support. The probes were threaded in the bottom and fixed with the help of a check nut which was insulated from the SS plate by a ceramic ring as shown in figure 2.18 (a). Kapton coated copper wire securely connected to probe between the ceramic and check nut of each probe. The wires were secured inside ceramic bead until the port-15, where they were connected to the 25 pin hermetic feedthrough. Figure 2.18 (b) shows complete assembly with 6 probes on plate-1 and 9 probes on plate-2. The assembly was then fixed inside the vacuum vessel. The electrical properties and radial length of each probe were measured inside the vessel after assembly. The details of probes radial, poloidal and toroidal positions of the 15 probes, are presented in the following table 2.4.

Table 2.4: Radial, poloida and toroidal position of Garland Langmuir Probes in ADITYA-U

	Probe location in ADITYA-U		
Probe name	*Radial (r) (cm)*	*Polidal (θ)*	*Toroidal (φ)*
G LP1	24.5	276.132	89.61
G LP2	25	279.672	89.25
G LP3	25	283.212	88.89
G LP4	24.5	286.752	89.61
G LP5	23.9	290.292	89.25
G LP6	24.5	293.832	88.89
G LP7	24.4	327.381	88.11
G LP8	24.6	330.93	87.75
G LP9	25.3	334.479	87.39
G LP10	24.5	338.028	88.11
G LP11	25.3	341.577	87.75
G LP12	24.5	345.126	87.39
G LP13	25.3	348.675	88.11
G LP14	25	352.224	87.75
G LP15	24.8	355.773	87.39

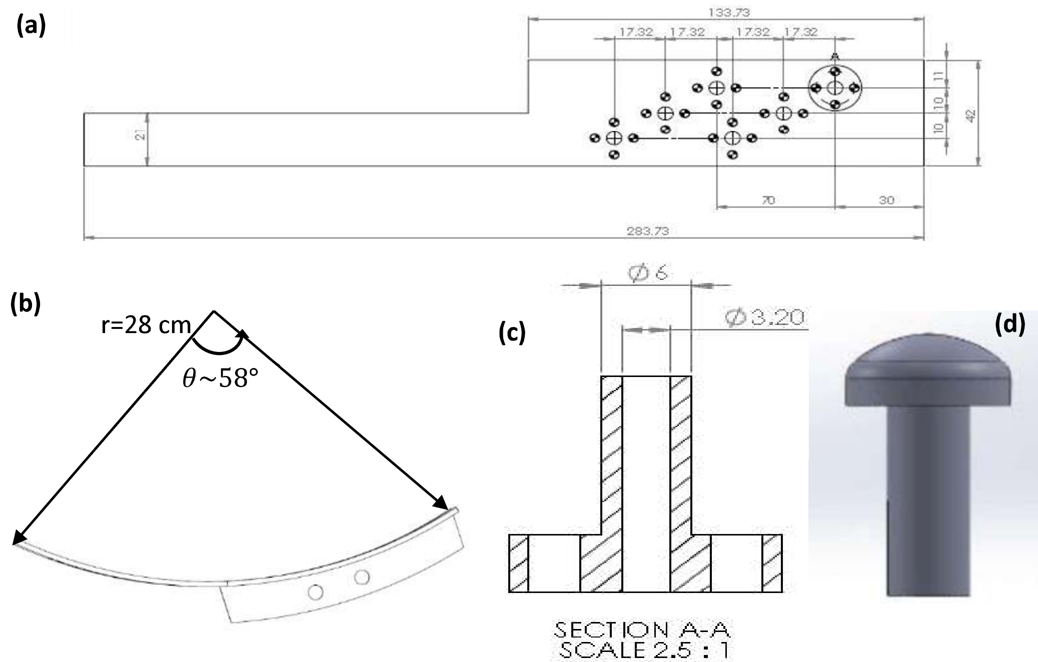

Figure 2.16: Drawing of (a) One section of SS support plate (b) after bending (c) ceramic bush and (d) molybdenum probe

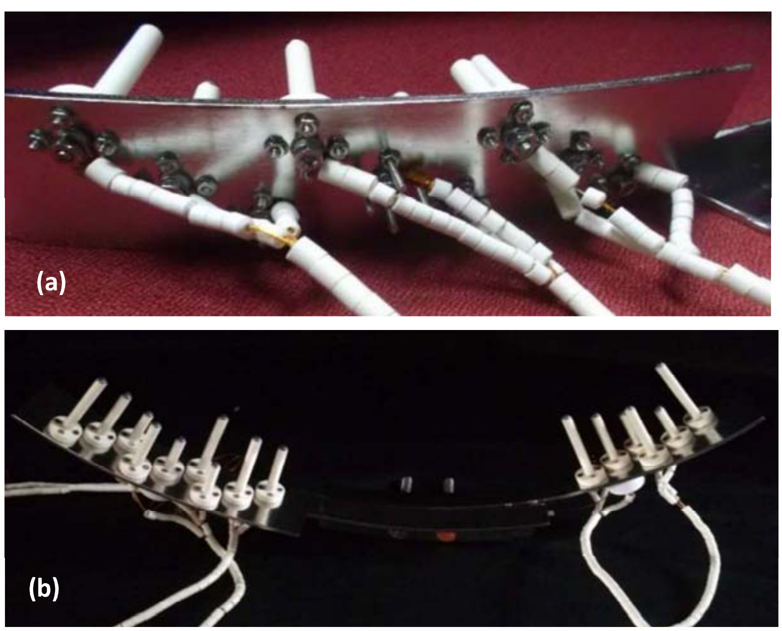

Figure 2.17: (a) bottom view of the probe assembly with wires connection to Langmuir probe and kapton coated wire secured inside ceramic beads (b) complete assembly of garland Langmuir probe.

Figure 2.19 (a) shows a basic schematic of the Langmuir probe and figure 2.19 (b) depicts a typical I-V curve for plasma as measured by the LP.

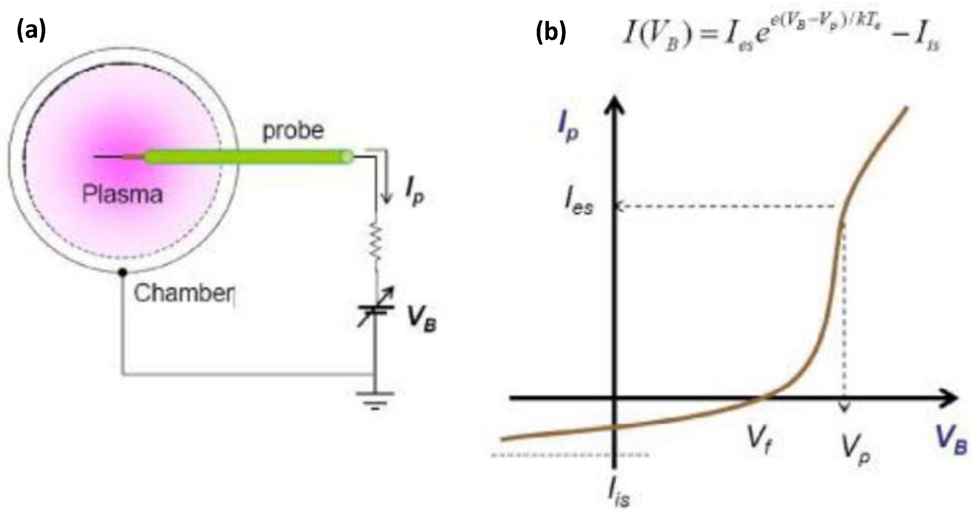

Figure 2.18: (a) Schematic of a Langmuir probe assembly (b) Plot showing typical I-V characteristic of plasma as measured by a Langmuir probe

Langmuir probes are operated in three different modes: [181]

2.6.2.1 Density measurement:

A negative bias voltage on the probe repels electrons, at sufficiently high voltage (~80V in ADITYA-U) all the electrons are repelled and only the ions reach the probe, generating ion current which is almost saturated. The equation for this ion current is (I_{sat}) is

$$I_{sat} = 0.5 e n_i A v_B \qquad 2.27$$

where A is probe area, and $v_B = \sqrt{kT_e/m_i}$ is Bohm velocity and m_i is ion mass.

$$n_i = \frac{2I_{sat}}{eA}\sqrt{\frac{m_i}{T_e(eV)}}. \qquad 2.28$$

For ADITYA-U: $A = 2.5 \times 10^{-5} m^{-2}$ and $v_B = 2 - 4 \times 10^4 m/s$ ($T_e \sim 5 - 15\ eV$). Plasma densities measured at different radial locations in ADITYA-U are plotted in figure 2.20. The oscillations in the density signal are due to edge fluctuation which is studied in detail in chapter 5.

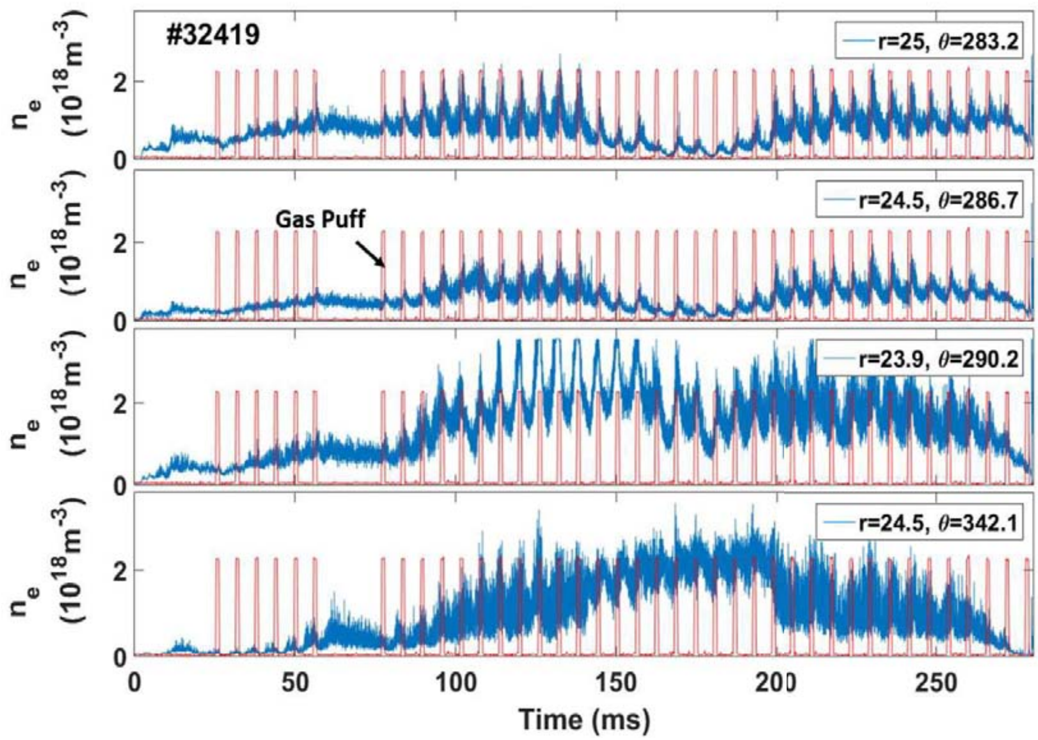

Figure 2.19: Plot showing the time evolution of plasma densities measured at different radial locations in ADITYA-U and the red bars denote the gas puffs.

2.6.2.2 Floating Potential measurement:

The floating potential (V_f) is defined as the potential at which $I_i = I_e$ and estimated as

$$V_f = V_s - \frac{kT_e}{2e}\ln\left(\frac{2m_i}{m_e}\right) \quad \ldots 2.28$$

where V_s is space potential. V_f is obtained by measuring the potential across a floating probe terminated in a high impedance ($R \sim 1\ M\Omega$) without any bias voltage. In general, $R >> T(eV)/I_{sat}$. The plasma potential is then calculated using equation 2.28. Figure 2.21 shows floating potential fluctuation measured at 2 different radial location in ADITYA-U.

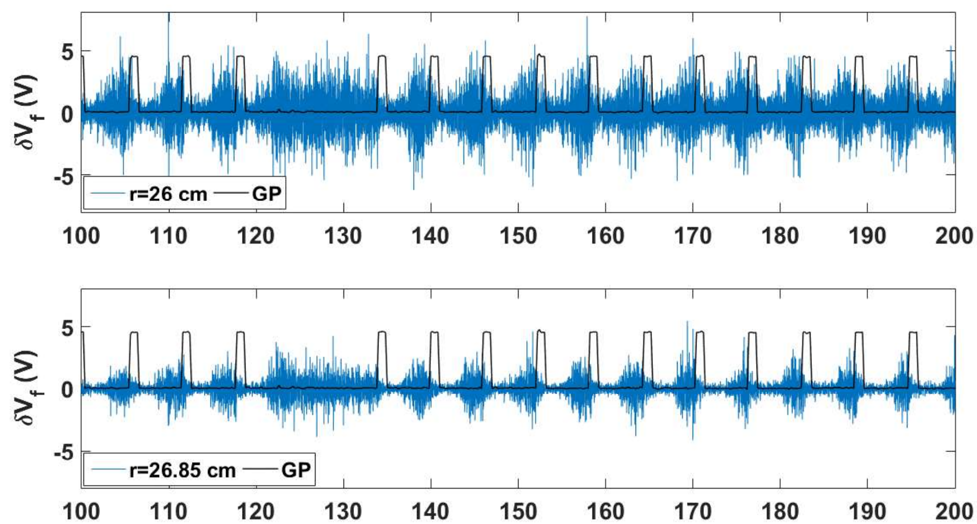

Figure 2.20: Plot showing fluctuations filtered from the floating potential measured at 2 different radial location in ADITYA-U.

2.6.2.3 Temperature measurement:

The exponential part of the I-V curve, when plotted semi logarithmically vs. the probe voltage, should be a straight line if the electrons are Maxwellian, and the electron current in this region is :

$$I_e = I_{es}\, exp\left(\frac{e(V_p - V_s)}{kT_e}\right) and\ T_e = \frac{dV_p}{d(lnI_e)} \quad \ldots 2.29$$

where I_{es} is electron saturation current. The slope of $(ln\ I_e) - V_p$ curve can thus provide the plasma temperature. In figure 2.22 (a) the bias current applied to Langmuir probes along with (b-c) acquired current through two Langmuir probes during the current flat top of a typical discharge are plotted. Figure 2.23 shows one typical I-V curve for the same discharge and figure 2.24 shows time profile of edge density and temperature calculated using the slope of the $(lnI_e) - V_p$ curve. Ideally $I_{es} > 50\ I_{is}$ for low-density un-magnetized plasma. However in tokamaks, magnetic fields are strong enough to make the electron Larmor radius smaller than the probe radius the probe depletes the field lines that it intercepts, further electrons are be collected only if they diffuse across the B-field which decreases with increase in B field.

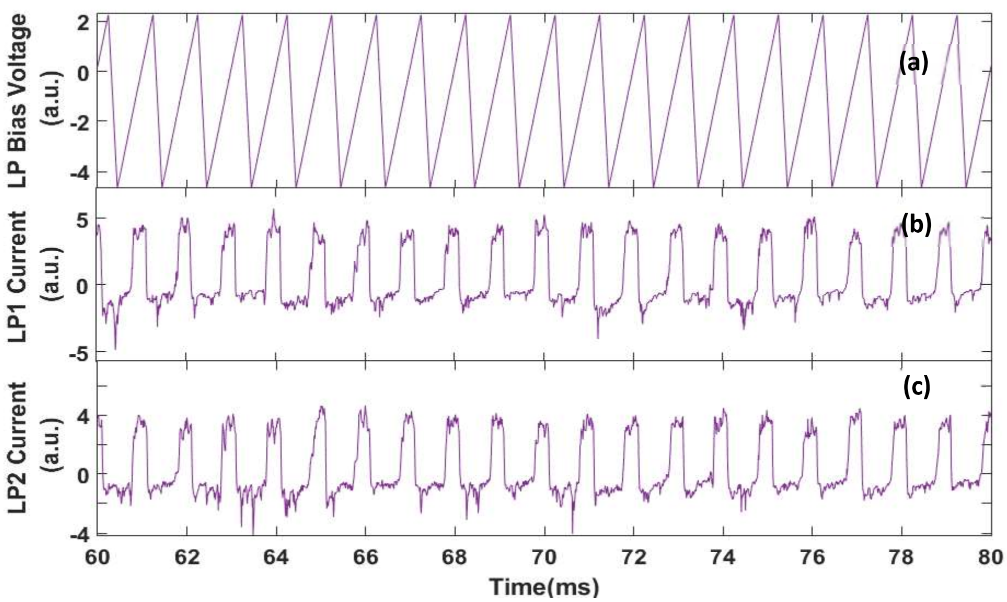

Figure 2.21: Plot showing (a) time evolution of bias current applied to Langmuir probes (b-c) current through two Langmuir probes.

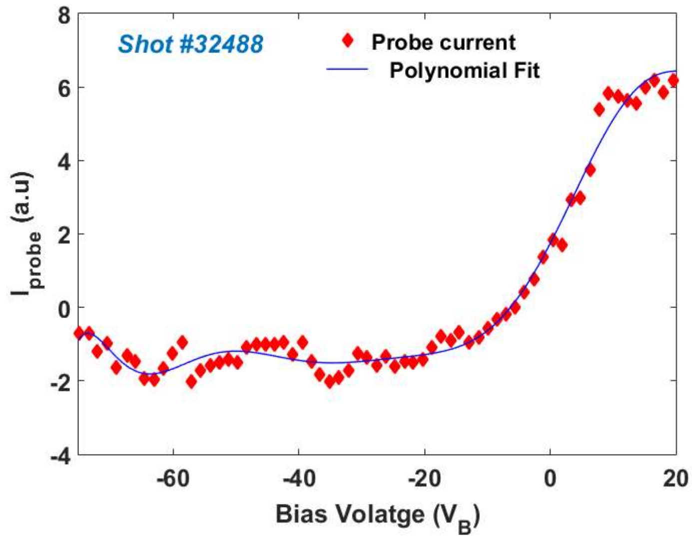

Figure 2.22: Plot showing typical I-V curve during the current flat top of a typical discharge from ADITYA-U

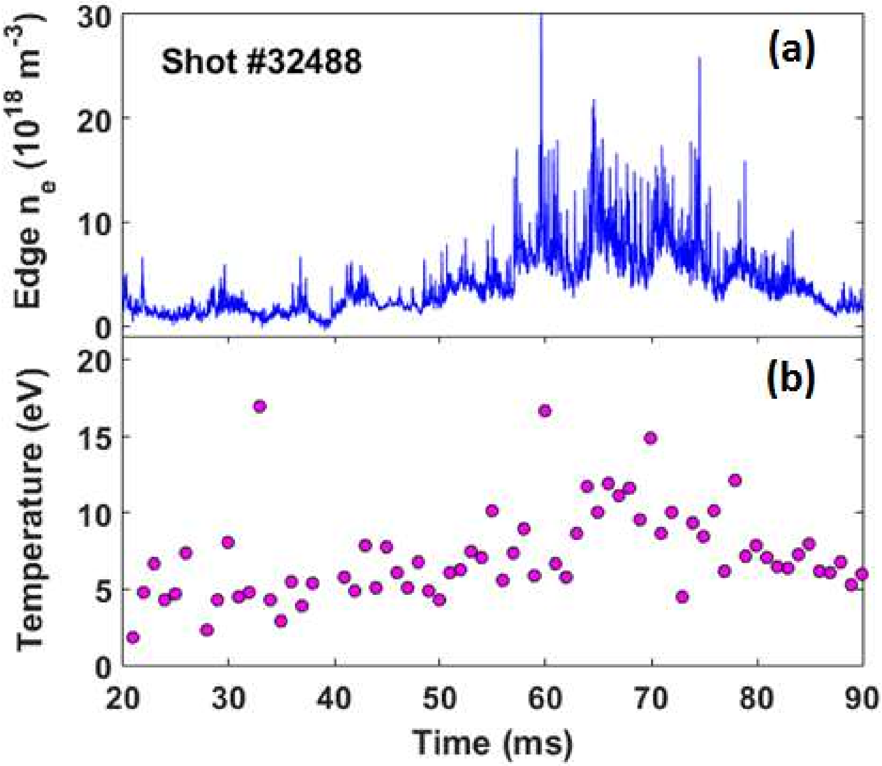

Figure 2.23: Plot showing time profile of (a) edge density and (b) temperature calculated using the slope of the $(lnI_e) - V_p$ the curve for a typical discharge

2.7 Basic Studies in ADITYA and ADITYA-U tokamak

In pursuit of understanding the basic tokamak machine operation, achieving repeatable discharges, their confinement properties and parameter regimes, the following studies have been carried out in both ADITYA and ADITYA-U during the course of this thesis work and hence constitute the part of this thesis. These studies are discussed in brief.

2.7.1 Confinement time studies in ADITYA tokamak

The time evolution of various discharge parameters of typical high current long pulse ADITYA discharges is shown in figure 2.25(i), showing repeatable plasma discharges with a maximum plasma current of $\sim 150\ kA$ and a discharge duration $> 200\ ms$ with a plasma current flattop duration of $> 140\ ms$. Repeatability of high-performance discharges has been established in different toroidal field operations as plotted in figure 2.25 (ii). Plasma position control using 2 Fast Feedback Coils (FFB) and 2 more Correction Coils (B.C.C) with pre-programmed current pulse played a significant role in achieving this discharge regime. Pre-programmed gas puffing has been used to increase mean plasma density and improve confinement in the majority of plasma discharges. A plot of chord average electron density versus shot label, estimated with microwave interferometer and central electron temperature versus shot label, estimated using SXR diagnostic for selected high confinement discharges are shown in Figure 2.26 (a) and (b) respectively. These plots showed that a significant number of discharges having a higher density ($2.7 - 3.8 \times 10^{19} m^{-3}$) and higher electron temperature ($500\ eV - 700\ eV$) have been achieved in ADITYA. The energy confinement time (τ_E), is one of the most important characteristics parameters of a tokamak plasma. The scaling of the energy confinement time with density constitutes one of the basic elements in the development of tokamak devices to a fusion reactor. The neo-ALCATOR scaling law for ohmically heated plasma discharges at moderate density was empirically established from a large number of plasma discharge database from many tokamaks in order to get a better insight into various operational limitations of tokamaks with varied parameters [182]. The neo-ALCATOR scaling law is [183]

$$\tau_{E(neo)} = 7 \times 10^{-2}\, n_e\, a\, R^2\, q_{eff} \qquad \text{... 2.25}$$

where τ_E is measured in seconds, a~minor radius, R~major radius measured in meters, n_e is core plasma density measured in $10^{20}m^{-3}$, q_{eff} - edge safety factor.

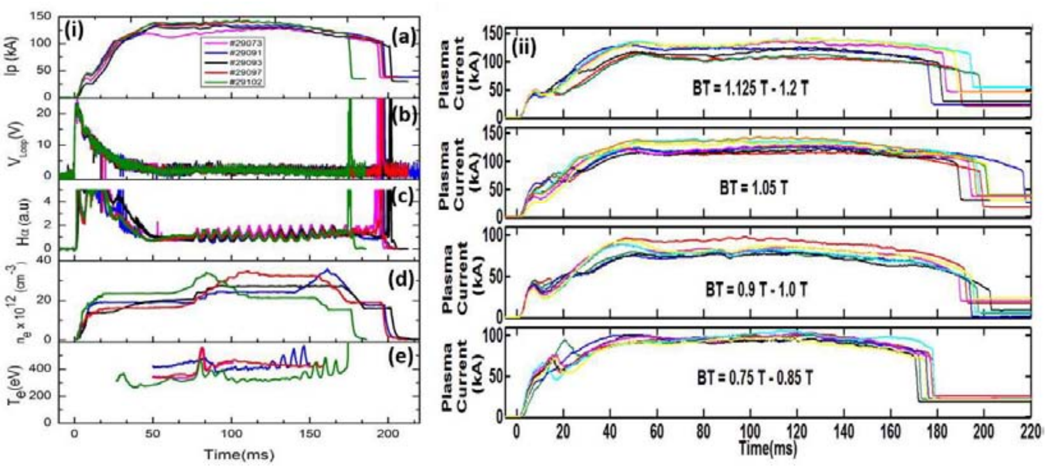

Figure 2.24: (i) The time evolution of typical ADITYA discharges (a) plasma current (kA), (b) loop voltage (V), (c) Hα line emission, (d) line average electron density (ne), (e) central electron temperature (eV), (ii) Plasma current time profiles of multiple discharges

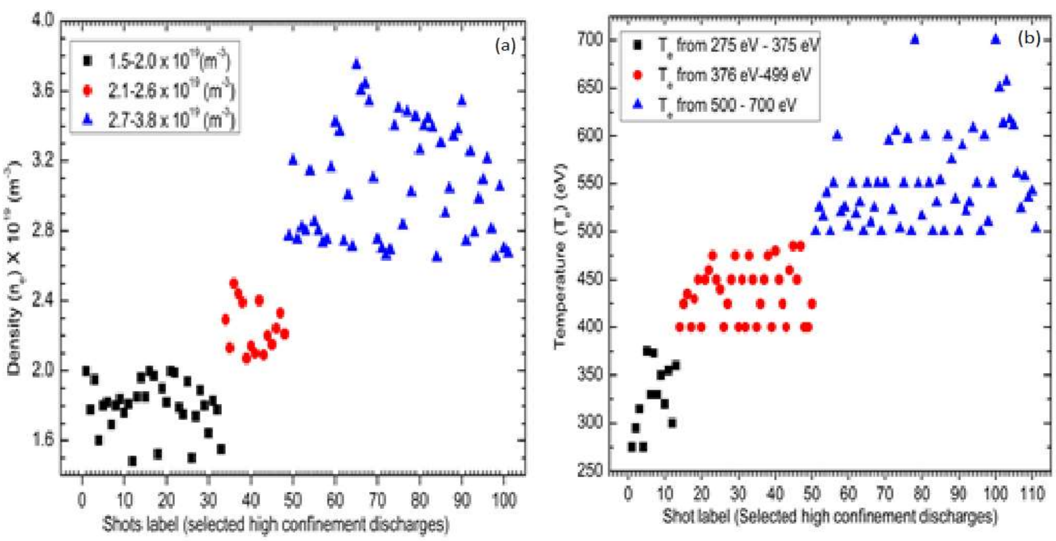

Figure 2.25: Plot showing (a) electron density and (b) electron temperature for selected shots versus shot label from ADITYA.

In ASDEX, improved Ohmic confinement (IOC) regime was discovered in which linear scaling of $\tau_E \sim n_e$ was extended up to density limit [184]. Experimentally, the energy confinement time can be estimated as

$$\tau_E = \frac{\frac{3}{2} < n_e T_e + n_i T_i > V}{I_p V_l - P_{rad}} \qquad \text{... 2.26}$$

where I_p is the plasma current, V_l is the loop voltage, V is the plasma volume, T_e is the core temperature and P_{rad} is the total radiated power. The radiation power, P_{rad} $\sim 10 - 15\,\%$ of total input power was measured using bolometers, and Z_{eff} is estimated from visible continuum measurement varies from ~ 1.5 to 2.3 in the studied discharges. The transition to improved confinement in ADITYA was characterized by a spontaneous increase of plasma density by a factor of 2 and an increase in the electron temperature by a factor of 1.5 to 2. The total stored energy also increased and consequently the ohmic heating power (V_L) dropped. Both effects yielded an improvement in β and the global energy confinement time.

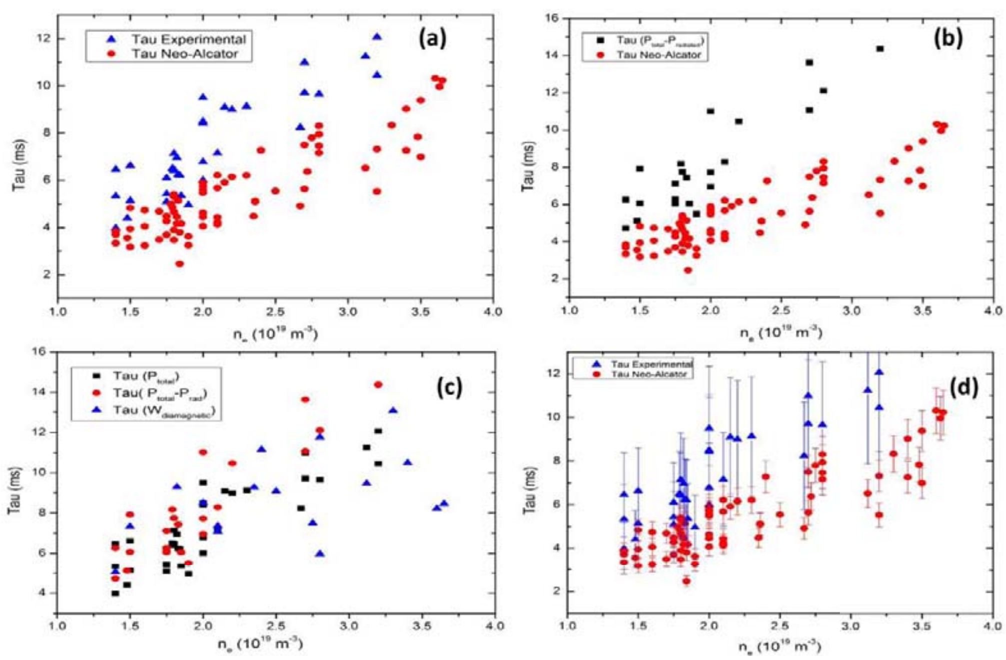

Figure 2.26: $\tau_E$experimental and neo-ALCATOR versus density (n_e) plot calculated (a) with P_{total} (b) with $P_{total}- P_{rad}$, (c) with P_{total}, $P_{total}- P_{rad}$, and $W_{diamagnetic}$ and (d) along with error bar

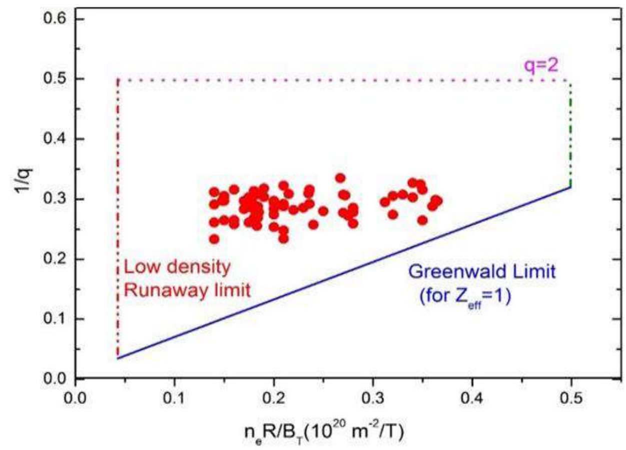

Figure 2.27: 'Hugill' plot describing operating space for ADITYA discharges

The experimental estimated energy confinement time (τ_E) was compared with confinement time estimated from neo-ALCATOR scaling for a large number of high-performance discharges from last campaigns of ADITYA tokamak. The results are plotted in figure 2.27. Confinement times have been calculated and compared using different power inputs taken into consideration, i.e. $\mathrm{P_{total}}$ ($\mathrm{I_p V_L}$), $\mathrm{P_{total}} - \mathrm{P_{rad}}$ and $\mathrm{W_{diamagnetic}}$ determined using diamagnetic loop diagnostic [185].

The results of energy confinement time analysis as shown in figure 2.27 demonstrates that confinement time of presented shots was considerably ($>$ 1.5 times) higher than that predicted by neo- ALCATOR scaling. Also, a good number of discharges lie in IOC (improved ohmic confinement) regime. Strong inward pinch during the periodic gas puff as mentioned later may be one of the possible explanations for the above.

2.7.2 Operation at Parameter Space of ADITYA

The operating space of a tokamak is restricted by several limitations amidst which the plasma performance is optimized. Plasma discharges in a tokamak can be realized only within a definite range of densities [186] determined by the plasma current. The lower density limit leads to the generation of runaway electrons. The upper Greenwald density limit, for a given plasma current, exists due to radiation loss and recycling at higher Z_{eff} , and is defined as $n_G(10^{20}) \ = I_p\ (MA)/\pi a^2\ (m^2)$ for circular plasma. However, over the past few years, this limit has increased due to the application of advanced wall conditioning and better fuelling techniques. The plasma current itself is limited due to the MHD instabilities, where strong MHD oscillations accompanied by shrinkage of the current channel were often observed at $q_{edge} = 2$, which imposes a disruptive limit [10,27,171]. The 'Hugill' plot includes a disruptive limit for high current (low q=2) operation, the density limit as well as low-density runaway regime and became a standard method of displaying the operating space for tokamaks. The 'Hugill' diagram for improved Ohmic confinement discharges of ADITYA is shown in figure 2.28 where the inverse edge safety ($1/q_a$), is plotted against the Murakami number, ($n_e\ R/B_T$) for a large number of discharges. The edge safety factor is calculated as $q_{edge} = 5\ a^2 B_T/I_p R$. The upper line at $1/q\ =\ 0.5$ is the safety factor limit beyond which disruptive m=2 kink MHD mode becomes unstable. The right lower limit is the maximum density limit i.e. Greenwald limit. The left low density is determined experimentally by analyzing density in runaway discharges. The Hugil plot from the last campaigns of ADITYA shows that densities quite close to Greenwald limit were attained with improved lithium wall conditioning, radial plasma position control and optimized adjustment of gas puffing.

2.7.3 Observation of Anomalous Inward Pinch Velocity in ADITYA

Majority of discharges with multiple periodic gas puff displayed a periodic modulation in the temporal evolution of SXR intensity as well as the neutral (H_α) emission intensity. The modulation arises from the peaking of H_α emission intensity, n_e and SXR intensity after each gas pulse, as shown in figure 2.29 and 2.30.

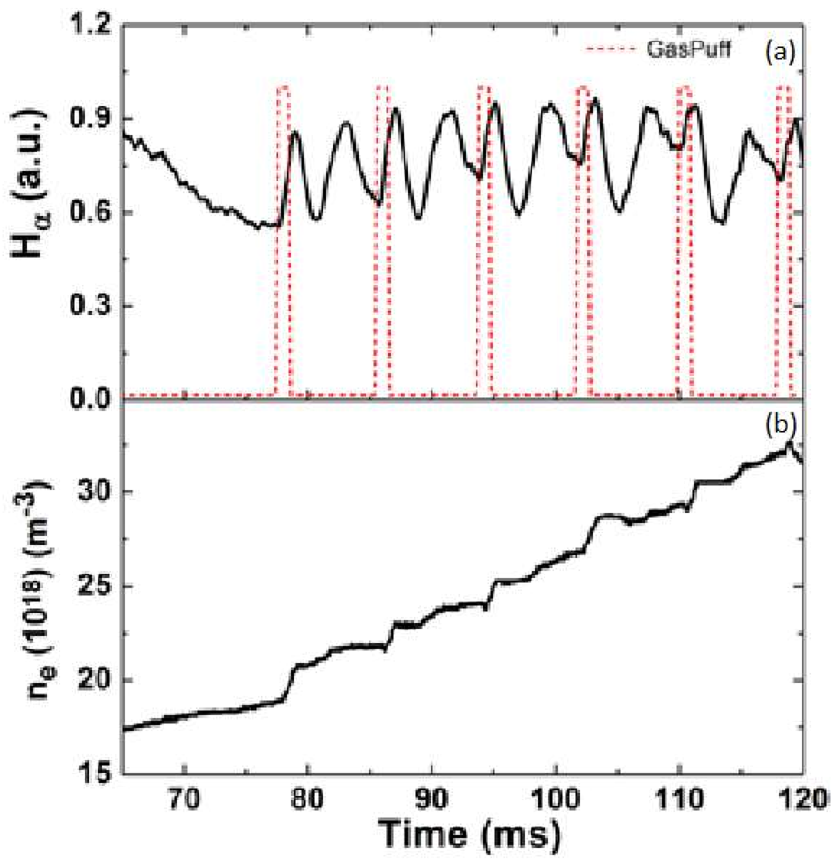

Figure 2.28: Plot showing the time evolution of H_α emission intensity and gas puff (b), n_e in #29078 from ADITYA.

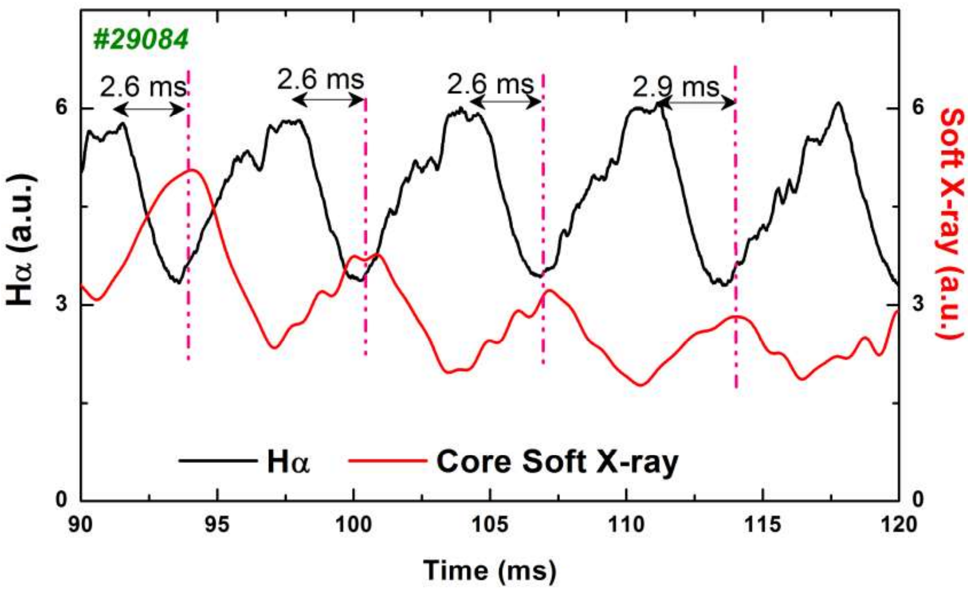

Figure 2.29: Plot showing the time delay between of H_α emission intensity and SXR in #29078 from ADITYA.

The H_α emission intensity, $I(H_\alpha) \propto n_H n_e \chi(T_e)$ where n_H is neutral H density and $\chi(T_e)$ is excitation cross-section. A time delay between both the signal was also consistently observed as depicted in figure 2.30. Since the SXR emission is emitted from the core region and the H_α emission originates mainly from the edge region, the delay in observed SXR peak with respect to H_α peak suggested inward particles transport. Investigation of the variations in H_α emission intensity and SXR emission from core immediately after each gas-puff pulse revealed that the peak in SXR lags the peak in H_α emission by $\sim 2-3\ ms$. The central electron temperature was almost unaltered by the gas-puffs, hence the increase in the SXR intensity with the gas-puff can be safely assumed to reflect the increase in the electron density. Dividing the plasma radius by the time delay of $\sim 2-3\ ms$ between the soft x-ray and H_α peaks, we get the velocity of $\sim 125\ m/s$ for this inward movement. The following figure 2.31 shows a cartoon of the poloidal cross-section of ADITYA displaying the radial location of SXR and H_α chord used for the analysis.

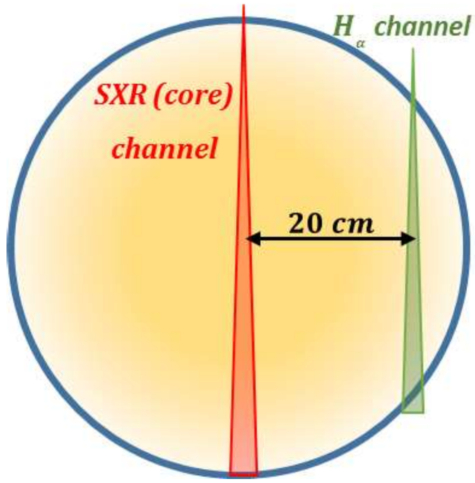

Figure 2.30: Poloidal cross-section of ADITYA displaying the radial location of SXR and H_α chord used for the analysis.

The increase in electron density in the core region due to the gas-puff can be due to either ionization of the penetrated neutrals to the core, else it may be due to the inward drift of the particles ionized at the edge injected via the gas-puff. Assuming the gas injected at room temperature during the gas-puff, the neutral should reach much faster to the core through diffusion having thermal velocity $\sim 600\ m/s$. Further, neutral penetration analysis carried out by DEGAS2 Code [187] has clearly shown that very few neutral ~ 10^{-4} particles reach to the plasma center. Hence, it seems that the increase in plasma density in the core after the gas-puff may be due to inward drift of the particles from the gas-puff getting ionized at edge region of ADITYA. Calculating the pinch velocity for Aditya parameter, which is understood to be one of the reasons for inward particle movement, originating from $E_\varphi \times B_\theta$ drift gives a value of $\sim 12\ m/s$. Anomalous inward pinch velocities, higher than the classical drift velocities has been reported in many tokamaks [188]. Further, the electrostatic fluctuations present in the edge region may also enhance this inward drift. Hence, the observations of soft x-ray peaking just after the application of a gas-puff pulse in Aditya seems to be due to inward convection of particles due to pinching caused by the $E_\varphi\ x\ B_\theta$ drifts. This inward pinch may be responsible for observation of higher confinement times compared to Neo-Alcator scaling in these ADITYA discharges [182].

2.8 ADITYA-U Operation

2.8.1 Basic studies in ADITYA-U

Basic studies in ADITYA-U include mainly two phases of plasma experiments conducted since December 2016, with the inclusion of a new graphite toroidal belt limiter as the primary PFC. The key objectives of the Phase-I operation are: (1) to achieve the first circular hydrogen plasma in ADITYA-U with purely Ohmic discharges, assisted by filament pre-ionization; (2) to check the overall functionality of the system, and; (3) to compare the discharge characteristics of ADITYA and ADITYA-U. During the Phase-I operation, the toroidal magnetic field varied from $\sim 0.5\ T\ to\ 1\ T$ and a gas breakdown was obtained in each of ~700 discharges without a single failure. Consistent plasma discharges of plasma currents of $\sim 80\ kA - 95\ kA$ were achieved, with durations of $80 - 180\ ms$, a chord averaged electron density of $\sim 2.5 \times 10^{19}\ m^{-3}$, and an estimated temperature of $>\ 200\ eV$ [176]. A discharge analysis study of the Phase-I operation of ADITYA-U is carried out in detail. Furthermore, magnetohydrodynamic (MHD) experiments and studies have been carried out in ADITYA-U. An interesting correlation between runaway electrons and MHD amplitude has been found and studied in detail. Comparison of volt–sec consumption in ADITYA and ADITYA-U tokamak showed that Sufficient burn-through of C and O impurities requires peak loop voltage for a longer duration in ADITYA-U (>15 ms) than in ADITYA (<8 ms) (figure 2.32 (i)(a)). The reason for the higher consumption of volt–sec during the burn-through phase in ADITYA-U is perhaps the installation of the new toroidal belt limiter on the high field side in ADITYA-U, instead of the single poloidal ring limiter in ADITYA, which has increased the graphite surface area by ~5 times [189]. Pre-filled gas pressure range has increased from $4 - 8 \times 10^{-5}\ Torr$ (ADITYA) to $1.5 - 3 \times 10^{-4}\ Torr$ (ADITYA-U) (figure 2.32 (i)(e)), initial hard X-rays during start-up phase were significantly reduced (figure 2.32 (i)(f)) and initial plasma current rise rate was reduced from $7 - 9\ MA/s$ to $4 - 5\ MA/s$ (figure 2.32 (i)(b)). Figure 2.33 (a) shows ramp-up failure due to insufficient loop voltage for impurity burn-through during initial operation phase of ADITYA-U and figure 2.33 (b) shows achieved repeatable standard discharges after increasing the loop voltage during the burn-through period.

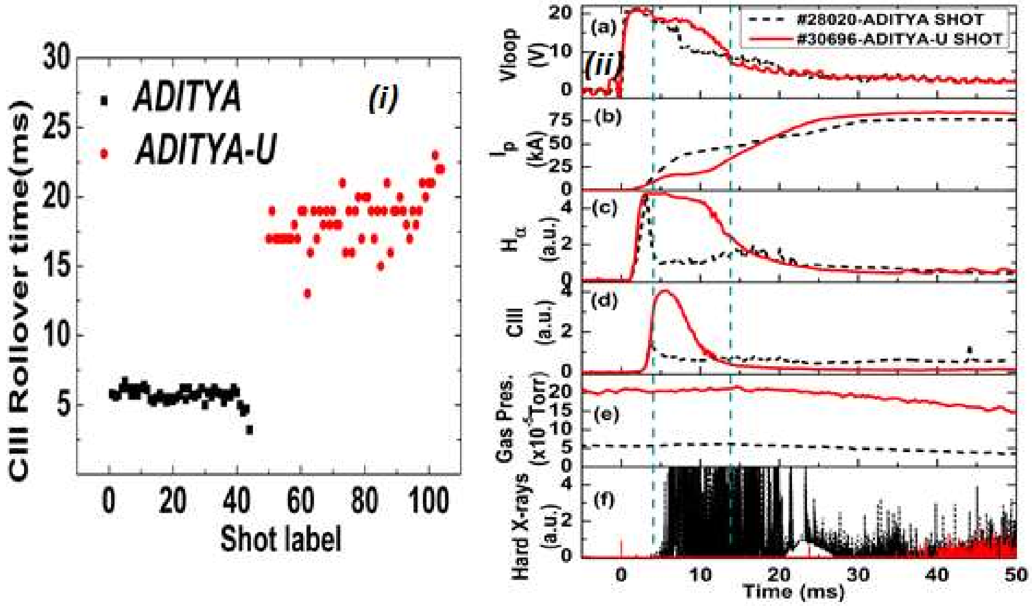

Figure 2.31: (i) Time traces of (a) loop voltage (b) plasma current (c) H_α line emission (d) CIII line emission (e) H2 gas pre-fill pressure and (f) hard X-rays showing the discharge initiation comparison of ADITYA plasma (shot #28020,black) versus ADITYA-U plasma (red).

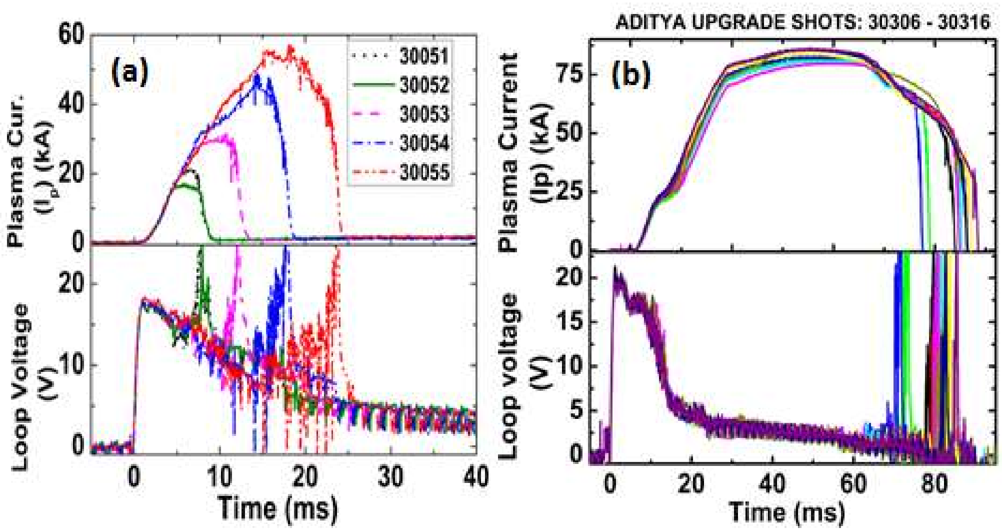

Figure 2.32: a) shows ramp-up failure due to insufficient loop voltage for impurity burn-through and (b) shows achieved repeatable standard discharges after increasing the loop voltage during the burn-through period.

The typical value of E/p ~ $225 - 625\ (V.cm^{-1}Torr^{-1})$, where E is the peak electric field and p is H_2 filling pressure at the time of breakdown. It is noteworthy that no breakdown failure has occurred in ADITYA-U, possibly due to reduced error field.

2.8.2 Phase II Operation of ADITYA-U

In phase II of the ADITYA-U operations, higher discharge duration, plasma density, and plasma current has been achieved. The feat can be attributed to the operation experience gained from ADITYA, improved base pressure, better wall conditioning and the real-time position control. The typical high current, high density discharges with discharge duration more than 300 ms is shown in figure [2.34].

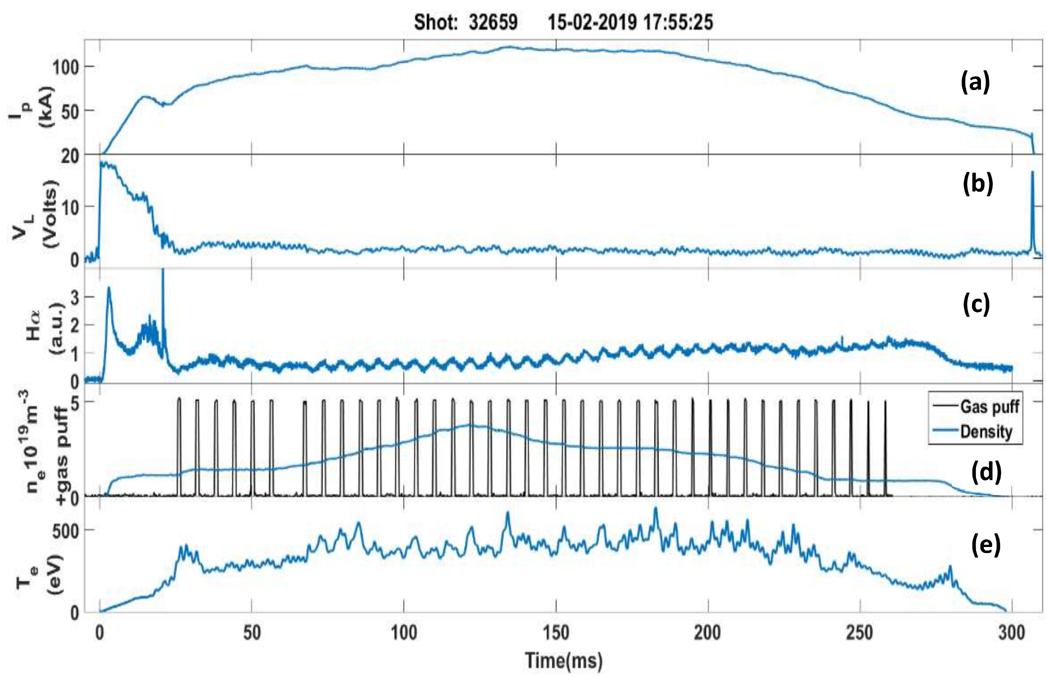

Figure 2.33: Time traces of ADITYA-U shot # 32659 showing plasma parameters (a) Plasma current (kA) (b) Loop voltage (V) (c) H_α line emission (a.u.) (d) Gas puff & Density (n_e) (e) Spitzer electron temperature (T_e) for Z_{eff} ~ 2.

Following chart compares the basic plasma parameter of ADITYA and ADITYA-U tokamak.

Table 2.5: Designed and achieved plasma parameter of ADITYA and ADITYA-U Tokamak.

ADITYA Tokamak		ADITYA-UPGRADE Tokamak		
Parameters	Achieved	Design		Achieved
		Circular Plasma	Shaped Plasma	
Major radius (R)	0.75 m	0.75 m	0.75 m	0.75 m
Minor radius (a)	0.25 m	0.25 m	0.18 - 0.22 m	0.25 m
Plasma Shape	Circular-Pol. limiter	Circular-tor. limiter	D shaped	Circular-tor. limiter
Toroidal Field (B_T)	1.34 T	1.5 T	1.5 T	1.4 T
Plasma Current	160 kA ± 10%	250 kA	150 kA	177 kA
Plasma Duration	250 ms	300 ms	300 ms	335 ms
Electron Density	3.5×10^{19} m^{-3} ± 10%	3.5×10^{19} m^{-3} ± 10%	5.0×10^{19} m^{-3} ± 10%	3.0×10^{19} m^{-3} ± 10%
Electron temperature	700 eV ± 20%	500 eV	500 eV-1 keV	400 eV ± 20%
Elongation	1	1	1.1-1.2	1
Triangularity	1	1	0.45	1

2.9 Analysis of Mirnov data

As the major part of thesis deals with the Magnetohydrodynamic (MHD) modes, their structures, the mode rotaion frequencies and the MHD island widths, before concluding this chapter, the data analysis of Mirnov data is presented in detail in this section. MHD studies have been carried out using one set of 16 Mirnov coils in ADITYA and two sets of 16 Mirnov coils in ADITYA-U as mentioned in the diagnostics section. The analysis and techniques used to obtain the magnetic island rotation frequency, direction of rotation, island structure and island width are as follows.

2.9.1 Mode Rotation frequency

Each magnetic island rotates toroidally and poloidally under the combined influence of various toroidal and poloidal drifts in a tokamak. At every instant, the rotation frequency of an island carries a large amount of information which may be related to plasma edge density temperature, current and density gradient, etc. The mode rotation frequency can be obtained by carrying out Fast Fourier Transform (FFT) of any of the Mirnov coils at a particular time instant as shown in figure 2.35. Presence of dominant peak denotes the presence of a coherent mode structure. Each island generally has a unique rotation frequency which evolves along with plasma density temperature and their gradients.

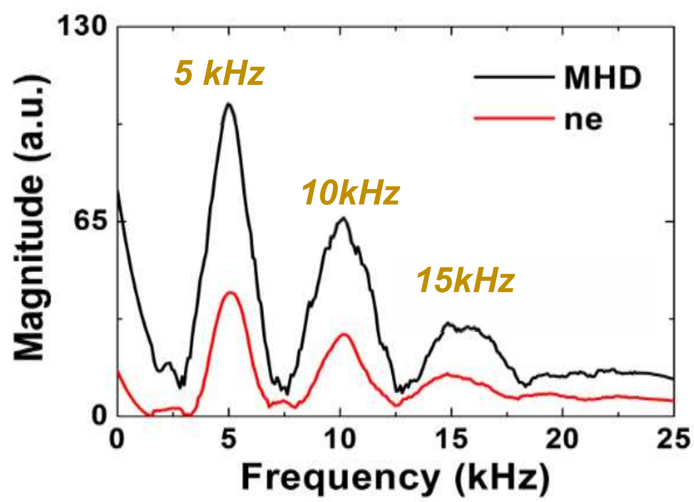

Figure 2.34: Frequency vs. magnitude plot showing FFT of MHD activity from a Mirnov signal.

These island rotation frequencies can be traced through a discharge to infer a basic idea of the island dynamics. The time evolution of the frequencies of MHD modes has been obtained by using the Specgram function in MATLAB, which computes the windowed discrete-time Fourier transform of a signal using a sliding window.

$$B = specgram(a, nfft, Fs, window, noverlap)$$

where a is the Mirnov data, $nfft$ specifies the FFT length that specgram uses, and determines the frequencies at which the discrete-time Fourier transform is computed. Fs is a scalar that specifies the sampling frequency of Mirnov diagnostic. '$window$' specifies a windowing function (e.g. hanning, hamming) and the number of samples specgram uses in its sectioning of vector a. $'noverlap'$ is the number of samples by which the sections overlap. Figure 2.36(a) shows multiple frequency bands in specgram of MHD data from shot # 32419.

Island width

An island is characterized by its toroidal and poloidal mode number. At any given time the magnetic field induced in a Mirnov coil is proportional to the amplitude of magnetic fluctuation of the island and its distance from the probe. In the simplest picture for a large island approximation the island width (W) is calculated as [140]:

$$\frac{W}{rs} = 2\left[\left(\frac{2}{m}\right)\left(\frac{r_c}{r_s}\right)^m (\tilde{B}_\theta/B_\theta\ )\right]^{1/2}$$

where m = mode number, r_s and r_c = radial location of the mode resonant surface & Mirnov probe respectively, $\tilde{B}_\theta$ is the magnetic fluctuation acquired from Mirnov and B_θ is the total poloidal magnetic field at that instant. The magnetic fluctuation corresponding to the frequency of the magnetic island is filtered from the Mirnov output to obtain the required $\tilde{B}_\theta/B_\theta$ value. Figure 2.36 shows specgram of MHD activity (b) normalise MHD amplitude $\tilde{B}_\theta/B_\theta$and island width calculated using $\tilde{B}_\theta/B_\theta$ in given formula for a typical high MHD discharge from ADITYA-U.

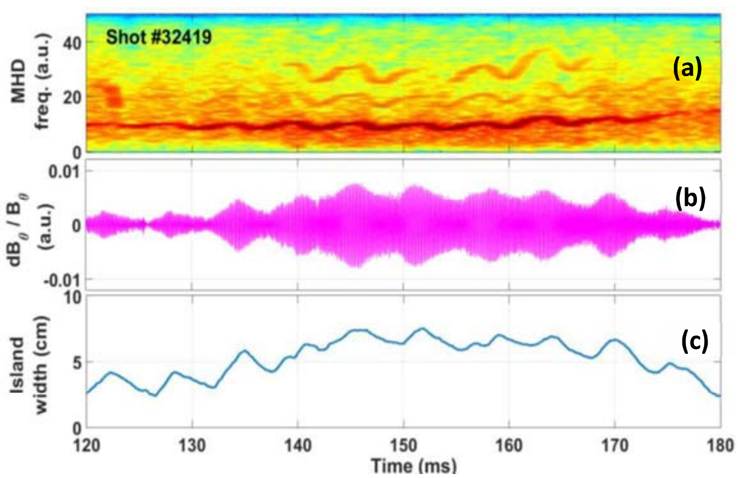

Figure 2.35: Plot showing temporal evolution of (a) specgram of MHD activity (b) normalise MHD amplitude ($\tilde{B}_\theta/B_\theta$) and (c) island width calculated using $\tilde{B}_\theta/B_\theta$ for a typical high MHD discharge from ADITYA-U.

Often in the presence of two mutually existing islands, the output in Mirnov is a resultant due to flux induced by both islands. In case these islands have different frequencies the magnetic fluctuation due to each can be easily filtered and used to calculate the island width of each. However, if both modes have nearly same rotation frequency the fluctuation corresponding to individual islands cannot be extracted by frequency filtering method. A technique called singular value decomposition (SVD) can be used to resolve the problem [190].

2.9.2 Island structure:

A magnetic island is defined by its poloidal (m) and toroidal mode number (n) and is centred at their mode rational flux surface$q = m/n$. The magnetic fluctuation of an island induces a voltage output of different magnitude in all Mirnov coils depending on their spatial location at every time instant [34,126]. For example, if an m=2 mode is present the Mirnov coils closest and to the two lobes of the island will have the highest amplitude. By counting the number of peaks in the output of spatially distributed Mirnov coils at one time instant one can find the mode number. For example, in the following figure 2.37. , the data from 16 Mirnov coils are arranged in sequence of their poloidal location starting from Mirnov coils at $\theta = 11.5° \ to \ \theta \ = 358.5°$ in a poloidally anticlockwise direction. $\theta = 0°$ is the outboard high field side and $\theta = 180°$ is the inboard high field side. A peak in the MHD fluctuation data is followed through all 16 probes and the number of peaks in time this peak competes one rotation in the last coil gives the poloidal mode number [184].

A polar plot the MHD amplitude acquired by each Mirnov coil with respect to their poloidal angle location at one time instant, one can also obtain the MHD mode structure. For example the MHD mode structure corresponding to an m=2 mode at different time instants is plotted in figure 2.38. The plot also shows the direction of island rotation which is in clock-wise direction (same as electron diamagnetic drift). It shall be noted that the maximum poloidal number that can be identified in a given system is limited by the half of the number of poloidally distributed Mirnov coils and the same is true for toroidal mode number. The SVD technique can provide more actuate mode structure.

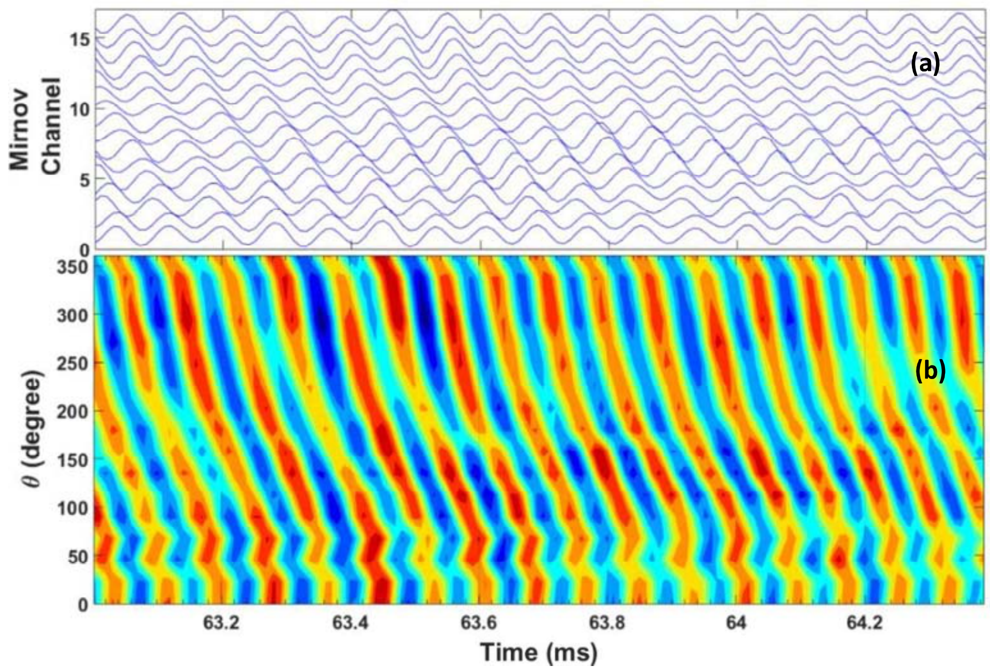

Figure 2.36: plot showing time evolution of (a) MHD data from 16 Mirnov coils arranged sequentially in anti-clock wise poloidal direction (b) its corresponding contour plot.

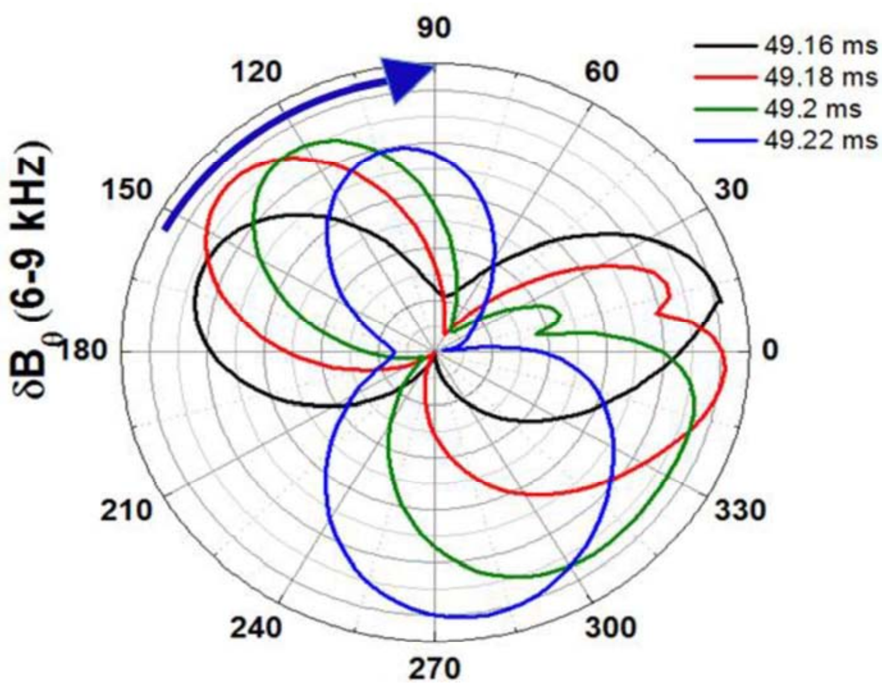

Figure 2.37: Plot showing m=2 mode structure at different time instant from a typical ADITYA-U discharge in poloidal cross section.

2.9.3 SVD Technique

The SVD technique is used for identification of mode structures [190]. In simple words, the SVD technique uses data from multiple coils distributed symmetrically around the poloidal cross-section and extracts the dominant coherent mode structures present in the system. An analogy can be made with frequency FFT technique; like FFT technique extracts modes with dominant amplitude in the frequency-time domain, SVD extracts mode structures with dominant amplitude.

In principle, two or more MHD modes with different mode number and frequencies are extracted by SVD into distinct pair of principle axis. Following steps are involved in SVD analysis of a vector X (multiple Mirnov coil time series)

- A $n \times m$ Matrix of m (time) data points from n Mirnov channels is constructed.
- Singular value decomposition of X is nothing but its factorization in the form of $X = U\Sigma V'$, where U is a $n \times m$ real or complex unitary matrix.
- Σ is a non-negative, real, $m \times n$ rectangular diagonal matrix, where $\Sigma_{i,i}$ are the eigenvalues, of X and the square root of $\Sigma_{i,i}$ are singular values of x.

V is a $m \times m$ real or complex unitary matrix, with columns forming eigenvectors of X i.e. orthogonal basis on which signal is decomposed. V' is its conjugate. After transforming to poloidal co-ordinates and fitting a polynomial curve to eigenvectors in V can provide mode structures. The corresponding weight of each mode hence the dominant can be identified by assessing their corresponding eigenvalues obtained.

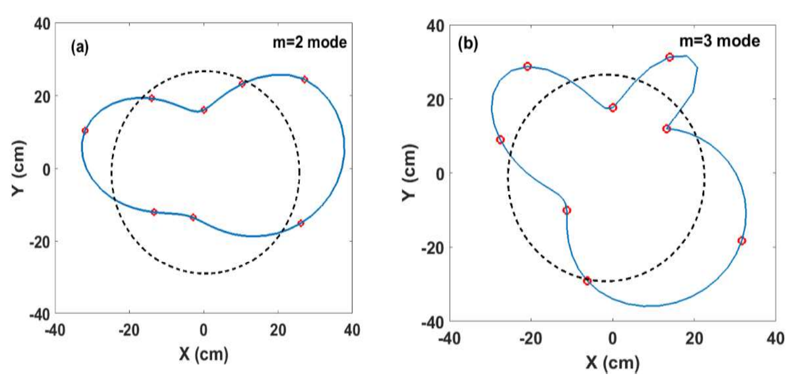

Figure 2.38: Poloidal mode structure of simultaneously existing (a) m=2 and (b) m=3 MHD mode obtained using SVD technique.

Special care must be taken to incorporate the polarity of Mirnov coils which is not evident in raw Mirnov signal and can easily lead to misinterpretation of data. The easiest way to verify is to integrate the Mirnov data and verify if it matches the plasma current shape. Figure 2.39 shows the mode structure of simultaneously existing (a) m=2 and (b) m=3 MHD mode obtained using SVD technique for shot #24025.

2.10 Summary

This chapter provided a brief introduction of both ADITYA and ADITYA-U tokamak, the upgrade process and diagnostics that are used in studies presented in this thesis. Further, the studies carried out for basic understanding of tokamak operation is also reported in brief. The data analysis of Mirnov data is also presented during the end of the chapter. This thesis includes experiments carried out on both ADITYA and ADITYA-U and all the results presented in this thesis are more or less consistent in both the tokamaks. It is interesting to note here that, with ADITYA having a poloidal ring limiter at one toroidal location and ADITYA-U having a continuous toroidal belt limiter with limiter poloidal extent, the edge/SOL characteristics do not change much and the experiments on REs carried out in both the machine bear exactly the same results. The above points to the universality of the edge/SOL plasma characteristics in mid-sized tokamaks worldwide.

Chapter 3

Sawtooth Instability Generated Runaway Electrons and their Transport

The sawtooth instability is a common MHD instability observed in fusion devices including tokamaks, which appears as periodic relaxation oscillation of the plasma temperature and density in the core plasma region when the safety factor on-axis, decreases below 1 ($q_0 \leq 1$) [54]. The temporal evolution of core plasma temperature exhibits a slow increase followed by a relatively sharp fall, which looks like sawteeth and hence these oscillations are called 'sawteeth' oscillations, commonly observed in almost all tokamaks including ADITYA/ADITYA-U tokamak [191]. Generation of non-thermal electrons during sawteeth crashes has been reported in several tokamaks like T-10 [192], DIII-D [56] and TCV[57]. RE generated HXR bursts during sawtooth crash have also been observed in COMPASS tokamak [60], however, they are often attributed to the throwing-off of already present REs in core plasma due to sawteeth. In typical discharges of ADITYA, bursts of Hard X-Ray (HXR), generated due to the interaction of runaway electrons (RE) with the limiter surface, during sawteeth crash are regularly observed during the plasma current flat-top. These HXR bursts are highly correlated with the sawtooth-crash, in time, which suggests that a sawtooth crash generates these runaway electrons, which then yield the HXR bursts due to their interaction with the limiter. The electric field induced in the toroidal direction due to change in the poloidal magnetic field during the sawtooth crash is found to be higher than the critical electric field required for runaway generation. This induced toroidal electric field during each sawtooth crash generates the REs, which then travel to the limiter to give the HXR bursts. Furthermore, it has been observed in ADITYA that the HXR bursts do not continue to appear over the complete time-span of the plasma current flat-top of the discharge. No HXR bursts accompany the sawtooth crash in the later period of plasma current flat-top in the studied discharge. This observation indicates toward different transport mechanisms of runaway electrons in the initial and later parts of plasma current flat-top of a single discharge. Further investigation revealed that the overlapping inflated magnetic islands seem to be responsible for the loss of sawtooth-crash generated REs and subsequent HXR bursts in the initial phase. Whereas no overlapping of magnetic islands and the presence of good magnetic surfaces in between the islands restricts the transportation of REs leading to the absence of correlated HXR bursts in the later phase of plasma current flat-top [193].

3.1 Sawteeth Generated Runaway electrons in ADITYA

3.1.1 Sawteeth Instability

The sawtooth instability is a periodic MHD instability, during which the core plasma temperature and density inside the q ~ 1 surface rise slowly in time ($\sim 1 - 3\ ms$) and falls off relatively sharply ($\sim 50 - 100\ \mu s$) [54]. This effect is most evident on line integrated Soft X-Ray (SXR) measurements of the plasma core since SXR intensity is dependent on plasma density and temperature, $\mathrm{I_{SXR}} \propto \mathrm{n_e^2 T_e}$ [96]. SXR intensity measurements remain as a preferred tool to investigate the sawtooth instability in tokamaks. The temporal evolution of core SXR intensity displays a repetitive sequence of slow rise and sudden dip as illustrated in figure 3.1 from ADITYA tokamak [58], mainly during the plasma current flat-top period in tokamak discharges.

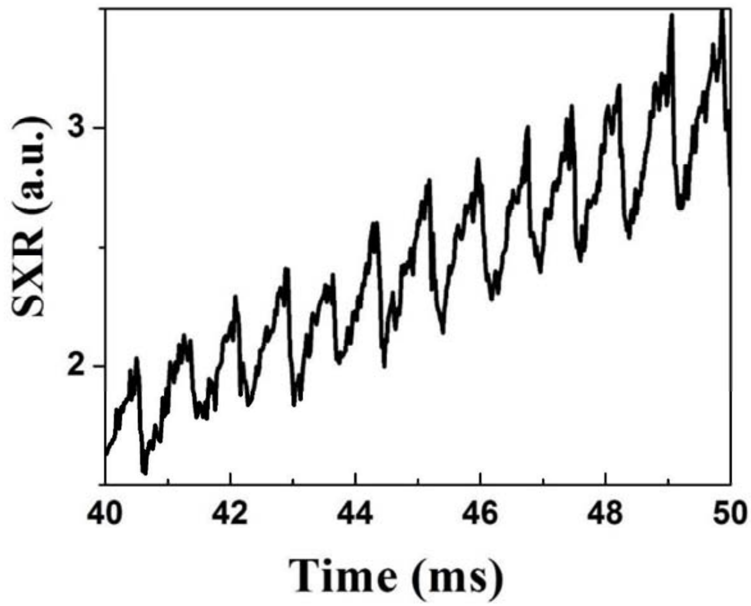

Figure 3.1: Typical time profile of the SXR intensity exhibiting sawteeth instability in ADITYA tokamak.

The sawtooth instability is believed to be a manifestation of m/n= 1/1 internal kink mode ever since its initial observation on ST tokamak [194]. According to the first model proposed by Kadomstev [59], when $q_0 < 1$ at the magnetic axis, the m=1 mode becomes unstable and grows, initiating a rigid radial displacement of plasma column residing inside the q=1 surface. This radial displacement of plasma column leads to the squeezing of magnetic flux surfaces in direction perpendicular to the helical flux surfaces between the plasma core and q=1 surface, ultimately leading to rearrangement of flux surfaces through (complete/ partial) reconnection of magnetic field lines between magnetic axis and q = 1 surface with those outside and q = 1 surface [54]. However, the complete physical processes involved in the rearrangement of flux surfaces during the sawtooth crash still remains to be completely understood. Several uncertainties related to saturation of island and the occurrence of complete magnetic reconnection still exist.

An explanation of the sawtooth-crash has provided the motivation for several theoretical efforts. Von Goeler et al. observed that the growth rate of the m = 1 ideal MHD internal kink mode is approximately seven times too large to explain the observed growth rate of the m = 1 oscillations [194]. Furthermore, Rosenbluth [195] showed that in the low-q limit, the ideal internal kink instability should saturate at an amplitude much lower than the amplitude inferred from experiments [56]. Later, however, Kadomtsev heuristically argued that the resistivity should prevent the saturation of the internal kink at low amplitudes and thus allow the magnetic field to evolve in such a way that current density, safety factor, and temperature profiles flatten inside the singular or mode rational surface where the safety factor equals unity [24]. The literature on the subject [196] claims that island saturation requires $\beta_p > 2$. Figure 3.2 schematically depicts the sequence of events in the poloidal cross-section of tokamak that take place during a typical sawteeth period.

On the backdrop of vast theoretical and experimental studies, it is quite well-established that the sudden change in the poloidal magnetic flux during the sawtooth crash occurring in a typical time scale $\leq 100\ \mu s$ [59], leads to the generation of an electric field in the toroidal direction. And the amplitude of the electric field induced due to the sawtooth crash can be fairly estimated using Kadomtsev's model [54].

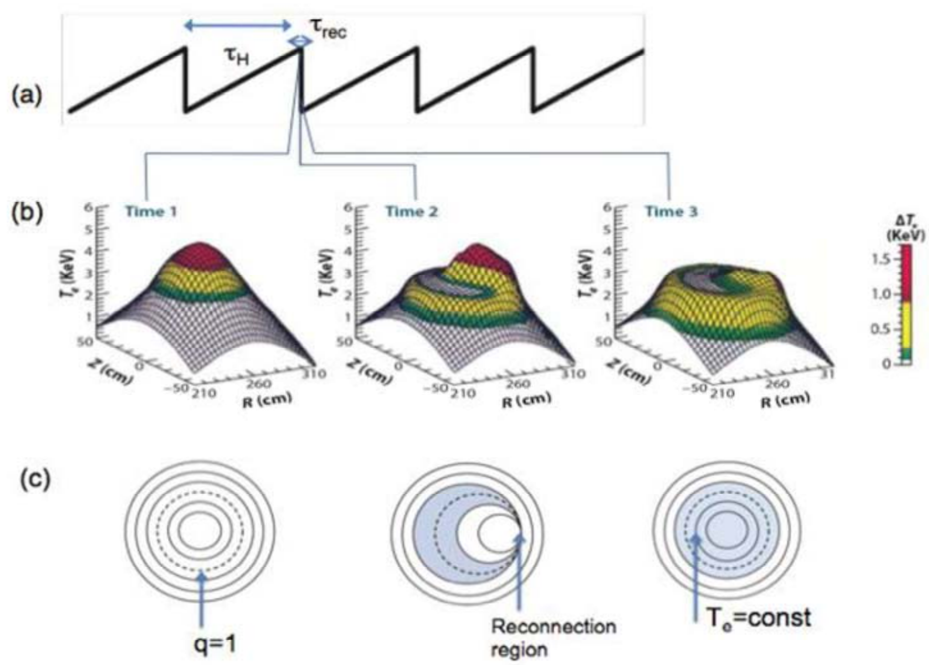

Figure 3.1: Schematic showing (a) Sawtooth time profile, (b) evolution of plasma temperature and (c) plasmas core and q=1 flux surfaces during various stages of sawtooth crash.

3.2 Experimental Observations of correlated SXR and HXR bursts in ADITYA/ADITYA-U

In a typical discharge of ADITYA with sawteeth, periodic spikes in HXR coinciding with each sawtooth crash has been observed multiple times. The time evolution of the plasma current, loop voltage, soft and hard X-ray emission intensities, the time derivative of the poloidal magnetic field, $\delta\dot{B_\theta}$, (measured by one of the 16 Mirnov coils) and central chord-averaged density of a typical plasma discharge (with sawtooth) of ADITYA tokamak is shown in Figure 3.3 (a, b, c, d and e) respectively. The loop voltage ~ 20 V initiates the discharge and the plasma current reaches its flat-top at $\sim 40\,ms$ and stays constant till the end of the discharge. During the current rise initiation phase, the loop voltage, i.e., the toroidal electric field (required for the gas breakdown and impurity rollover) is much higher than the critical electric field, E_c , generating runaway electrons and subsequently producing a significant amount of HXRs during the first $\sim 25\,ms$ of the discharge. After that phase, as the loop voltage and hence the toroidal electric field is substantially reduced, the HXR intensity goes down significantly and the SXR intensity started rising indicating the increase in plasma temperature. As soon as the plasma current approaches its flat-top, the sawtooth activity in the SXR emission starts appearing. Along with that, the base level of HXR intensity rises again, however significantly lower than the initial phase, and periodic bursts having energies in the range of $\sim 3 - 5\,MeV$ start appearing. These bursts last till $\sim 55\,ms$ (in these typical discharges) into the discharge and then they disappear along with the reduction in the base level of HXR intensity, however, the sawtooth activity continues almost till the end of the discharge. A correlation to this sequence of events is also observed in the MHD activity as shown in Figure 3.3(c). During the initial current rise phase, high MHD activity is observed which subsides as the plasma current approaches the flat-top. The MHD activity increases again during first ~ 15 ms of the current flat-top (till 55 ms in this typical discharge) and reduces significantly thereafter. Based on these sequence of events the discharge has been categorized into three different time zones which are marked in Figure 3.3. In first time zone (TZ1) the plasma current initiates and reaches to its flat-top. The second time zone (TZ2) represents the first $15 - 20\,ms$ of plasma current flat-top region, which exhibits strong bursts in HXR emission correlated with each sawtooth-crash in SXR emission and a rise in MHD activity. Third time zone (TZ3) represents the later phase of plasma current flat-top, where the HXR bursts disappear and the MHD activity subsides, however, the sawtooth activity continues.

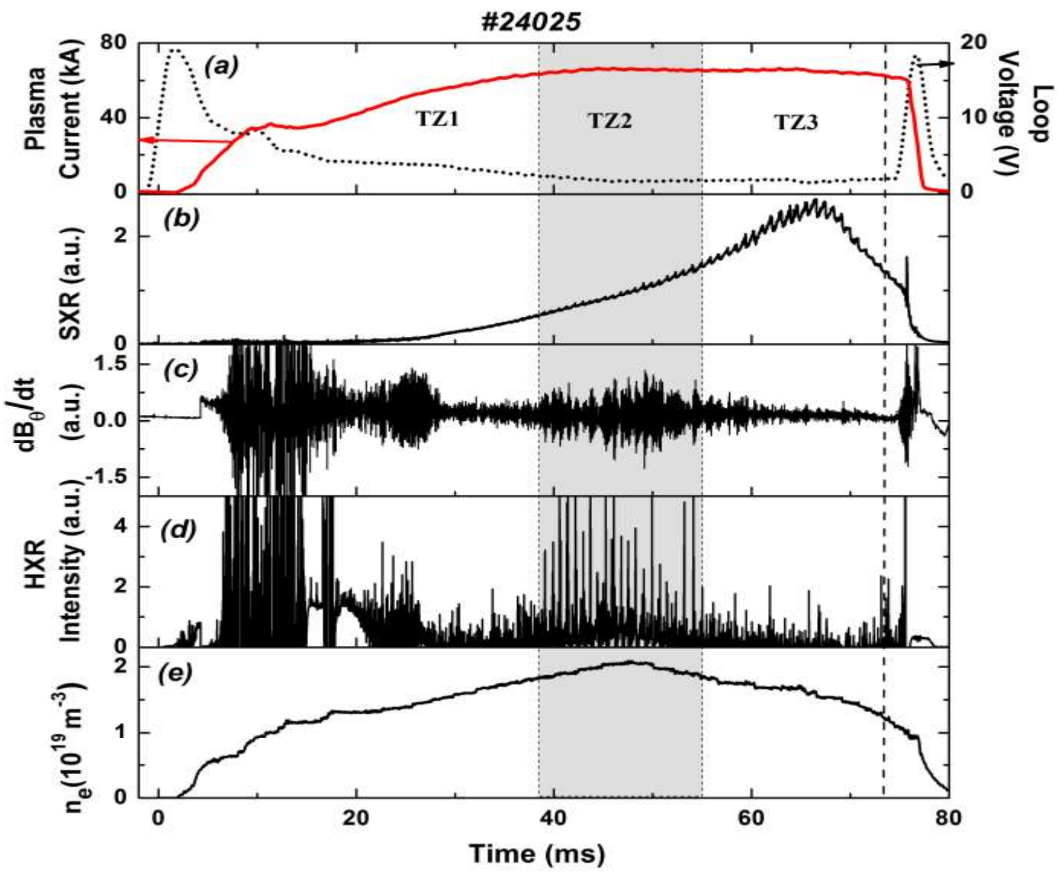

Figure 3.2: Time evolution of a typical plasma discharge (#24025) of ADITYA tokamak (a) plasma current and loop voltage (b) intensity of SXR showing sawteeth activity (c) fluctuations in the time derivative of the poloidal magnetic field, $\sim B_\theta$ (d) intensity of HXR

Expanding the TZ2 in time reveals that the HXR bursts coincide exactly with each sawtooth crash. The sawtooth activity in SXR emission along with HXR intensity and MHD activity in TZ2 are plotted in Figures 4.4 a, b and c respectively. Figure 3.4 clearly demonstrates that after each sawtooth crash, a peak in HXR intensity is observed. The time lag between the sawtooth peak and the HXR burst peak is $\sim 60 - 80\ \mu s$ (figure 3.4 d and 3.4 e). In contrast to the time TZ2, no HXR burst peak associated with the sawtooth crash has been observed in TZ3 as shown by expanding the time TZ3 in figure 3.5. Investigating several discharges (with HXR peaks correlated with sawtooth in

SXR) for a systematic variation in time-zone TZ2 and TZ3, a consistent and pronounced dissimilarity in the MHD activity has been observed in these two zones. In TZ2, higher amplitude of MHD fluctuation $\left(\delta\dot{B_\theta}\right)$ has been detected compared to that in TZ3 (Figure 3.4c and 3.5c). Periodic HXR bursts in the current flat-top phase have only been observed in discharges where the sawtooth activity is present.

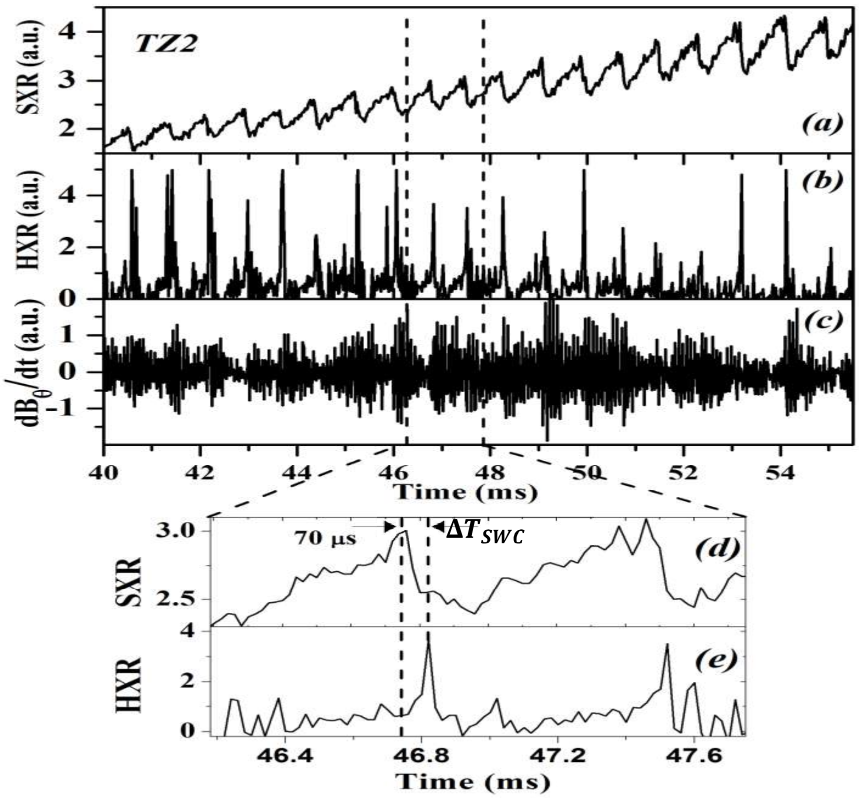

Figure 3.3: Time evolution of (a) intensity of Soft X-ray emission, (b) intensity of Hard X-Rays emission (c) fluctuations in the time derivative of poloidal magnetic field, $\delta\dot{B_\theta}$ in time zone 2 (TZ2). (d) SXR intensity and (e) HXR intensity, respectively

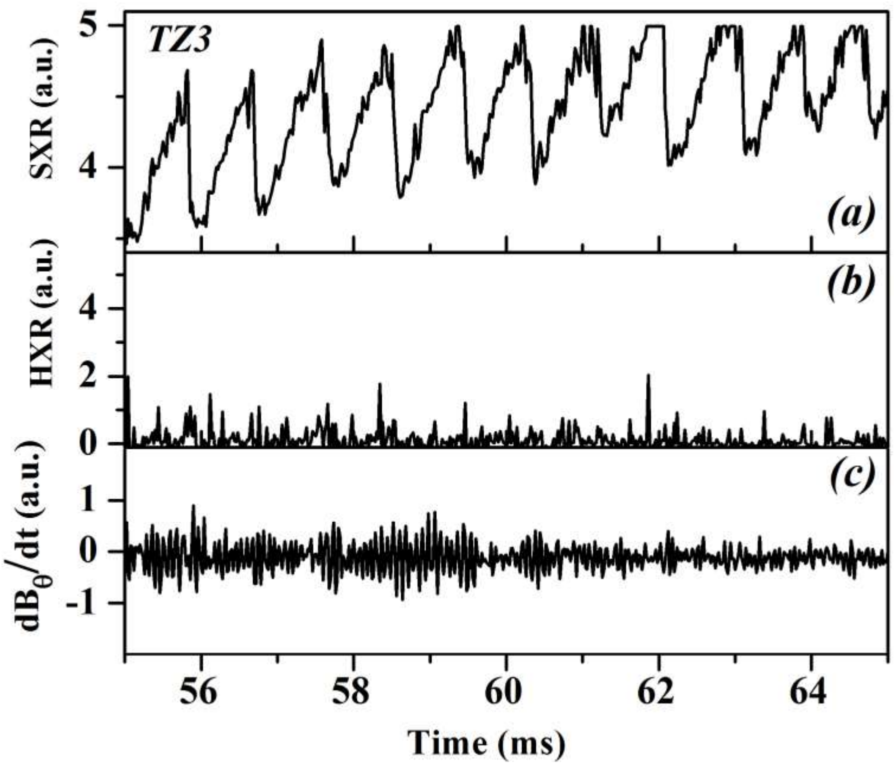

Figure 3.4: Time evolution of (a) intensity of Soft X-ray emission, (b) intensity of Hard X-Rays emission (c) fluctuations in the time derivative of poloidal magnetic field, , $\delta \dot{B}_\theta$ in time zone 3 (TZ3).

Periodic HXR bursts with a time period of $\sim 1\ ms$ remained absent when there is no sawtooth activity in discharge as shown in Figure 3.6. This further confirms that the observed HXR bursts in #24025 are related to the sawtooth crash. The significant build-up of REs in shot # 24020 is due to low plasma density ($< 1 \times 10^{19}\ m^{-3}$) in the current flat-top region as shown in Figure 3.6(e).

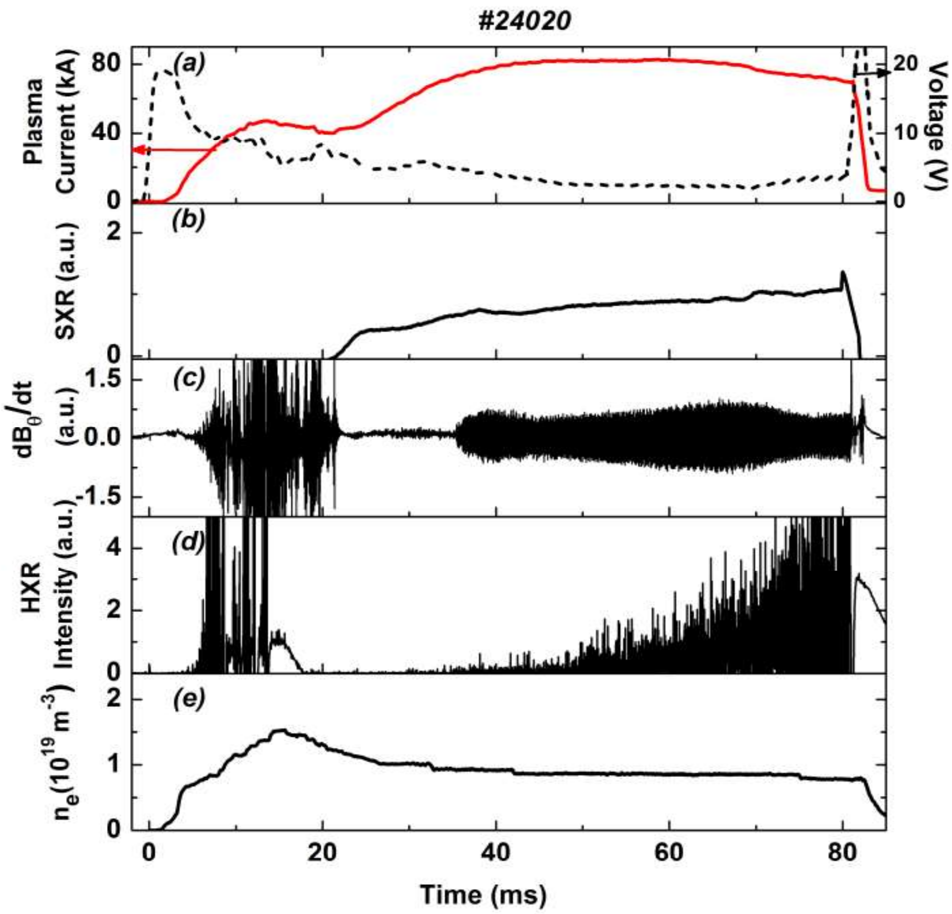

Figure 3.5: Time evolution of a typical plasma discharge of ADITYA tokamak (#24020) with no sawteeth activity in SXR emission (a) Plasma current and Loop Voltage (b) intensity of Soft X-ray emission (c) fluctuations in the time derivative of poloidal magnetic field

In the following sections, it has been demonstrated that the observed periodic HXR bursts are due to generation or acceleration of new REs due to the presence of an additional electric field apart from the loop voltage and not an artefact of the expulsion of existing REs generated in presence of background loop voltage. Exactly similar observations are also made in typical discharges of ADITYA-U tokamak as shown in Figure 3.7.

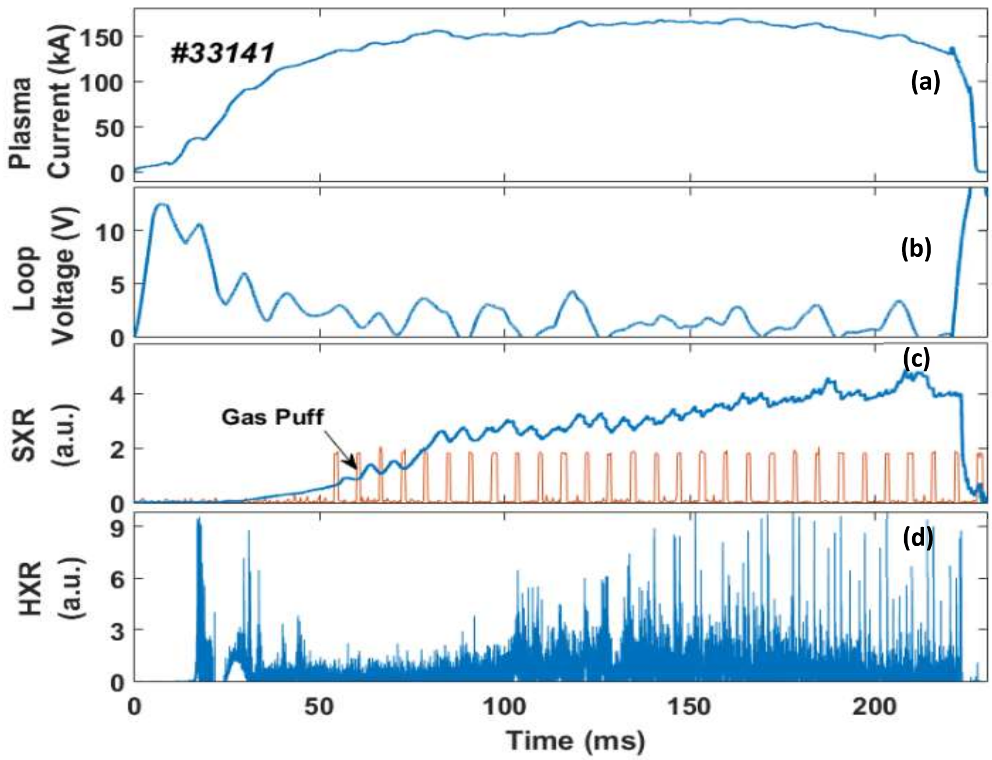

Figure 3.6: Plot showing time evolution of (a) Plasma Current (b) Loop Voltage (c) SXR with sawtooth activity and Gas puff and (d) HXR intensity with periodic HXR burst following the sawteeth crashes.

3.3 Sawtooth generated Runaway electrons in ADITYA/ADITYA-U

It is well known that the HXR emission from the limiter is due to the interaction of REs (non-thermal electrons), with the limiter surface [197]. RE generation and associated HXR emission during the breakdown and start-up phase (TZ1) is a regular feature of ADITYA tokamak plasma [58] and can be explained by the Dreicer model. During this phase the plasma density remains low (< 1 x 10^{19} m^{-3}) and the applied electric field remains much higher than the critical electric field required for Runaway generation, E_{crit} and Dreicer Electric field $E_D$required for thermal electrons to runaway, which can be calculated using the formula

$$E_{crit} = n_e\, e^3\, ln\,\Lambda / 4\pi\varepsilon_0^2 mc^2 \qquad \text{... 3.1}$$

$$E_D = n_e\, e^3 \ln\Lambda / 4\pi\varepsilon_0^2 T_e \qquad \text{... 3.2}$$

Therefore the initial loop voltage leads to the generation of a significant population of REs and subsequent HXR emission having energies up to a few MeV. In the plasma current flat-top, a single cluster of HXR bursts has also been observed quite often, due to enhanced MHD activity causing sudden loss of REs [198]. The experimental observations of the periodic bursts of high-intensity HXRs in TZ2 [see Figure 3.4(b)], presented in this paper, indicate periodic generation of REs and/or acceleration of existing low-energy REs and subsequent loss of these REs from the plasma. Figure 3.3 (d) further shows that a band of intense HXR emission is produced during the breakdown and start-up phase of the plasma current (TZ1) due to the generation of REs by high loop voltage during this phase. This band of intense HXR emission is terminated at $\sim 25\ ms$ into the discharge, indicating that a significant fraction of RE population generated during the breakdown and start-up phase is lost by $\sim 25\ ms$. Thereafter, the HXR intensity remains low from $\sim 25\ ms\ to \sim 40\ ms$ (end of TZ1). Afterward, HXR bursts with intensities up to 10 times higher than the intensity of HXR emission observed in the time interval of $25 - 40\ ms,$ are observed in TZ2, accompanying each sawtooth crash. This suggests a possible generation of REs and/or acceleration of existing REs to higher energies during the sawtooth-crash event, which when lost to the limiter, leads to HXR burst with higher intensity.

The periodic expulsion of residual REs (breakdown and start-up generated REs, surviving the initial loss) pre-existing inside the q = 1 surface, during the sawteeth crashes, may also seem to be a possible mechanism of observance of the HXR bursts. However, in our experiments, this mechanism is highly improbable and the observed HXR bursts cannot be explained without the generation of new REs or acceleration of existing REs, due to following reasons. The spatial distribution of residual REs generated during the breakdown and start-up phase is essentially determined by the spatial distribution of REs at the time of breakdown and start-up along with the prevailing confinement and loss-rate. It is well documented that because of the relatively slow penetration of the applied electric field, the REs are most likely to be generated predominantly in the outer regions of the plasma, in the breakdown and start-up phase [48,199]. Therefore, the residual breakdown and start-up generated REs in the #24025, surviving the initial loss, are expected to remain in the outer region of plasma as they are mostly generated there. It is also well known that independent of their generation location inside the plasma, the REs continuously move towards the outer regions as they gain energy [48,199]. So, even if the REs are generated in the central region during the start-up phase, they move towards the outer region as they gain energy. It is also to be noted here that up to the first $\sim 35\ ms$ of the discharge, the absence of sawteeth activity indicates that the m = 1 island has not come into existence until this time and hence there is no possibility of residual REs being trapped in the island and remain confined inside the q = 1 surface.

Consequently, it is logical to conclude that the residual REs, generated during start-up in #24025, would remain predominantly in the outer region. And periodic expulsion of REs from inside the q = 1 surface during each sawtooth event may not explain the observed high intensity HXR bursts accompanying each sawtooth crash. To substantiate this claim further, the following analysis of the observed HXR intensity in the time-interval between the sawtooth crashes(ΔT_{SWC}), as shown in Figure 3.4 (b), is presented. In the entire time duration of TZ2, the increased MHD activity, identified as m = 2 and m = 3 modes, majorly controls the radial loss of REs as described in next section. If a sawtooth-crash event expels a part of the residual REs present in plasma volume contained in q =1 surface, $V_{q<1}$, they will be lost to the limiter only by the prevailing loss rate in the intermediate region between q = 1 and the limiter. The residual REs present in the plasma volume between the q = 1 surface and the limiter, $V_{q>1}$, are also being expelled by the same rate amounting to the observed HXR intensity during ΔT_{SWC}. As $V_{q>1}/\ V_{q<1} \sim$ 10, the number of residual REs inside $V_{q<1}$will be $\sim 1/10^{th}$ of those present in $V_{q>1}$, if the residual REs being uniformly distributed in total plasma volume. So, even if a sawtooth-crash throws away all the residual REs present in $V_{q<1}$, without accelerating them, the total HXR intensity during the sawtooth-crash should only be 1.1 times more intense than its value during ΔT_{SWC} in TZ2. If we consider the spatial distribution of REs predominantly present in the outer region, the total HXR intensity during the sawtooth-crash should be even less. However, the observed HXR bursts accompanying each sawtooth-crash in TZ2 are $5 - 10$ times more intense than that of the HXR intensity during ΔT_{SWC} in the same time zone (TZ2). If the observed RE bursts are to be explained by the periodic expulsion of residual REs (no new generation or acceleration of existing REs), the above analysis demands that the number density of residual REs inside the q = 1 surface should be $\sim 50\ to\ 100$ times more than those outside the q = 1 surface. This is again quite unlikely as reasoned in the above paragraphs. The above discussion strongly suggests that the REs are being produced and/or the existing REs are accelerated, particularly around the q = 1 surface, during each sawtooth-crash event and leading to observed HXR bursts.

The generation and/or acceleration of REs can be through the primary generation mechanism (Dreicer acceleration) or due to knock-on avalanche (secondary) mechanism. The avalanche mechanism is an exponential process with a growth rate $\gamma_{sec} \propto [(E/E_{crit}) - 1]$ [195]. With $E_{crit} \sim 0.02\ V/m$, and $E = (V_L/2\pi R) \sim 0.4\ V/m$ in the current flat-top of reported discharges, the secondary generation time scale, $\tau_{sec} \sim 100\ ms$ is much larger than the time interval between two HXR bursts in TZ2 and almost of the order of the total discharge duration. Hence, it is quite unlikely that the RE bursts in TZ2 are generated due to the knock-on avalanche or secondary mechanism. Therefore, the primary (Dreicer) mechanism remains the only possible mechanism by which the REs can be generated in TZ2. It is well known that a minimum electric field, E_{crit} is required to generate any runaway in tokamak plasma, $E \gtrsim E_{crit}$. However, Granetz et al [71] have reported that for a significant RE production, only $E \gtrsim E_{crit}$ is not sufficient, and $E/E_{crit} > 10$ is required for significant RE production in TEXTOR, DIII-D and FTU tokamaks. Furthermore, the primary runaway growth rate at a given value of E/E_{crit} inherently depends on the temperature. Because the width of velocity distribution functions describing the particle speeds is determined by the temperature and hence the number of particles with speed above any threshold speed is temperature-dependent [200]. In the plasma current flat-top region of the reported discharges (TZ2 and TZ3), the $E/E_{crit} \sim 20$ and with the plasma temperature $\sim 500\ eV$, negligible runaway population is expected due to available loop voltage ($\sim 0.4\ V/m$) in the current flat-top region. This is quite evident in TZ3 where $E/E_{crit} \sim 20$ and negligible HXR intensity is observed. Therefore, an additional source of the electric field is required for RE generation leading to observed HXR bursts associated with the sawtooth crash in TZ2.

The experimental observations described in Sec. 3.1.2 evidently indicate that the HXR bursts during a sawtooth crash in TZ2 are connected to the phenomena of magnetic reconnection associated with the abrupt growth of m = 1, n = 1 perturbations. The absence of HXR bursts in TZ3 excludes the possibility of non-thermal electron generation due to plasma-wall interaction during the sawtooth crash. The observations in TZ3 further refute the possible role of ballooning origin of HXR bursts [192]. Furthermore, the periodic HXR bursts are not observed in discharges in which the sawteeth are not present. Due to all the above-mentioned reasons, RE generation due to the electric field induced during a sawtooth crash is intuitively the most suitable explanation for the observed periodic HXR bursts. In order to verify this possibility, the Electric field induced due to the sawtooth crash has been estimated in the following section.

3.3.1 Sawteeth Induced Electric Field

According to Wesson [54], the rate of change of reconnected flux per length is given by the radial velocity of the plasma multiplied by the helical magnetic field, B^*. Using this model we can calculate the Electric field produced due to change of the magnetic flux as following. The helical magnetic field is calculated as

$$B^* = (1 - q_0)B_{\theta 1}, \qquad \ldots 3.3$$

where $B_{\theta 1} = \mu_0 I_{r_1}/2\pi r_1$ is the initial poloidal magnetic field at q = 1 surface, r_1 is the radius of q = 1 surface and I_{r_1} is the total current inside q = 1 surface, and q_0 is the safety factor at the plasma axis. Thus the electric field in the reconnection layer is,

$$E \sim v_r B^* \qquad \ldots 3.4$$

v_r is the radial velocity of plasma. The reconnection time, t_{rec}, which is experimentally observed as the sawtooth crash time, is theoretically calculated as [18]

$$t_{\mathrm{rec}} = r_1/v_r \qquad \ldots 3.5$$

The inversion radius, same as r_1 can be experimentally estimated from Soft X-ray tomography, which is typically $\sim 6.5\ cm$ for these discharges. The mean crash time of several crashes during the current flat top for the representative discharge #24025 $\sim 50\ \mu s$. From the experimental r_1 and t_{rec}, the calculated $v_r \sim 1.3 \times 10^3 ms^{-1}$. The reconnection time may also be calculated using the formula

$\tau = (r_1 \omega_P / c)\tau_A$ ...3.6

where the Alfven time, $\tau_A = \mathrm{r}_1/(B/\sqrt{\mu_0 m_i n_e})$ and plasma frequency, $\omega_P = n_e \mathrm{e}^2/\varepsilon_0 m_e$. For the representative discharge the plasma density $n_e \sim 2 \times 10^{19}\ m^{-3}$ and $B = 0.75\ T$, therefore $\tau_A \sim 2.1 \times 10^{-8} s$ and $\omega_P = 2.5 \times 10^{11} s^{-1}$. Hence, $\tau = 50\ \mu s$ which is in agreement with the observed crash time in the experiment. In order to calculate B^*, the total plasma current inside the q = 1 surface (at $r_1 \sim 0.065\ m$), I_{r1} has been calculated using a reconstructed current density profile of the form

$j(r) = j_0\,[(1 - r^2/a^2)]^{\nu}$ ...3.7

where plasma radius, $a \sim 25\ cm$, and peaking factor, $\nu \sim 4$ [140]. The total plasma current inside the q = 1 surface, i.e. $I_{r1} = j(r_1)\pi r^2 \sim 23\ kA$. The initial poloidal magnetic field at the $q = 1$ surface With $I_{r1} \sim 23\ kA$, comes out to be $B_{\theta 1} \sim 7.4 \times 10^{-2}\ T$. The peaking factor ν follows the relation,

$q_a/q_0 = \nu + 1,$ ...3.8

where $q_a \sim 4$ is the edge safety factor for the studied discharge. q_a is calculated using equation 2.4 and putting $r = a$. Putting the values ν and q_a in the above relation we get $q_0 \sim 0.8$ [54,140]. The calculation also verifies that the on-axis safety factor $q_0 < 1$, which is a necessary condition for sawtooth instability in tokamaks. Substituting the values of $B_{\theta 1}$ and q_0 in equation 1 we get $B^* = \sim 1.5 \times 10^{-2}\ T$. Finally, putting the value of v_r and B^*in the equation (2) the electric field induced due to the sawtooth crash in ADITYA, E_{swc} is calculated to be

$$E_{swc} \sim 20\ V/m.$$

In the following section, the possibility of RE generation by this sawteeth induced E field has been investigated and a crude estimation of REs that may be generated is also calculated.

3.3.2 Generation of REs by Sawteeth Induced Electric Field

As mentioned in Chapter 1 the necessary condition for RE generation in presence of an electric field, E in a tokamak is $> E_{crit}$ [49,53]. For studied discharge, the estimated critical electric field was calculated using the formula 3.1.

$$E_{crit} = n_e\, e^3 \ln\Lambda / 4\pi\varepsilon_0^2 mc^2$$

which for given discharge results to be $E_{crit} \sim 0.02\ V/m$ and is much greater than the E_{SWC} estimated in section 3.1.4. According to Driecier's RE generation theory, all thermal electrons may runway if the Electric field exceeds E_D. However, in reality, the electric field required for all thermal electrons to runaway is much higher, nevertheless at $E > E_D$ the RE production is significantly high [71]. For the presented discharge the E_D has been calculated using the following formula [48]

$$E_D \cong 4 \times 10^{-2}(n_e/10^{19})(10^3/T_e)(ln\Lambda_c/15) \qquad \ldots 3.9$$

where density n_e is in m^{-3}, electron temperature, T_e is in eV and $ln\Lambda_c$ is the Coulomb logarithm. Taking $n_e \sim 2 \times 10^{19} m^{-3}$, $T_e \sim 500\ eV$ and $ln\Lambda_c \sim 15$, the calculated value of $E_D = 16\ V/m$. Therefore, in the typical sawteeth discharge of ADITYA tokamak presented in this paper, the induced electric field due to sawtooth crash is higher than the critical electric field required for thermal electrons to runaway, $E_{swc} > E_D$. Hence, it can be established that the REs can be generated by induced parallel electric fields during the sawtooth crash in ADITYA tokamak. In order to estimate the number of REs generated during each crash, the following formula for the production rate of the primary REs can be used [49]

$$\tau_{dr}^{-1} \approx 0.3\, \upsilon_e \varepsilon_d^{-3(Z_{eff}+1)/16} exp\left(-1/4\varepsilon_d - \left(\{Z_{eff}+1\}/\varepsilon_d\right)^{1/2}\right) \qquad \ldots 3.10$$

where $\varepsilon_d = E_{swc}/E_D$, υ_e is collision frequency of electrons at a thermal velocity v_{th} and Z_{eff} (≈ 1.5) is the effective plasma charge . For the studied discharge $n_e \sim 2 \times 10^{19}\ m^{-3}$, $T_e \sim 500\ eV$ and $E_{swc} \sim 20\ V/m$. Putting these values in equation 3.10 and assuming there is no loss of runaway electrons during the sawtooth crash, number of primary REs that can be produced during the crash time ~ 50 μs due to the induces E_{swc} at q = 1 surface can be estimated, using the relation $dN_{re}/dt = n_e/\tau_{dr}$. The number of REs generated is calculated to be $10^{18} m^{-3}$, which is sufficient to generate the observed HXR bursts.

3.4 Radial Transport of Sawteeth generated REs

3.4.1 Fast Radial transport of REs

Together with the generation of the REs by induced $E_{\|}$, the perturbed magnetic field (B^*) during the sawtooth crash simultaneously throws out the REs from the reconnection layer to larger radii ($r > r1$). When these REs reach to the limiter traveling through the intermediate plasma region extending from q = 1 surface to the limiter, they emit HXR bursts upon colliding with the limiter. The de-confinement of high energy electrons in case of macro-scale magnetic turbulence is quite well known [95]. The loss of REs, governed by magnetic turbulence can be determined by the diffusion coefficient using Rochester and Rosenbluth formula [201]

$$D_{RE} \cong \pi q R_0 \mathrm{v}_{||RE} (\delta B_r / B_T)^2 \qquad \ldots 3.11$$

where B_T is the background magnetic field and δB_r is it's a radial perturbative part, R_0 is major radius, q is the safety factor, and $v_{||RE}$ is the RE velocity. Estimating the radial magnetic field perturbations using

$$\delta B_r = (r_1/r)^{m+1} \delta B_{\theta,q=1} \qquad \ldots 3.12$$

$\delta B_r / B_T$ during the sawtooth crash is found to be $\sim 1.3 \times 10^{-3}$. Putting this value in equation 3.11 and taking $\mathrm{v}_{||RE} \sim c$, the velocity of light, $D_{RE} \sim 1300\ m^2/s$ is obtained. The time for the REs generated during a sawtooth crash to reach the limiter surface, t_{RR} , has been calculated by using the formula

$$t_{RR} \approx a^2 / C D_{RE} \qquad \ldots 3.13$$

where, 'a' is the size of the medium through which the REs propagate and C is inversion radius position [202,203]. Taking inversion radius, $C = r1 = 6.5\ cm$ [203], the REs generated near $q = 1$ surface due to sawtooth crash should reach to the limiter ($r = 0.25\ m$) in $\sim 700\ \mu s$. Hence the HXR bursts due to sawtooth crash generated REs should have appeared after $\sim 700\ \mu s$ of the crash, according to Rochester and Rosenbluth diffusion model. However, in the experiments HXR burst appears within $\sim 10 - 30\ \mu s$ after the crash as shown in figure 5 during TZ2, which is $\sim 20 - 70$ times faster than diffusion time estimated using the theoretical model. Interestingly, no

HXR bursts appear in the time zone TZ3 even though the sawteeth are present in this time zone. As demonstrated in earlier section due to the continuation sawtooth oscillations, significant REs must be generated with each sawtooth crash near the q~1 surface, hence the absence of REs may be due to the effect of modified magnetic topology on radial REs transport. This observation suggests that sawteeth generated REs fail to reach the limiter hence do not produce the HXR bursts like those in TZ2. In order to investigate the reason behind the disappearance of periodic HXR bursts, the state of magnetic surfaces in the intermediate region ($r_1 < r \leq r_{lim}$) in time TZ2 & TZ3 have been extensively analysed and presented in the following section.

3.4.2 Magnetic Island Characterization and Evolution

As explained in detail in chapter 2, the magnetic islands are studied using the set of Mirnov coils which detect the time varying poloidal magnetic fluctuations induced by the islands. Figure 3.4(c) and 3.5(c) compares the MHD activity in TZ2 and TZ3 respectively measured by the Mirnov coils for shot #24025. The figures clearly show that the amplitude of Mirnov oscillations is higher in TZ2 as compared to TZ3 indicating a difference in the magnetic island topology in TZ2 and TZ3. The periodic high HXR burst period coincides with the high Mirnov oscillation amplitude phase whereas the no HXR burst period coincides with low Mirnov oscillation amplitude period To characterize the observed Mirnov oscillations in these two zones, Fourier spectrum analysis of these fluctuations has been performed. Figure 3.8(a) and (b) compares the spectral properties of these fluctuations for both the zones, the Figure 3.8 (a) show the spectral properties of the fluctuations for TZ2, which has higher MHD activity and Figure 3.8 (b) show the spectral properties of the fluctuations for TZ3 with low MHD activity. It is evident from the figures that in TZ2 with high MHD activity, the fluctuations in the magnetic field exhibit multiple coherent peaks in the frequency range of $\sim 12 - 15\, kHz$, whereas in TZ3, the intensity of these peaks have been reduced by ~ 10 times. Investigating further the Mirnov oscillations in TZ2, the mode structures, obtained using singular value decomposition (SVD) technique [190,203], show the presence of m = 2 and m = 3 modes as shown in Figures 3.9(a) and 3.9(b).

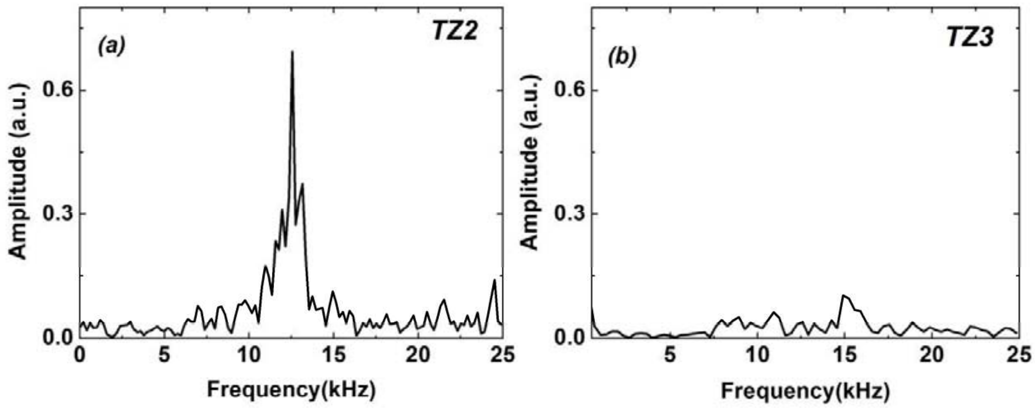

Figure 3.7: Frequency spectra of fluctuations in the time derivative of poloidal magnetic field, $\dot{B_\theta}$, (a) in time zone 2 (TZ2) and (b) in time zone 3 (TZ3)of discharge #24025

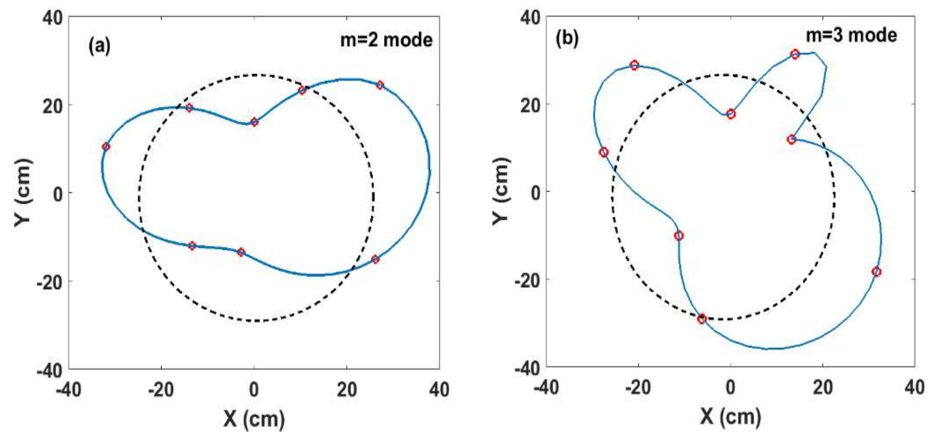

Figure 3.8: Spatial structures of (a) m = 2 and (b) m = 3 modes in time zone 2 (TZ2) of discharge #24025.

Both the modes have almost similar frequencies$\sim\ 12 - 15\ kHz$. The island widths associated with these modes are estimated from the measured amplitudes of $\widetilde{B_\theta}/B_\theta$ using the relation [140]

$$W/r_s = 2\left[(2/m)(r_c/r_s)^m\left(\widetilde{B_\theta}/B_\theta\right)\right]^{1/2} \qquad \ldots 3.14$$

where W is the island width, m is the mode number, r_s is the radius of the mode resonant surface and r_c is the radius of the Mirnov probe location. The radius of the mode resonant surface, r_s for m = 2 and 3 modes are estimated to be $\sim 16\ cm$ and $\sim\ 20\ cm$, respectively, using reconstructed q (safety factor) profile for which, current profile of the form given above with $\nu\ \sim\ 4$ is used [140]. Island widths associated with m = 2 and m = 3 islands are found to be $\sim 6\ cm$ and $\sim 4\ cm$ respectively in TZ2, whereas the widths in TZ3 for m = 2 and m = 3 islands are found to be ~ 3 cm and ~ 2 cm respectively which is quite narrow. Assuming the island grow equally on either side of the mode resonant surface, r_s, Figure 3.10 shows the time evolution of the outer (low field side) boundary of m = 2 island ($r_s \sim 16\ cm$) and the inner (high field side) boundary of m = 3 island ($r_s \sim 20\ cm$) in TZ2 and TZ3.

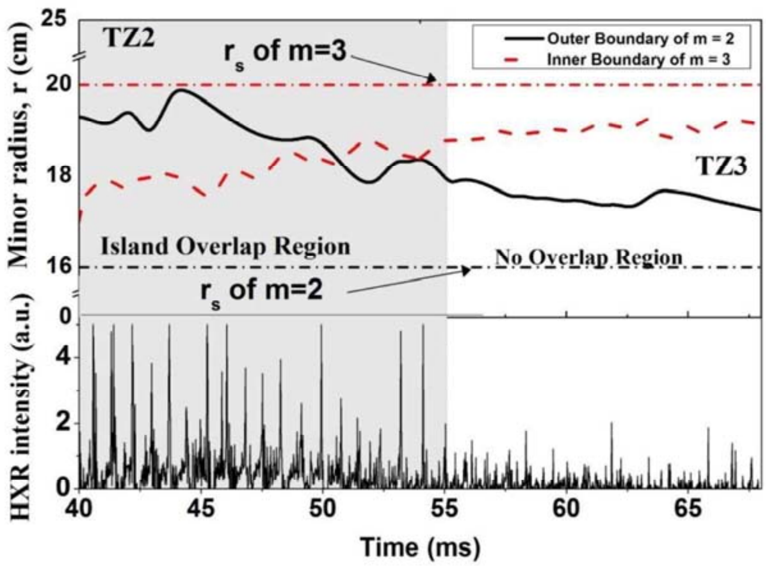

Figure 3.9: (a) Time evolution of outer boundary of m = 2 (solid line) island and inner boundary of m = 3 (dashed line). The location of mode rational surfaces is indicated by dash-dot line. (b) Time evolution of HXR emission intensity (shot# 24025).

Interestingly, Figure 3.10 reveals that in time zone TZ2 both the m = 2 and m = 3 islands grow so large that they overlap each other. Whereas in the time TZ3 the width of the islands reduces and they remain well separated from each other indicating that good magnetic surface prevails in between the islands in TZ3. The above analysis of the intermediate plasma lying between the q = 1 surface and the limiter explains the presence and absence of HXR burst in TZ2 and TZ3 respectively. The strong ergodization of the magnetic field with no good surfaces in the area traversed by the REs is considered as a possible mechanism of the rapid loss of REs. It is hypothesized that the ergodization is due to the overlap of large, low poloidal mode number magnetic islands. The ergodized magnetic field structure would affect the REs more than 10 times faster than they affect the thermal plasma [97,98]. Such a situation arises in time TZ2 in our experiments where the two islands m = 2 and m = 3 overlap in the intermediate region of $r_1 < r \leq r_{lim}$. The ergodization in this intermediate region facilitates the rapid loss, faster than their diffusion due to magnetic perturbation associated with each sawtooth crash, of REs generated due to sawtooth crash, leading to HXR bursts within $\sim 10 - 30\ \mu s$ of the crash. Furthermore, a small number of the good surfaces are known to reduce the transport of the energetic electrons [204] which is the situation in TZ3, where both the islands get separated due to a reduction in their sizes indicating the presence of good surface in between the islands. This significantly brings down the transport of REs to prevent them from reaching the limiter surface and hence no HXR bursts are observed in TZ3 although the sawteeth remain present during this time. Figure 3.11 shows a cartoon of m=2 and m=3 island during TZ2 and TZ3, in a poloidal cross-section.

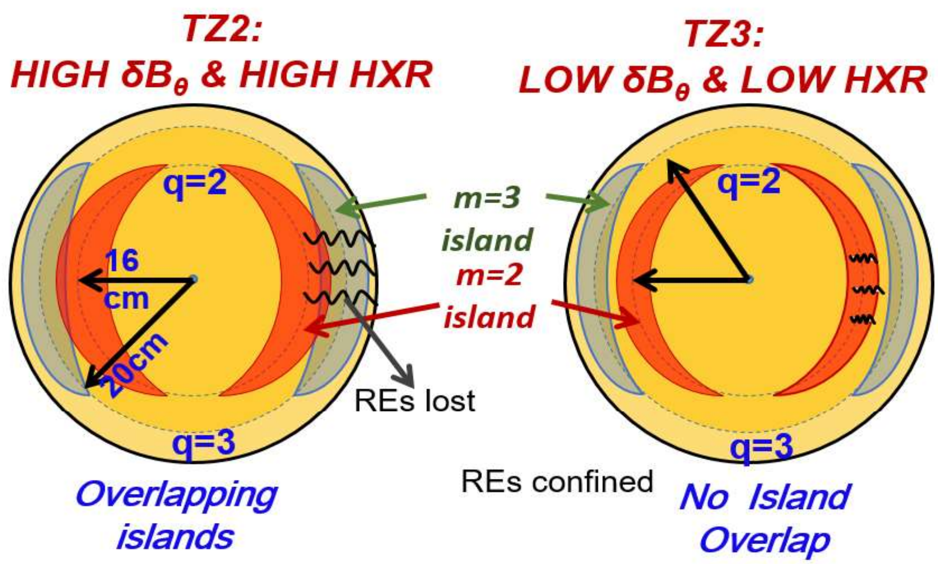

Figure 3.10: Cartoon representation of m=2 and m=3 islands in a poloidal cross-section during TZ2 (island overlapping) and TZ3 (No overlapping)

3.5 Conclusion

In this chapter it has been established that the sawtooth instability can induce electric fields strong enough to generate Runaway electrons and these REs travel to the limiter in different fashion depending the plasma conditions in terms of presence and absence of individual or overlapped MHD islands, prevailing between the q = 1 surface and the limiter, to excite HXR emission. HXR burst, produced due to RE-limiter interaction, accompanying each sawtooth crash have been observed during first 15–20 ms of the current flat-top of Ohmic discharges in ADITYA/ADITYA-U tokamak. These HXR bursts remained absent in the later period of current flat-top although the sawteeth event continued during this time. Detailed analysis revealed that a toroidal electric field is induced due to the change in poloidal magnetic field associated with the growth of m = 1, n = 1 mode during the sawtooth crash at q = 1 surface. The amount of induced electric field due to sawtooth crash is found to be higher than the critical electric field required for thermal electrons to runway. This leads to the generation of REs during each sawtooth crash in typical discharges of ADITYA/ADITYA-U tokamak. The REs, hence generated at q = 1 surface during a sawtooth crash, when they reach the limiter, give rise to bursts of HXRs leading to the observation of associated HXR burst with each sawtooth crash during first $15\text{–}\ 20\ ms$ of plasma current flat-top region. It has been observed that the travel time to the limiter, of these crash-induced REs, depends on the presence of magnetic islands having different widths and overlapping in the intermediate plasma situated between the q = 1 surface and limiter. The measured Mirnov fluctuations show the presence of high MHD activity in this intermediate region of plasma during the extent of plasma current flat-top where sawtooth crash-associated HXR bursts are observed. The MHD activity subsides in the later period of plasma current flat-top where the HXR bursts are not observed in the presence of sawteeth crash. A thorough analysis of MHD activity, in both the time periods where HXR bursts are present and absent, revealed presence of overlapping m = 2 and m = 3 islands in the intermediate plasma region when sawtooth crash-associated HXR bursts are observed. The width of these islands reduces in the later period of plasma current flat-top and they lay separated from each other when sawtooth crash-associated HXR bursts are not observed. Hence, it is concluded that ergodization due to island overlapping in intermediate region facilitates the rapid loss of REs generated due to sawtooth crash to limiter leading to HXR bursts. And a small number of the good surfaces present between the islands substantially reduce the transport of the REs leading to non-observance of HXR bursts in the later period of plasma current flat-top, although the REs are still being generated due to the sawtooth crash.

To understand further the role of MHD islands present in the discharges, mainly the m/n=2/1 MHD mode, in the generation/loss/trapping mechanism of REs, multiple discharges from both ADITYA and ADITYA-U with the presence of MHD islands of smaller and larger island-widths have been analysed and studied in detail. These results are presented in the next chapter to gain a better perspective on RE dynamics in presence of MHD islands of different widths.

Chapter 4

Drift tearing modes and its interplay with Runaway electrons in ADITYA and ADITYA-U tokamak

As mentioned earlier in the thesis, the uncontrolled growth of resistive magnetohydrodynamic (MHD) modes leading to disruptions and generation of high energetic runway electrons($\sim 3 - 10 MeV$), both pose severe threats to a successful operation of bigger tokamaks including ITER. Both of these have been studied separately for a very long time, however, studies on the interplay between the two have fast-tracked in recent years [27,71,73,108,205]. Several experimental, as well as theoretical studies, have been reported in the literature describing the effect of MHD modes on runaway electron transport [41,95,105,206,207]. The transport of runaway electrons is found to be sensitive to magnetic perturbations and techniques like the application of resonant magnetic perturbations are tested with limited success for mitigating the REs on various tokamaks [87,97,208] Recently, runaway electron generation has been reported as a possible trigger for the enhancement of magnetohydrodynamic plasma activity and fast changes in runaway beam behavior in EAST tokamak [78,209,210]. The possible relation between the magnetohydrodynamic (MHD) phenomena and runaway electrons (REs) in standard discharges are investigated in ADITYA as well as ADITYA Upgrade tokamak. Analysing a large number of discharges, it has been observed that discharges with strong MHD activity always have low limiter-generated hard-X ray (HXR) emission compared to those having weak MHD activity. Interestingly, a gradual increase in HXR emission intensity closely following a gradual decrease in MHD mode amplitude has been observed during the course of a single discharge in several discharges. Furthermore, spontaneous increase in MHD mode amplitude along with the appearance of harmonics, strongly coinciding with a burst of HXR emission is also observed during a discharge. These observations suggest the existence of a possible interaction between the RE dynamics and the MHD modes in ADITYA and ADITYA-U tokamaks, as the limiter HXR emission is a consequence of REs interacting with the limiter. The study reveals that the discharges in which large 2/1 island width may confine runaways leading to decrease in observed hard X-ray emission from the limiter.

The above analysis has mainly been carried out statistically on a shot-to-shot basis along with analysing the spontaneous events occurring in the discharges with no control on their repeatability. It can very well be argued that even though the external confining fields, loop voltage, and plasma parameters remain the same, the generation, as well as the dynamics of REs, may be different in different discharges leading to conclusions arrived at. Hence it has been attempted to modify the MHD characteristics with the application of a train of short gas-puff pulses of hydrogen (fuel gas) during the plasma current flat-top phase of a single discharge and RE dynamics have been studied. The short gas puffs, injecting approximately $\sim 10^{17} - 10^{18}$ molecules of fuel gas (hydrogen) at one toroidal location, are found to concomitantly decrease the drift-tearing mode rotation frequency and the mode amplitude during the period of injection and then recover back to its initial values when the gas pulse is over. This leads to a periodic modulation of the rotation frequency and amplitude of the drift-tearing modes that is correlated with the periodicity of the gas pulse injection. The underlying mechanism for this change in the mode characteristic appears to be related to a gas puff induced a change in the radial profile of the plasma pressure in the edge region that brings about a reduction in the diamagnetic drift frequency. Detailed experimental measurements and BOUT++ code simulations support such a scenario. Our results reveal a close interaction between the edge dynamics and core MHD phenomena in a tokamak that could help us better understand the rotation dynamics and amplitude pulsations of magnetic islands and subsequent changes in RE dynamics.

This chapter is mainly sub-divided into two parts. In part one, the RE dynamics are studies in different discharge having strong and weak MHD activity statistically. Part two consists of adaptation of MHD mode characteristics using shot gas-puff pulses in a single discharge and its effect on the RE dynamics. Discharges over a wide range of plasma parameters from both the machines are used for the study presented in this chapter unless otherwise mentioned specifically. The plasma parameters of the studied discharges are : toroidal magnetic field, $B_T \sim 0.8 - 1.1\ T$; plasma current, $I_p \sim 80 -$

$120\ kA$; chord average plasma density, $n_e \sim 1.5 - 3 \times 10^{19} m^{-3}$; electron temperature, $T_e \sim 250 - 700\ eV$; discharge duration, $90 - 200\ ms$.

4.1 Relation between REs and 2/1 Drift Tearing Modes and its Harmonics in ADITYA and ADITYA-U tokamak

4.1.1 Drift Tearing mode and its Harmonics in ADITYA and ADITYA-U tokamak

The resistive tearing instabilities and growth of magnetic islands leading to plasma disruption are reviewed in detail in chapter 2. The classical resistive tearing instability, a purely growing mode, changes its character when electron pressure gradient effects are important[134,211,212]. In the regime where the electron diamagnetic frequency is larger than the tearing mode growth rate, the growth rate of the unstable mode is significantly reduced. In this so-called linear 'Drift-tearing' regime, the magnetic islands rotate in the electron diamagnetic drift direction with frequencies close to the diamagnetic drift frequency, ω^* [146,213,214]. In the non-linear phase, the pressure gradient around the magnetic islands is flattened and the diamagnetic drift frequency is modified[146,215]. The amount of flattening depends on the perpendicular transport and the electron temperature. Experimentally, the onset and growth of tearing modes and the island structures can be obtained by measuring the variations of the perturbed poloidal magnetic field [24]. These variations are conveniently picked up by Mirnov coils, a set of small magnetic loops placed around the poloidal periphery of the tokamak at one or several toroidal locations. The frequency spectra of the poloidal magnetic field fluctuation exhibit coherent peaks corresponding to different modes present in the plasma. Again, the measurement and analysis of poloidal magnetic field fluctuations in ADITYA and ADITYA-U are described in Chapter 2. In the purely Ohmic discharges of ADITYA [157,182] as well as of ADITYA Upgrade tokamak[189] the frequency spectra of the poloidal field fluctuations show single as well as multiple peaks indicating the presence of one or several MHD modes in these discharges. These modes are found to be rotating with a frequency close to the electron diamagnetic frequency and hence can be identified as drift-tearing modes (DTMs) in the low β plasma of ADITYA and ADITYA-U plasmas. A detailed analysis from many discharges (> 2000), reveals that the observed multiple peaks in the frequency spectra of the Mirnov signal are the harmonics of a dominant m/n = 2/1 mode since the frequencies of these peaks are found to be integral multiples of the fundamental frequency of the m/n = 2/1 mode. As many as seven harmonics have been observed in these discharges with the number of higher harmonics varying from two to seven. They are found to last through the entire life time of a discharge or in some cases appear and disappear during the temporal evolution of a discharge. Our experimental observations also indicate that the number of harmonics appearing in a discharge is strongly related to the frequency of the fundamental m/n = 2/1 mode and they do not occur above a threshold value of the frequency. The lower the frequency of the fundamental m/n = 2/1 mode, the higher the number of harmonics and the amplitude of the MHD fluctuation. Although the presence of harmonics in destabilised non-linear tearing modes (NTMs) are quite common in high β tokamaks, very few investigations of harmonics of DTM have been reported in tokamaks [216–219] and in some cases, they have been attributed to island distortion [219]. Bicoherence investigation of Mirnov signals reveals that there are periodic, non-sinusoidal, oscillations are present in the observed time series of Mirnov oscillations. In addition, the observations also show that above a threshold value of mode-rotation frequency, the harmonics cease to exist and only the m/n = 2/1 mode with very low amplitude remains throughout the discharge.

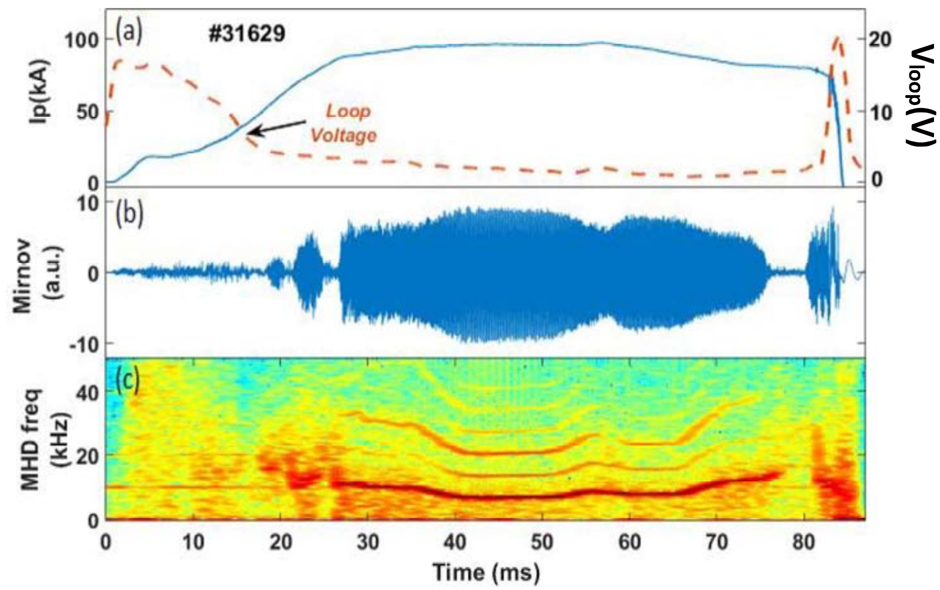

Figure 4.1: Time evolution of (a) Plasma current and loop voltage (b) $\dot{\tilde{B}}_\theta$ acquired by Mirnov and its (c) frequency spectrum with multiple frequency bands for discharge #31629

Temporal evolution of loop voltage, plasma current, fluctuation of the poloidal magnetic field, $\dot{\tilde{B}}_\theta$ from one of the 16 Mirnov probes and its frequency spectra, for a typical discharge of ADITYA tokamak with strong MHD activity is shown in Figure 4.1.

It can be clearly seen in the figure that during $40\ to\ 50\ ms$ in the current flat-top of presented discharge, seven coherent modes appear in the time-frequency plots of Mirnov Oscillations. The frequency of each band is a positive integral multiple of the frequency of the mode with the lowest frequency at every instant during the current flat top. The lowest frequency mode (~ 7 kHz) has the highest power. The subsequent MHD modes with relatively lower power have frequencies of ~ 14, 21, 28, 35, 42, and 49 kHz respectively. The MHD mode ($\sim 7\ kHz$) has a mode structure of *m/n* = 2/1 mode (where *m* and *n* are the poloidal and toroidal mode numbers respectively). To identify the *m* value, $\dot{\tilde{B}}_\theta$ data acquired from all 16 Mirnov probes filtered for the frequency between $6 - 9\ kHz$ at a single time instant has been plotted in a polar plot where θ is the poloidal location of the respective Mirnov coil. To identify the *n* value of the MHD mode, $\dot{\tilde{B}}_\theta$ acquired from Mirnov at same poloidal location θ but situated at the opposite toroidal location have been compared. The 1st harmonic mode at $\sim 14\ kHz$ has been identified as *m/n* = 4/2 mode. The mode structures of these two modes are plotted in Figures 4.2a and 4.2b.

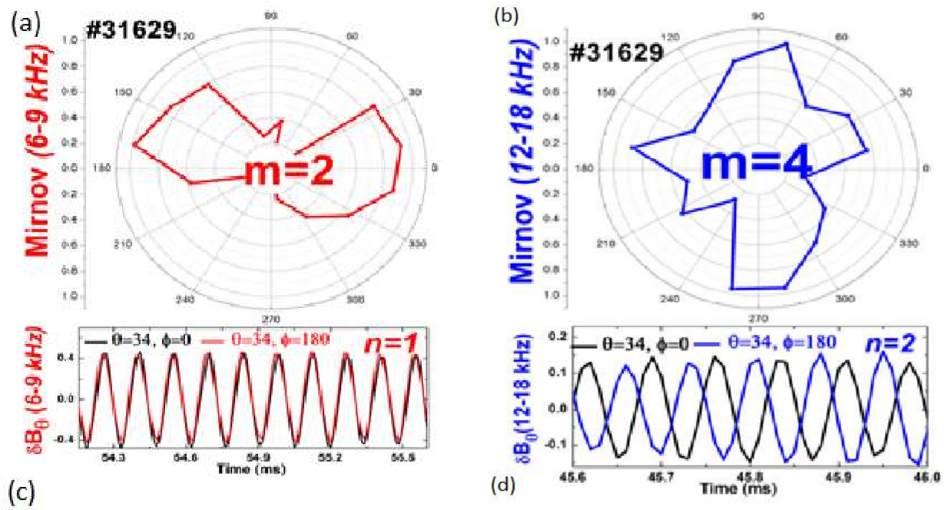

Figure 4.2: Plot showing poloidal mode structure plotted using poloidal magnetic fluctuation from Mirnov coils (a) filtered for the range of lowest frequency band (6-9 kHz) (b) filtered for the second lowest frequency band range (12-18 kHz). (c) Integrated poloidal magnetic fluctuation from Mirnov coils at (θ, φ)=(34˚, 0˚) (black) and (θ, φ)=(34˚, 180˚) (red).

For the discharges presented in this thesis, the toroidal magnetic field, B_{ϕ}, is in the anti-clockwise direction and the plasma current is in the clockwise direction as viewed from the top, both in ADITYA and ADITYA-U [189]. Hence, the electron diamagnetic drift has a poloidal clockwise direction. Before the gas injection, the observed coherent m/n = 2/1 MHD modes are found to be rotating in a poloidal clockwise direction. The direction of rotation of these modes is obtained by plotting the filtered Mirnov fluctuations at the coherent frequency $\sim 5 - 14\ kHz$ of the dominant m/n = 2/1 mode for all the 16 coils. Figure 4.3 (a) and (b) shows the raw Mirnov fluctuations at different poloidal angle arranged in a clockwise direction starting from outboard 0° and the poloidal phase angle plot using all 16 Mirnov coils and corresponding contour plot, respectively.

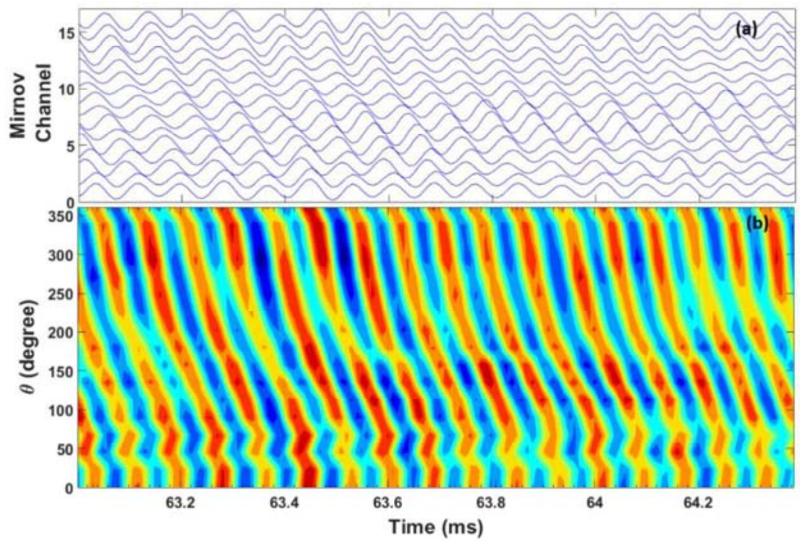

Figure 4.3:Poloidal magnetic fluctuations from 16 Mirnov coils (b) and their Contour plot.

Figure 4.4 shows a series of mode structures obtained at an interval of 0.02 ms during plasma current flat top, showing clockwise rotation of m=2 mode, i.e. in electron diamagnetic drift direction.

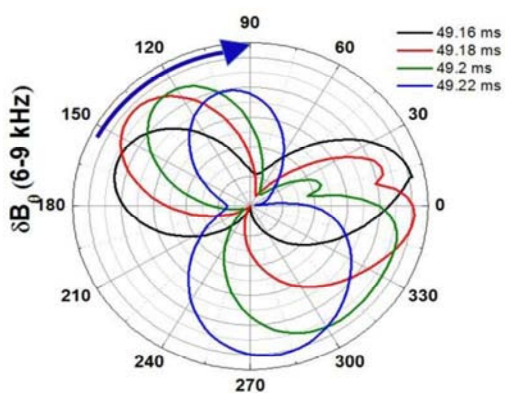

Figure 4.4: Series of mode structure obtained at an interval of 0.02 ms during plasma current flat top, showing clockwise rotation of m=2 mode, i.e. in electron diamagnetic drift direction.

Furthermore, coherent peaks at a frequency similar to that of the dominant m/n = 2/1 mode are observed in the frequency spectra of electron density fluctuations obtained from microwave interferometer diagnostic, as shown in figure 4.5.

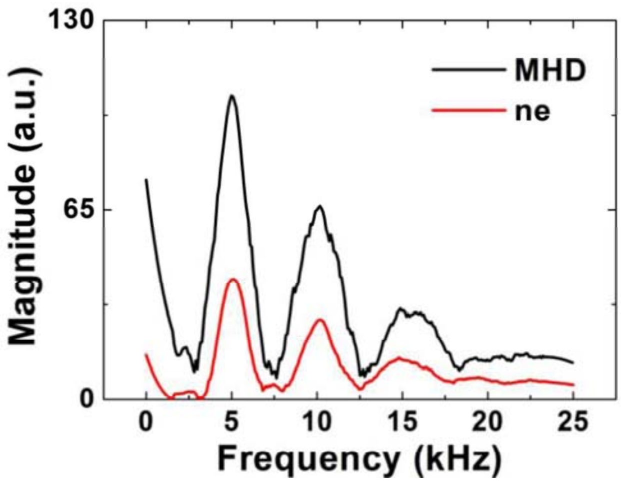

Figure 4.5: Frequency vs. magnitude plot obtained by FFT of MHD (black) and density (red) data for shot #29078

These observations suggest that the observed MHD modes fall in the drift-tearing mode category and rotate with a real frequency of $\sim 5 - 14$ kHz in the electron diamagnetic direction. We note here that these observations are repeated for a good number of discharges prior to gas-puff pulse injection.

From these plots, it is concluded that the observed m/n = 2/1 MHD modes are rotating in electron diamagnetic direction prior to the gas puff. The observed rotation frequency of the dominant m/n = 2/1 mode $\sim 5 - 10\ kHz$ matches well with the diamagnetic frequency calculated using

$$\omega_e^* = \frac{k_y T_e}{eBL_n} \qquad \dots (4.1)$$

where the electron temperature $T_e \sim 50\ eV$ and density scale length [220] $1/L_n \sim 4\ cm^{-1}$, $k_y\ (= m/r)$ is the wavenumber, $B_\phi = 1\ T$, at the location of m=2 island assuming parabolic plasma profiles [187,221]. Furthermore, coherent frequency bands with frequencies similar to that of the dominant m/n = 2/1 mode and its harmonics are observed in the frequency spectra of electron density fluctuations both in the edge and SOL region of ADITYA/ADITYA-U tokamak as shown in figure 4.6.

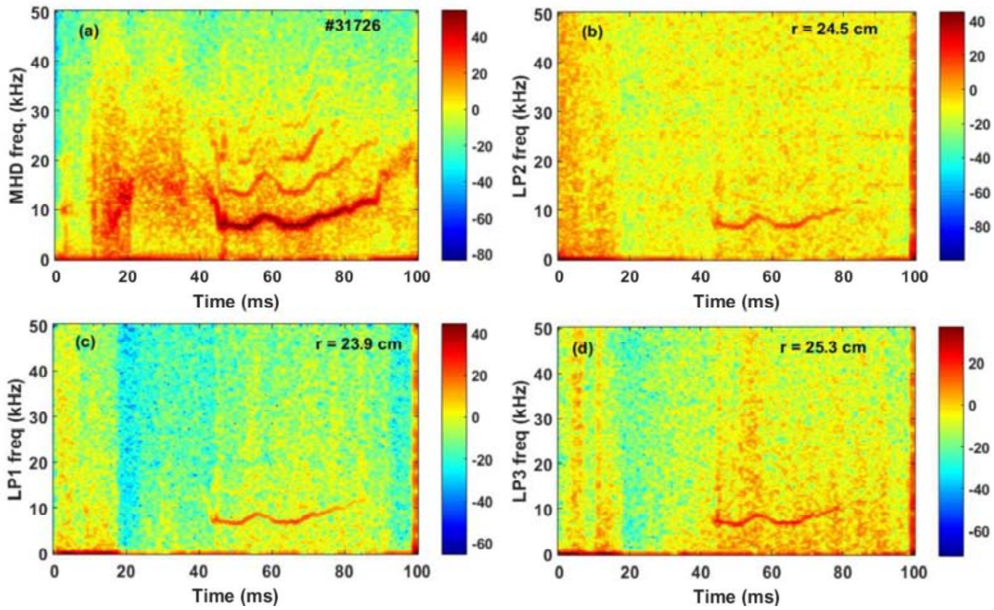

Figure 4.6: Plot showing the time evolution of frequency spectrum of (a) MHD, and (b-d) density fluctuation acquired from Langmuir probes at different radial locations in #31726 from ADITYA-U.

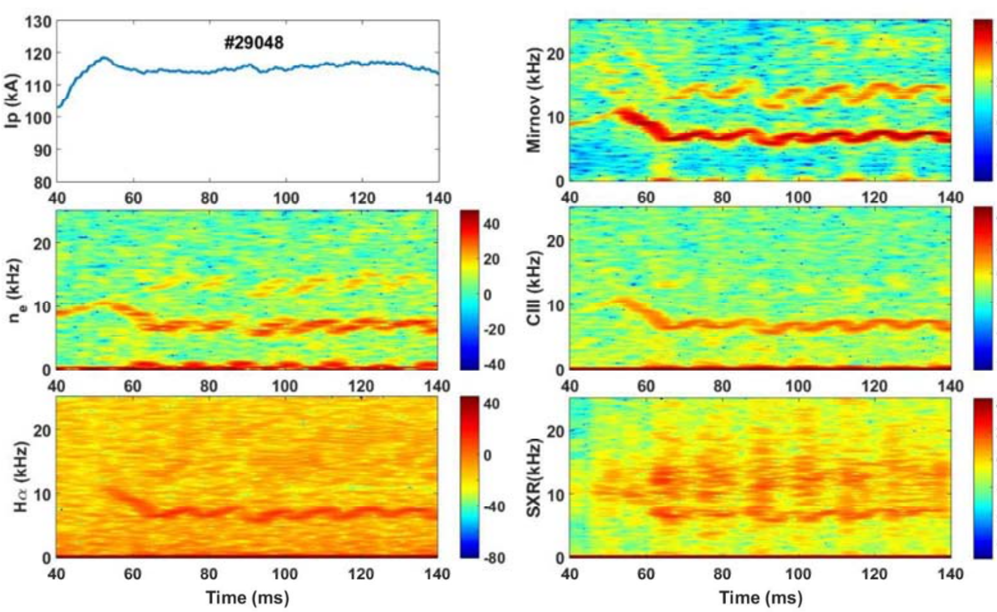

Figure 4.7: Plots showing the time evolution of (a) plasma current and frequency spectrum of (b) MHD (c) density, (d) C^{2+}emission intensity (e) H_α line emission intensities and (f) SXR exhibiting frequency band corresponding to m/n= 2/1 mode in shot#29048.

Furthermore, the fluctuations in the spectral line emission intensities of H_α and C^{2+} originating from edge/SOL region of the plasma and are mainly caused by the density fluctuations [222], also exhibited the presence of the coherent frequency bands in their time-frequency plots with same frequencies that of the 2/1 MHD mode and its harmonics as shown in figure 4.3. These observations further imply that the observed MHD modes fall in the drift-tearing mode category and rotate with a real frequency of $\sim 5-14$ kHz in the electron diamagnetic direction. We note here that these observations are repeated for a good number of discharges.

As can be seen from figure 4.1, all the frequency peaks corresponding to frequencies $\sim 7, 14, 21, 28, 35$ and 42 kHz appear simultaneously at ~ 40 ms. This suggests that these frequency modes may not be the independent primary modes corresponding to m/n = 4/2, m/n = 6/3, etc. Since the growth rates of primary m/n = 4/2 and higher modes at the q=2 mode rational surface are robustly stable with negative growth rates according to linear MHD theory [223]. Hence, the observed higher frequency bands in the Mirnov oscillations in discharges with strong MHD activity, suggests that they are the harmonics of the m/n = 2/1 tearing mode may be either due to the presence of non-sinusoidal periodic oscillations in a large amplitude m/n = 2/1 mode or generated through non-linear interaction among these modes.

4.1.2 Threshold conditions for the observation of harmonics of 2/1 mode

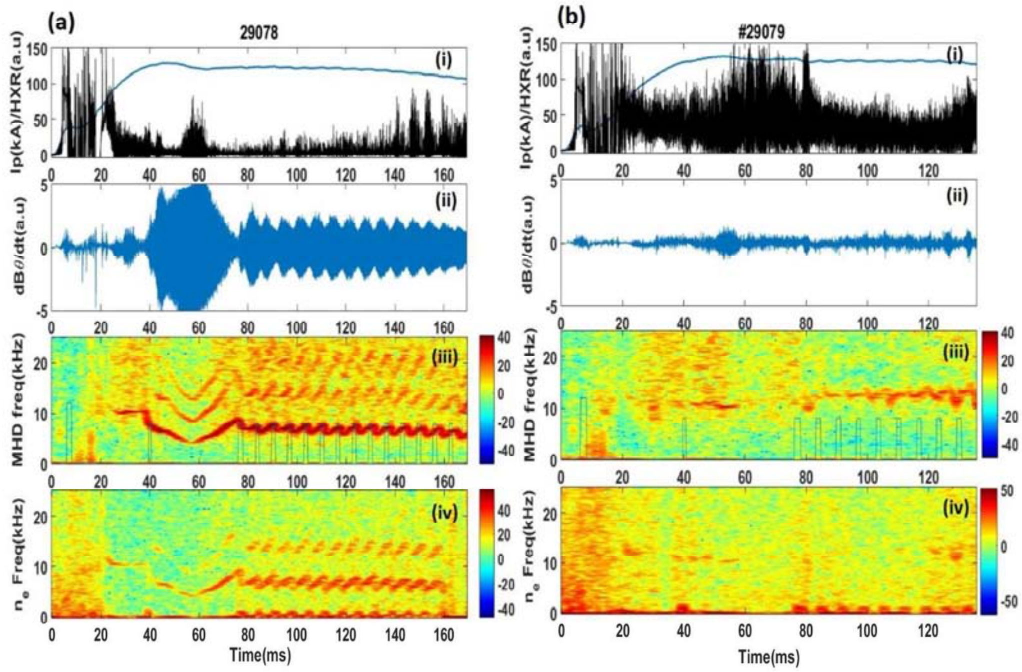

Figure 4.8: Time evolution of (i) Plasma current (blue), HXR (grey), (ii) frequency spectrum of $\dot{\tilde{B}}_\theta$ *(iii)* $\dot{\tilde{B}}_\theta$ *and (iv) frequency spectrum of ne for (a) shot#29078 (Type I) and (b) shot#29079 (Type II)*

In the search for a parametric dependency for the onset of harmonics in MHD activity, several discharges from ADITYA and ADITYA-U tokamaks have been analysed and categorized in two groups, namely, Type I – discharges with harmonics and Type II-discharges without harmonics. Figure 4.8 shows the temporal evolution of plasma current, HXR, MHD amplitude, and frequency spectrum and density frequency spectrum for type I (figure 4.8 (a)) and type II figure 4.8 (b)) discharges. A statistical analysis based on a few parameters related to these discharges reveals several interesting conditions favorable for the appearance of harmonics. One such condition is the existence of a threshold in MHD amplitude as well as in the rotation frequency of the m/n = 2/1 mode for the appearance of harmonics in a discharge. The MHD amplitude of 2/1 mode at one instant during current flat-top was studied in comparison with its rotation frequency at that instant, for multiple discharges in ADITYA-U. Figure 4.9 shows a plot of MHD amplitude vs. rotation frequency of m/n=2/1 mode in ADITYA-U. It has been found that the MHD amplitude during a discharge is inversely proportional to its rotation frequency at that instant. It has also been discovered that harmonics are generated only beyond a threshold in poloidal magnetic fluctuation i.e. $\tilde{B}_\theta/B_\theta > 5 \times 10^{-4}$ (poloidal magnetic fluctuation due to 2/1 mode normalized with the total poloidal magnetic field) during a discharge. In terms of rotation frequency, it has been found that the harmonics ceased to exist when the rotation frequency of 2/1 mode was greater than ~14 kHz. Also, in several discharges as the rotation frequency of 2/1 mode decreased, larger number of harmonics are generated as shown in figure 4.10.

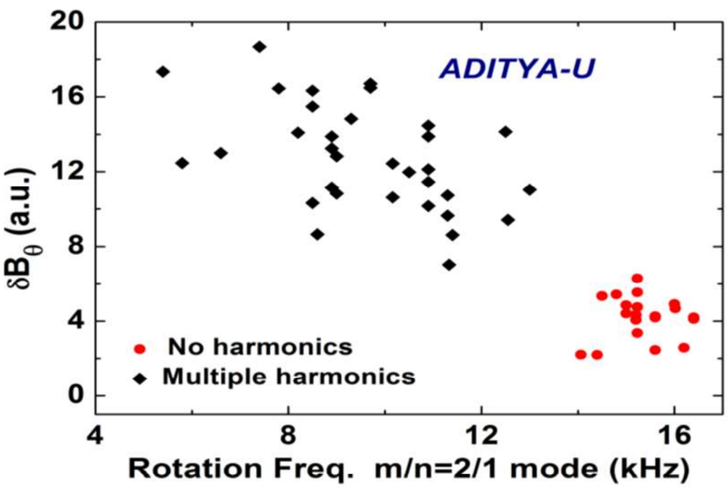

Figure 4.9: Plot showing (a) δB_θ amplitude corresponding the rotation frequency of m/n=2/1 mode for Type I discharges (in black) and Type II discharges (in red).

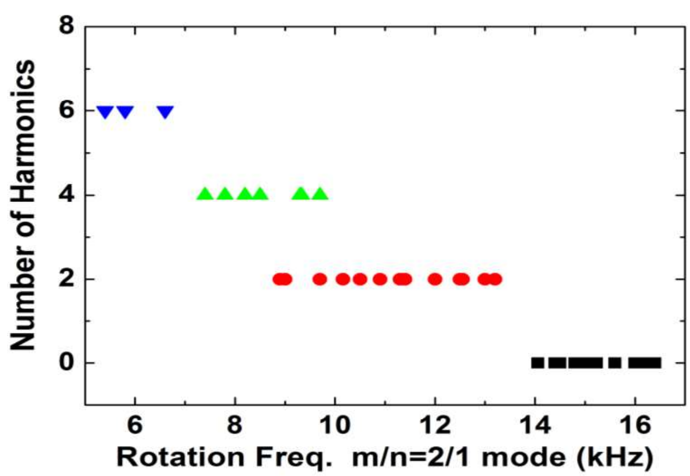

Figure 4.10: Total number of harmonics observed in different discharges plotted with respect to the rotation frequency of m/n=2/1 mode at single time instant during current flat-top of respective discharge

It has been realized that the number of harmonics present in a discharge is inversely proportional to the rotation frequency of the 2/1 mode. Since the MHD amplitude is inversely proportional to the 2/1 mode rotation frequency, the number of harmonics in a discharge may be regarded as proportional to the MHD amplitude during the discharge. Also, since the dimensionless quantity $\tilde{B}_\theta/B_\theta$, is directly proportional to the width of island associated with 2/1 mode, it is appropriate to state that the 2/1 mode island when attains a sufficiently large width, harmonics are generated at q=2 surface. The amplitude of fluctuations corresponding to m/n=4/2 is observed to be more than 10 times lower than that of m/n = 2/1 mode amplitude and should be well contained within the 2/1 island. The same argument may be put forth for other higher harmonics.

The relationship between MHD amplitude, the rotation frequency of the 2/1 mode and the appearance of a number of harmonics is also spontaneously observed during the course of a single discharge as shown in figure 4.11. It can be clearly seen from the figure that during $\sim 20\ to\ 27\ ms$ into the discharge, when the rotation frequency of the 2/1 mode is $\sim 11-12\ kHz,$ only two harmonics are present. However, as soon as the rotation frequency decreases to $\sim 8\ kHz$ after $40\ ms$ into the discharge, the MHD amplitude increases and four harmonics appear in the time-frequency plot of Mirnov oscillations. The strong dependence of the presence and absence of harmonics of 2/1 drift tearing modes on its amplitude, indicates that the generation of harmonics is the non-linear in nature. The overall performance of the discharges has also been found to be affected by the presence or absence of the harmonics, which is intuitive since the presence or absence of the harmonics are directly related to the island width of 2/1 mode. The type I discharges with relatively lower rotation frequency of 2/1 mode and higher MHD amplitude with harmonics have relatively lower $\beta_N{\sim}0.3\ \%$ and lower confinement times (β_N calculated using equation 2.20). The type II discharges, on the other hand, with relatively higher rotation frequency and lower amplitude of the fundamental m/n = 2/1 mode and absence of harmonics have relatively higher $\beta_N{\sim}0.6\%$ and high confinement times. Since larger size 2/1 islands have been known to increase the transport across the field lines and thereby degrade the confinement, this observation is in good agreement with past experimental and theoretical studies[151,224,225]. These observations further validate the strong dependence of generation of harmonics on the 2/1 mode island width, which is a signature of non-linear interactions.

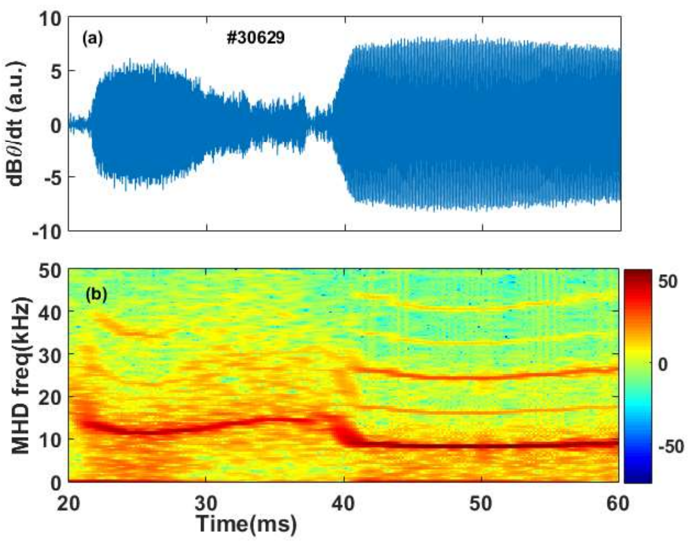

Figure 4.11: Time evolution of (a) $\dot{\tilde{B}}_\theta$ (b) MHD frequency spectrum showing two harmonics at ~25 ms when rotation frequency of m/n=2/1 mode is 12 kHz and four harmonics at t~45 ms when rotation frequency of m/n=2/1 mode is 9-10 kHz for #30629.

4.1.3 Correlation of Presence and absence of Harmonics of 2/1 mode with Hard X-Ray

In this section, the correlation between the presence and absence of strong MHD activity and runaway electron behavior in a large number of discharges from ADITYA and ADITYA-U is reported. As mentioned earlier, the RE loss dynamics during a discharge is inferred by the detection of Hard X-rays (HXR) produced by the interaction of REs with the limiter. In most of Type I discharges (with harmonics), the intensity of HXR emission remained low as compared to those in Type II discharges as shown in figure 4.8. A Type II discharge (#29079, figure 4.8 (i)) with 2/1 mode having lower MHD amplitude, exhibits high HXR intensity throughout the discharge current flat-top whereas the HXR intensity remains quite low in a Type I discharge (#29078, figure 4.8 b) throughout the discharge. Both the discharges have similar macroscopic discharge parameters accountable for the generation of runaway electrons i.e. loop voltage responsible for the parallel electric field ($E_{||}$) and pre-fill pressure (p), hence the generation of REs is expected to remain the same in both the discharges. Figure 4.8

shows the identical loop voltage and prefill pressure for #29078 and #29079. We note here that the generation of REs majorly happens at the beginning of the discharge, both in ADITYA and ADITYA-U as already detailed in chapter 3. Therefore, in principle, the RE population which is grossly dependent on $E_{||}/p$ during the high loop voltage (current ramp-up phase), should same for both the discharges. The RE (Dreicer) generation rate τ_{dr} is given as

$$\tau_{dr}^{-1} \approx 0.3\, \upsilon_e \varepsilon_d{}^{-3(Zeff+1)/16}\, exp\,(-1/4\varepsilon_d - (\{Z_{eff} + 1\}/\varepsilon_d)^{1/2} \quad \ldots (4.2)$$

where $\varepsilon_d = E_{||}/E_D$, $E_{||} \sim V/2\pi R$, where V ~ Loop voltage and R (~0.75 m) is plasma major radius. υ_e is collision frequency of electrons at a thermal velocity υ_{th} and Z_{eff} (≈ 1.5) is the effective plasma charge. The Dreicer electric field, $E_D = 4 \times 10^{-2} \frac{n_e}{10^{19}} - \frac{10^3}{T_e} - \left(\frac{ln\Lambda_c}{15}\right)$, density n_e is in m^{-3} , electron temperature, T_e is in eV and $ln\Lambda_c$ is the Coulomb logarithm ($\sim 15 - 17$). Taking, $n_e \sim 10^{19} m^{-3}$, T_e ~ 100 eV and $V = 20V$ the RE (Dreicer) generation rate is calculated to be $\tau_{dr}^{-1} \sim 10^{17-18} s^{-1}$, during the initiation of the discharge. Whereas taking $n_e \sim 2 \times 10^{19} m^{-3}$, T_e ~ 500 eV and d $V = 2\,V$ the RE generation rate is estimated to be $\tau_{dr}^{-1} \sim 10^{13-14} s^{-1}$, during current flat-top. Since the generation rate during flat-top is ~ 4 orders lesser than RE generation rate during the ramp-up phase, the majority of RE population is generated during the current ramp-up duration and the contribution of flat-top generated RE in total RE population is negligible. Note here that since the plasma duration is $\sim 100 - 300\, ms$, the secondary generation [226] is relatively small and the pitch-angle scattering remains a remote possibility in the reported experiments [199,227]. Several experimental observations and theoretical predictions established that the loss rate of REs is determined by the prevailing magnetic stochasticity associated with the MHD modes during the current flat-top of the discharges. In several other tokamaks, the HXR generated due to RE loss has been used as a measure to estimate the level of stochastic magnetic fluctuation [115] associated with different MHD modes. Hence, the difference in HXR emission intensity between the two consecutive ADITYA discharges (#29078 and #29079) is a result of different loss rates of REs due to the difference in MHD activity assuming that the relatively slower drift RE losses in both the discharges are similar. According to the above-mentioned arguments, the REs loss in the discharge with high MHD amplitude containing harmonics should be larger than that in the discharge with low MHD amplitude containing no harmonics. Furthermore, as the MHD island with bigger width spans a bigger radial extent, the loss of REs should be higher in Type II case, hence they should exhibit higher HXR intensity, in principle. However, in reality the opposite has been observed in these two representative discharges as shown in the figure 4.8 (i) (a) and (ii) (a). This observation, recorded in hundreds of discharges, indicates that the confinement of REs in discharges with large 2/1 island with harmonics is better than the confinement of REs in discharges with small 2/1 mode island with no harmonics. The confinement of REs in large magnetic island has been also observed earlier in several tokamaks like TEXTOR[228] J-TEXT [113] etc. More theoretical arguments in support of this proposition have been presented in the discussion section. This observation motivated us to conduct experiments in which alteration of MHD amplitude of 2/1 mode by means of gas puffing, SMBI, and/or by moving the plasma position has been carried out to understand further the interplay of REs and 2/1 modes.

The correlation between the RE dynamics with the harmonics of 2/1 mode is further confirmed, when the harmonics appear or disappear in the lifetime of a single discharge. One such discharge (#29081) presented in figure 4.12 (a).

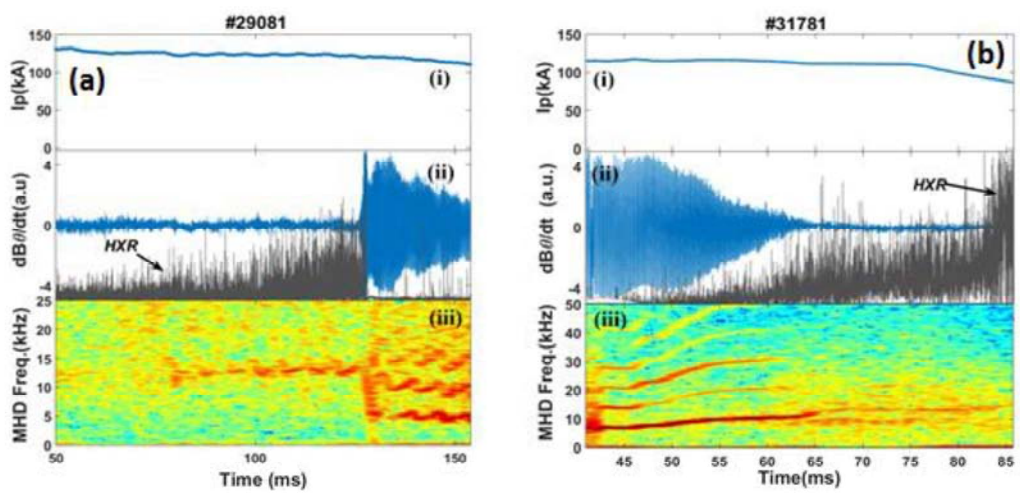

Figure 4.12: Time evolution of (i) Plasma current (ii) $\dot{\tilde{B}}_\theta$ (blue) and HXR (grey) and (iii) frequency spectrum of $\dot{\tilde{B}}_\theta$ for (a) shot #29081 and (b) shot #31781 showing low HXR emission coinciding with the presence of multiple harmonics

During the plasma current flat-top, until ~135 ms into the discharge the amplitude of 2/1 mode remains low, it rotates with $f \sim 14\ kHz$ and the harmonics of 2/1 mode are absent. In this duration, i.e., until$\sim 135\ ms$, the intensity of HXR emission remains high, and as soon as the rotation frequency of 2/1 mode decreases, its amplitude increases and multiple harmonics of the 2/1 mode appear, simultaneously, the intensity of HXR decreases sharply in comparison to its value prior to$\sim 135\ ms$. This sudden decrement on HXR intensity signifies improved confinement of REs which may be attributed to the presence of large 2/1 mode with harmonics, which is again consistent with our proposition. In another representative discharge (#31781) shown in figure 4.12 (b) (ii), it has been observed that during the initial part of the current flat-top the MHD amplitude due to 2/1 mode is high (large 2/1 mode island), the rotation frequency of 2/1 mode low ($f < 14\ kHz$) and five harmonics are present as can be seen in time-frequency plot of MHD fluctuations in figure 4.12 (b) (iii). The HXR intensity has been found to be low during this period, signifying lower RE loss rate. At around $\sim 50\ ms$ into the discharge, the amplitude of 2/1 mode starts decreasing gradually, the higher harmonics disappear consecutively, starting from the highest 5th harmonic of 2/1 mode, which is the first to disappear. Simultaneously, as the MHD amplitude decreases, i.e. the 2/1 mode island width decreases, the HXR intensity starts increasing. The above experimental evidence substantiates that with the decrease in 2/1 mode island width RE loss increases. Similar observations have been made in a wide range of discharges where the presence of harmonics of 2/1 mode is marked by a lower amplitude of HXR intensity, whereas the absence of harmonics of 2/1 mode during a discharge is often accompanied by higher HXR intensity. The confinement of REs and energetic particles in presence magnetic islands has been reported in Tokamaks [112,113,229]as well as in Stellarator [230].

To achieve deep penetration of fuel H_2 inside the plasma, an SMBI (Sonic molecular beam injection) system has been installed on the low field side (LFS) of the Aditya-U tokamak. A particle flux of $\sim 2 - 3 \times 10^{22}\ particles/s$ is achievable at a plenum pressure of $1\ MPa$ [45]. Few milliseconds after the SMBI injection, a significant decrease in the island rotation frequency ($\Delta f \sim 3 - 4\ kHz$) as shown in figure 4.13(a). The decrease in the frequency of 2/1 mode is accompanied by an increase in MHD amplitude as well as the appearance of harmonics of 2/1 mode. In addition to this, the

HXR intensity also decreases as soon as the harmonics appear. More than 15 discharges have been repeated with SMBI pulse, demonstrating the improvement in RE confinement owing to increase in island width and presence of harmonics of 2/1 mode.

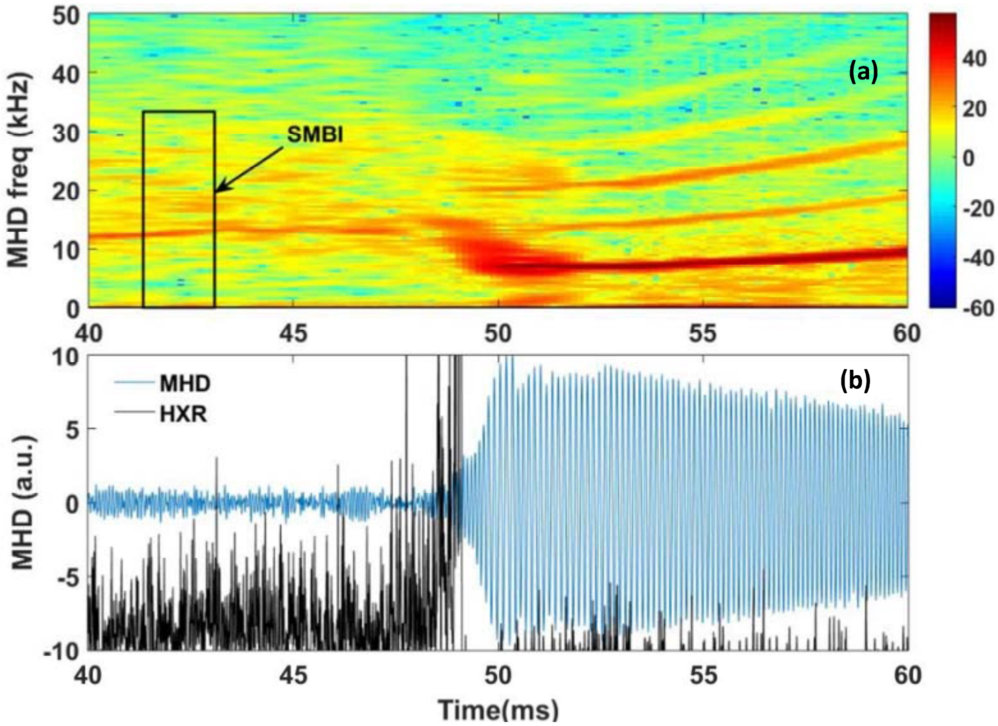

Figure 4.13: Time evolution of (i) frequency spectrum of MHD with SMBI pulse (ii)) MHD amplitude (blue) and HXR (black) for shot #31263.

It is essential to state that in all the discharges exhibiting improvement in RE confinement in the presence of harmonics of 2/1 mode during current flat-top, the current disruption is accompanied by a strong HXR intensity burst. The large HXR spike at the time of current disruption of the discharges is indicative of the significant population of REs which remain confined during the current flat-top and expelled during the current disruption as shown in figure 4.14.

This observation also negates the possibility of the decrease in HXR intensity due to a decrease in the total RE population inside the plasma. In case of discharges where total REs in the plasma are completely lost, mostly in situation where the sudden onset of turbulent magnetic stochasticity leads to complete expulsion of REs, the HXR intensity becomes zero after the HXR intensity peak at the time of magnetic turbulence and no HXR intensity burst appears during the current disruption.

4.2 Modulation of drift-tearing mode using short periodic gas-puff pulses and their effect on RE dynamics

The dynamics of magnetic islands in a tokamak is influenced by many factors such as the free energy sources, thermal transport [27], ion-sound wave [231], drift waves [139,146], magnetic curvatures [232,233], external perturbations[36], polarisation current [149], etc. In general, the rotation frequency of islands, which is given by a combination of the plasma rotation frequency and the phase velocity of the island in the plasma frame, plays an important role in the growth, decay, and saturation of magnetic islands [137]. The rotation of magnetic islands around the tokamak in both poloidal and toroidal directions in the kilohertz (kHz) range of frequencies is widely observed in tokamak discharges [140,184]. It is well known that the rotation of magnetic islands is driven by the electron diamagnetic effect [139,146] when the drift modes couple to tearing modes and the growth rate of the tearing modes is then significantly reduced in this so-called drift-tearing regime [147,148]. In the linear drift-tearing regime, the rotation frequency of an island is approximately equal to the diamagnetic drift frequency. While rotating, the island interacts with the background plasma to produce rotating perturbations in the plasma pressure and velocity profiles, which in turn affect the island width[234]. Furthermore, interaction with the resistive wall also halts the rotation of magnetic islands leading to slow down of plasma rotation and causing a degradation of the confinement [155,235]. Controlling the rotation of the magnetic islands is attempted in order to produce damping forces that induce a reduction in the island size[155,184]. The external control system alters the island motion, which then, in turn, changes the plasma behaviour. The interaction of magnetic islands with the background plasma, particularly with the ion fluid velocity, is crucial to understanding and improving rotation control techniques [234].

An externally applied non-axisymmetric magnetic field is one of the simplest and most direct approaches to control of MHD instabilities since it can interact directly with the non-axisymmetric magnetic field of an instability [36,236]. Many tokamaks and reversed-field pinch devices now have single or multiple rows of non-axisymmetric coils/ resonant magnetic perturbation coils (RMP), external or internal to the vacuum vessel, that provide the capability to apply magnetic perturbations of different toroidal and poloidal mode numbers [237,238]. However, the effectiveness of RMP heavily depends on the initial state of the tearing mode, such as mode frequency and island width. Furthermore, a strong RMP can even stimulate a tearing mode even if the initial plasma is tearing stable and in some cases, it can lead to mode-locking too.

There exists an abundance of experimental evidence of short gas puff (GP) pulses significantly influencing the scrape-off-layer (SOL) and edge plasma characteristics in tokamak discharges. Gas puffing experiments on the PBX-M [239], ADITYA [240], NSTX [241], and T-10 [242] have reported significant modifications in the SOL/edge plasma parameters and the SOL/edge turbulence due to the application of fuel gas-puff pulses. Apart from the modifications in SOL/edge plasma parameters and turbulence, the presence of neutrals in the edge plasma are also known to influence the global confinement [243] and play a major role in the transition from low (L) to high (H) confinement mode which are critical to the performance of tokamak based fusion reactors. The poloidally localized fueling is also known to influence the plasma rotation [244,245]. A flattening of the edge floating potential profile along with a reduction in edge floating potential fluctuations in the SOL/edge plasma region of ADITYA tokamak has been observed with the application of gas-puff pulse [163]. A decrease in edge density gradient and an increase in global confinement time have also been reported in these experiments. Furthermore, these gas puffs are also known to reduce the edge poloidal flow speed and cause a reversal in the toroidal flow speed due to the localized edge particle source [240,246]. Similar results have also been reported from STOR-M tokamak [247], where a two-fold increase in the line averaged density, decrease in electron temperature along with a reduction in the floating potential fluctuations have been observed by injecting gas in short pulses. A decrease in the loop voltage has also been observed, indicating an increase in the core electron temperature and global confinement in STOR-M [247]. In addition to the modifications in the characteristics of electrostatic fluctuations with the application of short gas-puff pulses, the Edge localized Modes (ELMs) are also reported to be influenced by pulsed supersonic molecular beam injection (SMBI) in K-STAR and HL-2A tokamak [248]. Bifurcation of tearing modes due to SMBI has been observed in J-TEXT tokamak [249].

In this section, the influence of short gas-puff pulses on the amplitude and the rotation frequency of drift-tearing magnetic islands is presented. It has been observed that the amplitude and rotation frequency of pre-existing m/n = 2/1 islands reduce significantly with the application of fuel (hydrogen) gas-puff pulses (neutral injection) of suitable magnitude in the SOL/edge region of ADITYA and ADITYA-U tokamaks. The decrement in the rotation frequency of the mode scales up with the number of particles injected up to ~10^{19} particles, after which complete cessation of the mode rotation generally leading to disruption has been observed. The decrease in rotation frequency as well as in the amplitude occurs within $\sim 1 - 2\, ms$ of the application of gas puff pulse. The time interval between the gas-pulse application and reduction in amplitude of the mode also reduces with an increasing amount of injected gas molecules. As these m/n = 2/1 islands are observed to be rotating in the electron diamagnetic direction, the reduction in rotation frequency is most likely due to a change in the diamagnetic frequency caused by a reduction in the plasma temperature and a flattening of the density profile in the SOL/edge region due to the gas puffs. The density and floating potential fluctuations in the SOL/edge region are suppressed due to the gas-puffs. However, the observation of a decrease in mode amplitude along with the decrease in the rotation frequency is counter-intuitive to the analytical prediction of an increase in growth-rate of MHD modes with a decrease in the mode-rotation frequency. These experimental observations are well supported by simulations using the BOUT++ code [250]. The modification of the diamagnetic drift frequency in the edge and SOL region of ADITYA/ADITYA-U tokamak due to a gas puff (neutral injection) has been investigated using two-dimensional (2D) interchange plasma turbulence. The simulation results suggest $\sim 25 - 65\%$ reduction in the diamagnetic drift frequency due to an injection of $\sim 10^{18}$ neutral fuel particles in the edge region of ADITYA tokamak.

In case of periodic gas puffs with a period of $t_{GP} \sim 4 - 6\, ms$, after the effect of the one gas puff, is over, the mode regains its pre-gas-puff value, both in magnitude and its rotation frequency, and the sequence of events is repeated after each gas-puff. Hence a train of periodic gas puff pulses leads to a periodic modulation of the frequency and amplitude of the drift-tearing modes in ADITYA/ADITYA-U tokamak. This demonstration of alteration of drift-tearing modes using periodic gas-puffs may be useful for understanding the interaction of magnetic islands with the background plasma and may help in improving MHD control techniques. Multiple hydrogen gas puffs are injected through a bottom port (poloidal angle, $\theta \sim 270^{\circ}$ and toroidal angle, $\varphi \sim 90^{\circ}$) during the plasma current flat top by activating a piezo-electric valve (500 SCCM at 100V) with appropriate voltage pulses. These gas-feed pulses have been pre-fixed through a programmable voltage pulse generator prior to the initiation of the discharge, using a computer-controlled electronic circuitry specially designed for gas feed system [251]. The magnitude and pulse-width of the voltage pulse are varied to inject a particular number of gas molecules in the plasma. A pulse width of $1 - 2\ ms$ and amplitude of $\sim 5 - 7\ V$, with $1\ V$ corresponding to $10\ V$ on the piezo valve, generally injects $\sim 0.7 - 1 \times 10^{18}$ particles in the plasma. A representative discharge from ADITYA tokamak with 15 periodic gas-puff pulses applied during the plasma current flat-top at a frequency of $\sim 200\ Hz$ is shown in figure 4.14. Time evolution of loop voltage, plasma current, H_{α} emission intensity and MHD activity acquired from one of the Mirnov coils (at $\theta \sim 320°$) are shown in the figure 4.14.

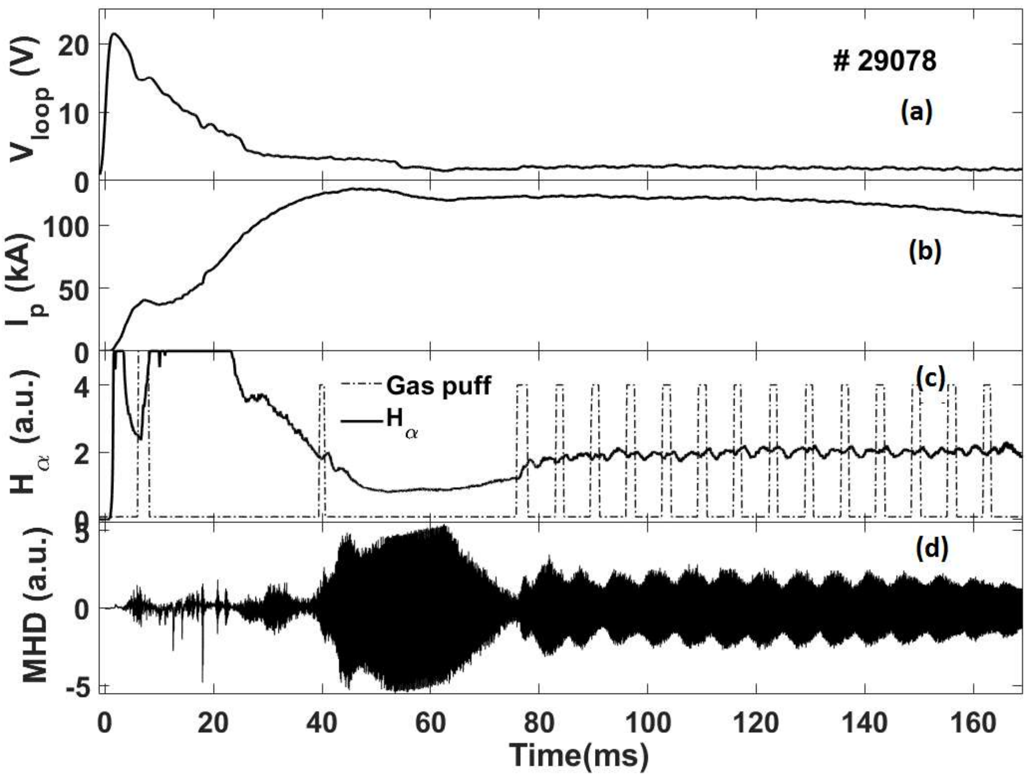

Figure 4.14: Plot showing the temporal evolution of (a) loop voltage, (b) plasma current, (c) H_α emission intensity and periodic gas puffs (d) MHD activity from shot #29078.

The prime objective of fuel (hydrogen) gas-puffing during the discharge is to maintain the plasma density which is clearly reflected in the plasma particle inventory, both from the central line averaged and edge density measured by microwave interferometry and Langmuir probes respectively. Along with this, the gas-puffs trigger several other events in the discharge such as suppression of edge density and potential fluctuations, runaway electron ejection and changes in the characteristics of MHD modes[182] present in the discharges. As mentioned earlier, Hydrogen gas is injected through a piezoelectric valve located at the bottom-central port, $\sim 6\ cm$ behind the limiter radius. The amount of injected gas is controlled by varying the amplitude and time duration (width), of the voltage pulse applied to the piezoelectric valve. In the discharges studied for this chapter, the applied pulse-voltage has been varied between $\sim 4.5 - 6\ V$ and the pulse duration has been varied from $\sim 1 - 2\ ms$ leading to the injection of $\sim 10^{17}$ - 10^{18} hydrogen neutrals during each pulse. The delay between two pulses has been varied from $\sim 5 - 8\ ms$ over a large number of discharges. Experiments have been carried out by varying the number of gas-puff pulses and the time gap between the gas-puffs in different discharges.

4.2.1 Impact of multiple periodic gas-puffs on MHD modes

The parameter $\widetilde{B_\theta}/B_\theta$ has been investigated during the current flat-top for > 3000 discharges in ADITYA/ADITYA-U tokamak, since it is a measure of the island width/ MHD activity of a tearing mode [193]. To investigate the effect of gas puffs on the MHD mode characteristics in ADITYA and ADITYA-U tokamak discharges with moderate to strong m/n = 2/1 ($\widetilde{B_\theta}/B_\theta > 5\%$) have been considered for the study. A large number of discharges in which these modes are present throughout the plasma current flat top with a nearly constant rotation frequency as well as amplitude have been analysed both in presence and absence of gas puffs. As mentioned in the previous section, the mode structures corresponding to mainly $m/n = 2/1$ MHD mode are observed as shown in figure 4.2. The rotation frequencies of these MHD modes have been observed to be in the range of $\sim 5\ to\ 12\ kHz$, with a bandwidth of $\sim 1 - 2\ kHz$. In the absence of the gas-puffs, the temporal evolution of MHD activity remains nearly constant in its amplitude and frequency as shown in figure 4.15(a) and (b).

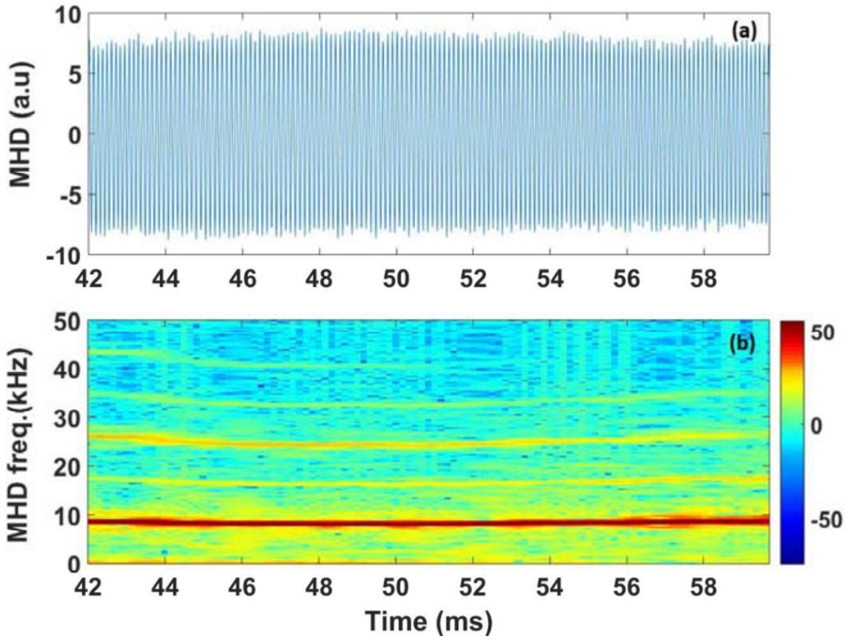

Figure 4.15: Plot showing (a) MHD activity and (b) its corresponding frequency spectrum of a discharge duration without the gas puff.

However, it can be clearly seen from figure 4.14 (c), as soon as the train of gas-puffs starts at$\sim 76\ ms$, a distinct periodic change strongly correlated with the gas-puff pulses appears in the temporal evolution of MHD amplitude (figure 4.14 (d)). The MHD amplitude has been observed to decrease by ~ 20 - 40 % within $1\ ms$. The MHD activity remains at this reduced amplitude for the next $\sim 1 - 2\ ms$ before increasing again until the next gas-puff pulse comes, whereupon the mode amplitude decreases again and the whole cycle is repeated after each gas-puff.

Furthermore, the frequency spectral analysis of MHD oscillations from these discharges reveals that not only the amplitude of MHD activity is reduced due to the application of the gas-puff, the rotation frequency of these MHD modes also reduces after each gas-puff pulse. Figure 4.16 shows the time evolution of the frequency spectrum of MHD oscillations exhibiting the presence of multiple frequency bands.

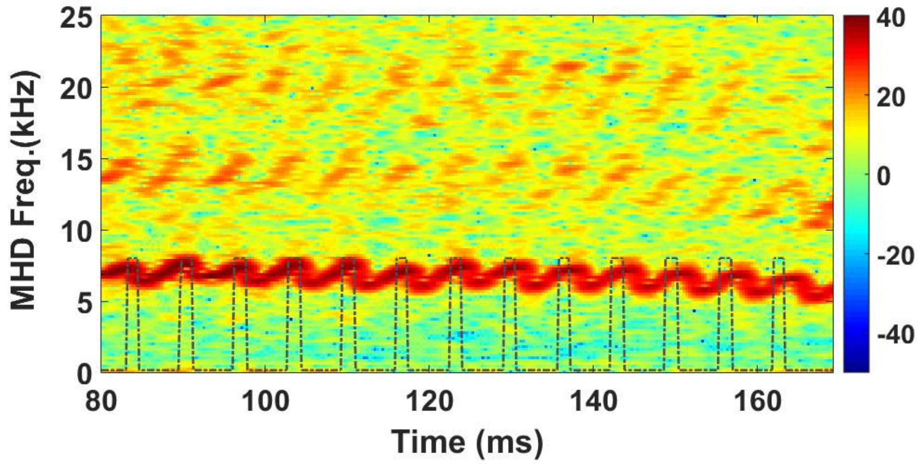

Figure 4.16: Plot showing frequency MHD modulation correlated with gas puffs specgram of Mirnov data from shot #29078.

The dominant frequency corresponds to the rotation frequency of m/n =2/1 mode. The other peaks are harmonics of the m/n = 2/1 mode, as explained in the previous section. Going back to figure 4.9, the dominant m/n = 2/1 mode and its harmonics rotate with constant frequency $\sim 8\ kHz, 16\ kHz\ and\ 24\ kHz$ respectively during the plasma current flat-top, prior to the application of gas-puff train. After the application of the gas-puff the mode rotation frequency of the fundamental m/n = 2/1 mode decreases by $\sim 2\ kHz$ within $\sim 1\ ms$ after the application of the gas puff pulse. The mode rotates at $\sim 6\ kHz$ under the influence of the gas-puff pulse for next $\sim 2 - 3\ \ ms$ and thereafter regains and maintains its initial value of $\sim 8\ kHz$ till the next gas puff pulse reduces its frequency again and thus the whole cycle is repeated after each gas puff pulse. The higher frequency harmonics are also influenced in a similar fashion as the frequency of the first harmonics $\sim 16\ kHz$) decreases by $\sim 4\ kHz$, after the gas-puff pulse. Carrying forward the argument from the previous section regarding the multiple bands in the time-frequency plots of MHD oscillation we note the following. If the observed harmonics belonged to independent modes rotating with different frequencies and located at different rational surfaces inside the plasma, the observed systematic effect of the gas injection at the edge would be extremely improbable. This observation again suggests that the observed modes are harmonics of 2/1 mode and not independent MHD modes at different mode rational surfaces. The above-mentioned observations clearly establish that the amplitude and rotation frequency of MHD modes have been influenced by puffing an appropriate amount of fuel (hydrogen) gas in plasma discharges of ADITYA and ADITYA-U tokamak. To investigate further the nature of the interaction between the gas-puff and the MHD modes, the amount of injected gas has been varied either on a shot-to-shot basis or during the course of a single discharge. The decrement in rotation frequency of the MHD modes appeared to be higher with higher amount of injected neutrals. The decrement in rotation frequency has been plotted with respect to the amount of neutrals injected in figure 4.17. Each data point corresponds to the decrement in rotation frequency after gas puff in during the current flat-top of different discharges with different amount of injection of gas puff.

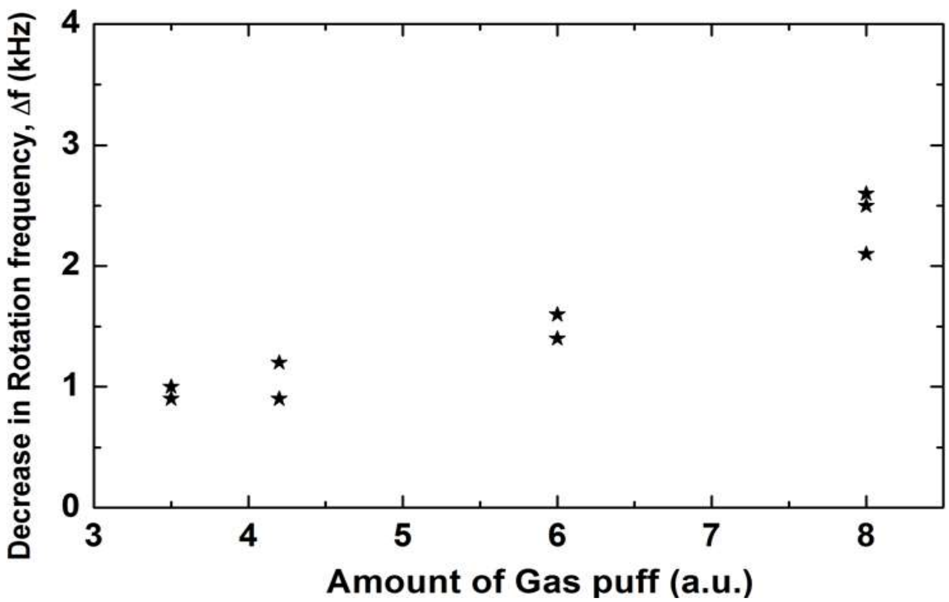

Figure 4.17: Decrement in 2/1 mode rotation frequency after gas puff plotted with respect to the amount of gas puff injected.

The figure shows that the decrease in the rotation frequency is almost proportional to the amount of neutrals injected up to ($\sim 10^{19}$) neutrals injected for these discharges after which they induce disruptions. Similarly, the decrement in the MHD amplitude has also been found to be increasing systematically as shown in figure 4.18 (a). Figure 4.18 (b) further shows that the rate of decrease of the amplitude is also increased with increasing the amount of injected molecules, i.e., the mode amplitude decreases with a faster rate after the application of the gaspuff pulse as the amount of injected neutrals are increased. We again note here that these observations are repeated for a good number of discharges prior to gas-puff pulse injection.

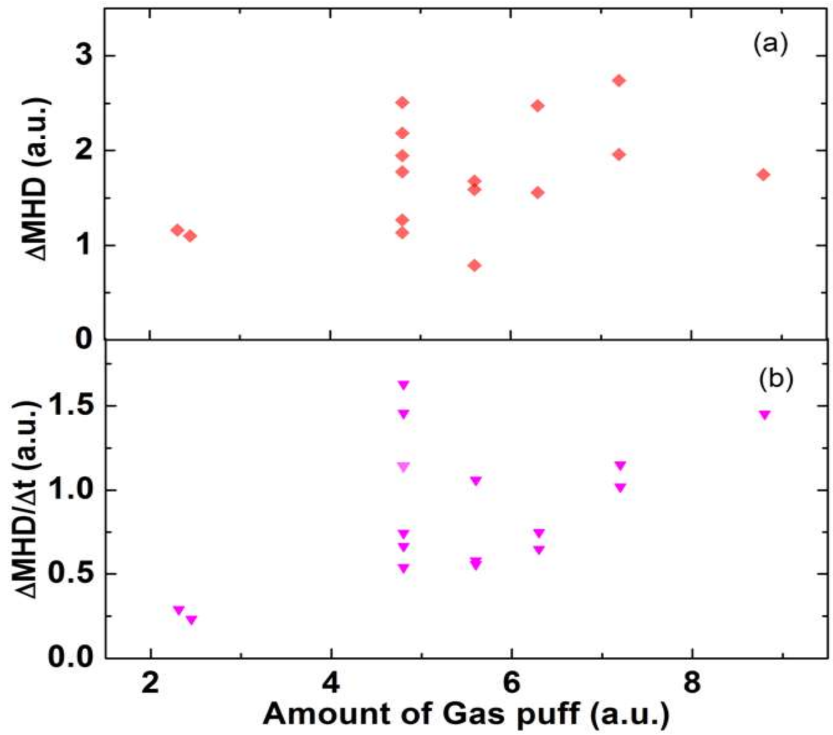

Figure 4.18:(a) Decrease in MHD amplitude and (b) Rate of change of MHD amplitude plotted with respect to the amount of gas puff injected for several discharges from ADITYA.

The reason for the above-mentioned modifications of MHD characteristics due to short gas-puff pulses is as follows. As established in the previous section that the observed MHD modes in the reported discharges fall in the drift-tearing mode category and rotate with a real frequency of $\sim 5 - 14$ kHz in the electron diamagnetic direction. When the neutrals are injected through a gas-puff pulse at the current flat-top in the discharges with existing high-amplitude ($\widetilde{B_\theta}/B_\theta > 5\%$) m/n = 2/1 MHD modes, a reduction in the frequency of rotation of these modes along with a reduction in the amplitude of the MHD fluctuations have been observed. The rotation frequency of the MHD island in the laboratory frame is a combination of the plasma rotation frequency and the phase velocity of the island in the plasma frame. Hence, the rotation frequency downshifts after a gas-puff pulse may either be due to the reduction in the frequency of the electron diamagnetic drift or that of the $E \times B$ plasma rotation. Since the radial electric field (E_r) has a radially outward direction, the resultant $E \times B$ rotation would be in the poloidally anti-clockwise direction. Figure 4.19 shows the direction of different drifts in ADITYA and ADITYA-U.

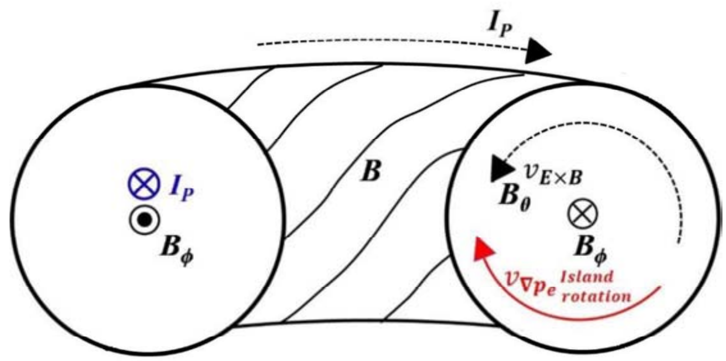

Figure 4.19: Schematic of ADITYA showing the toroidal direction of plasma current, toroidal magnetic field and the direction of electron diamagnetic drift, $E \times B$ drift, and the island rotation.

With the introduction of the gas puff, the island continues to rotate in the electron diamagnetic drift direction but with a reduced frequency, which indicates that the diamagnetic drift appears to have the dominant influence on the mode rotation in both ADITYA and ADITYA-U. The $E \times B$ rotation also reduces, due to a reduction in the potential fluctuation (and hence E), as has been noted before in the edge region of the ADITYA tokamak [221]. However, the reduction in $E \times B$ cannot decrease the mode rotation frequency as it is in the opposite direction. Earlier experiments in ADITYA have demonstrated that neutral injection significantly reduces the edge temperature (T_e) and increases the edge density scale length (L_n) [170]. The radial profile of electron density in the edge/SOL region of ADITYA-U is measured using Langmuir probes. The radial profile of density at two time intervals, before and after the gas-puff are shown in figure 4.20. The light-coloured open circle and open triangle symbols in figure 4.20 represent the measurements at different radial locations from different gas-puff cycles and from different discharges before and after the gas-puff pulse injection respectively. The bigger, brighter, filled-symbols (circle and triangle for before and after gas-puff respectively) represent the average of all measurements at a single radius. It can be clearly seen from the figure that after the application of the gas puff the density profile in the edge/SOL region flattens, i.e. the density gradient in the edge/SOL region decreases after the gas-injection from its value in absence of the gas injection.

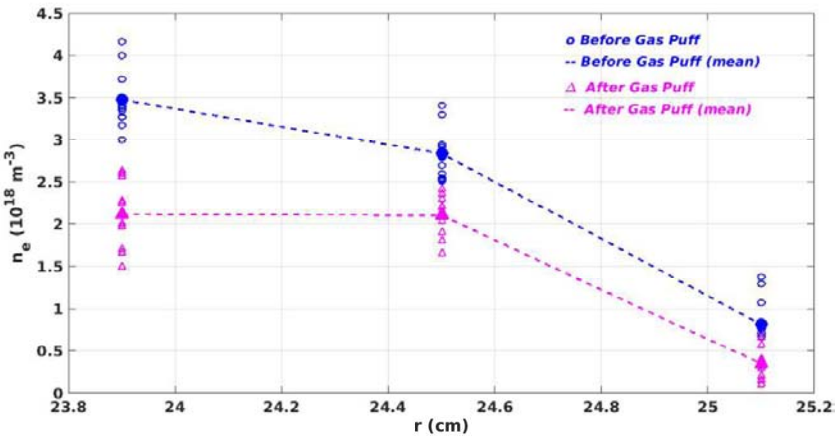

Figure 4.20: Radial profile of density measured by 3 Langmuir probes placed at different radial locations in the edge region before (Black circles with solid line) and after the gas-puff (Red triangles with dotted line). Smaller open symbols are the measurements from different gas-puff cycles and from different discharges. Larger, solid-symbol represents the average of all measurements at each radial location.

Similar observations of reduction in edge/SOL temperature and flattening of density profiles have also been reported by other tokamaks. As the electron temperature and the density gradient decrease with the application of the gas puff, the diamagnetic drift frequency also decreases according to equation 4.a. The decrease in the drift frequency is further corroborated with the observation of a significant reduction in the density and floating potential fluctuations measured with Langmuir probes in SOL region of ADITYA-U tokamak after the gas injection as shown in figure 4.21.

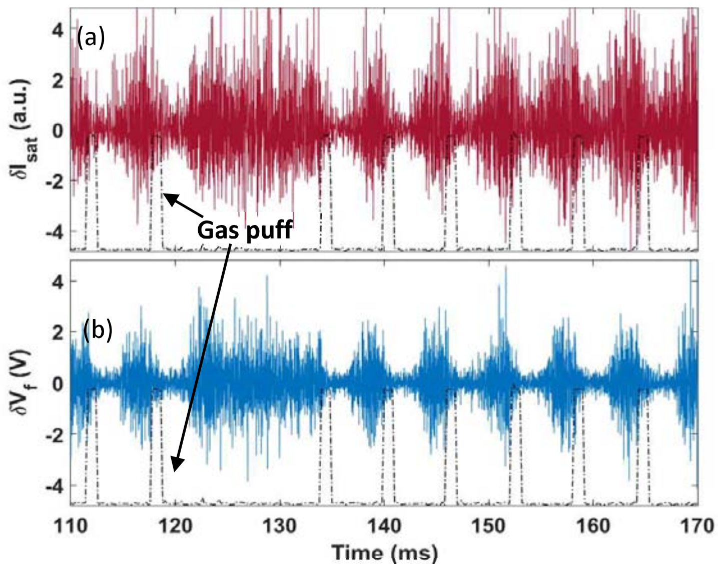

Figure 4.21: Plot showing (a) edge density fluctuations filtered from Ion saturation current signal and (b) potential fluctuations acquired from Langmuir probes in ADITYA-U tokamak, exhibiting fluctuation suppression after each gas puff.

As the drift frequency reduces with the application of short gas-puff pulse, the rotation frequency of the island also reduces due to their coupling, which fairly describes our experimental observations. The argument attributing the observed downshift of the rotation frequency of the island to be due to the reduction in ω^* is further substantiated by changing the amount of injected gas in one gas-puff pulse. As the amount of the injected gas is increased the electron temperature decreases and L_n increases in the edge/SOL, leading to a further decrease in island rotation frequency as shown in figure 4.17. Interestingly in the majority of discharges, where a train of gas-puff pulses is applied with a repetition frequency of $\sim 200\ Hz$ (time period ~ global confinement time of the plasma), the rotation frequency of the m/n = 2/1 mode and its harmonics are observed to be modulated with the rotation frequency decreasing after each gas puff and regaining its prior-to-gas-puff value once the effect of gas-puff is gone. The short gas-puff pulse reduces the temperature and density gradient in the edge/SOL region for a short duration and after the neutrals are completely ionized the edge/SOL region is heated again in presence of the loop voltage and ω^* increases again. The modulation of rotation frequency and the amplitude of the 2/1 mode and its harmonics continue throughout the plasma current flat-top with the application of a train of short gas-puff pulses. Furthermore, these trains of gas-puff pulses have been observed to affect the global plasma parameters including the energy confinement favorably as improvement in these parameters are observed with the application of gas-puff pulses [182]. It has also been observed that in discharges where a gas-puff pulse of larger duration ($\geq 5\ ms$) is applied, instead of usual short gas-puff pulse ($\leq 2\ ms$), the 2/1 mode regains its rotation frequency prior-to-gas-puff value, after a decrease in the rotation frequency, even while the gas pulse in still on. To further understand the observations mentioned in the above sections, the effect of short gas-puff pulses on the ADITYA/ADITYA-U tokamak plasma discharges has been simulated using the BOUT++ code [252]. In edge and SOL regions, in the presence of the ionizing electrons and the neutral gas, a number of atomic and molecular reactions such as electron impact molecular dissociations, ionization, molecular ionic dissociations, and ionic recombination, etc. occur. Details of these reactions are given in Refs.[187,253] which indicate that the plasma in the SOL region consists of electrons, H^+, H^{+2}, and H_2 molecules mainly. Details of the model equations and normalization of each parameter have been given in [252]. The main equations are as follows:

$$\frac{dn}{dt} - D\nabla_\perp^2 n + g\left(T_e\frac{\partial n}{\partial y} + n\frac{\partial T_e}{\partial y} - n\frac{\partial \phi}{\partial y}\right) = \xi_{ion}(T_e)nN + \chi_{edge}\chi_0\bar{T}_{e0}^{3/2}\{\phi - T_e\ln(n)\} - \sigma_{sol}\sigma_0 f_{cs} n\sqrt{T_e}e^{\Lambda-\phi/T_e} + S_n \tag{1}$$

$$\frac{dn_2}{dt} - 2n_2\frac{d\nabla_\perp^2\phi}{dt} - D_{n2}\nabla_\perp^2 n_2 - gn_2\frac{\partial\phi}{\partial y} = -\sigma_0\sigma_{sol}f_{cs}n_2 + \xi_{ion}(T_e)nN - \xi_{eff}^{n_2}nn_2 + S_{n2} \tag{2}$$

$$\frac{d\nabla_\perp^2\phi}{dt} - \nu\nabla_\perp^4\phi + \frac{g}{n+n_2}\left(T_e\frac{\partial n}{\partial y} + n\frac{\partial T_e}{\partial y}\right) = \sigma_{sol}\sigma_0 f_{cs}\sqrt{T_e}\left(1 - e^{\Lambda-\phi/T_e}\right) \chi_{edge}\chi_0\frac{T_e^{3/2}}{\bar{n}+\bar{n}_2}\{\phi - T_e\ln(n)\} - \nu_{in}N\nabla_\perp^2\phi \tag{3}$$

$$\frac{dT_e}{dt} - k_e\nabla_\perp^2 T_e + \frac{2}{3}g\left(\frac{7}{2}T_e\frac{\partial T_e}{\partial y} + \frac{T_e^2}{n}\frac{\partial n}{\partial y} - T_e\frac{\partial\phi}{\partial y}\right) = -\frac{2}{3}f_c\xi_{eff}^{loss}N - \frac{2}{3}f_E f_{cs}\sigma_{sol}\sigma_0 T_e^{3/2}e^{\Lambda-\phi/T_e} + S_{Te} \tag{4}$$

$$\frac{\partial N}{\partial t} - \vec{\nabla}_\perp\cdot\left[D_n(n)\vec{\nabla}_\perp N\right] = -\xi_{ion}^N nN + f_{cs}f_r\sigma_{sol}\sigma_0 n\sqrt{T_e} \tag{5}$$

where n, n_2, ϕ, T_e, and N indicate electron density, H_2^+ density, potential, electron temperature, and neutral gas density, respectively. The contribution of hot or energetic ions has been ignored and each ion species is assumed to be collected at the limiter plate with a common sound speed. It is to be noted that for quantitative comparison with the experimental results the above equations should be solved in the toroidal coordinate system using a kinetic description of the neutral gas. But here a simple 2D rectangular coordinate system and a fluid description of the neutral gas have been used as we are interested in the qualitative matching of the experimental observations and results. Equations (1) - (5) have been solved numerically using BOUT++ code. The above equations are solved using $S_n = 1 \times 10^{-4}$ and varying the magnitude from $S_{N0} = 1 - 6 \times 10^{-5}$. It is to be noted that $S_n = 1 \times 10^{-4}$ corresponds to the injection of $\sim 3 \times 10^{20}$ particles from the core plasma to the edge-SOL regions and $S_n = 1 \times 10^{-5}$ corresponds to the injection of $\sim 3 \times 10^{19}$ particles in the outermost SOL region through an area of $\sim 1\ m^2$ in the yz plane. In the simulation, the contribution of hot or energetic ions has been ignored and each ion species is assumed to be collected to the limiter plate with their own Bohm sheath criteria. A finite-difference in the radial x-direction and FFT in the poloidal y-direction have been used for spatial integration. The time integration has been done using stiffly stable fourth-order Adams-Bashforth predictor-corrector method. Details of the input parameters as given in the model equations can be found in Ref. [252] and references therein.

Figure 4.22 shows the simulated variation of ω^* (normalized to ion gyro-frequency) versus the distance from separatrix (normalized to ion gyroradius) in absence and presence (gas injection rate of $\sim 5 \times 10^{20}$ molecules per second as in the case of experiments) of injected gas. The figure clearly shows that ω^* reduces significantly when neutral gas is injected and thereby suggests that the observed decrease of MHD mode rotation frequency is due to the reduction in ω^*. A maximum of 60% reduction has been found in the ω^*, from the numerical investigations with an injection of $\sim 10^{17} - 10^{18}$neutrals in the edge/SOL region.

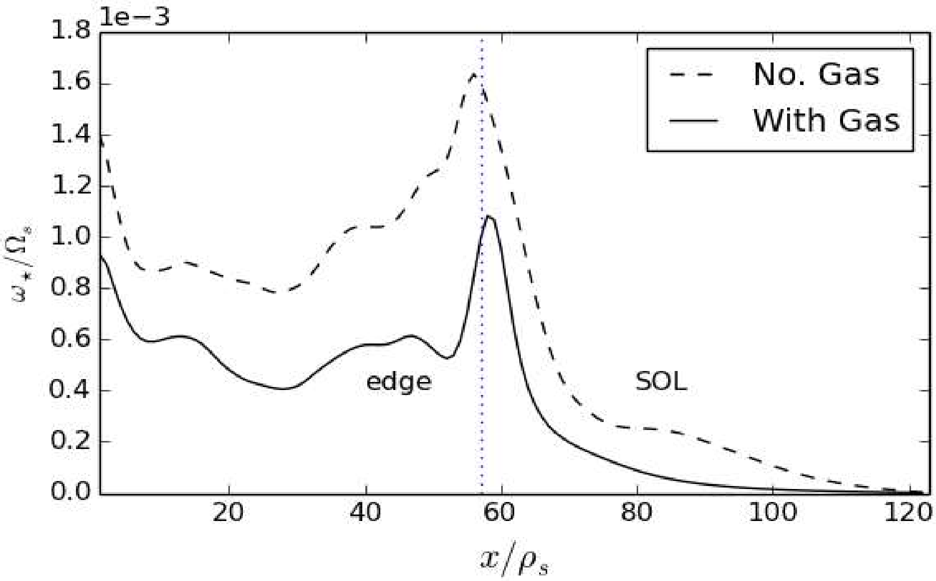

Figure 4.22: BOUT++ Simulation results comparing drift frequency in edge/SOL of ADITYA with and without gas puff.

The almost linear increase in the decrement of mode rotation frequency with the increase in the amount of injected gas molecules is also reproduced in the simulations as shown in figure 4.23.

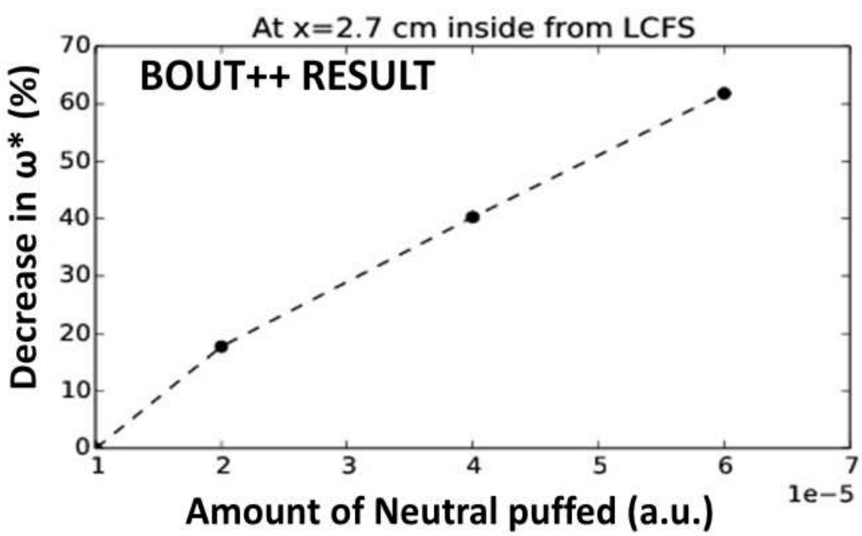

Figure 4.23: Plot showing simulation results for decrease in ω with increase in the amount of neutrals injected.*

The other interesting observation with the short gas-puff pulse application is the reduction of the amplitude of the m/n = 2/1 MHD mode when the mode rotation frequency decreases. We note here that the observed reduction in amplitude of the mode is not due to measurement error. With the reduction in the mode frequency, the amplitude of the voltage induced in the Mirnov coil will decrease, however, the observed decrease in amplitude of the voltage is much larger than that calculated by taking a rotation frequency reduction of $\sim 2 - 4\ kHz$ due to the gas injection. This result is counter-intuitive as higher mode rotation frequencies are known to stabilize the tearing modes [254]. However, as suggested by Biskamp [146], in contrast to the analytical prediction [138] the growth rate of tearing modes increases for large ω_e^* to almost the purely resistive values Biskamp has shown that a transition point exists in the $\gamma/\gamma_T\ vs\ \omega^*/\gamma_T$ plot at $\omega^*/\gamma_T \sim \gamma_T^{-3/8}$ (see figure 6 in Biskamp et.al), after which the growth rate of tearing mode increases with increasing ω^*. Here γ is tearing-mode growth rate and γ_T is the tearing-mode growth rate for $\omega^* \rightarrow 0$.The reason behind this increase in growth rate is that the drift mode gets reflected from the inner boundary r = 0 of the resistive layer, forming a standing wave and its energy is fed back into the resistive layer, hence increasing the growth rate of tearing mode. Furthermore, it has been shown [146] that the transition point depends on plasma resistivity and shifts towards lower values of ω^*/γ_T with increasing resistivity of the plasma. For the relatively lower temperature discharges of ADITYA/ADITYA-U, the values of ω^*/γ_T remains on the side of the transition point where the γ/γ_T is an increasing function of ω^*/γ_T. And in this region of the γ/γ_T versus ω^*/γ_T, reducing the ω^* may reduce the growth rate of the tearing mode. This may be a plausible reason for the experimental observation of reduced amplitude of m/n=2/1 mode with decreasing mode rotation frequency after the application of a short gas-puff pulse.

4.2.2 Influence of MHD modulation using short gas-puff pulses on RE dynamics

As described above the MHD characteristics can be modified by short gas-puff pulse application in a single discharge and hence forms a good platform for studying the relation between the MHD modes and the dynamics of REs. The temporal evolution of HXR emission intensity along with MHD activity, modulated with the application of a train of gas-puff pulses during the plasma current flat-top is shown in figure 4.24 for a representative discharge from ADITYA tokamak.

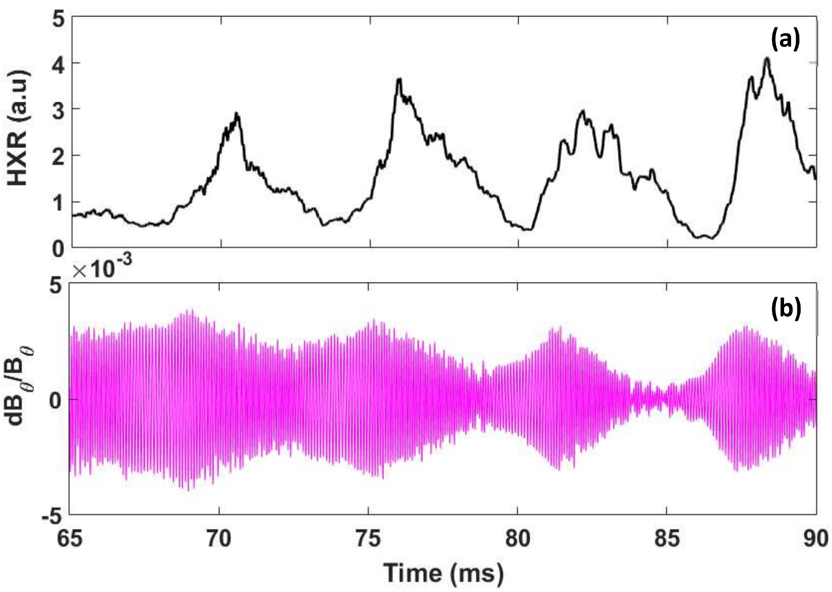

Figure 4.24:Plot showing temporal evolution of (a) HXR emission intensity (b)MHD amplitude modulated with the application of a train of gas-puff pulses.

As mentioned earlier the gas-puff decreases the rotation frequency of the mode as well as the amplitude of the mode is also reduced immediately after each gas-puff. In subsequent 1 – 3 ms of the gas-puff application, the amplitude of the MHD mode increases again to its value before the gas-puff, until the next gas-puff again reduces it. Similar signatures of significant decrease and increase have been observed in HXR emission intensity with the application of each gas-puff. At a first glance, this periodic amplitude modulation of HXR emission intensity with gas-puffs indicate some kind of correlation with MHD modifications, indicative of a relation between of MHD modes and RE loss. However, detailed investigation of events during a single gas puff revealed that the onset time of MHD mode suppression lags or leads the HXR emission reduction. Often, the HXR emission intensity remains suppressed even well after the MHD amplitudes retain their original (high) values after going through suppression due to gas puff and the overall duration of suppression of MHD mode amplitude also does not match with that of the HXR emission. Analysing over 2000 discharges in ADITYA and ADITYA-U, no correlation could be observed between the modification of amplitude and rotation frequency of the m/n = 2/1 mode and the systematic variations in HXR emission intensity, both of which are instigated by the application of a periodic train of gas-puff pulses.

4.3 Discussion and Conclusion

The effect of magnetic stochasticity or MHD modes on REs confinement has been a subject of intense research in the fusion community ever since the REs confined in the MHD island has been first reported in TEXTOR tokamak [112]. In most of the present theoretical models used for simulation of REs in a tokamak, the presence of MHD modes is always considered to be a contributing factor to the RE loss i.e proportional to the $\tilde{B}_\theta/B_\theta$due to the MHD mode. However, the experiments from several tokamaks have often shown signatures of RE confinement inside well-formed magnetic islands [88]. In the experiments conducted in ADITYA and ADITYA-U tokamak, results from discharges having a presence of different MHD modes, support the fact that REs can indeed be confined inside the magnetic island and the effective RE loss rate may be a combination of the loss due to $\tilde{B}_\theta/B_\theta$ and the confinement in the island, when saturated no-overlapping islands are present in a tokamak discharge. As stated by Boozer [95], the complete destruction of magnetic surfaces are required to mitigate the REs. The theoretical model for RE dynamics in tokamak, proposed by Boozer et. al [95] has shown that the REs may get confined inside magnetic islands if the island width increases above a certain threshold. Using that threshold condition for ADITYA and ADITYA-U plasma parameters, the island size should be more than 1 cm for confining the REs. The island width for the type I and type II discharges has been calculated using measured values of $\tilde{B}_\theta/B_\theta$ in the equation $\frac{W}{rs} = 2\left[\left(\frac{2}{m}\right)\left(\frac{r_c}{r_s}\right)^m \left(\tilde{B}_\theta/B_\theta\right)\right]^{1/2}$, where W is the island width, m is the mode number, r_s is the radius of the mode resonant surface and r_c is the radius of the Mirnov probe location [58]. The island width in discharge without harmonics of 2/1 mode has been estimated to be $\leq 1\,cm$ whereas in the discharges with the presence of harmonics of 2/1 mode, the island width$\geq 3\,cm$. The calculations for island width agree very well with the Boozer's island threshold for RE confinement. The generation of harmonic of 2/1 mode i.e 4/2 mode which must be nested inside the 2/1 island may also have some role on the improvement in RE confinement, which may be an interesting subject of theoretical investigation or simulations. Furthermore, it has been theoretically predicted that the saturation amplitude of the MHD modes increases in the presence of runaway or energetic electrons [255,256]. Hence, it may be speculated that in discharges with the presence of harmonics of 2/1 mode, the REs are confined in the m/n = 2/1 islands and increases their saturation amplitude leading to strong non-linear coupling and hence the appearance of harmonics. While in type I discharge, the island size remains low and does not confine the REs. It has also been reported that the loss of RE changes the current profile which can lead to increase and decrease of amplitude of MHD modes [256]. To enhance the understanding of the interplay between the MHD modes and RE dynamics, MHD mode characteristics are modified during a discharge in a controlled fashion. With the application of short gas-puff pulses, the rotation frequency as well as the magnitude of the drift-tearing mode, existing prior to the gas-puff, is observed to be decreased systematically in typical discharges of ADITYA/ADITYA-U Tokamak. A train of periodic short gas-puff pulses applied at the plasma current flat-top leads to periodic modifications of the mode rotation frequency and magnitude of drift-tearing modes. Mode analysis showed that the dominant m/n = 2/1 and its harmonics are rotating in the electron diamagnetic direction prior to the gas puff with a rotation frequency of $\sim 5 - 14\ kHz$. After the application of short fuel (hydrogen) gas-puff pulse injecting 10^{17} – 10^{18} molecules, the 2/1 mode continues to rotate in the electron diamagnetic direction, however with a lower rotation frequency and the amplitude of the mode is also observed to be reduced. The decrease in the rotation frequency, as well as the amplitude of the MHD mode, is found to be proportional to the number of neutrals injected until the gas injection disrupts the plasma. As the electron temperature decreases and the density scale length increases with the gas injection, the drift wave frequency also decreases leading to a reduction in the observed rotation frequency of the m/n = 2/1 mode and its harmonics. Although the $E \times B$ plasma rotation also reduces with the gas-puff, however, it may not be causing the decrease in the mode rotation frequency as it is in the opposite direction to the direction of the mode rotation. The BOUT++ code simulation corroborates the experimental results of plasma pressure profile modifications in the edge/SOL region, leading to a reduction in diamagnetic drift frequency, subsequently reducing the rotation frequency of drift-tearing mode. Interestingly, the amplitude of the mode is also observed to be reduced after the gas puff along with the reduction in rotation frequency. This result of reduction in MHD amplitude with reduction in mode rotation frequency is counter-intuitive as higher mode rotation frequencies are known to stabilize the tearing modes [140] and reduction in mode rotation frequency should increase the amplitude of the drift-tearing modes. However, as suggested by Biskamp [146], in contrast to the analytical prediction [138], the growth rate of drift tearing mode γ, increases with increasing drift frequency ω^*, for $\omega^* > \gamma_T$. Biskamp [146] further argued that for larger ω^* the drift waves do not get damped and propagates across the whole plasma and in case of $d\omega^*/dr \leq 0$, they remain confined to the interior of the singular surface, $0 \leq r \lesssim r_s$. The boundary condition at r = 0 can impose reflection of the drift wave, forming a standing wave, leading to energy transport back into the resistive layer reinforcing the tearing instability. The transition point in the values of ω^*/γ_T, from where the formation of drift standing wave starts and the growth rate of tearing mode, instead of decreasing, increases with increase in ω^*, depends on the plasma resistivity. As the resistivity of the plasma decreases, this transition point moves towards the lower values of ω^*/γ_T. For the relatively lower temperature discharges of ADITYA/ADITYA-U (with normalized resistivity [146], $\eta \sim 10^{-6}$ and $\gamma_T \lesssim 1\ kHz$ [140]), the values of ω^*/γ_T remains on the side of the transition point where the γ/γ_T is an increasing function of ω^*/γ_T, i.e., the amplitude of the drift-tearing mode increases with increasing ω^*. Hence, in the reported discharges of ADITYA/ADITYA-U, reducing the ω^* by the gas injection should decrease the amplitude of the drift-tearing modes.

Although ample evidence towards establishing that the MHD modes do influence the RE dynamics in the discharges without any gas puff, it has been observed that when the MHD mode characteristics are modified in a single discharge, the modifications in the RE dynamics do not seem to follow the changes in the MHD mode amplitude as well as their rotation frequency. Investigation thoroughly the events occurring during and after a single gas-puff pulse exposed that the onset time of MHD mode suppression due to gas-puff lags or leads the observed reduction in the HXR emission intensity. In several discharges, the HXR emission intensity remained suspended even well after the MHD amplitudes retain their original (high) values after going through the suppression phase due to gas puff. The overall duration of suppression of MHD mode amplitude by the gas-puff pulse also does not match with that of the HXR emission intensity. Furthermore, the time is taken for the HXR emission intensity to reach its minimum value after each gas-puff always remains much faster than the time required for the REs to reach to the limiter from the m=2 surface even with Rochester-Rosenbluth diffusivities calculated from the observed amplitudes of MHD mode [17]. Another important observation has been made when the gas-puff pulses are applied in Type-I discharges, where the MHD activity remains weak. In a large number of discharges with very low MHD amplitudes where no well-formed m/n = 2/1, 3/1 island structures are observed, the MHD amplitude remains indifferent to the periodic gas-puffs, i.e., devoid of any periodic activity. Interestingly, the periodic variations in HXR emissions are still observed in such discharges strongly correlated to the periods of the gas-puff pulse train. These observations strongly indicate the presence of another factor controlling the RE dynamics in ADITYA/ADITYA-U, which is strongly affected by the gas-puffs as well. Extensive investigations reveal the presence of a completely new mechanism influencing the RE dynamics, seldom reported in the available literature on REs, which is the subject matter of the next chapter.

Chapter 5

Influence of Turbulent Fluctuations in Edge Density and Floating Potential on RE loss in ADITYA-U

5.1 Introduction

Carrying forward the arguments made in the conclusion of the last chapter, it has been observed that during the periodic gas-puffs, the RE dynamics in ADITYA/ADITYA-U is not correlated with the induced variations in the MHD mode characteristics, instead, they are observed to be strongly affected by the density and potential fluctuations present in the edge/SOL region. Owing to the well-established fact that the magnetic turbulence dominates the runaway transport [references given in earlier chapters], several experiments have been attempted to modify the magnetic turbulence in tokamaks in order to device a mechanism for RE mitigation worldwide, e.g., application of RMPs, fast variations of vertical fields, etc. RE transport effected by electromagnetic resistive ballooning modes is reported in ADEX tokamak [116]. However, to the best of our knowledge, direct experimental evidence of the effect of density and floating potential fluctuations in the edge/SOL region on the RE loss or confinement are not reported. Indirect evidence include the JET tokamak [257] experiments, in which the contribution of electrostatic turbulence is attributed to the observed difference in the measured and estimated diffusion coefficient of REs taking into account the magnetic turbulence. Further, it has been observed in limiter biasing experiments in IR-T1 [258] that the REs are suppressed during the biasing of the limiter. As the electrode or limiter biasing are known to suppress the electrostatic fluctuations in the edge/SOL region, suppression of REs might be due to the suppression of electrostatic fluctuation due to biasing. Furthermore, it has been observed in ASDEX tokamak, that the RE flux increases significantly when the discharge makes the transition to L-mode from the Ohmic mode. The RE flux again decreases significantly, well below of its value in the Ohmic mode, when the discharge makes a transition from L to H mode. As it is well known that the electrostatic fluctuations in the edge/SOL make similar transitions at Ohmic to L to H modes, an indirect correlation may be foreseen between the electrostatic fluctuations and the RE flux.

In the previous chapters of this thesis, it has been observed that magnetic fluctuations due to the presence of MHD modes do effect the RE generation and loss in ADITYA and ADITYA-U tokamak. However, when both the amplitude and frequency of the m/n= 2/1 drift tearing modes in ADITYA and ADITYA-U are varied during a discharge by applying short gas-puff pulses, no correlation has been observed between the MHD variations and the HXR emission intensity variation. Furthermore, the HXR emission intensity variation has been observed after each short gas-puff pulse application in the discharges with very low ($\tilde{B}_\theta/B_\theta < 1 \times 10^{-4}$) the magnetic fluctuations in which the m/n=2/1 modes are not visible or barely visible. In these discharges with low magnetic fluctuations, the variation of amplitude correlated with gas puffs is also not observed. This observation clearly suggests a mechanism other than the magnetic fluctuations is responsible for the observation of strong modification of HXR emission intensity with the application of short gas-puff pulses.

The effect of gas puff on the edge/SOL electrostatic fluctuations has been investigated in detail by Jha et.al. [221,240,246] in ADITYA tokamak. It has been observed that the short gas-puff pulses suppress the edge/SOL electrostatic fluctuations. In this chapter, direct experimental evidence of the strong influence of electrostatic fluctuations on the RE transport is presented.

5.2 Experimental Observation

5.2.1 Variation in HXR emission intensity with short gas-puff pulses

As mentioned earlier in the thesis, the HXR emissions from the limiter are observed in ADITYA as well as ADITYA-U REs using NaI detector collimated to view the graphite limiter. The HXR emission is generated by the REs hitting the limiter surface. The REs are generated inside the plasma and due to their cross-field (radial) transport, they reach the limiter, thereafter generate HXRs. Mainly two types of discharges of ADITYA-U are chosen for this study. In the type-I discharges the HXR emission intensity remains almost constant or varies very slowly compared to the gas-puff pulse width ($1 - 2\ ms$) and interval between the two pulses, during the plasma current flat-top and in type-II discharges the HXR emission intensity increases monotonically, again with slow time-scales compared to gas-puff pulse width and interval, after its initiation at some time-point during the current flat-top. The type-II discharges are obtained by pushing the plasma column towards the inboard (high-field side), where the toroidal belt limiter is located in ADITYA-U. After obtaining stable repeatable discharges, periodic gas puffs with ON time of $\sim 0.5 - 2\ ms$ and OFF time of $\sim 4 - 7\ ms$ is applied, during the current flat top (> 40 ms into the discharge), until the end of the discharge. The gas-puff pulse width, magnitude and period are varied according to the experimental requirements from shot-to-shot. The temporal evolution of plasma current, loop voltage, H_α emission intensity and HXR emission intensity in a representative discharge with the application of a train of short gas-puff pulses is plotted in figure 5.1. The temporal profile of HXR emission clearly shows a periodic variation strongly time-correlated with the period of gas-puff pulses as shown in the figure 5.1(d).

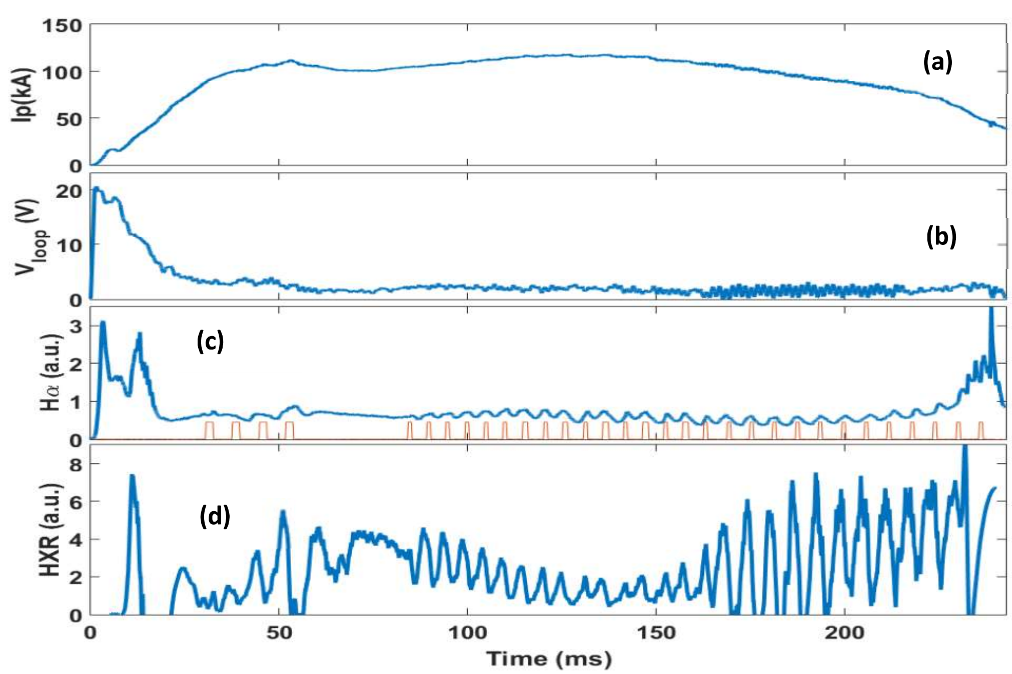

Figure 5.1:Time profile of (a) Plasma Current (b) Loop voltage (c) H_α emission intensity, multiple gas puffs (orange) and (d) HXR intensity for a typical discharge shot#32544 from ADITYA-U

These fast variations in the HXR emission intensity remains absent when no short gas-puff pulse is applied. Systematic analysis of large number of discharges database from ADITYA-U reveals that the observed fast periodic variations in HXR emission intensity are strongly correlated with periodic gas puffs applied during plasma current flat-top. To elaborate the variation in HXR emission intensity during and after a short gas-puff, a time-slice of the HXR emission intensity along with a single gas-puff from the plasma current flat-top period is plotted in figure 5.2.

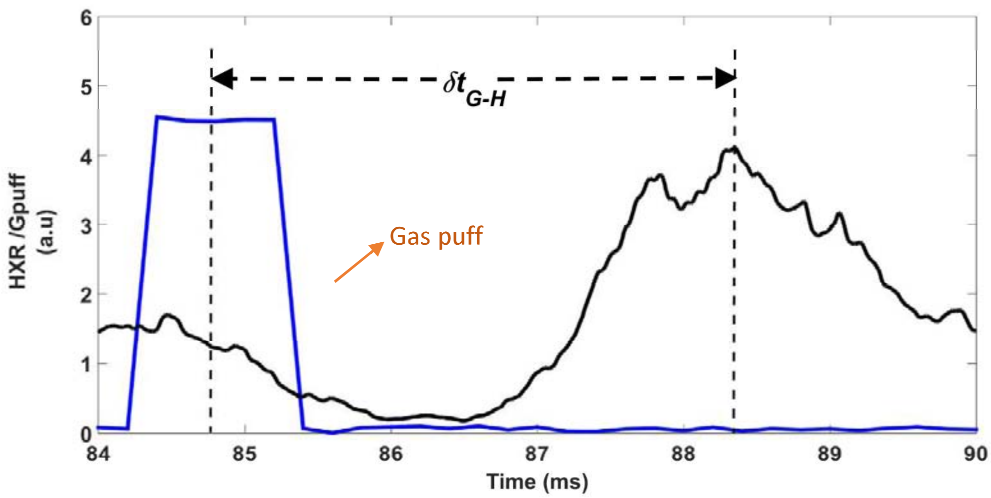

Figure 5.2: Plot showing Gas puff and peak in HXR intensity following the gas puff, and defining the time delay (δt_{G-H}) between gas puff and HXR peak.

When a short gas-puff pulse is applied, the HXR emission intensity decreases from its value prior to the gas-puff almost simultaneously and attains a minimum value. The HXR emission intensity remains at this minimum value for $\sim 2 - 3\, ms$ from the gas injection and then increases to a value higher than its value prior to the gas-puff in subsequent$\sim 2 - 3\, ms$. The HXR intensity decrease again and attains its value which it had before the gas puff. The overall variation in the temporal evolution of HXR emission intensity during and after a single gas-puff pulse hence depict a peak with $FWHM \sim 1 - 2\, ms$. The sequence repeats itself during the next gas-puff cycle. The ratio of peak-value (attained after the gas injection) to mean-value (value of HXR intensity before the gas-puff) varies from $\sim 40\% - 80\%$ in different discharges (Figure 5.3(a)). The occurrence of these periodic peaks in HXR intensity has been found to be strongly dependent on gas puffs and such pronounced HXR intensity peaks are absent in discharges without periodic gas puffs. The number, as well as time period of HXR intensity peaks observed in each discharge, is the same as the number of gas puffs injected and time period of periodic gas puffs. Also, the observed HXR intensity peaks always followed the gas-puff pulse and they have never been observed precede the gas-puff pulse in any discharge. The time duration between the gas-puff pulse and the peak of the HXR emission intensity is named as 'δt_{G-H}' as shown in figure 5.2. The time delay between a gas puff and its subsequent HXR peak has been plotted with number of observed peaks from multiple randomly selected discharges in ADITYA-U in figure 5.3(b). The average time delay (δt_{G-H}) between gas puff injection and the appearance of HXR peak is found to be $\sim\ 2 - 4\ ms$.

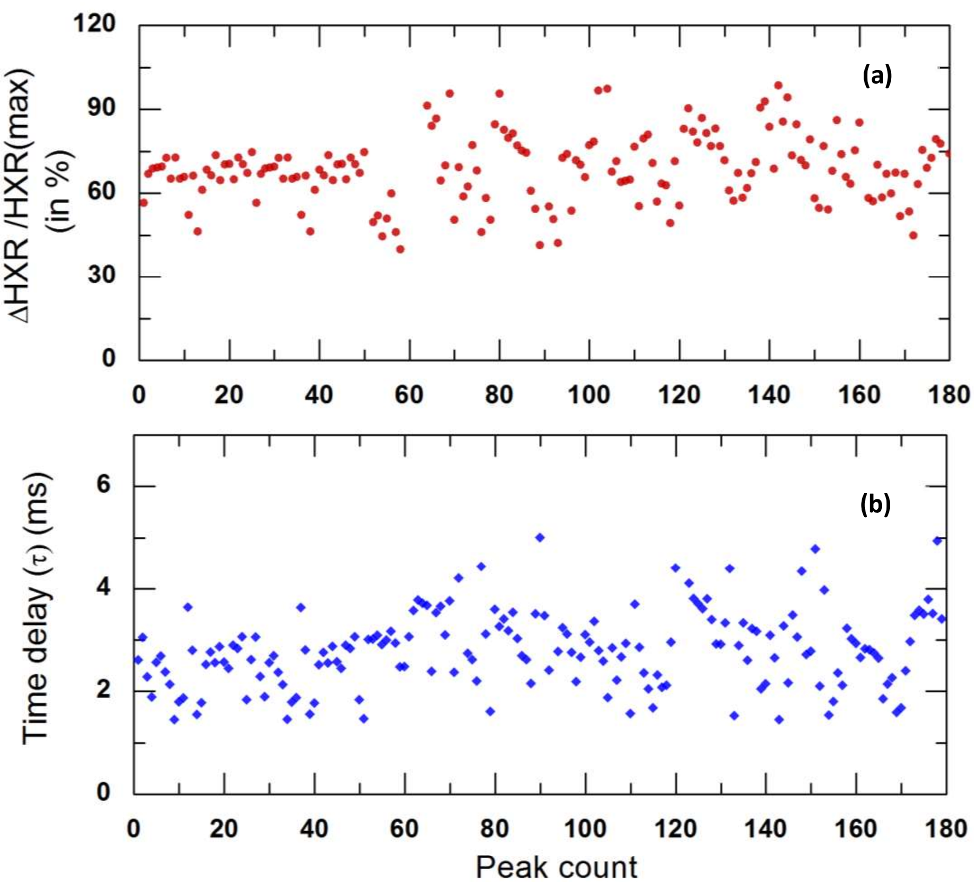

Figure 5.3:(a) Percentage of decrease in HXR intensity after each gas puff and (b) Time delay between gas puff and HXR intensity peak afterward plotted for 180 gas puff pulses from randomly selected discharges.

As mentioned in Chapter 4, often no correlation has been observed between the periodic variations in the MHD mode characteristics and the observed variations in the HXR emission intensity due to the short gas-puff pulse application. Apart from that, in a large number of discharges the periodic variations in the HXR emission intensity have been observed even in absence of periodic modulation in poloidal magnetic fluctuations during the plasma current flat-top duration with the application of short gas-puff pulses. Two representative discharges from this category of discharges (Type II of chapter 4) are shown in figure 5.4 (a, b) for shot #31544 and for shot #32567 in 5.5 (a, b). Note here again that in these discharges, the amplitude of Mirnov fluctuations remain very low ($\tilde{B}_\theta/B_\theta < 1 \times 10^{-4}$) and mode structures are not observed.

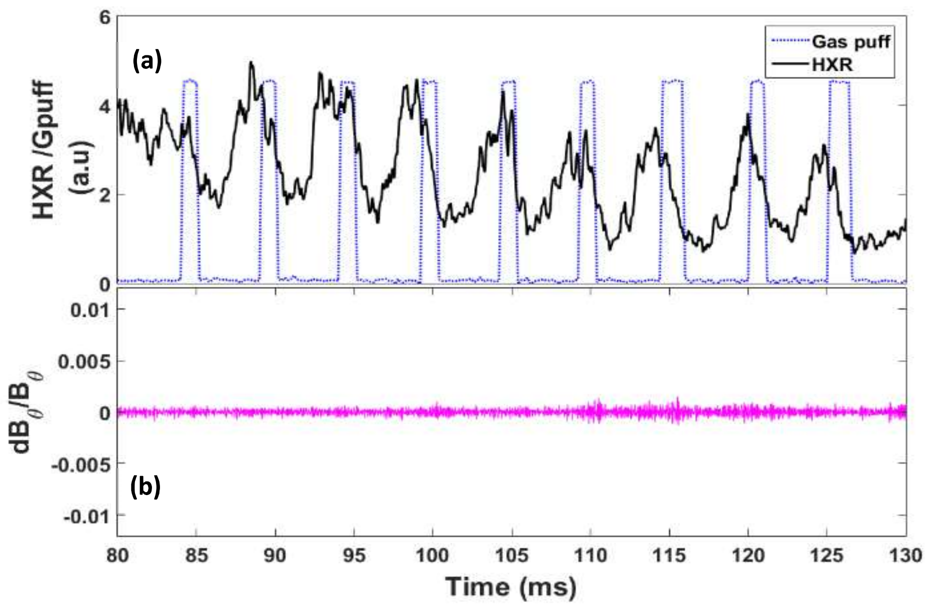

Figure 5.4: Plot showing the temporal evolution of (a) HXR intensity, and gas puffs (blue) (b) normalized poloidal magnetic fluctuations with negligible amplitude and no modulation with gas puff for shot #32544.

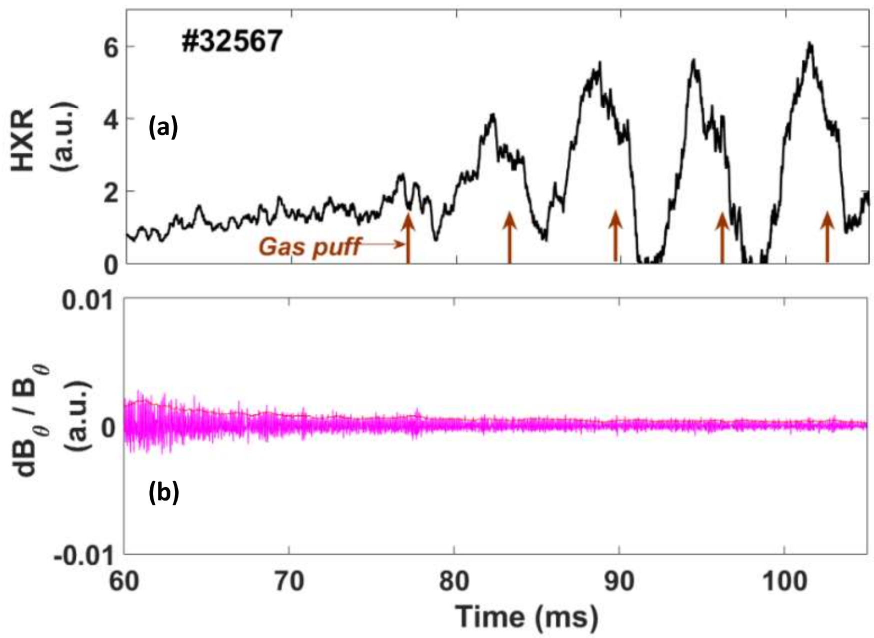

Figure 5.5: Plot showing the temporal evolution of (a) HXR intensity, and gas puffs (vertical arrows) (b) normalized poloidal magnetic fluctuations with negligible amplitude and no modulation with gas puff for shot #32567.

After finding no correlation of the HXR emission intensity variation with the observed with the magnetic fluctuations in several discharges, a wider investigation revealed that the edge/SOL density and potential fluctuations exhibited a strong correlation with the presence and absence of these HXR peaks. Thereafter, multiple experiments and detailed analysis have been carried out in order to investigate and establish the effect of the edge fluctuations on REs in ADITYA-U tokamak.

5.3 Turbulent Electrostatic Edge Fluctuation

The edge of a tokamak plasma is widely known to be dominated by turbulent electrostatic fluctuations [26,30,163,216]. In ADITYA tokamak these fluctuations had been studied in detail. It has been shown that application of gas puff leads to suppression of the edge fluctuations [163,240]. The fluctuation suppression is observed in a broad extent of the edge region and is not limited to the narrow gradient region. A reduction in the particle flux during the gas puff has also been reported which lead to a substantial increase in particle confinement time in ADITYA [163].

5.3.1 Edge Fluctuation in ADITYA-U Tokamak

In ADITYA-U these fluctuations have been studied with the help of multiple Langmuir probes independently as well as in correlation with the RE generated HXRs. The edge density has been acquired by 2-5 Langmuir probes at different radial and poloidal locations in ion saturation current mode and the floating potential at the edge has also been acquired at a sampling frequency of 100 kHz. The details of the Langmuir probe have been described in detail Chapter 2. The following figure 5.6 shows the temporal evolution of electron density measured by the Langmuir probes placed at different radial and poloidal locations in the edge/SOL region of ADITYA-U tokamak. Sharp variations in the mean edge density are due to the application of short gas-puff pulses.

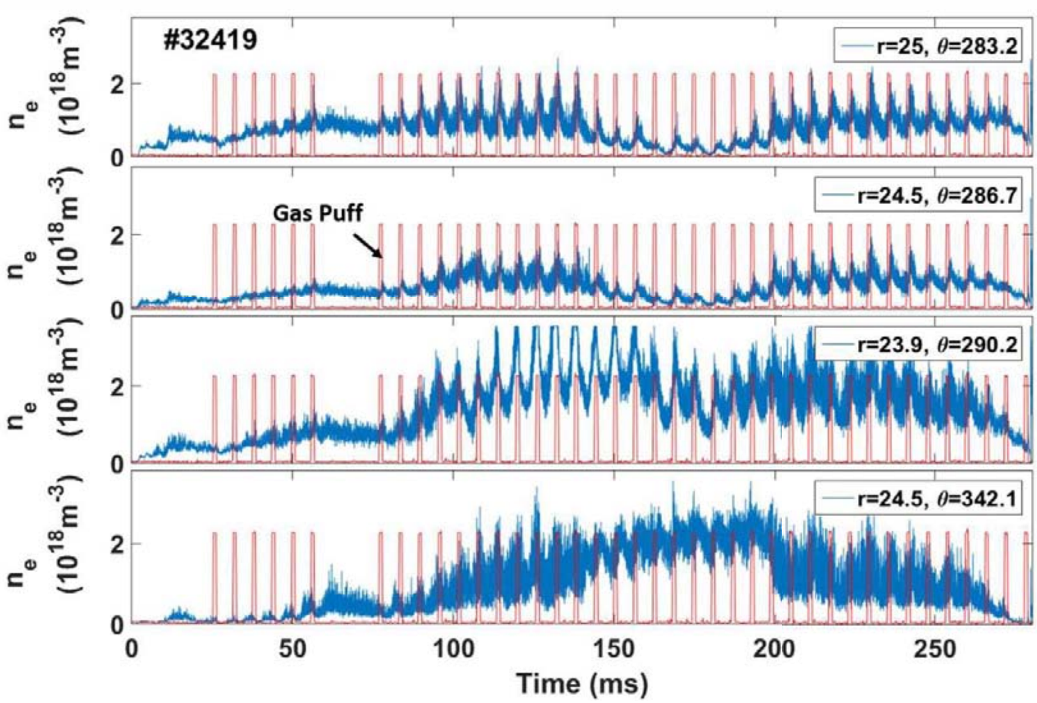

Figure 5.6: Plots showing time evolution density obtained from 5 Langmuir probes at different radial (r) and poloidal (θ) locations in ADITYA-U with gas puff (red).

In order to extract the edge fluctuation information, the following steps have been performed on ion saturation current acquired by the Langmuir probes for multiple discharges. The edge electron density is calculated by using the ion saturation current (I_{sat}) acquired by the Langmuir probes using the formula [177,259,260] , $n_e = \frac{I_{sat}}{0.6\, Av_{th}}$, where A is the probe area and v_{th} ~ is the ion thermal velocity at the edge. The I_{sat}

data is then smoothened by 100- 200 points to obtain the time profile of the mean ion saturation current as shown by the black curve in figure 5.7.

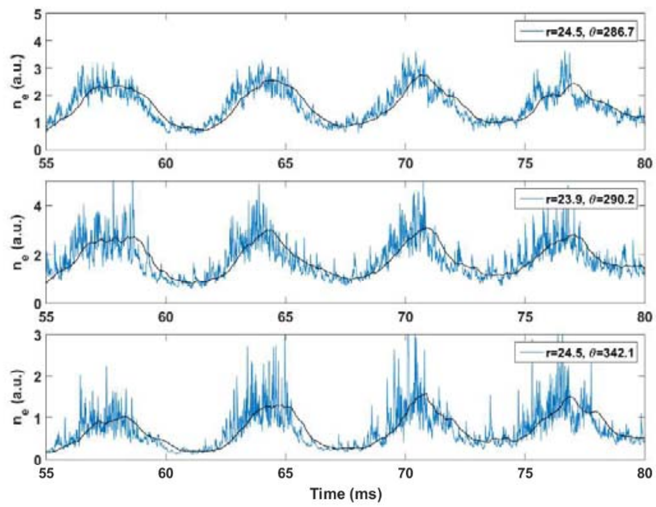

Figure 5.7: Plots showing the time evolution of I_{sat} acquired by 3 Langmuir probes at different radial (r) and poloidal (θ) locations, along with 100 points smoothened mean I_{sat} for each probe (black).

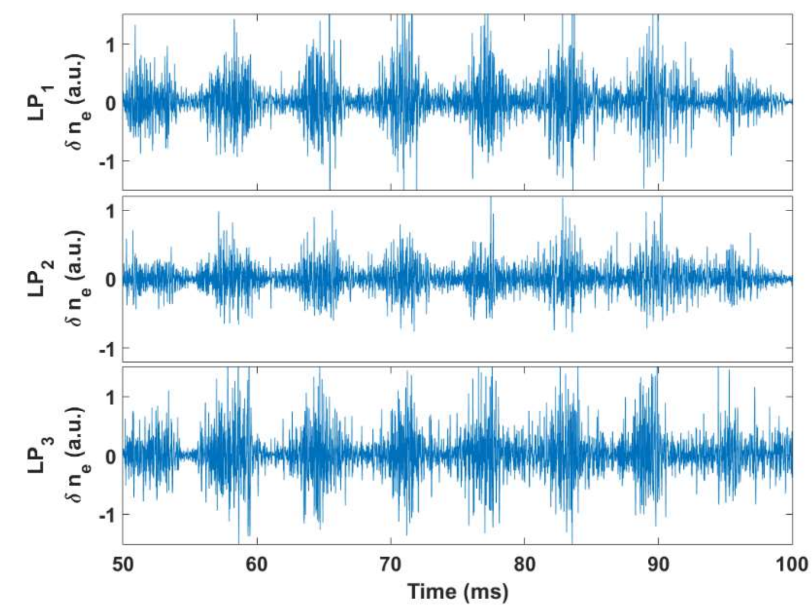

Figure 5.8:Plots showing the time evolution of Isat fluctuation data obtained by filtering >0.5 kHz from 3 Langmuir probes, exhibiting periodic fluctuation suppression.

The raw data is then filtered with a high pass filter ($> 0.5\ kHz$) to extract the temporal evolution of density fluctuation δn_e as shown in figure 5.8 (a, b, c). Density fluctuations with amplitude $\left(\frac{\delta n_e}{n_e}\right) \sim 40 - 60\%$ are generally observed in edge/SOL region of

ADITYA-U, which decrease up to $\sim 10 - 20$ % after the application of short gas-puff pulse. Similar observations are recorded in the temporal evolution of floating potential in the edge/SOL region as shown in figure 5.9. Figure 5.9 shows the time evolution of fluctuation in floating potential fluctuations, exhibiting decrement in fluctuation amplitude after each gas puff, similar to that observed in I_{sat} fluctuations.

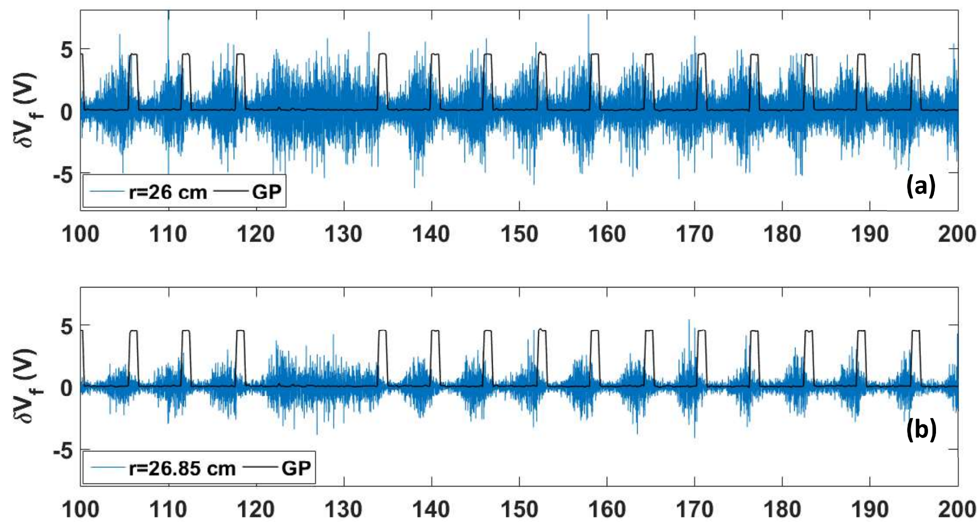

Figure 5.9:Plots showing the time evolution of edge potential fluctuation filtered from floating potential acquired by 2 Langmuir probes showing suppression in amplitude after each gas puff (black).

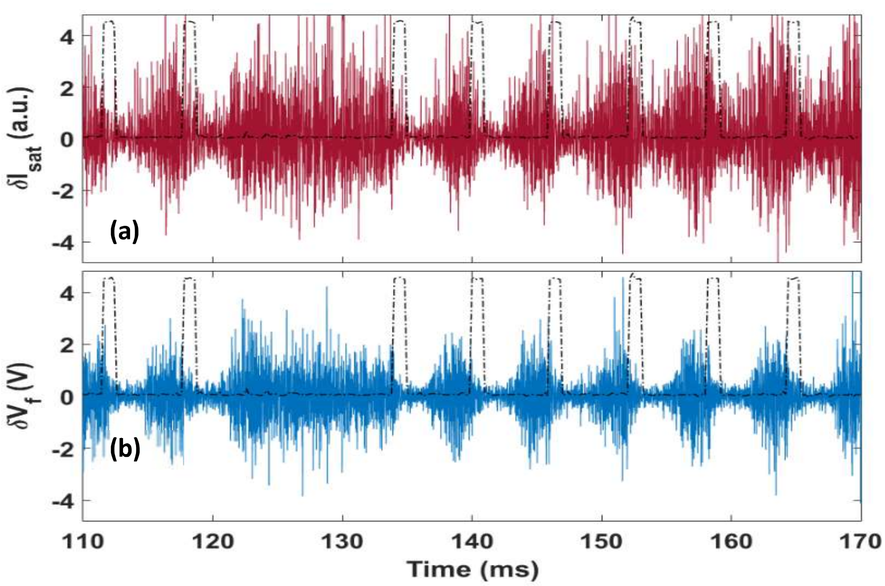

Figure 5.10: Plot showing (a) time evolution of fluctuation in edge potential and Isat exhibiting identical amplitude suppression in time.

Thereafter, the density fluctuation time series has been compared with the potential fluctuation time series, and the results are plotted in figure 5.10. It shows that both edge density and potential fluctuations decrease simultaneously after the gas puff. Note here again that no such sharp variation in density and floating potential fluctuations has been observed without the application of gas-puffs. Again, looking at the variations in density and potential fluctuations after the application of a single gas-puff pulse, it has been observed that the fluctuations are suppressed almost simultaneously with the gas injection. The fluctuations remain suppressed for a time duration of $\sim 2 - 4\ ms$ after the injection of each gas-puff pulse and then increase again regaining the amplitude they had prior to the gas-puff pulse. After the next gas-puff pulse injection these fluctuations decrease again and the cycle continues with each of the gas-puff pulses. As can be seen from figure 5.10, that around $\sim 115\ ms$ in the figure, where the interval between the two gas-puff pulses is increased, the fluctuations get suppressed after the gas-puff pulse is applied (at $\sim 117\ ms$), remains suppressed for $\sim 3\ ms$, then increase again to retain a saturated value until the next gas-puff pulse comes at $\sim 134\ ms$. The fluctuation suppression is observed over a broad extent spreading over the edge and SOL regions of ADITYA-U ($r \sim 23.9 - 27\ cm$). Further to characterize the fluctuations, the frequency power spectra of these fluctuations are generated using Fast Fourier Transform (FFT) as shown in figure 5.11.

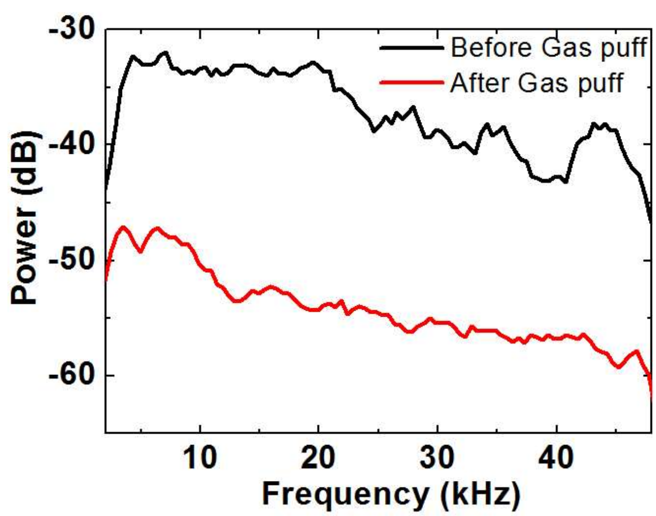

Figure 5.11: Frequency power spectrum of edge fluctuations before (black) and after gas puff (red).

The power spectrum shows that these fluctuations are broad-band in nature with no coherent peaks in the spectra. As the edge turbulence mainly consists of broadband density fluctuations [29] the observed broadband density fluctuations indicate presence of edge turbulence in edge/SOL region of ADITYA-U. Interestingly, after the application of the gas-puff pulse, the fluctuation power decreases by $\sim 20\ dB$ over the frequency band of $5 - 40\ kHz$, although the nature of fluctuations remained broadband.

5.3.2 Effect of Turbulent edge fluctuations on REs Loss

The turbulent edge fluctuations are observed to be suppressed by the application of short gas-puff pulses in ADITYA-U tokamak. Further, by applying a train of short gas-puff pulses, periodic suppression of edge/SOL turbulence is observed during the plasma current flat-top. Comparing the time-sequence of these periodic edge turbulence suppression with the HXR emission intensity variations by the application of gas-puff train, a one to one correspondence has been observed between the two in the discharges where the magnetic fluctuation are very low. The variation in HXR emission intensity along with the suppression of edge/SOL turbulence from a time-slice of the plasma current flat-top is plotted in figure 5.12.

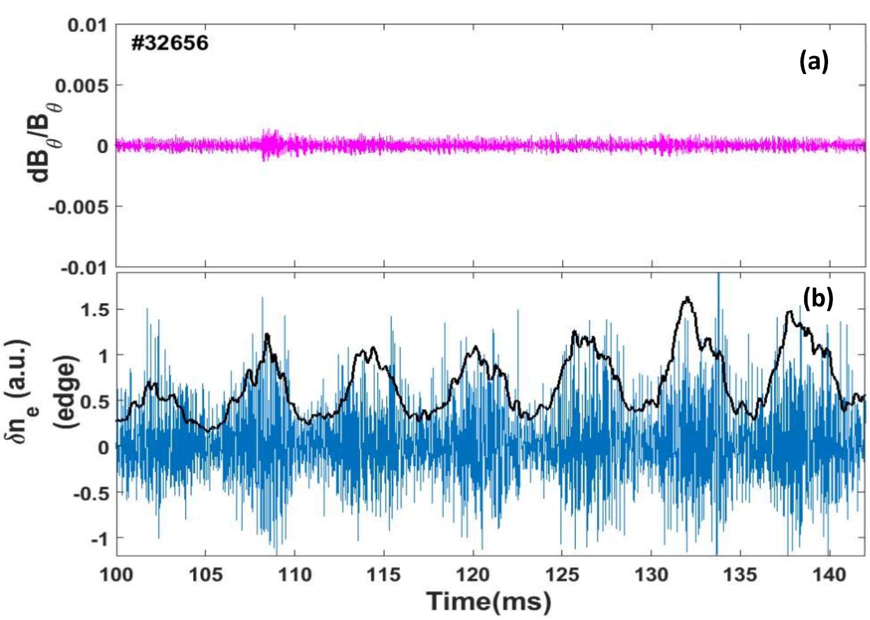

Figure 5.12: Plot showing the temporal evolution of (a) normalized poloidal magnetic fluctuations (Mirnov) (b) HXR intensity,(black) and edge density fluctuations (blue) for shot #32656.

The temporal variation of poloidal magnetic field fluctuation from a Mirnov coil is also plotted for comparison. The one-to-one correspondence between the edge/SOL turbulence suppression and the variation in the HXR emission intensity is clearly evident in this figure. As soon as the gas is injected the turbulence is suppressed, the HXR intensity decreases to attain a minimum value, thereafter the turbulence remains suppressed the HXR intensity remains at its minimum value. After the effect of the gas puff is over, the turbulence increases again and the HXR intensity also increases attaining its maximum value. This sequence of events repeats after each gas-puff pulse. The strong time-correlation between the turbulence suppression and the HXR intensity in ADITYA-U is further confirmed by plotting the time evolution of frequency spectrum (specgram) of edge/SOL turbulence and HXR emission intensity on top of each other in figure 5.13.

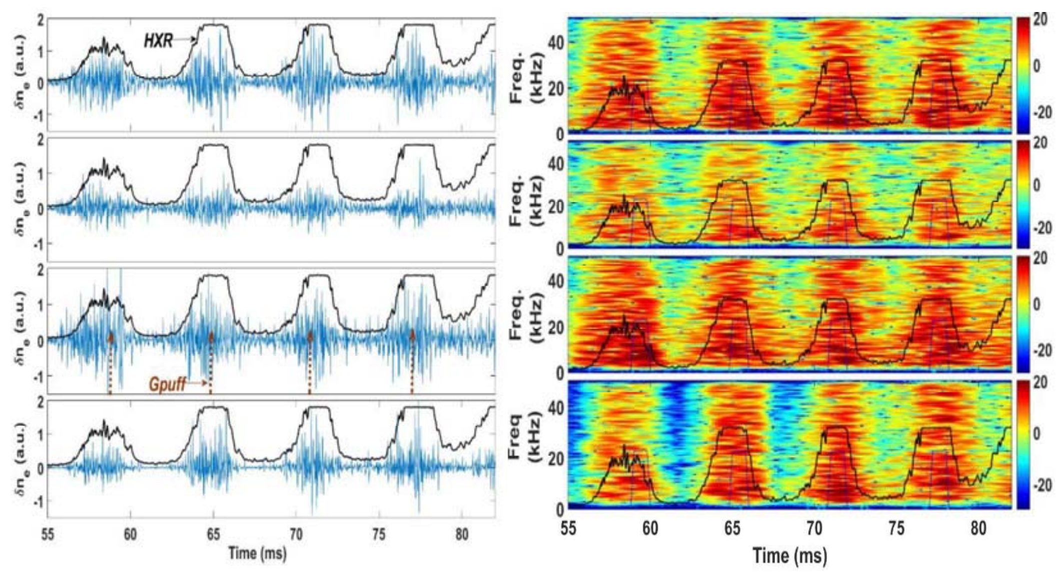

Figure 5.13: Plot showing temporal evolution of (a) HXR intensity (black), and edge density fluctuations from 4 Langmuir probes and gas puff (vertical arrows) for shot #32567 and (b) specgram of density fluctuations.

The left-hand panel of the figure shows the time evolution of density fluctuations (in blue) obtained from four Langmuir probes located at different poloidal and toroidal locations in the edge/SOL, overlapped with HXR intensity (in black). Whereas the right-hand panel shows the 'specgram' of the same fluctuations overlapped with HXR intensity (in black). The time-frequency plot depicts the power of fluctuations (in dB) that is color-coded in 'JET' style where red denotes highest power and blue denotes the lowest power. The vertical red band in the time-frequency plot implies broadband nature of the fluctuation and the following blue band denotes a decrease in the fluctuation amplitude with the application of gas-puff pulses. The gas-puff pulses are also shown by arrows in the figure. Note here that the time-slices are from the plasma current flat-top region. It can be observed in both the figures that the minima the HXR intensity coincides well with minima in the density fluctuation power and the HXR intensity peak lie in the time-zone where the fluctuation power is maximum. These observations are recorded from several discharges (>500) irrespective of major changes in the bulk plasma parameters, such as plasma current and toroidal magnetic field in the operation range of ADITYA-U tokamak.

In order to further confirm the role of edge/SOL turbulence on RE loss, the experiments are repeated in the discharges where continuously increasing HXR emissions are obtained during the plasma current flat-top. The discharges with continuously increasing HXR emissions are obtained by deliberately pushing the plasma column towards the inboard toroidal belt limiter. The specgram of density fluctuations overlapped with HXR intensity is plotted for two representative (consecutive) discharges are plotted in figure 5.14 where the initiation time of gas-puff pulse train has been varied, while the rest of the operation parameters are kept constant. Figure 5.14 (a) and (b) show HXR intensity plotted on top of specgram of δn_e for shot #32764 in which the periodic gas-puff train is initiated at $\sim 125\ ms$ and for shot #32765 where gas-puff train is initiated at 160 ms, respectively.

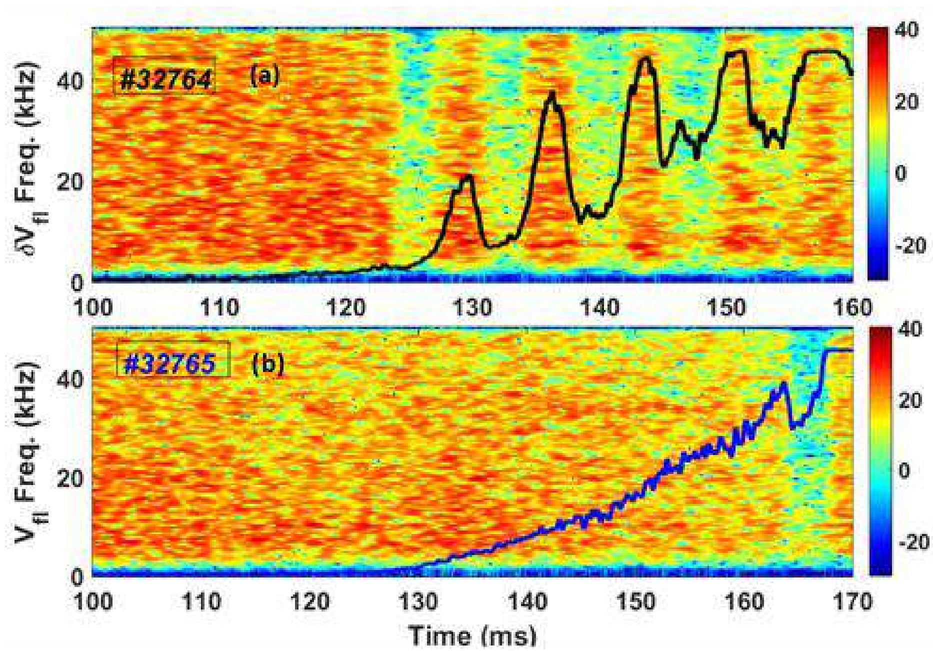

Figure 5.14:Plot showing temporal evolution of HXR intensity plotted over specgram of density fluctuations, for two consecutive discharges (a) shot #32764 where periodic gas puff starts from 122 ms (b) shot #32765 where periodic gas puff starts from 160 ms.

It can be seen from the figure that the baseline of HXR emission intensity starts rising slowly around $\sim 125\,ms$ in both the discharges. As soon as the gas-puff pulse is injected at $\sim 120\,ms$ in shot # 32764, it suppresses the density fluctuation and the HXR emission intensity decreases. The HXR emission intensity rises again between the two consecutive gas-puff pulses where the fluctuations are high. Another interesting observation is related to the rise rate of the HXR intensity subsequent to its decrease after the gas injection. The HXR intensity increases much faster than its rise rate before the gas puffing. The sequence repeats again during the next gas puff. It may be noted that each HXR intensity peak attains a higher value than the value of peak preceding it. This may be due to the continuously rising trend of the HXR related to the continuous increase in the loss of REs. However, as the gas-puff is initiated at a later time ($\sim 160\,ms$) in shot# 32765, the HXR emission, starts, rising continuously from $\sim 125\,ms$ mostly due to increasing RE loss as the plasma column is pushed inboard until the gas is injected around $\sim 165\,ms$, where it again decreases simultaneously with the decrease in edge/SOL fluctuation power due to the gas injection. The above experimental observations persuasively suggest that edge/SOL turbulence facilitates the RE loss in ADITYA-U tokamak.

5.3.3 Effect of edge/SOL turbulence on Sawteeth generated REs

As described in chapter 3, the sawtooth crash generate/accelerate the REs, which subsequently generate HXR bursts coinciding with each sawtooth crash, when they interact with the limiter. To further confirm the capability of edge/SOL turbulence to facilitate the RE loss the effect of gas-puff induced turbulence suppression on the transport of the sawtooth-crash generated REs has been studied in a unique experiment. As already explained in detail in Chapter 3, the toroidal electric field induced during a sawtooth crash is strong enough to generate REs that may lead to the observed HXR bursts after reaching the limiter. The observations of HXR burst coinciding with each sawteeth crash are repeated in typical discharges of ADITYA-U tokamak. Figure 5.15 shows the time evolution of plasma current, loop voltage, SXR, and HXR emission from shot #33141 in presence of train of gas-puff pulses, showing the bursts in HXR emission coinciding with each sawtooth crash.

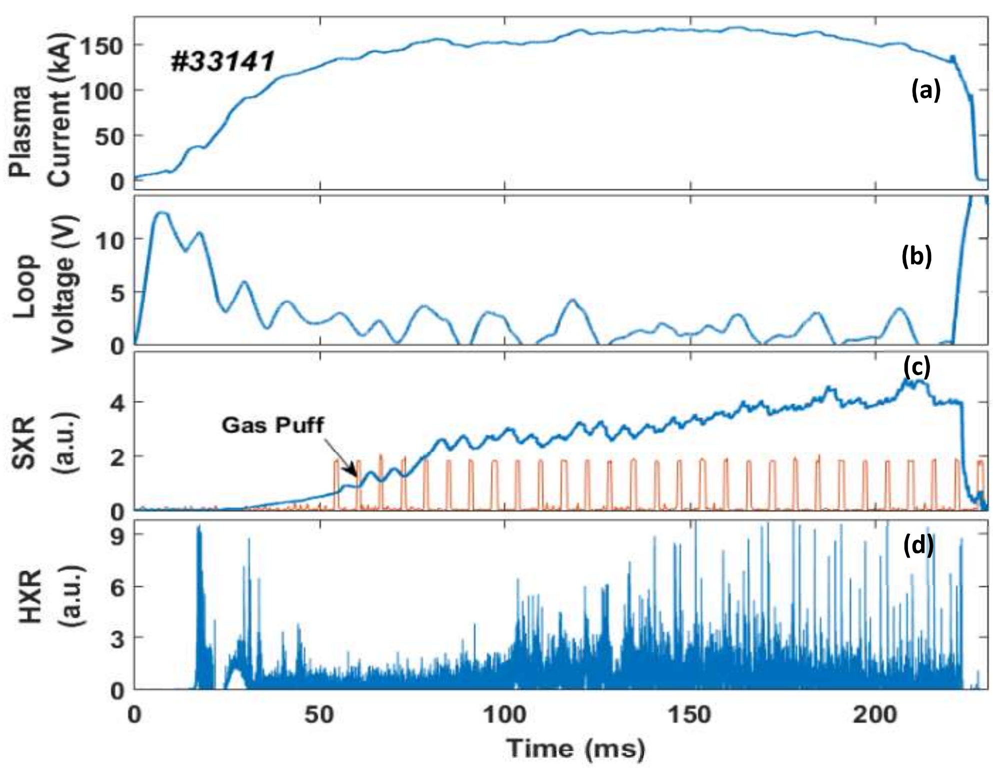

Figure 5.15:Plot showing the time evolution of (a)Plasma current, (b) Loop Voltage, (c) SXR and periodic gas puffs, (d) HXR intensity from shot #33141 from ADITYA-U.

The interval between two gas-puff pulses ($\sim 4\ ms$) is so chosen that $2 - 3$ sawteeth cycle falls during that interval. To elaborate the effect of short gas-puff pulses on sawtooth-crash generated HXR bursts, the temporal evolution of SXR, HXR and gas-puff pulses are plotted on top of each other in figure 5.16 in an expanded time zone of $\sim 130 - 190\ ms$ of the plasma current flat-top of shot #33141. As noticeable in the figure, the amplitude of the HXR bursts shows a systematic variation during the presence and absence of the gas-puff pulses. It is clearly evident from the figure that the amplitude of sawtooth-generated HXR bursts are strongly reduced after each gas-puff pulses.

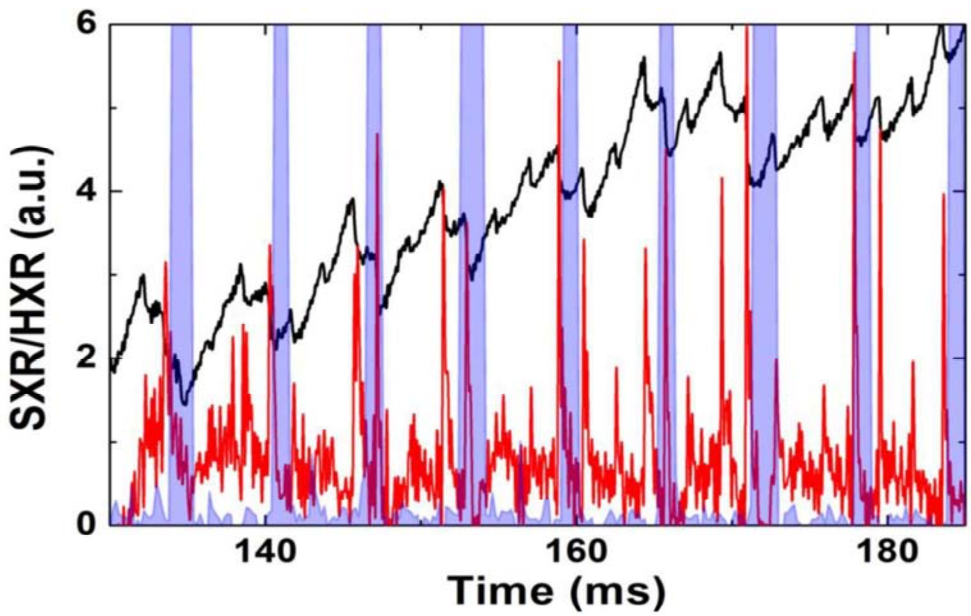

Figure 5.16: Plot showing the time evolution of SXR (black), filtered HXR intensity (red) and periodic gas puffs (blue) from shot#33141 from ADITYA-U.

The sawteeth generated HXR bursts are suppressed by > 5 times, immediately after each gas puff. These HXR bursts reappear $\sim 2 - 3\ ms$ thereafter, before the injection of subsequent gas puff pulse. The same sequence of events is repeated after each gas puff. As mentioned earlier in the chapter that the edge/SOL turbulence is strongly correlated with the gas-puff pulses, a direct correlation between the amplitude variation of sawtooth-generated HXR bursts and the variations in the edge/SOL turbulence is observed as shown in figure 5.17. It has been observed that when a sawtooth crash occurs just after the gas injection, where the edge/SOL turbulence remains suppressed, the sawtooth-crash generated HXR burst show a relatively reduced amplitude.

Whereas, when the sawtooth crash occurs $\sim 3 - 4\ ms$ after the gas injection (in between two gas-puff pulses), where the edge/SOL turbulence remained high, a relatively high amplitude saw-tooth generated HXR burst is observed. This may be due to the fact that, in presence of high edge/SOL turbulence, a larger number of sawteeth generated REs reach the edge from the q=1 surface leading to the high intensity HXR bursts. After the gas injection, the edge/SOL turbulence is suppressed leading to a reduction in the RE loss due to the turbulence and hence, a lesser number of the sawteeth generated RE reach the limiter, leading to absence/suppression of HXR bursts coinciding with the sawtooth-crash. This observation further strengthens the notion that edge/SOL turbulence facilitate the RE loss. In retrospect, it is worth emphasizing that no gas puffs are injected during the current flat-top of shot # 24025, and therefore the edge/SOL turbulence has not been externally disturbed. Hence, the presence/absence of HXR bursts coinciding with sawteeth crashes, signifying RE loss, was solely dependent on the overlapping/non-overlapping of m/n=2/1 and 3/1 island in #24025 (ADITYA). However, in # 33141(ADITYA-U) the periodic gas puffs have been injected during the current flat-top, which modifies the edge/SOL turbulence in the discharge affecting the RE dynamics, which is comparable to the effect of magnetic island dynamics in #24025. Again, note here that shot #33141 has very low MHD activity, $\tilde{B}_\theta/B_\theta < 1 \times 10^{-4}$ or $\tilde{B}_\theta/B_T < 1 \times 10^{-5}$, where the mode structures are not visible and do not show any significant characteristics changes due to the gas-puff pulses as shown in figure 5.17. The experiments in TEXTOR have revealed presence of threshold in the amplitude of magnetic turbulence $\tilde{B}_\theta/B_T < 4 - 5 \times 10^{-5}$ below which the RE loss is strongly supressed, leading to onset/increase in avalanche generated the RE current [261]. It is therefore safe to eliminate the role of magnetic fluctuations in the observed RE dynamic in presented discharge.

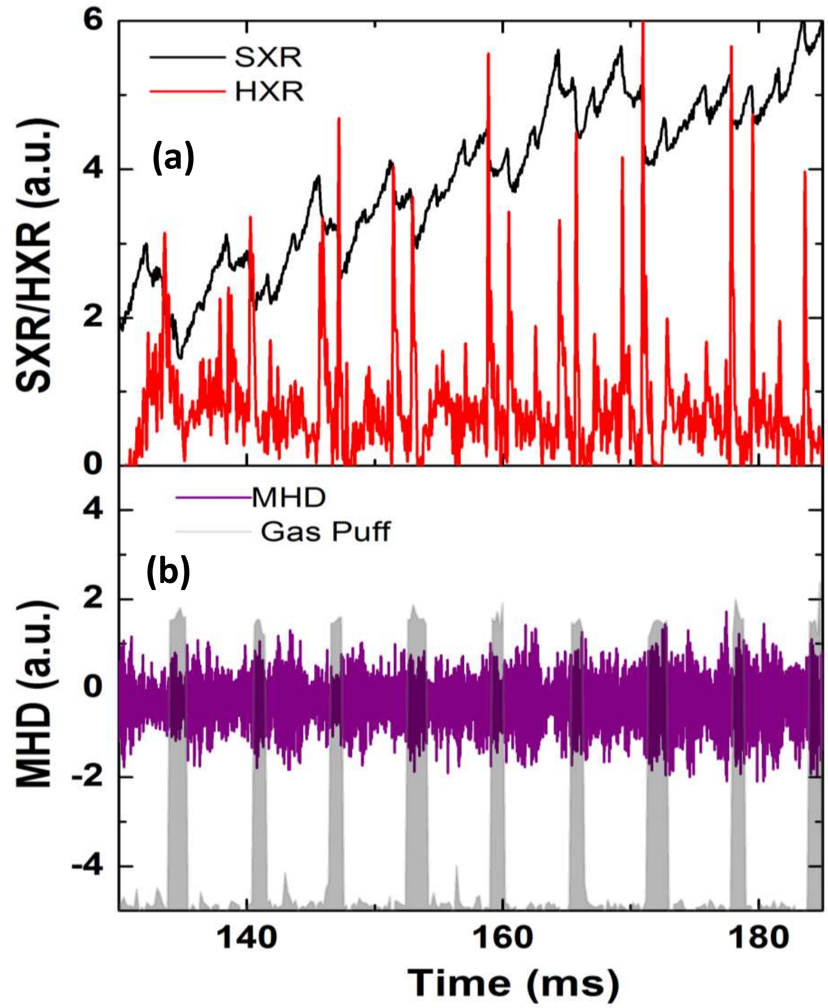

Figure 5.17:Plot showing the time evolution of (a) SXR (black), filtered HXR intensity (red) and (b) MHD activity with periodic gas puffs (gray) from shot#33141 from ADITYA-U.

5.4 Discussion and conclusion

All the above-mentioned observations provide first direct experimental evidence of edge/SOL turbulence facilitating RE loss in ADITYA and ADITYA-U tokamak. The presence of turbulence in the edge region is a common observation in tokamaks [262]. Further, the edge turbulence is usually interpreted as the nonlinear saturated state of drift wave or interchange instabilities in the edge plasma. The prevailing turbulence and its suppression by the gas-puff in the ADITYA edge has been investigated in detail by Jha et al. [221]. It has been observed that the fluctuation suppression is accompanied by a flattening of the radial profiles of the floating potential, plasma density. Similar observations are made during the gas-puff pulse applications in ADITYA-U. With the very low values of plasma β in the edge/SOL region of ADITYA-U, β being the ratio of plasma pressure and magnetic field pressures, the observed turbulence may safely be regarded as electrostatic in nature. Since, the regime where the electromagnetic fluid description is valid is rather limited in narrow ranges of plasma parameters where high-beta and high-collision conditions are satisfied simultaneously [263]. The edge electrostatic turbulence is known as the dominant mechanism of the cross-field plasma transport through the edge [30,242,264]. Furthermore, simultaneous reduction in particle flux along with the fluctuation suppression throughout the observed region of the plasma edge has been observed in the gas-puff experiments in ADITYA [221]. The experimental results described in the previous section suggest the electrostatic turbulence not only affect the thermal particles, but they also facilitate the loss of high-energetic particles (RE). Further, as the influence of magnetic fluctuations on RE dynamics is well established, the results presented in this chapter are the first direct evidence of electrostatic turbulence influencing the RE dynamics.

The observed decrease and subsequent increase of the HXR emission intensity after the application of gas-puff pulse within a time-span of ~ 5 ms cannot be explained by the existing RE loss theories. Because except the RE loss induced by magnetic fluctuation, which is proven not to be the loss mechanism in our experiments, all other loss mechanisms such as RE orbit drift losses and collisional losses which are long timescale phenomena [38,84,265]. Note here that the amount of gas injected in our experiments is $\sim 10^5$ times less than the injected amount in the massive gas injection experiments. With the prevailing loop voltage $\geq 2\,V$ (electric field $\sim 0.4\,V/m$) and $n_e > 2 \times 10^{19} m^{-3}$, the generation rate of REs through Decrier generation mechanism as well as secondary generation mechanism is also much more than $\sim 5\,ms$. Therefore, the decrease and increase of HXR emission intensity may be understood by following simple model. In ADITYA-U the observed REs have energies typically in the range $\sim 0.5 - 3\,MeV$. Before the application of the gas-puff, the REs are continuously lost to the limiter from the plasma, due to the drift-orbit loss [38,266] in presence of the relatively high electrostatic turbulence prevailing in the edge/SOL. As soon as the gas puff is injected, the electrostatic turbulence reduces and loss of REs due to the electrostatic turbulence is obstructed. This may lead to RE accumulation in the edge region where the turbulence was prevalent prior to its suppression since the loss of REs from the inner region is not affected by the gas puff. As soon as the effect of gas-puff is over and the turbulence increases again to its value of before gas-puff, the RE loss due to turbulence resumes, however, as the REs accumulated during the reduced turbulence phase are also thrown out now, larger HXR emission intensity as compared to its value before the gas puff, is observed. Also, it may happen that the during turbulence suppression period, the accumulated REs are accelerated to higher energies as the loop-voltage remains available. This may also be the possible reason behind the observance of higher values of HXR emission intensity during the subsequent turbulence switch-on period as compared to its minimum value during the turbulence switch-off period during and after the gas-puff pulse application. The diffusion coefficient due to the electrostatic turbulence has been estimated following these simple arguments. After attaining its minimum value during the turbulence switch-off phase, the HXR intensity rises to its maximum value, in the turbulence switch-on phase, $\tau_{rise} \sim 3\ ms$ (from figure 5.3 (b)). Considering roughly the edge is the region outside $r/a\ \sim 0.9$ where $T_e \sim 10 - 12\ eV$ [187]. including the whole region from the last closed flux surface to the first wall, i.e. the 'SOL' [29], the radial extent of edge fluctuation region is taken to be $x \sim 5\ cm$. Therefore the RE diffusion due to edge electrostatic turbulence estimated using $D_{EF} = \pi\,(a1^2 - a2^2)/\tau_{rise}$. Taking $a1 \sim \left(\frac{r}{a}\right) * a \sim (\ 0.9 \times\ 25)cm \sim 22.5\ cm$ and limiter boundary, $a2 \sim\ \sim 25$ cm, the estimated diffusion coefficient of RE due to electrostatic turbulence comes out to be $\sim D_{EF} \sim 1.2\ m^2/s$. The Loss of Runaway electrons due to magnetic and electrostatic fluctuations has been theoretically studied by Martin Solis et. al[88]. The diffusion coefficient of REs due to electric fluctuations is given as, $D_{RE} = \frac{D_{\tilde{E}}}{v_{||}}$, where $v_{||}$ is the parallel electron velocity and $D_{\tilde{E}}$ is the magnetic line diffusion coefficient given by $D_{\tilde{E}}$=$L_{||}v_{\tilde{E}}{}^2$ and $v_{\tilde{E}}$ is drift electron velocity induced by the fluctuating poloidal electric field $\tilde{E}v_{\tilde{E}} = \tilde{E}/B_0$. The calculated value of diffusion coefficient of REs due electrostatic fluctuation is plotted in figure 5.18 (a) with respect to δE_θ in the range, typically observed in tokamak edge, of $\sim 0.5 - 5\ kV/m$. REs velocity, $v_{||}$ is taken to be $\sim 10^8\ m/s$ for the calculations. It can be seen from the figure that, the experimentally observed value of diffusion coefficient of REs due to electrostatic turbulence $\sim 1.2\ m^2/s$, matches with the theoretically estimated value for $\delta E_\theta \sim 3\ kV/m$, which is quite possible in the edge region of ADITYA-U. For the sake of completion and comparison, the diffusion coefficient of REs in the presence of magnetic fluctuation is also calculated using [88]. $D_{RE} = D_{\tilde{B}} v_{||}$, where $v_{||}$ is the parallel electron velocity and $D_{\tilde{B}}$ is the magnetic line diffusion coefficient, $D_{\tilde{B}}$=$L_{||}\tilde{b}$ with $\tilde{b}$ is the normalized radial magnetic fluctuation amplitude, $\tilde{b} = \widetilde{B_r}/B_0$ and B_0 is Toroidal magnetic field and $L_{||}$ is the parallel correlation length of the magnetic field fluctuations, $L_{||} = \pi q_0 R_0$. Figure 5.18 (b) show the magnitude of diffusion of REs due to magnetic fluctuations with respect to $\tilde{b}$ in a range typically observed in the tokamaks i.e. $(10^{-5} - 10^{-4})$. In discharges with very low magnetic fluctuation amplitude ($\tilde{b} \leq 10^{-5}$) e.g. shot #32544 and #32567 shown in figure 5.4 and 5.5. The diffusion due to magnetic fluctuations is $< 0.5\ m^2/s$ whereas the diffusion due to electrostatic fluctuations is $\sim 1.2\ m^2/s$. It is, therefore, possible that even in the absence of sufficient magnetic fluctuations, the electric fluctuation can facilitate the RE loss, which is reflected in our experiments.

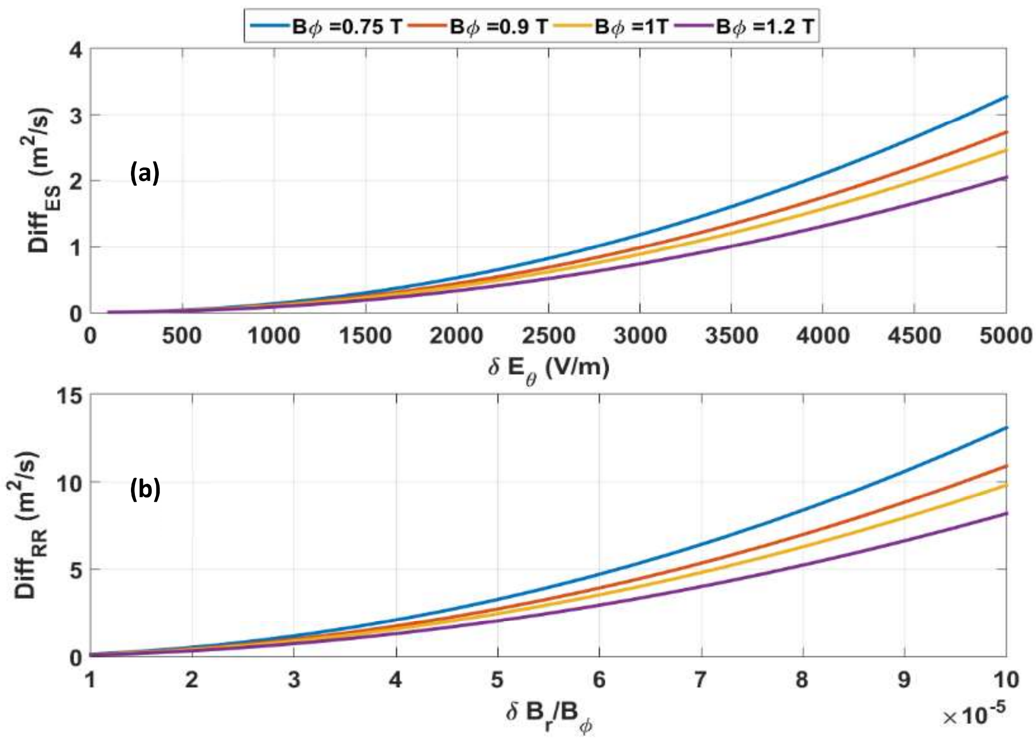

Figure 5.18:(a) Runaway Diffusion due to electrostatic fluctuation versus amplitude of electrostatic fluctuation, (b) Rechester- Rosenbluth Diffusion due to magnetic fluctuation versus amplitude of radial magnetic fluctuation normalized with a toroidal magnetic field

<u>Keywords</u>

Name of the Student: Harshita Raj

Name of the CI/OCC: Institute for Plasma Research

Enrolment No.: PHYS06201304012

Thesis Title: Study of generation and transport of Runaway Electrons in ADITYA and ADITYA-U tokamak

Discipline: Physical Sciences **Sub-Area of Discipline:** Plasma Physics (Tokamak)

Date of viva voce: 22 Jan 2020

1. Tokamak
2. Runaway electrons
3. ADITYA Tokamak
4. ADITYA-U Tokamak
5. MHD instabilities
6. Drift tearing modes
7. Runaway electron transport
8. Turbulent Edge fluctuations
9. Mirnov coils
10. Langmuir probes

<u>**Thesis Highlight**</u>

Name of the Student: Harshita Raj **Enrolment No.: PHYS06201304012**

Name of the CI/OCC: Institute for Plasma Research

Thesis Title: Study of generation and transport of Runaway Electrons in ADITYA and ADITYA-U tokamak

Discipline: Physical Sciences **Sub-Area of Discipline:** Plasma Physics (Tokamak)

Date of viva voce: 22 Jan 2020

Prevention and mitigation of runaway electrons, electrons that are collisionally decoupled from the bulk plasma and accelerate freely to very high energies ($\geq$ 10 MeVs), in tokamak plasma is a major thrust area of ongoing thermonuclear fusion research as they pose a severe threat to the peripheral plasma facing components. Scaling the energy of the RE beam produced during plasma disruption in present day experiments give a very alarming projection for ITER. The REs are known since the birth of tokamak and the generation mechanism of REs is understood to an extent, however, the loss or mitigation mechanisms of these REs are not very well understood. This thesis makes remarkable contribution in the study of the generation and loss mechanisms of RE. The experiments have been carried out in ADITYA and ADITYA-U tokamak (minor radius, $a = 25\ cm$ and major radius, $R = 75\ cm$) will be discussed in detail. The studied discharges have: plasma current$\sim 80 - 150\ kA$, chord-averaged electron density $\sim (1 - 4) \times 10^{19} m^{-3}$, chord-averaged electron temperature $\sim 200 - 500\ eV$ and toroidal magnetic field $\sim 0.75\ -\ 1.3\ T$. It has been observed that in majority of the cases the conventional sources of generation and loss do not explain the observed RE dynamics in ADITYA/ADITYA-U. Correlated HXR bursts with the each sawteeth-crash in several discharges suggested that sawtooth crash generates REs. Studies carried out in this thesis show that the electric field induced in the toroidal direction during the sawtooth crash is higher than the critical electric field required for REs generation, hence capable of generating REs during current flat-top. Further analysis revealed that overlapping of two magnetic islands (m/n=2/1 & 3/1) significantly enhances the radial RE loss, whereas the RE loss is reduced when good magnetic surfaces exist between the islands, as shown in figure 1. It has also been found that the presence of well-formed large magnetic islands with harmonics tends to confine the RE. A threshold in magnetic fluctuation amplitude and island rotation frequency has been observed for the generation of harmonics of 2/1 MHD mode. The 2/1 MHD mode amplitude and rotation frequency have been altered in a controlled fashion by periodic gas puffing during the course of a single discharge. The role of neutral injection in decreasing the diamagnetic drift frequency which results in decrease of island rotation has also been studied in detail. These periodic gas-puffs also resulted in reduction of turbulent edge fluctuations (TEF) in edge/SOL plasma region. A comparative study of magnetic and edge fluctuation in presence and absence of periodic gas puffs for several discharges in ADITYA-U indicates that the TEF in the edge of ADITYA-U also facilitates the RE loss mechanism and can be exploited as a mitigating mechanism for the REs.

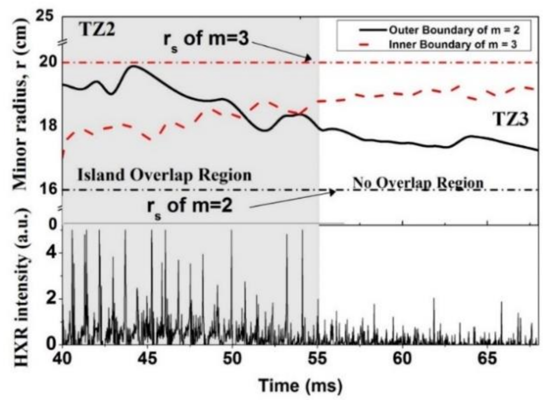

Figure 1: (a) Time evolution of outer boundary of m = 2 (solid line) island and inner boundary of m = 3 (dashed line). The location of mode rational surfaces is indicated by dash-dot line. (b) Time evolution of HXR emission intensity (shot# 24025). Nucl. Fusion 58 076004 (2018)